

# **New approaches to improve prediction of drug-induced liver injury**



Dissertation zur Erlangung des  
naturwissenschaftlichen Doktorgrades  
der Julius-Maximilians-Universität Würzburg

vorgelegt von  
Melanie Adler  
aus Greiz

Würzburg 2012



Eingereicht am 02.02.2012

bei der Fakultät für Chemie und Pharmazie

Gutachter der schriftlichen Arbeit

1. Gutachter PD. Dr. Angela Mally

2. Gutachter Prof. Dr. Ulrike Holzgrabe

1. Prüfer PD Dr. Angela Mally

2. Prüfer Prof. Dr. Ulrike Holzgrabe

3. Prüfer Prof. Dr. Wolfgang Dekant  
des öffentlichen Promotionskolloquiums

Datum des öffentlichen Promotionskolloquiums: 27.02.2012

Doktorurkunde ausgehändigt am .....



Für meine Eltern

*"Wer immer tut, was er schon kann,  
bleibt immer das, was er schon ist."*

Henry Ford



# INDEX

Index .....	I
Abbreviations .....	V
<b>1 Introduction .....</b>	<b>1</b>
<b>1.1 The liver as a critical target organ of drug toxicity .....</b>	<b>1</b>
1.1.1 Liver morphology and function .....	3
1.1.2 Xenobiotic metabolism .....	4
1.1.3 Types and mechanisms of drug-induced liver injury .....	6
<b>1.2 Methods for detection of hepatotoxicity .....</b>	<b>10</b>
1.2.1 Primary hepatocytes as an <i>in vitro</i> model to study hepatotoxicity .....	10
1.2.2 Traditional approaches .....	11
1.2.3 Application of omics technologies .....	12
1.2.3.1 Novel biomarker candidates for hepatotoxicity .....	13
1.2.3.2 Mechanistic understanding of hepatotoxicity .....	15
1.2.4 RNA interference as an investigative tool in mechanistic toxicology .....	17
1.2.4.1 Mechanism of siRNA-mediated gene silencing .....	18
<b>1.3 Aims of this work .....</b>	<b>21</b>
<b>2 Materials and Methods .....</b>	<b>22</b>
<b>2.1 Materials .....</b>	<b>22</b>
2.1.1 Technical equipment .....	22
2.1.2 Chemicals and reagents .....	23
2.1.3 Culture media and supplements .....	25
2.1.4 Kits .....	25
2.1.5 Buffers and solutions .....	26
2.1.6 Antibodies .....	28
2.1.7 Oligonucleotides .....	29
2.1.8 Software .....	30
<b>2.2 <i>In vivo</i> studies .....</b>	<b>30</b>
2.2.1 Standardized study design of the InnoMed Predictive Toxicology Project .....	30
2.2.2 Clinical examination .....	32
2.2.3 Construction of tissue microarrays .....	33
<b>2.3 <i>In vitro</i> studies .....</b>	<b>33</b>
2.3.1 Isolation of primary rat hepatocytes .....	34
2.3.2 Trypan Blue exclusion test .....	35
2.3.3 Culture conditions of hepatocytes .....	36

---

2.3.4 Transfection of siRNA duplex .....	36
2.3.5 Treatment with compound BAY16 .....	37
2.3.6 WST-1 assay .....	38
2.3.7 CellTiter-Glo <sup>®</sup> Luminescent cell viability assay .....	39
<b>2.4 Molecular biological methods .....</b>	<b>40</b>
2.4.1 Isolation of total RNA from tissues .....	40
2.4.2 Isolation of total RNA from rat hepatocytes .....	41
2.4.3 RNA quantification and quality control .....	41
2.4.4 cDNA synthesis and qRT- PCR using SYBR <sup>®</sup> Green .....	42
2.4.5 cDNA synthesis and qRT- PCR using hydrolysis probes .....	45
2.4.6 Microarray experiments .....	46
2.4.6.1 Preparation of labeled aRNA .....	48
2.4.6.2 Hybridization and microarray processing .....	49
2.4.6.3 Data extraction and analysis .....	50
<b>2.5 Biochemical methods .....</b>	<b>51</b>
2.5.1 Protein preparation from tissue .....	51
2.5.2 Protein preparation from rat hepatocytes .....	52
2.5.3 Protein separation by SDS polyacrylamid gel electrophoresis .....	52
2.5.4 Protein detection by western blot analysis and immune detection .....	53
2.5.5 Immunofluorescence .....	55
2.5.6 Immunohistochemical analyses .....	55
2.5.7 Quantification of proteins by ELISA .....	57
2.5.7.1 Development and validation of the rat NGAL ELISA .....	58
2.5.7.2 Thiostatin ELISA .....	59
2.5.7.3 Clusterin ELISA .....	60
2.5.8 PON1 activity assay .....	60
<b>3 Assessment of candidate biomarkers of drug induced liver injury in preclinical toxicity studies .....</b>	<b>61</b>
<b>3.1 Background .....</b>	<b>61</b>
<b>3.2 Results .....</b>	<b>62</b>
3.2.1 Biomarker responses to BAY16 in relation to traditional endpoints of toxicity ..	62
3.2.1.1 Clinicopathological and histopathological observations .....	62
3.2.1.2 Gene expression of biomarkers .....	65
3.2.1.3 Detection and quantification of biomarkers in serum and urine .....	67
3.2.1.4 Immunolocalization of putative biomarkers .....	70
3.2.1.5 Summary .....	72
3.2.2 Biomarker responses to EMD335823 in relation to traditional endpoints of toxicity .....	73
3.2.2.1 Histopathological and clinicopathological observations .....	73



---

3.2.2.2 Gene expression of biomarkers .....	76
3.2.2.3 Detection and quantification of biomarkers in serum and urine.....	77
3.2.2.4 Immunolocalization of putative biomarkers.....	79
3.2.2.5 Summary.....	80
3.2.3 Biomarker responses to BI-3 in relation to traditional endpoints of toxicity .....	81
3.2.3.1 Clinicopathological and histopathological observations.....	81
3.2.3.2 Gene expression of biomarkers .....	84
3.2.3.3 Detection and quantification of biomarkers in serum and urine.....	85
3.2.3.4 Immunolocalization of putative biomarkers.....	88
3.2.3.5 Summary.....	90
3.2.4 Evaluation of candidate biomarkers using ROC analyses .....	90
<b>3.3 Discussion .....</b>	<b>92</b>
3.3.1 NGAL as a non-invasive marker of acute tissue injury.....	92
3.3.2 Thiostatin as a sensitive marker of hepatotoxicity.....	92
3.3.3 Evaluation of PON1 activity for detection of liver damage .....	93
3.3.4 Expression of clusterin as a marker for liver damage .....	94
<b>3.4 Conclusion .....</b>	<b>95</b>
<b>4 Application of toxicogenomics to improve mechanistic understanding of drug-induced hepatotoxicity .....</b>	<b>96</b>
<b>4.1 Background.....</b>	<b>96</b>
4.1.1 Selection of BAY16 as model compound for studying hepatotoxicity .....	97
4.1.2 Experimental approach to discriminate between omics responses related to pharmacological vs. toxic effects .....	100
<b>4.2 Effect of BAY16 <i>in vitro</i>.....</b>	<b>101</b>
4.2.1 Results .....	102
4.2.1.1 Evaluation of BAY16 cytotoxicity in primary rat hepatocytes.....	102
4.2.1.2 Gene expression profile induced by BAY16 <i>in vitro</i> and comparison with existing <i>in vivo</i> data .....	104
4.2.1.3 Pathway analysis of transcriptional changes induced by BAY16 <i>in vitro</i> and comparison with <i>in vivo</i> .....	108
4.2.1.4 Functional analysis of deregulated genes.....	112
4.2.2 Discussion.....	117
<b>4.3 Effect of GCGR gene silencing by siRNA-mediated transfection <i>in vitro</i>.....</b>	<b>120</b>
4.3.1 Results .....	120
4.3.1.1 Efficiency of GCGR knockdown in primary rat hepatocytes .....	120
4.3.1.2 Effect of GCGR knockdown on cell viability .....	122
4.3.1.3 Transcriptional changes induced by gene silencing of <i>GCGR</i> .....	123
4.3.2 Discussion.....	125

<b>4.4</b>	<b>Discrimination of gene expression changes induced by BAY16 in the presence and absence of the GCGR .....</b>	<b>127</b>
4.4.1	Results .....	127
4.4.1.1	Morphological examination .....	127
4.4.1.2	Comparison of gene expression profile.....	128
4.4.1.3	Comparative pathway analysis and biological interpretation of transcriptional response related to BAY16-induced hepatotoxicity .....	129
4.4.2	Discussion .....	132
<b>4.5</b>	<b>Conclusions .....</b>	<b>133</b>
<b>5</b>	<b>Summary .....</b>	<b>137</b>
<b>6</b>	<b>Zusammenfassung .....</b>	<b>139</b>
<b>7</b>	<b>References .....</b>	<b>141</b>
<b>8</b>	<b>Acknowledgements .....</b>	<b>160</b>
<b>9</b>	<b>Publications .....</b>	<b>162</b>
<b>10</b>	<b>Appendix .....</b>	<b>164</b>

## ABBREVIATIONS

18s rRNA	nuclear ribosomal RNA small subunit
ABC	avidin-biotin complex
ALF	acute liver failure
ALP	alkaline phosphatase
ALT	alanine aminotransferase
ANOVA	analysis of variance
APS	ammonium persulfate
AR	aldose reductase
aRNA	amplified ribonucleic acid
ASO	antisense oligonucleotide
AST	aspartate aminotransferase
ATP	adenosine triphosphate
AUC	area under the curve
BA	bile acid
BAY16	(+)-(1R)-1-[4-(4-fluorophenyl)-2,6-diisopropyl-5-propyl-pyridin-3-yl]ethanol
BI-3	3-Pyrrolidineacetic acid, 5-[[[4'-[imino[(methoxycarbonyl) amino]methyl] [1,1'-biphenyl]-4-yl]oxy]methyl]-2-oxo-, methyl ester, (3S-trans)
BSA	bovine serum albumin
BSEP (ABCB11)	bile salt efflux pump
bw	body weight
C	control
cAMP	cyclic adenosine monophosphate
CAR	constitutive androstane receptor
cDNA	complementary deoxyribonucleic acid
CHAPS	3-((3-cholamidopropyl)-dimethylammonio)-1-propanesulfonate
C <sub>t</sub>	threshold cycle
CV	coefficient of variation
Cy	cyanine
CYP	cytochrome P450 enzymes
DAB	3,3'-diaminobenzidine
DAPI	4',6-diamidino-2-phenylindole
DEPC	diethylpyrocarbonate
DF1	lipid transfection reagent DharmaFECT 1

## ABBREVIATIONS

---

DILI	drug-induced liver injury
DMEM	dulbecco's modified eagle medium
DMSO	dimethyl sulfoxide
DTT	dithiothreitol
dNTPs	deoxynucleotide triphosphate
dsRNA	double stranded ribonucleic acid
EGTA	Ethylene glycol-bis-(2-aminoethyl)-N,N,N', N'-tetraacetic acid
ELISA	enzyme linked immunosorbent assay
EMD335823	1-(2-trifluoromethoxyphenyl)-2-nitroethanone
FXR	farnesoid X receptor
GAPDH	glycerine aldehyde-3-phosphate-dehydrogenase
GCGR	glucagon receptor
GCGR <sup>-/-</sup> mice	glucagon receptor knockout mice
GCOS	Gene Chip <sup>®</sup> Operating Software
GGT	$\gamma$ -glutamyltranspeptidase
GLDH	glutamate dehydrogenase
GSH	glutathione
GST	glutathione S-transferase
HD	high dose
HKG	housekeeping gene, reference gene
HRP	horseradish peroxidase
IF	immunofluorescence
IHC	immunohistochemistry
IL	interleukin
IPA	Ingenuity Pathway Analysis
IPG	immobilized pH gradient
ITS	insulin-transferrin-sodium selenite
IVT	<i>in vitro</i> transcription
LD	low dose
LLD	lower limit of detection
LXR	liver X receptor
MAS5	Microarray Analysis Suite 5.0
MDR	multidrug resistance protein
mRNA	messenger ribonucleic acid
MRP	multidrug resistance-associated protein
NAC	no amplification control

---

NGAL	neutrophil gelatinase-associated lipocalin
NOEL	no observed effect level
NTCP	Na <sup>+</sup> -taurocholate cotransporting polypeptide
OA	organic anions
OATP	organic anion transporting polypeptides
OST	organic solute transporters
PAGE	polyacrylamid gel electrophoresis
PB1	perfusion buffer 1
PB2	perfusion buffer 2
PBS	phosphate buffered saline
PCA	principal component analysis
PCNA	proliferating cell nuclear antigen
PCR	polymerase chain reaction
PKA	protein kinase A
PON1	paraoxonase-1
PPAR	peroxisome proliferator-activated receptor
PVDF	polyvinylidene difluoride
PXR	pregnane X receptor
qRT-PCR	quantitative real-time polymerase chain reaction
RIPA	radioimmunoprecipitation assay
RNA	ribonucleic acid
RNAi	RNA interference
ROC	receiver operating characteristic
rpm	rounds per minutes
RT	room temperature
RXR	retinoid X receptor
SC	scrambled siRNA (control siRNA)
SD	standard derivation
SDS	sodium dodecyl sulfate
siGCGR	siRNA targeting GCGR (knockdown GCGR)
siRNA	small interfering RNA
SULT	sulfotransferase
TEMED	tetramethylethylenediamine
TIMP-1	tissue inhibitor of metalloproteinases-1
TBS	tris buffered saline
TMA <sub>s</sub>	tissue microarrays
TMB	3,3',5,5'-tetramethylbenzidine

## ABBREVIATIONS

---

TNF	tumor necrosis factor
UGT	uridine diphosphate glucuronosyltransferase
UPL	Roche Universal Probe Library
UT	untransfected cells
WB	western blot
WST-1	4-[3-(4-Iodophenyl)-2-(4-nitrophenyl)-2H-5-tetrazolio]-1,3-benzene disulfonate

# 1 INTRODUCTION

The discovery and development of new drugs is a time-consuming and expensive process requiring a large number of animal testing. However, more than 90% of drug candidates fail in preclinical or clinical studies due to a lack of safety and efficacy [1, 2]. Drug-induced liver injury (DILI) is a major reason for the high failure rate of new pharmaceutical agents [3]. The high loss of new drug candidates due to hepatotoxic side effects in late stages of the drug development process represents a considerable problem for the pharmaceutical industry. Hence, there is an urgent need to develop new approaches for early and reliable prediction of drug-induced hepatotoxicity that enable a better selection of drug candidates by filtering out those compounds with high potential for toxicity at early stages of drug development. More knowledge about underlying key mechanism of toxicity and the identification of more sensitive biomarkers, linked to toxic responses, is of critical importance for improving the predictivity of drug-induced hepatotoxicity [4, 5].

## 1.1 The liver as a critical target organ of drug toxicity

The liver is the central organ for intermediate and xenobiotic metabolism and the largest gland in the human body that produces and secretes hormones, enzymes and other molecules involved in a wide range of physiological processes. Due to its pivotal role in bioactivation, detoxification and clearance of exogenous and endogenous substances, the liver is the main target of chemical- and drug-induced injury [6, 7]. The occurrence of hepatotoxicity is a major problem during development of novel drug candidates and the main cause for drug withdrawals from the market [8, 9]. It has been reported that more than 900 drugs can induce liver injury [10]. DILI can generally be categorized as dose-dependent and predictable (high incidence, type 1) or unpredictable (idiosyncratic, low incidence, type 2) [6]. Under the top 5 drugs associated with fatal liver injury reported to the WHO Collaborating Centre for International Drug Monitoring are acetaminophen, troglitazone, valproate, stavudine and halothane [11]. Clinical and epidemiological studies have established that acetaminophen toxicity, a typical case of DILI type 1, were the most common cause in 39 % and 42 % of cases of acute liver failure (ALF) in the US and Sweden [12, 13]. Another example of well-studied DILI drug is the peroxisome proliferator-activated receptor gamma (PPAR $\gamma$ ) agonist troglitazone (Rezulin®). This drug was the first thiazolidinedione approved in the US for treatment of type 2 diabetes in 1997 and removed from the market in 1999 in the United Kingdom (UK) and in 2000 in the US, or stopped during the registration procedure in the rest of Europe due to fulminant liver

failure [14, 15]. There are several factors that may contribute to the pathogenesis of drug-induced injury which usually involve the exposure to a high drug concentration and/or its metabolic activation to a toxic intermediate [6]. It is generally known that induction of cell damage and the response of the liver to such injury combined with fundamental changes in biochemical processes can be very varied and extensive after exposure of drugs. The mechanisms whereby some drug candidates induce hepatic injury are not yet fully understood. Possible targets of toxic agents are several structures, such as liver cells and cell membranes, or molecules, like intracellular proteins, lipids or nucleic acids, bile duct transporter and members of the nuclear receptor family [16-19]. Dysfunction of molecules involved in cell signaling pathways leads to dysregulation of gene expression and/or cellular function, resulting in initiation of apoptosis, proliferation, immunological and mitochondrial reactions [20, 21] (Figure 1). If the target molecule plays a key role in synthesis, metabolism, transport and energy mediated processes, or represent a cellular structure, then cell homeostasis may be disturbed (Figure 1).

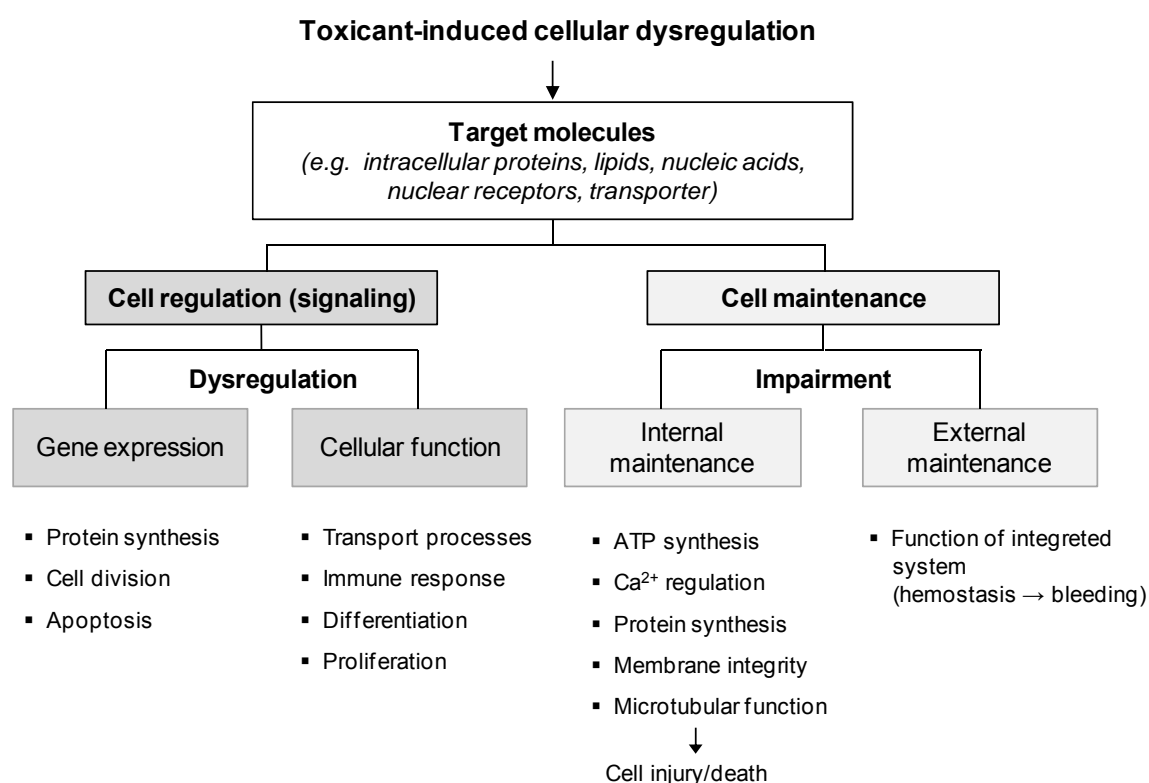


Figure 1. Effect and consequence of toxic-mediated cellular dysregulation (modified from Casarett and Doull's Toxicology: The Basic Science of Poisons, Klaassen CD. (Ed), Chapter 3. Mechanism of Toxicity (Zoltán Gregus), [22]).



### 1.1.1 Liver morphology and function

The liver has an important role in many vital functions including uptake, processing and storage of amino acids, carbohydrates, proteins, lipids, cholesterol and vitamins, synthesis of plasma proteins and bile as well as their release into the bile or blood [23, 24]. Anatomically, the rat liver can be divided into four lobes: the left lateral lobe, the median lobe, the right lateral lobe and the caudate lobe. The liver has two blood supplies, the portal vein and the hepatic artery. The portal vein carries venous blood to the liver and contains substances absorbed from the gastrointestinal tract, while the hepatic arteries supply oxygenated blood. The blood leaves the liver via the central veins which drain directly into the hepatic vein (*inferior vena cava*). Orally administered xenobiotics are absorbed from the intestine and are directly transported via the portal vein to the liver where they can be metabolized and/or detoxified before reaching other target organs (first pass effect). The metabolites are excreted into the bile or urine, depending on their molecular weight and polarity. The liver is composed of parenchymal cells, mainly hepatocytes, which represent 60 % of the cells in the liver, and non-parenchymal cells such as endothelial cells, stellate cells, Kupffer cells and pit cells [25-27]. A hexagonal shaped hepatic lobule is the functional unit of the liver, structurally organized by a vein in the center and the portal triads at the periphery [28]. The portal triad consists of the portal vein, hepatic artery and bile ducts (Figure 2). The hepatocytes are distributed into three zones, namely the periportal zone, the midzone and the central zone [29].

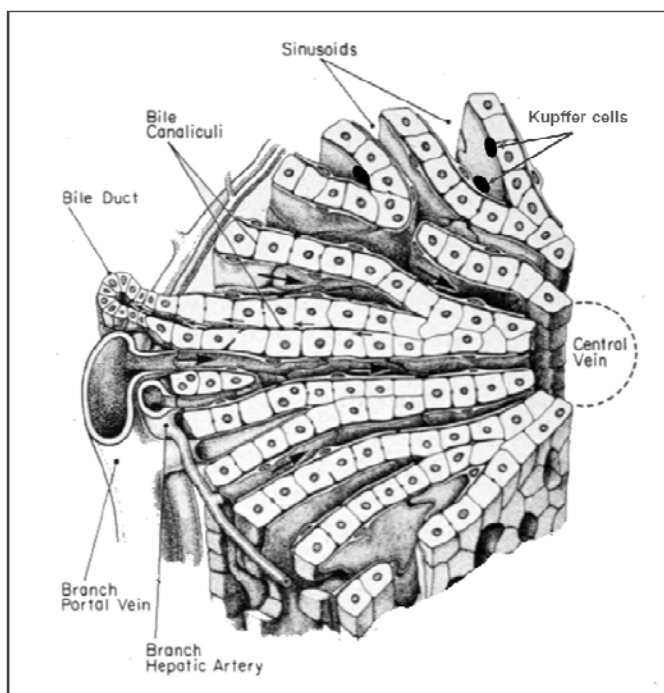


Figure 2. Schematic diagram of liver lobule structure showing the portal triad and the central vein, surrounded by hepatocytes, sinusoid and Kupffer cells (modified from Bloom and Fawcett. A Textbook of Histology (10th ed.) Philadelphia, PA: Saunders, 1975, and [30]).

Hepatocytes are required to not only detoxify endogenous and exogenous molecules, but to maintain metabolic function such as glucose and lipid metabolism, synthesis of proteins and bile to induce acute phase response [29]. The hepatic sinusoidal endothelial cells represent the barrier between blood and hepatocytes and are responsible for filtering and clearance of molecules or substances by endocytotic processes [31]. Independent of that function as antigen presenting cells, liver sinusoidal cells may also regulate the immune response through the control of effector T cell function [32] and an inhibitory effect on antigen presenting cell function of dendritic cells [33].

Kupffer cells are resident macrophages, located at the sinusoidal surface. They have proliferative and phagocytic properties and are involved in inflammatory processes via the secretion of eicosanoids, cytokines (e.g. interleukin-1, interleukin-6, tumor-necrosis factor  $\alpha$ ), nitric oxide and proteolytic enzymes [34]. This suggests that Kupffer cells play an important role in host defence as well as in the pathophysiology of liver disease [34].

Hepatic stellate cells are also known as Ito or fat-storing cells that reside in the space of Disse between sinusoidal endothelial cells and hepatocytes. A characteristic feature of this cell type is the presence of lipid droplets for storage of retinoid [35]. They have the ability to synthesize extracellular matrix proteins and it has been suggested that activation of stellate cells contribute to fibrosis, cirrhosis and immune response [36-38].

### 1.1.2 Xenobiotic metabolism

The role of the liver in bioactivation and detoxification of xenobiotics is of central importance. There are three groups of metabolic reactions, called phase I, phase II and phase III. The first phase of metabolic reactions involves introduction of functional groups into the molecules by oxidation, reduction or hydrolysis which usually result in formation of a more polar metabolite. This is followed by phase II reactions, the conjugation of active metabolites with hydrophilic groups, such as glucuronide, glutathione, sulfate, acetyl coenzyme A and amino acid, leading to more water-soluble products and thus facilitating their excretion into urine or bile. Although the conjugation of xenobiotics mostly leads to the detoxification of reactive intermediates, in some cases, chemically reactive metabolites can be produced that are more toxic than the present compound (activation).

Coordinated regulation of export processes plays an important role in detoxification and clearance of metabolites or endogenously produced substances and is also referred to as phase III of xenobiotic metabolism (Figure 3). Several basolaterally located influx transporters have been identified in the liver of rat, such as Na<sup>+</sup>-taurocholate cotransporting polypeptide (NTCP) and organic anion transporting polypeptides (OATP2, OATP4, OATP8), mediating uptake of drugs, organic anions, cations, and bile acids [39-

41]. Canalicular export pumps in the hepatocyte, such as multidrug resistance proteins (MDR) isoform 3, multidrug resistance-associated proteins (MRP) isoform 2, ATP-binding cassette sub-family G (ABCG) member 5 or member 8 and bile salt efflux pump (BSEP) are responsible for hepatic export of cholesterol, bile acids and products of metabolic pathways into the bile [41]. In addition, export transporter like multidrug resistance-associated protein isoform 3 (MRP3) and organic solute transporters (OST)  $\alpha$  and  $\beta$  are located along the basolateral membrane (Figure 3). Alterations in the functionality or expression of transport proteins are often associated with liver injuries in response to drugs [42].

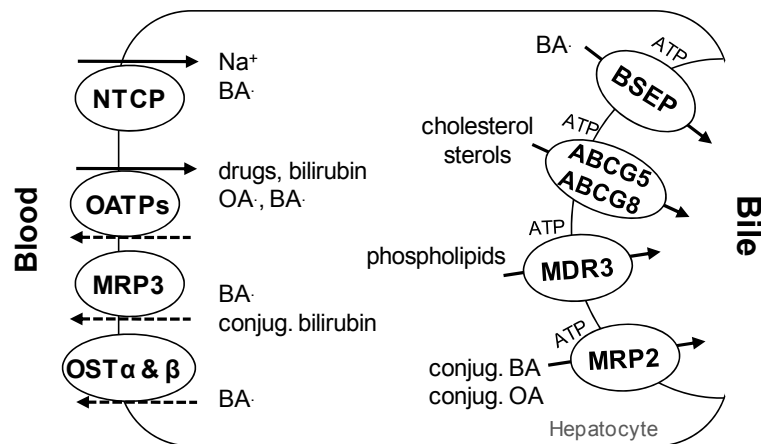


Figure 3. Overview of hepatocyte transporters on the sinusoidal (blood) and canalicular membrane (bile) that are involved in import and export of drugs, bile acids and metabolic end products (BA = bile acids, OA = organic anions; modified from Walker's Pediatric Gastrointestinal Disease Vol. 2; Kurbegov and Karpen, Physiology: Bile formation and cholestasis).

The expression of metabolizing enzymes is transcriptionally regulated through activation of nuclear receptors, including the pregnane X receptor (PXR), the constitutive androstane receptor (CAR), the farnesoid X receptor (FXR), the liver X receptor (LXR), the peroxisome proliferator-activated receptor (PPAR) and the aryl hydrocarbon receptor (AhR). They are activated by a broad range of endogenous compounds and clinical drugs (Table 1). After binding of a ligand, the receptors translocate from the cytosol to the nucleus as heterodimers or homodimers where they act as transcription factors by binding to specific DNA response elements. Depending on the kind of receptor and the ligand, nuclear receptors can positively or negatively regulate the expression of genes encoding several isoforms of cytochrome P450 (CYP), UDP glucuronosyltransferase (UGT), glutathione S-transferase (GST), sulfotransferase (SULT) as well as transport proteins (Table 1). The activation of PXR or CAR which have overlapping ligand specificity can result in increased expression of the same enzymes due to stimulation of similar response elements [43-46].

Table 1. Overview of nuclear receptors including ligands, target genes and biological function (based on [19]).

Nuclear Receptor	Drug/Ligand	Transcriptional activation of genes	Function
Pregnane X receptor (PXR/RXR)	rifampicin, phenobarbital, dexamethasone, statins, clotrimazole, paclitaxel	CYP2B6, CYP3A4, CYP2C6, CYP2C19, CYP1A2, CYP3A7, CYP7A1, CYP2C9, UGT1A1, UGT1A2, SULT2A1 GSTs, MRP2, SHP, BSEP, MDR1, MDR2,	BA synthesis, BA transport, BA detoxification, drug metabolism and detoxification
Constitutive androstane receptor (CAR/RXR)	bilirubin, phenobarbital, 1,4-bis-[2-(3,5-ichloropyridyloxy)] benzene (TCPOBOP), dimethoxycoumarin, dimethylesculetin, acetaminophen, phenytoin	CYP2A6, CYP2B1, CYP2B2, CYP2B10, CYP2B6, CYP2C9, CYP2C19, CYP2C29, CYP3A4, SULT1A1, SULT2A1, SULT2A9, UGT1A1, MRP2, MRP3,MRP4, ALAS	BA synthesis, BA transport, BA detoxification, drug detoxification
Farnesoid X receptor (FXR/RXR)	cholic acid, deoxycholic acid, chenodeoxycholic acid, synthetic: GW4064, 6-ECDCA	CYP3A4, SULT2A1, UGT2B4, UGT2B7, MRP2, ASBT, SHP, BSEP, MDR3, MDR2	Regulation of BA synthesis, BA transport, drug detoxification
Liver X receptor (LXR/RXR)	Oxysterols, fatty acids, 6 $\alpha$ -hydroxylated bile acids	CYP7A1, SULT2A9, MRP2, MRP4	BA synthesis, BA transport, BA detoxification
Peroxisome proliferator-activated receptor (PPAR $\alpha$ )	Fatty acids, fibrates, statins, eicasonoids, leukotriens, NSAIDs	CYP7A1, SULT2A1, UGT2B4, UGT1A3, MDR2, ASBT	BA synthesis, BA transport, BA detoxification, indirect induction of FXR
Aryl hydrocarbon receptor (AhR)	Halogenated and polycyclic aromatic hydrocarbons, tryptamine, bilirubin, biliverdin and lipoxin A4	CYP1A1, CYP1A2, CYP1B1, UGT1A1, UGT1A6, GSTA1, MRP3, MRP5, MRP6, BCRP, NRF2	Drug detoxification
Nuclear factor E2-related factor 2 (NRF2)	Reactive oxygen species	MRP2, MRP3, MRP4, BSEP, GSTS, NQO1, CYP1A2, CYP2A4, CYP2A12, CYP3A13, CYP4A10, CYP4A14, CYP2C39, UGTS, MRP1	BA transport, drug metabolism

### 1.1.3 Types and mechanisms of drug-induced liver injury

It has long been established that administration of drugs may result in acute and/or chronic liver failure depending on time of exposure and class of toxins. Hepatotoxicity may manifest in different types of liver injury, including necrosis, steatosis, steatohepatitis, cholestasis, hepatitis, fibrosis, cirrhosis and liver tumors (Table 2). These pathophysiological changes in the liver may be attributable to a direct or indirect effect of a toxic drug or their metabolites mediated by a wide range of molecular or biochemical mechanisms.

Table 2. Types of drug-induced liver disease.

Type of injury	Drugs
Cell death (Necrosis)	Acetaminophen, carbon tetrachloride, diclofenac
Fatty Liver (Steatosis)	Amiodarone, tetracycline, valproic acid, tamoxifen, steroids
Cholestasis	Chlorpromazine, cyclosporine A, estrogens
Hepatitis	Isozianid, nitrofurantoin, troglitazone, halothane
Fibrosis and cirrhosis	Methodextrate, carbon tetrachloride
Liver tumors	PPAR $\alpha$ agonist, clofibrate

In most cases, the clinical manifestation of hepatotoxicity is caused by a combination of impaired biochemical and cellular mechanisms [20]. Several mechanisms have been implicated in the onset and progression of DILI, including disruption of intracellular calcium homeostasis that leads to cell membrane injury, oxidative stress, activation of apoptosis, interruption of canalicular transporter, inhibition of fatty acid oxidation, inhibition of mitochondrial function and immune response or cell death mediated by the formation of a reactive metabolite (Figure 4) [20, 47].

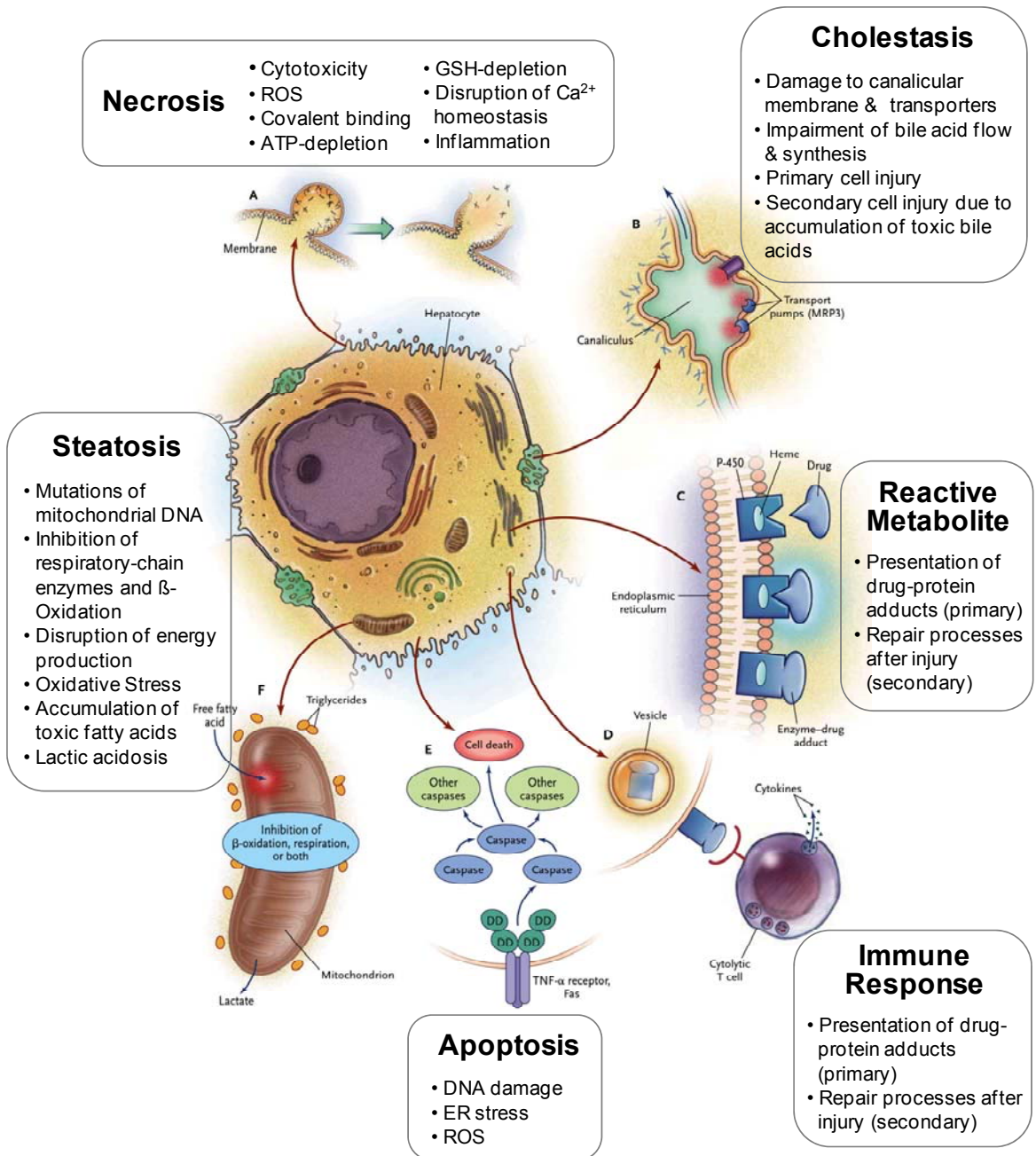


Figure 4. Types and mechanism of liver injury (adapted from [47], permission granted by New England Journal of Medicine).

*Hepatic cholestasis*

Cholestasis is characterized by impaired secretion of biliary substances or an obstruction of bile flow, resulting in accumulation of bile acids in the liver and blood. The mechanism underlying intrahepatic cholestatic injury has been linked to alterations of bile salt transport by inhibition or downregulation of ATP-dependent export pumps, and also to damage at the canalicular membrane, leading to impaired intracellular transport of bile to the canalicular membrane [48]. Maintenance of the balance between influx, efflux and

biosynthesis of bile acids is essential, because most bile acids are cytotoxic and may cause mitochondrial damage, apoptosis or necrosis in the liver [49]. The synthesis of primary bile acids cholic acid and chenodeoxycholic acid from cholesterol are catalyzed by several enzymes including cholesterol 7 $\alpha$ -hydroxylase (CYP7A1) and sterol 12 $\alpha$ -hydroxylase (CYP8B1) [50]. Bile acids are conjugated with taurine or glycine before they are excreted into the bile duct. Under physiological conditions, cholesterol and bile acid homeostasis is transcriptionally regulated by FXR, PXR, LXR and CAR [51]. The nuclear receptor FXR, which is activated by cholic acid, deoxycholic acid and chenodeoxycholic acid, plays a key role in the regulation of genes involved in cholesterol and bile acid homeostasis (Table 1) [52]. FXR inhibits intestinal reabsorption of bile acids through downregulation of basolateral NTCP uptake transporter and promotes the export of bile into the bile canaliculi through up-regulation of export pumps (BSEP, MRP2) [53-55]. Both mechanisms serve to prevent hepatocytes from accumulating toxic bile acids [53, 54]. Moreover, FXR is responsible for bile acid detoxification and repression of genes involved in bile acid synthesis, such as CYP8B1 or CYP7A1 (Figure 5) [56].

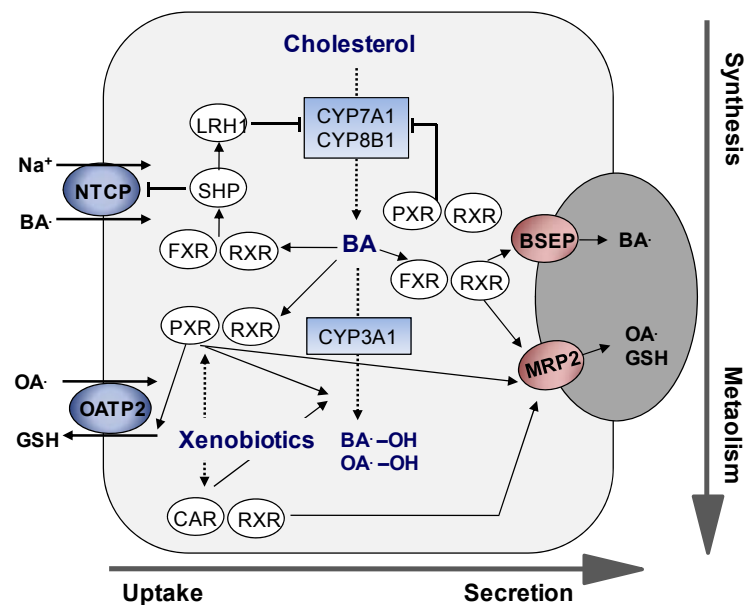


Figure 5. Transcriptional regulation of genes involved in synthesis, uptake, metabolism and secretion of bile acids (BA) and organic anions (OA<sup>-</sup>) through activation of FXR and PXR, which forms heterodimers with retinoid X receptor (RXR). The nuclear receptors prevent BA induced toxicity by inhibition of BA synthesis and import as well as increasing biliary detoxification and canalicular secretion (modified from [57]).

Drugs or their metabolites can inhibit hepatobiliary transport processes either directly through downregulation of canalicular transport proteins or indirectly through induction of pro-inflammatory cytokines produced by Kupffer cells in response to cellular injury,

leading to reduced expression of transport genes [42, 58]. For example, cyclosporine A, rifampicine and estradiaol have been shown to inhibit BSEP-mediated transport [59-61]. The model compound carbon tetrachloride decreased the expression of NTCP and OATP1/2, which might be associated with increased levels of the proinflammatory cytokine tumor necrosis factor alpha (TNF- $\alpha$ ) [18]. In the case of  $\alpha$ -Naphthylisothiocyanate, which is used as a model compound for cholestatic liver injury without clinical relevance,  $\alpha$ -Naphthylisothiocyanate induced several canalicular and basolateral transporter in mice, such as BSEP, MDR2, and MRP3 [62]. It has been shown that  $\alpha$ -Naphthylisothiocyanate is conjugated with glutathione and secreted into the canaliculi via MRP2 [63], where it injures bile duct epithelial cells, which results in intrahepatic increase of bile acids and hepatocyte necrosis [64].

### *Hepatic steatosis*

Hepatic steatosis is characterized by excessive accumulation of lipids within the hepatocytes and may be accompanied by hepatocellular necrosis, inflammation, fibrosis or cirrhosis, a progressive condition that is also referred to as non-alcoholic steatohepatitis. Steatosis may occur due to chronic alcohol consumption, hyperinsulinemia (diabetes mellitus type 2), obesity and drug or viral mediated effects [65]. Several molecular events may contribute to steatosis, including increased uptake of lipids, enhanced de novo fatty acid synthesis (lipogenesis), impaired lipid export, oxidative stress, decreased fatty acid oxidation and inhibition of the respiratory chain [66]. The antiarrhythmic drug amiodarone has been reported to induce steatosis by inhibition of the carnitine palmitoyltransferase 1A-dependent transport of long-chain fatty acids across the mitochondrial membrane, resulting in intracellular accumulation of free fatty acids [67]. On the other hand, amiodarone also has inhibitory effects on the mitochondrial respiratory chain [68, 69]. A reactive metabolite of valproic acid, a antiepileptic drug, is known to cause microvesicular steatosis by inactivation of  $\beta$ -oxidation enzymes [70-72].

## **1.2 Methods for detection of hepatotoxicity**

### **1.2.1 Primary hepatocytes as an *in vitro* model to study hepatotoxicity**

While *in vivo* models, limited by the animal welfare ethic, are used to study hepatic drug effects in the context of systemic influence, *in vitro* models derived from various cell types provide good systems to investigate specific mechanism in a controlled environmental [73]. The most frequently applied cell culture models in toxicology are primary hepatocytes [74], which are isolated from the liver and cultured in conventional monolayer on collagen or in a sandwich system with an collagen gel overlay [75-77]. The formulation of the media



and the extracellular matrix environment has a significant influence on the differentiation and morphology of the hepatocytes [78, 79]. Due to their metabolic activity, which are required to investigate the effect of a toxic drug metabolite, primary rat hepatocytes represent a good *in vitro* model for testing of drugs regarding their toxic potential [80].

For example, the observed hepatotoxicity of carbon tetrachloride and trichloroethylene studied in primary rat hepatocytes are consistent with data obtained from rats [81]. However, it needs to be considered that the use of cultured hepatocytes in comparison to the *in vivo* model is still limited due to the lack of physiological condition, especially the complexity of the whole liver, characterized by the presence of non-parenchymal cells (e.g. Kupffer cells, pit cells, stellate cells), biliary cells, blood flow and bile flow.

### **1.2.2 Traditional approaches**

Drug-induced hepatotoxicity may manifest in the form of several histopathological pattern of liver injury, including hepatocellular, cholestatic and mixed pattern [6]. The detection of drug-induced liver injury and differentiation between various hepatic lesions has been based primarily on histopathological findings and the quantitative measurement of enzyme biomarkers in serum or plasma using spectrophotometric methods in preclinical safety studies [82]. The term biomarker refers to a measurable biological parameter that can be used as an indicator of physiological or pathological processes, diseases or other conditions [83].

Hepatic enzymes, like alanine aminotransferase (ALT), aspartate aminotransferase (AST) and glutamate dehydrogenase (GLDH) are released from damaged hepatocytes into the circulation, resulting in elevated serum levels that can be used as indicators of hepatocellular injury [84]. However, elevation of ALT activity in the blood may be due to pathological conditions other than liver damage, such as muscle damage or cardiac injury [85, 86]. Increased levels of alkaline phosphatase (ALP),  $\gamma$ -glutamyltranspeptidase (GGT) and bilirubin indicate cholestatic injury [87]. A rise in serum ALP may also occur in bone disease or hyperthyroidism [88, 89]. Moreover, abnormal enzyme levels reveal only severe tissue injury and may not represent sensitive indicators of subtle toxic changes. Consumption of foods can also increase serum ALP activity in rats, which should be considered in the interpretation of this marker with regard to toxicological findings [84]. Although GGT serum levels are very low in the rat [90], this marker is considered to be more specific for cholestasis than ALP [84].

The use of these conventional clinical markers with respect to the prediction of liver injury is limited, because they lack specificity and are often only detectable when the liver function is already impaired.

### 1.2.3 Application of omics technologies

In the last 10 years, the application of new omics technologies like genomics, proteomics and metabonomics has become increasingly important in the drug development process [91-93]. These methods are widely used to measure changes at the transcript and protein level caused by exposure to a toxic compound to provide a better prediction and understanding of drug toxicities and adverse reactions [94]. The combination of toxicology and genomics has led to a new sub-discipline, called toxicogenomics [95]. Transcriptional analysis reveals changes in gene expression that might be linked to molecular or cellular processes in the liver, which in turn allows generation of mechanistic hypotheses of toxic drug response in accordance with histopathological observations [96-98]. Increased understanding of the underlying mechanism of toxicity is critical for the safety evaluation in the early phase of drug development [96] (Figure 6). Furthermore, it has been recognized that omics methods provide new possibilities for the discovery of new biomarkers for target organ toxicities. The identification and validation of sensitive and specific biomarkers for monitoring drug-induced liver injury is important to improve the selection of potentially toxic drugs in early preclinical stages and poses a great challenge [99, 100] (Figure 6). Additionally, toxicogenomics profiles enable to classify compounds with similar pathologies. It might be assumed that similar pathological phenotypes affect the same or related molecular mechanism of toxicity that might be associated with similar changes in gene expression [101]. The identification of such toxicity-related gene expression signatures (fingerprints) may be used as a diagnostic or predictive tool in toxicity testing [91, 102-104] (Figure 6).

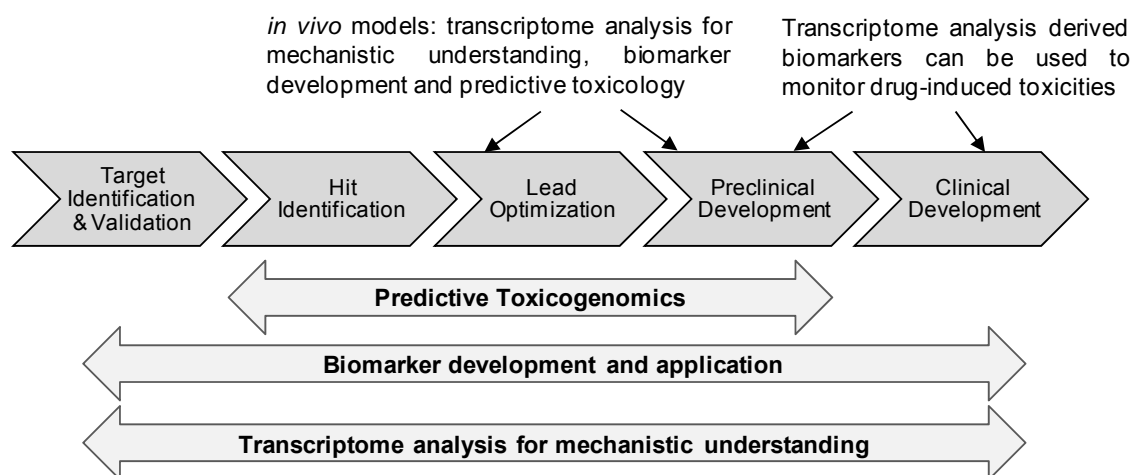


Figure 6. Application of genomics in the drug development process (modified from [99]).

*Innovative Medicine Predictive Toxicology Program (InnoMed PredTox)*

Over the last decade, several large-scale consortia have emerged with the aim of establishing new tools for improving the predictivity of drug-induced injuries [105]. Among these is the InnoMed PredTox project, a collaborative effort by 13 pharmaceutical companies, 2 small enterprises and 3 universities, partially funded by the EU as part of the Framework 6 program, which has been initiated in 2005 to evaluate whether conventional preclinical safety assessment can be significantly enhanced by incorporation of molecular profiling omics technologies. In short-term *in vivo* toxicological studies, transcriptomics, proteomics and metabolomics data were collected and analyzed in relation to routine clinical chemistry and histopathology [98]. To this end, male Wistar rats were treated for 1, 3 or 14 days with a low and a high dose of either a reference compound (troglitazone and gentamicin) or one of 14 proprietary compounds that previously failed during non-clinical drug development in part due to nephrotoxic or hepatotoxic effects [105]. A combination of omics technologies was applied to gain more mechanistic information of toxic endpoints and to identify novel biomarkers that are mechanistically linked to the observed drug-induced toxicities [97, 106, 107]. The compounds were classified in three major subgroups based on their toxicological endpoints: liver hypertrophy, bile duct necrosis and/or cholestasis (BDN), and kidney proximal tubular damage [98]. Four of sixteen drug candidates were characterized by bile duct damage and hyperplasia and/or increased bilirubin and cholestasis, hepatocyte damage including enzyme release, hepatocyte regeneration and hypertrophy, and inflammation in the bile duct and/or hepatocyte area [97]. The analysis of transcriptomics and proteomics data revealed potential candidate marker, such as neutrophil gelatinase-associated lipocalin (NGAL) and T-kininogen (thiostatin).

**1.2.3.1 Novel biomarker candidates for hepatotoxicity***Paraoxonase-1 (PON1) – a hepatic biomarker*

The enzyme paraoxonase-1 (PON1) is an ester hydrolase and has been implicated in the detoxification of organophosphates, carbamates, aromatic esters and unsaturated aliphatic esters [108, 109]. PON1 is mainly expressed in the liver and is secreted into the serum by high-density lipoprotein to prevent oxidation of low-density lipoprotein as part of the high-density lipoprotein complex [110, 111]. Besides the liver, PON1 activity has also been found in other rat tissues, such as kidney, brain and lung [112]. There is increasing evidence that PON1 is involved in the regulation of oxidative stress, however its physiological function in the liver remains unclear [97, 113-116]. Several studies have shown that serum PON1 activity is reduced in response to liver injury, including chronic

hepatitis, liver cirrhosis and steatosis, suggesting that reduced PON1 activity may be indicative of hepatotoxicity [115-119].

### *Clusterin – a kidney biomarker and a potential marker of hepatotoxicity*

Clusterin (apolipoprotein J), which is widely expressed in epithelial cells of many organs, is secreted as a 80 kDa heterodimeric glycoprotein into body fluids, such as urine, semen, breast milk and plasma [120-122]. It was first discovered and isolated from ram rete testis fluid, and named according to its ability to induce clustering of Sertoli cells [123, 124].

Because of its ability to bind a wide range of cellular molecules, clusterin is involved in several physiological processes such as lipid transport, regulation of the complement system and apoptosis, reproduction, cell differentiation, and clearance of proteins [121, 125, 126]. It has been reported that secretory clusterin promotes the lysosomal degradation of extracellular misfolded or denatured proteins through binding and internalization of such proteins, suggesting that overexpression of clusterin may help to protect cells against oxidative stress [125, 127]. Several studies have shown that the nuclear form of clusterin is linked to proapoptotic processes [128, 129], whereas the secreted form of clusterin may interact with Bax, which leads to inhibition of apoptotic signaling [130]. Induction of clusterin is observed under several disease conditions, including atherosclerosis, neurodegenerative diseases, glomerulonephritis, and cancer as well after kidney injury [121]. Clusterin has been shown to be upregulated in the kidney and released into urine in response to renal tubular injury in the rat. Urinary clusterin has been recently accepted by US and European regulatory authorities as a non-invasive kidney biomarker [131, 132].

Gene expression analysis in the liver of hepatotoxin-treated rats reveals a correlation between the increase of clusterin mRNA level and compound-induced liver injury [104]. Immunohistochemical analysis suggests that overexpression of clusterin in cholestatic or fibrotic liver disease may be due to its functional role as chaperone to stabilize or protect cells or cellular structure [133].

### *Neutrophil gelatinase-associated lipocalin (NGAL) – a urinary biomarker of renal injury and a potential marker candidate of liver injury*

Neutrophil gelatinase-associated lipocalin, also known as lipocalin-2, is a member of the lipocalin protein family, a group of extracellular proteins with a beta barrel calyx structure, which are able to bind and transport hydrophobe molecules [134-136]. It is released from neutrophile granules as a 25 kDa monomer, a 46 kDa disulfide-linked homodimer or as a 135 kDa disulfide-linked heterodimer conjugated with matrix metalloproteinase-9 [136, 137]. NGAL is expressed by immune cells, hepatocytes and renal tubular cells and is

secreted into urine and serum in a broad range of pathological conditions, including kidney injury, atherosclerosis and inflammatory bowel disease [138-140]. Several studies have demonstrated that NGAL inhibits the growth of bacteria by binding of bacterial siderophore, which is required to take up iron from the extracellular space [141, 142]. Thus, NGAL plays a role in the defense of bacterial infections [143, 144]. NGAL has been characterized as an acute phase protein, because it is expressed during the myelocyte stage in the course of neutrophil maturation and release after neutrophil activation as part of the immune response [145]. Expression of NGAL in hepatocytes is increased by exposure to IL-1 $\beta$ , but not to IL-6 [146]. NGAL has also been shown to be induced in response to inflammatory stimuli in the liver, accompanied by an increase in serum concentrations [142, 147]. Similar to clusterin, previous transcriptomics results from PredTox studies indicated that NGAL, which has been suggested as a urinary marker of renal injury [148, 149], was consistently up-regulated in livers of rats following treatment with compounds associated with hepatotoxicity [97].

*Thiostatin (T-kininogen) – a potential non-invasive biomarker of liver injury*

T-kininogen, also known as thiostatin or major acute phase alpha 1-protein, is a rat specific 68 kDa glycoprotein belonging to the kininogen family that is primarily expressed in the liver [150]. Thiostatin has been implicated in the protection of healthy tissues due to inhibition of cysteine proteinases that are released around damaged areas [150, 151]. Due to its role as an acute phase protein, mRNA expression and plasma concentration of thiostatin increase during acute inflammatory conditions, e.g. in response to endotoxemia [152, 153]. Thiostatin was identified within the PredTox project as a protein increased in urine of rats showing hepatobiliary damage by proteomic analysis using 2D-PAGE (unpublished data).

### **1.2.3.2 Mechanistic understanding of hepatotoxicity**

More mechanistic insight into the action of a toxic drug is needed to better understand the nature of toxicity and to optimize the design of drugs, especially in those cases where more than one compound in a lead series of drug candidates show the same pattern of toxicity [154]. In most cases, specific mechanisms or processes leading to hepatotoxic effects induced by pharmacologic compounds are not yet fully understood.

Toxicogenomics is commonly used to identify molecular changes in the expression of key genes involved in the regulation of signal transduction cascades and can provide valuable mechanistic insight into the mode of action of drugs and the action of toxicity.

Acetaminophen, a well-studied hepatotoxicant, is one example to show how transcriptional profiling has been successfully used to elucidate the cause of drug-induced toxicity in the liver of rats [96, 155-157]. Transcriptional profiling has shown that acetaminophen leads to dose-dependent decrease in expression of genes involved in ATP-consuming pathways, such as gluconeogenesis, fatty acid synthesis, cholesterol synthesis, and increase in the expression of genes associated with ATP-producing processes, like glycolysis as well as oxidative stress [96]. Results obtained in these studies, revealed that most of these effects occurred in the absence of morphological evidence for hepatotoxicity [96]. The mechanism underlying acetaminophen hepatotoxicity is associated with depletion of GSH [158, 159]. This has been attributed to CYP-catalyzed formation to toxic metabolite N-acetyl-p-benzoquinone imine that can covalently bind to proteins leading to increase of oxidative stress accompanied by mitochondrial injury and ATP depletion [160, 161].

However, one of the key difficulties associated with interpretation of genomics data in preclinical studies is the fact that alterations in gene profiles may present a combination of toxic, adaptive and pharmacological properties of the drug, particularly in those cases where the pharmacological target is also present in the organ in which pathological changes occur [96]. Examples of this include the PPAR $\gamma$  receptor agonist troglitazone, an antidiabetic agent which is associated with liver toxicity and has been shown by -omics technologies to cause alterations in gene expression associated with increased glucose uptake, reduced fatty acid oxidation, hepatic glucose production, inhibition of cholesterol biosynthesis and transport and up-regulation of ketogenesis in the rat liver [162-164]. All of these included pathways appear to be linked to the pharmacology of troglitazone rather than being informative about the mechanism of toxicity. Although the exact mechanism of troglitazone-induced hepatotoxicity has not been fully elucidated, there is evidence to suggest that toxicity does not seem to be PPAR $\gamma$ -mediated but is rather caused by the formation of reactive metabolite. Studies *in vitro* and *in vivo* have shown that troglitazone is metabolized by CYP3A to several reactive intermediates, especially quinones [165-167]. In this context, the metabolite troglitazone sulfate has been linked to an inhibitory effect on canalicular bile salt export pumps (BSEP) and organic anion transporting polypeptides (OATP), leading to hepatotoxicity [168, 169]. The induction of apoptosis as a toxic endpoint is likely initiated by stimulation of JNK signaling and/or decrease of mitochondrial membrane potential, leading to release of cytochrome and activation of caspases signaling [170, 171].

Taken together, it is possible that drug toxicity may be linked to the pharmacology of the drug, whereas in other cases, toxicity may occur independently of the therapeutic effect.

#### 1.2.4 RNA interference as an investigative tool in mechanistic toxicology

Over a long period, toxicology has traditionally focused on the observation and interpretation of adverse effects to establish safety and risk assessment strategies for the tested compound. The use of genomics technologies in toxicology provides a new tool to identify gene expression changes potentially involved in mechanism of toxicity, but its application in the assessment of pharmaceuticals is limited with regard to interpretation of toxic relevant effects. Thus, the additional utilization of RNA interference (RNAi) has become increasingly important in the field of mechanistic toxicology in the pharmaceutical industry. RNAi is a cellular regulatory process in eukaryotic cells in which small RNA molecules are used to inhibit expression of target proteins by degradation of complementary messenger RNA (mRNA). This process was found in many organisms where it plays an essential role in the defense against viruses, parasitic genes and transposons in general. The mechanism of posttranscriptional gene silencing was first discovered by Fire and his colleagues in 1998 [172]. This working group has demonstrated that injection of double stranded RNA (dsRNA) into the nematode *Caenorhabditis elegans* leads to effective and selective inhibition of gene expression [172]. In mammalian cells dsRNA can silence gene expression by processing into 21-23 nucleotides long siRNA with an antisense 3' end overhang, which enhances the efficiency of mRNA degradation [173].

In recent years, RNAi technology has been widely used in mammalian cells and animals to knockdown the expression of a specific gene in order to generate systems which allow the investigation of disease phenotypes and identification of new therapeutic strategies [174, 175]. Chemically synthesized siRNA has proven to be a useful tool for rapid identification of novel drug targets through investigation of functional consequences resulting from target gene silencing on a cellular level. Most pharmaceutical companies use siRNA high-throughput screening for drug target validation to investigate if downregulation of a specific gene results in an interesting phenotype or undesirable phenotype associated with toxicity [176].

Genetically modified animals are also increasingly being used to identify and validate novel drug targets, but such systems can also be helpful to assess the toxicity of pharmacologically active compounds [177]. In contrast to preclinical toxicity studies in wild type animals, the use of knockout mouse models lacking the pharmacological target may provide a good system to investigate if the toxicity caused by a drug candidate is closely related to its pharmacology resulting from interaction with the therapeutic target (primary pharmacology, on-target effects) and/or other unspecific targets (secondary pharmacology, off-target effects) or even mediated by chemical reactions [154]. This can be done using active but structurally diverse compounds and inactive compounds that are

similar in their structure [154] (Figure 7). In order to simplify this experimental approach, which can be extensive and time-consuming due to generation of suitable knockout animals, the RNAi-based gene silencing can also be applied in cell-based systems to observe toxic effects after treatment with a given drug in the presence or absence of a specific siRNA molecule. For example, stable expression of siRNA against activating signal cointegrator-2 in HepG2 cells demonstrated that this protein might be involved in acetaminophen-mediated hepatotoxicity as a coactivator of CAR *in vivo* [178]. Another study has shown that mouse hepatocytes were less susceptible to actinomycin D cytotoxicity after gene silencing of the FAS receptor [179].

The combined application of RNAi and transcriptomics for analyzing the gene expression profiling of a drug candidate after suppression of its pharmacological target may be a useful new experimental approach to distinguish between pharmacological mode of action and/or toxic action of the drug, and might provide more insight into molecular mechanisms underlying drug-induced hepatotoxicity.

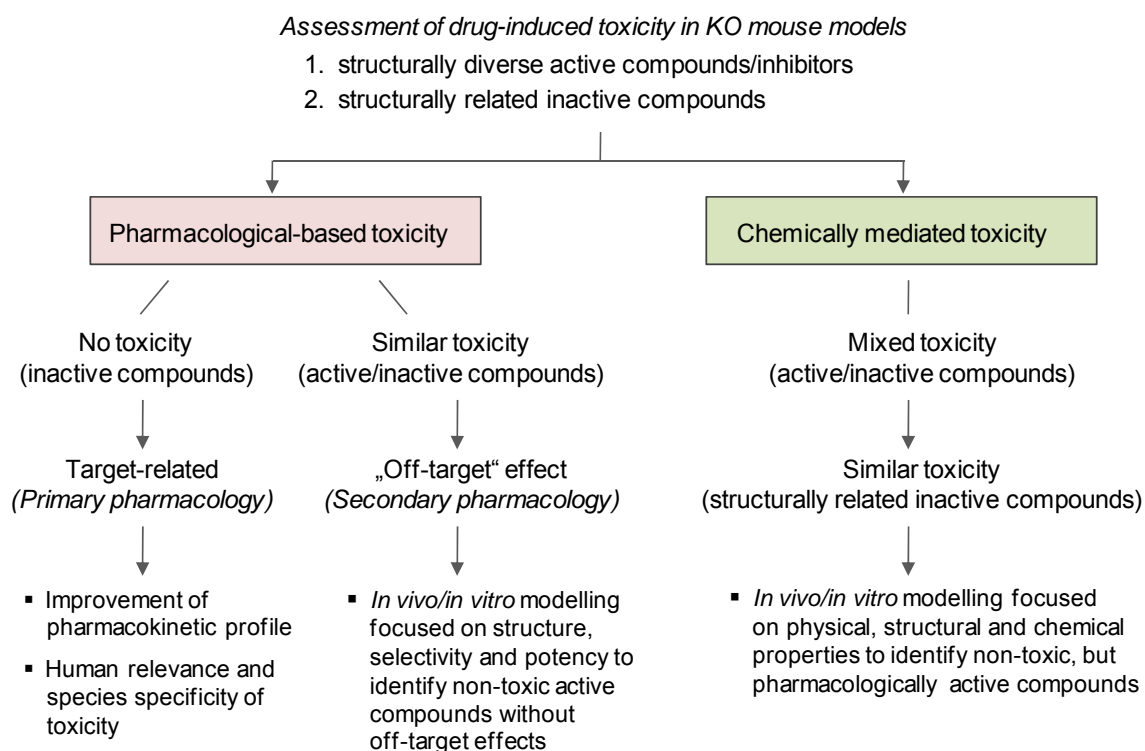


Figure 7. Approaches to assess if the toxicity of novel drug candidates represents a primary or a secondary pharmacological effect or a chemically mediated effect (modified from [154]).

#### 1.2.4.1 Mechanism of siRNA-mediated gene silencing

The mechanism of posttranscriptional gene silencing is based on the use of dsRNA, which triggers endonucleolytic processes resulting in degradation of specific mRNA. It has been shown that initiation of RNA processing through dsRNA can trigger an immune response



due to activation of interferon-induced protein kinase R signaling [180]. These unspecific off-target effects may be caused by activation of JAK/STAT transcription factor signaling, leading to an increased expression of interferon-stimulated genes [181]. To alleviate this problem, 2'-O-methyl modifications have been introduced into antisense strand to minimize off-target effects [182].

There are three general approaches for introducing dsRNA or siRNA into the cell. After co-transfection of exogenous dsRNA using viral vectors as carrier or transfection of siRNA using vectors expressing shRNA, both dsRNA and shRNA need to be pre-processed by the Rnase-III (Ribonuclease-III) enzyme Dicer and cleaved into RNA duplexes of 21-23 nucleotides in an ATP-dependent reaction [183, 184]. In contrast to pre-processed siRNA, synthetic siRNA may be directly transferred across the cell membrane using lipid transfection reagents that encapsulate the siRNA to promote its cellular uptake. The siRNA is then recognized by RNA-induced silencing complexes (RISC) which contains a Dicer helicase domain for unwinding of siRNA duplexes, endonuclease Argonaute 2 (Ago2) and a transactivating response RNA-binding protein (TRBP). TRBP is required to recruit Ago2 to the Dicer-bound-siRNA complex [185]. After activation of RISC, duplex siRNA is unwound and the less stable single strand with the 5'-end that has a complementary sequence to the target mRNA is integrated into the RISC. The antisense RNA strand guides the activated RISC to the homologous site of the target mRNA and the endonuclease Ago2 cuts the target mRNA into small fragments, resulting in mRNA degradation (Figure 8).

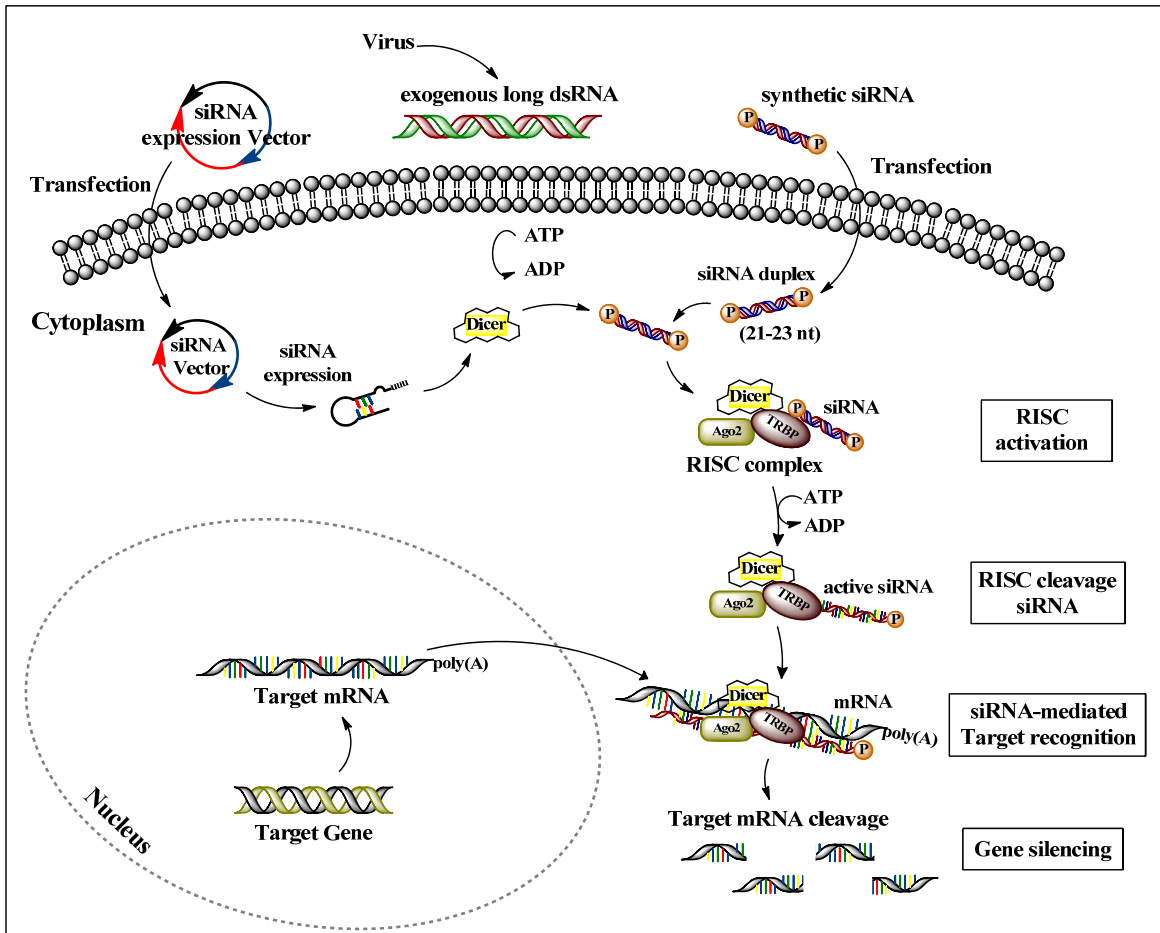


Figure 8. Mechanism of RNA interference using viral dsRNA, siRNA expression vectors or synthetically produced siRNA results in cleavage of target mRNA and subsequent inhibition of protein synthesis (modified from Ambion GeneAssist™ Pathway Atlas).

### 1.3 Aims of this work

Drug induced liver injury (DILI) represents a major cause for failure of new drug candidates due to late-breaking findings in preclinical safety studies. Thus, applications of new approaches in preclinical drug safety evaluation that can be used to identify or predict drug-induced hepatotoxicity and to better understand the mechanism underlying DILI are of fundamental importance to risk assessment and decision making in preclinical development. Therefore, the overall aim of this work was to improve the predictability of DILI in preclinical studies through improved mechanistic understanding and identification and evaluation of novel biomarkers of hepatotoxicity.

Conventional markers of liver injury are often not specific or indicate toxicity only when liver function is already impaired. Hence, it is important to evaluate additional novel biomarker that may be able to detect early signs of liver injury. Despite intensive worldwide efforts in the field of biomarker discovery, only few new biomarker candidates have been identified in the literature or within the PredTox project, such as clusterin, PON1, NGAL and thiostatin, but to date no novel marker for liver injury has been biologically validated.

Therefore, as part of the PredTox project, the first focus of this work was to assess a number of putative non-invasive marker for hepatotoxicity in preclinical safety studies in rats using a wide range of molecular biology and biochemical methods, including ELISA assays, immunohistochemical analysis and quantitative real-time polymerase chain reaction (qRT-PCR). The sensitivity and specificity of these markers were compared to established clinical chemistry parameters with regard to their use in preclinical safety studies for detection of DILI.

A second focus of this work was to investigate transcriptional changes associated with drug-induced hepatotoxicity to gain a better insight into key mechanism of drug toxicity. To this end, we were interested in establishing *in vitro* approaches which would allow us to discriminate between gene expression changes related to the pharmacologic action of a model drug and those changes which are associated with toxic effects of the drug to help identify key events responsible for the observed hepatotoxicities. Combined application of genomics profiling technology and RNAi to inhibit the pharmacological target of a drug candidate were used to determine if drug-induced hepatotoxicity represent a primary or secondary pharmacological effect or a chemically mediated off-target effect.

Finally, results obtained from this study were aimed to assess whether utilization of siRNA technology *in vitro* to specifically knockdown the expression of the pharmacological target of selected drugs may represent a suitable approach for early preclinical safety testing to improve mechanistic understanding of the molecular events involved in liver toxicity.

## 2 MATERIALS AND METHODS

### 2.1 Materials

#### 2.1.1 Technical equipment

Table 3. List of equipment and providers/manufacturers.

Equipment	Provider/Manufacturer
AB GeneAmp PCR system 9700	Applied Biosystems, Foster City, USA
Agilent 2100 Bioanalyzer	Agilent Technologies, Waldbronn, Germany
Autoclave	Melag Medical technology, Berlin, Germany
Bottle-top filter, 0.2 µm	Nalgene Nunc Internation, Rochester, USA
Cell scraper	Greiner Bio-One GmbH, Frickenhausen, Germany
Centrifuges (Hettich Universal/K2S Laborfuge 400e, Heraeus, Eppendorf Centrifuge 5415D)	Andreas Hettich GmbH & Co.KG, Tuttlingen, Germany; Eppendorf AG, Hamburg, Germany ThermoFisher Scientific, Waltham, USA
Confocal microscope TCS SP5	Leica Microsystems GmbH, Wetzlar, Germany
Cryostat CM3050S	Leica Microsystems GmbH, Wetzlar, Germany
Cups (0.5 ml, 1.5 ml, 2.0 ml)	Sarstedt AG & Co., Nümbrecht, Germany
Cuvettes	Hartenstein Laborbedarf GmbH, Würzburg, Germany
Glass/Teflon potter homogenizer	VWR International GmbH, Darmstadt, Germany
Dual Gel Caster	Hoefer Inc., Holliston, USA
Electrophoresis system	Biorad Laboratories GmbH, München, Germany
ELISA plate, Nunc-Immuno™ Maxisorp	Nunc-Immuno™ Maxisorp; Kamstrup, Denmark
Filter tips	Peqlab Biotechnology GmbH, Erlangen, Germany
Fluidics Station 450 Dx	Affymetrix, Santa Clara, USA
Gel Doc 2000	Biorad Laboratories GmbH, München, Germany
Gene Chip® Fluidics Station 450 Dx	Affymetrix, Santa Clara, USA
Gene Chip® Rat Expression Array 230 2.0	Affymetrix, Santa Clara, USA
Gene Chip® Scanner 7G	Affymetrix, Santa Clara, USA
Glassware	Schott AG, Mainz, Germany
Heat block	Eppendorf AG, Hamburg, Germany
Hybridization oven 640	Affymetrix, Santa Clara, USA
LightCycler® 480 Instrument	Roche Diagnostics GmbH, Mannheim, Germany
LB Mithras 940	Berthold Technologies GmbH & Co.KG, Bad Wildbad, Germany
Magnetic Stand-96	Applied Biosystems/Ambion, Austin, USA
Microplate photometer Spectramax340	Molecular Devices, München, Germany
Microscope	Nikon GmbH, Düsseldorf, Germany
Microtiterplates	Roche Diagnostics GmbH, Mannheim, Germany
Microtome RM2164	Leica Microsystems GmbH, Wetzlar, Germany

Equipment	Provider/Manufacturer
NanoDrop 2000c	Peqlab Biotechnology GmbH, Erlangen, Germany
Neubauer-Chamber	Hartenstein Laborbedarf GmbH, Würzburg, Germany
Nunc-Immuno™ Washer 12	Nunc, Wiesbaden, Germany
PCR microplate (white 96-well)	Roche Diagnostics GmbH, Mannheim, Germany
Peristaltic mini pump III (Model 3386)	Neolab Migge Laborbedarf-Vertriebs GmbH, Heidelberg, Germany
pH meter	WTW, Heidelberg, Germany
Pipettboy	Brand GmbH & Co.KG, Wertheim, Germany
Pipettes	Brand GmbH & Co.KG, Wertheim, Germany
Pipette tips	Sarstedt AG & Co., Nümbrecht, Germany
Plastic tubes	Sarstedt AG & Co., Nümbrecht, Germany
Power supplies	Biorad Laboratories GmbH, München, Germany
Spectralphotometer	Pharmacia Biotech Ltd, Cambridge, UK
SuperFrost® Slides	Gerhard Menzel GmbH, Braunschweig, Germany
Thermocycler	Eppendorf AG, Hamburg, Germany
Thermomixer comfort	Eppendorf, Hamburg, Germany
Ultra Turrax	IKA Werke GmbH & Co.KG, Staufen, Germany
Vortex	Bender & Hobein, Zürich, Switzerland
Water bath	Julabo Labortechnik GmbH, Seelbach, Germany

### 2.1.2 Chemicals and reagents

Table 4. List of chemicals and reagents including supplier.

Chemical/Reagent	Provider
Acetic acid (100 %)	Carl Roth GmbH & Co. KG, Karlsruhe, Germany
Acrylamide (Rotiphorese-Gel, 30 %)	Carl Roth GmbH & Co. KG, Karlsruhe, Germany
Ammonium persulfate (APS)	Carl Roth GmbH & Co. KG, Karlsruhe, Germany
Avidin	Sigma-Aldrich, Taufkirchen, Germany
Biotin	Sigma-Aldrich, Taufkirchen, Germany
Bovine serum albumin (BSA)	Carl Roth GmbH & Co. KG, Karlsruhe, Germany
Bromphenol blue	Carl Roth GmbH & Co. KG, Karlsruhe, Germany
D-(+)-Glucose	Sigma-Aldrich, Taufkirchen, Germany
DEPC (Diethylpyrocarbonate)-H <sub>2</sub> O	Carl Roth GmbH & Co. KG, Karlsruhe, Germany
Donkey serum normal	Vector/Linaris, Wertheim, Germany
ECL™ Western Blotting Detection and Hyperfilm ECL	GE Healthcare Life Science, Freiburg, Germany
Eosin	Carl Roth GmbH & Co. KG, Karlsruhe, Germany
Ethanol	Sigma-Aldrich, Taufkirchen, Germany

## 2 MATERIALS AND METHODS

Chemical/Reagent	Provider
Ethylene glycol-bis-(2-aminoethyl)-N,N,N', N'-tetraacetic acid (EGTA)	Sigma-Aldrich Chemie GmbH, Taufkirchen, Germany
4-(2-Hydroxyethyl)piperazine-1-ethanesulfonic acid, N-(2-Hydroxyethyl)piperazine-N'-(2-ethanesulfonic acid) (Hepes)	Sigma-Aldrich, Taufkirchen, Germany
Hydrogen peroxide	Carl Roth GmbH & Co. KG, Karlsruhe, Germany
Isopropanol	Sigma-Aldrich, Taufkirchen, Germany
Ketanest	Pfizer Pharma GmbH, Berlin, Germany
Laemmli buffer (2x)	Sigma-Aldrich, Taufkirchen, Germany
$\beta$ -Mercaptoethanol	Serva GmbH, Heidelberg, Germany
NGAL, recombinant protein	R & D Systems, Minneapolis, USA
Nonfat dry milk powder	AppliChem GmbH, Darmstadt, Germany
Nuclease free water	ABgene Ltd., Epsom, UK
PeqGOLD Prestained Protein-Marker IV	Peqlab Biotechnology GmbH, Erlangen, Germany
Ponceau S	Sigma-Aldrich, Taufkirchen, Germany
Protease inhibitor	Sigma-Aldrich, Taufkirchen, Germany
Rat tail tendon collagen	Roche Diagnostics GmbH, Mannheim, Germany
Rompun	Bayer Healthcare AG, Leverkusen, Germany
Roti®-Histol	Carl Roth GmbH & Co. KG, Karlsruhe, Germany
Rotiphorese® Protogel	Carl Roth GmbH & Co. KG, Karlsruhe, Germany
Sodium dodecyl sulfate (SDS)	Carl Roth GmbH & Co. KG, Karlsruhe, Germany
Secondary antibodies	Santa Cruz Biotechnology, Heidelberg, Germany
siRNA buffer (5x)	ABgene Ltd., Epsom, UK
Streptavidin-HRP solution	Vector/Linaris, Wertheim, Germany
Sulfuric acid	Sigma-Aldrich, Taufkirchen, Germany
TM (Thermolysin Medium) Liberase Research	Roche Diagnostics GmbH, Mannheim, Germany
3,3',5,5'-tetramethylbenzidine (TMB)	Sigma-Aldrich, Taufkirchen, Germany
tetramethylethylenediamine (TEMED)	Sigma-Aldrich, Taufkirchen, Germany
Tissue-Tek®	Hartenstein Laborbedarf GmbH, Würzburg, Germany
Trypan blue (0.4 %)	Sigma-Aldrich, Taufkirchen, Germany
Trypsin	Sigma-Aldrich, Taufkirchen, Germany
Transfection Reagent Dharmafect 1	ABgene Ltd., Epsom, UK
Tween-20	Sigma-Aldrich, Taufkirchen, Germany

### 2.1.3 Culture media and supplements

Table 5. Media and supplements used for cultivation of primary rat hepatocytes.

Media/Supplements	Provider
Bovine serum albumin (BSA)	Carl Roth GmbH + Co. KG, Karlsruhe, Germany
Collagen I (Rat Tail)	Roche Diagnostics GmbH, Mannheim, Germany
Dexamethasone	Sigma-Aldrich, Taufkirchen, Germany
Dulbecco's modified eagle medium (D-MEM)/Ham's F-12 (1x), liquid, without L-Glutamine	PAA Laboratories GmbH, Cölbe, Germany
D-MEM (10x)	PromoCell GmbH, Heidelberg, Germany
Dimethyl sulfoxide (DMSO)	Sigma-Aldrich, Taufkirchen, Germany
Fetal bovine serum (FBS)	PAA Laboratories GmbH, Cölbe, Germany
Hepes	PAA Laboratories GmbH, Cölbe, Germany
Insulin bovine solution	Sigma-Aldrich, Taufkirchen, Germany
Insulin-transferrin-sodium selenite (ITS+1), liquid (100x)	Sigma-Aldrich, Taufkirchen, Germany
L-Glutamine (100x)	PAA Laboratories GmbH, Cölbe, Germany
Opti-MEM <sup>®</sup> (modified eagle medium) I Reduced-Serum Medium (1x), liquid	Invitrogen GmbH, Darmstadt, Germany
Penicillin/Streptomycin (100x)	PAA Laboratories GmbH, Cölbe, Germany
Sodium pyruvate solution (100mM)	PAA Laboratories GmbH, Cölbe, Germany

### 2.1.4 Kits

Table 6. List of kits including provider used in this work.

Product	Provider
Absolute™ QPCR SYBR <sup>®</sup> Green Mix	ABgene Ltd., Hamburg, Germany
Cell Titer Glo Assay	Promega GmbH, Mannheim, Germany
DAB Peroxidase Substrate Kit	Vector/Linaris, Wertheim, Germany
DC Assay	Biorad Laboratories GmbH, München, Germany
2-D Quant Kit	GE Healthcare Life Science, Freiburg, Germany
EnzChek <sup>®</sup> Paraoxonase Assay Kit	Invitrogen GmbH, Darmstadt, Germany
GeneChip <sup>®</sup> 3' IVT Express Kit	Affymetrix, Santa Clara, USA
GeneChip <sup>®</sup> Hybridization, Wash and Stain Kit	Affymetrix, Santa Clara, USA
LightCycler <sup>®</sup> 480 Probes Master	Roche Diagnostics GmbH, Mannheim, Germany
Oligonucleotides	Biomers.net GmbH, Ulm, Germany
Probes for TaqMan <sup>®</sup> -qRT-PCR	Roche Diagnostics GmbH, Mannheim, Germany
Rat thioestatin ELISA	Immunology Consultants Laboratory, Inc., Newberg, USA
Rat clusterin ELISA	Biovendor GmbH, Heidelberg, Germany

## 2 MATERIALS AND METHODS

Product	Provider
RNA 6000 Nano LabChip Kit	Agilent Technologies GmbH, Böblingen, Germany
RNase-Free DNase Set	Qiagen GmbH, Hilden, Germany
RNeasy Mini Kit	Qiagen GmbH, Hilden, Germany
RNeasy QiaShredder	Qiagen GmbH, Hilden, Germany
Transcriptor First Strand cDNA Synthesis Kit	Roche, Mannheim, Germany
VECTASHIELD® Mounting Medium with DAPI	Vector/Linaris, Wertheim, Germany
Vectastain® Elite® ABC Kit	Vector/Linaris, Wertheim, Germany
Verso™ cDNA Kit	ABgene Ltd., Hamburg, Germany
WST Assay	Roche Diagnostics GmbH, Mannheim, Germany

### 2.1.5 Buffers and solutions

Table 7. Composition of sterile perfusion buffers used for *in situ* rat liver collagenase perfusion.

Buffers for rat liver perfusion	Composition (sterile)
Perfusion stock solution	6.30 g NaCl, 0.32 g KCl, 0.27 g MgSO <sub>4</sub> x 7 H <sub>2</sub> O, 0.15 g KH <sub>2</sub> PO <sub>4</sub> , 1.81 g NaHCO <sub>3</sub> , 3.58 g HEPES (C <sub>8</sub> H <sub>18</sub> N <sub>2</sub> O <sub>4</sub> S), 1.50 g D-Glucose
Perfusion buffer 1	Perfusion stock solution and 0.038 g EGTA, add H <sub>2</sub> O to 1 l and adjust to pH 7.4
Perfusion buffer 2	Perfusion stock solution and 0.58 g CaCl <sub>2</sub> x 2 H <sub>2</sub> O, adjust to pH 7.4 and add 5 mg Liberase TM to 300 ml

Table 8. Preparation of sterile solutions, culture media and wash buffer used for cultivation of hepatocytes.

Buffers and solutions for cell culture	Composition (sterile)
Coating solution	1 ml rat tail collagen (1 mg/ml) in 10 ml 0.2 % acetic acid (sterile-filtered) coating: 125 µl/well (24-well), 255 µl/well (12-well), 600 µl (6-well)
Culture medium (Attachment)	DMEM/Ham's F-12 (1:1) containing 10 % FBS, 2 mM L-Glutamin, 15 mM HEPES, 1 mM Pyruvate, 100 U/ml Penicillin/Streptomycin, 5 µg/ml Insulin
Culture medium (Maintenance)	DMEM/Ham's F-12 (1:1) containing 2 mM L-Glutamin, 15 mM HEPES, 1 mM Pyruvate, 100 U/ml Penicillin/Streptomycin, 1 % ITS+1 (Insulin-transferrin-sodium selenite, BSA, Linolic acid complex), 100 nM Dexamethasone
Culture medium (Transfection)	Culture medium (Maintenance) without Penicillin/Streptomycin
Trypan-blue solution	100 µl Trypan-blue (0.4 %), 900 µl PBS
Wash buffer	Perfusion stock solution and 0.58 g CaCl <sub>2</sub> x 2 H <sub>2</sub> O, 20.00 g BSA, add H <sub>2</sub> O to 1 l and adjust to pH 7.4



Table 9. Overview and preparation of buffers used for protein preparation and immunodetection.

Buffers for protein preparation and immunodetection	Composition
0.05 % Avidin solution	0.5 mg of avidin per ml of 1x PBS
0.05 % Biotin solution	0.5 mg of biotin per ml of 1x PBS
Blocking solutions	1. 1x TBST with 5 % nonfat dry milk (WB) 2. 1x PBS with 1 % BSA (IF) 3. 1x PBS with 1 %, 5 % or 10 % serum (IHC)
1 % BSA/PBS	1 % BSA in PBS
10 mM Citrate buffer	2.1 g citric acid (anhydrous), 12 ml 2 N NaOH, add H <sub>2</sub> O to 1 l and adjust to pH 6.0
Coating buffer	0.1 M Na <sub>2</sub> CO <sub>3</sub> (3.03 g/l), 0.1 M NaHCO <sub>3</sub> (6.09 g/l) pH 9.6 add H <sub>2</sub> O to 1 l and calibrate to pH 9.6
Eosin	30 µl acetic acid/200 ml eosin solution
3 % H <sub>2</sub> O <sub>2</sub>	1:10 dilution of 30 % H <sub>2</sub> O <sub>2</sub> in 1x PBS
Haemalaun	1 g hematoxylin, 200 mg NaIO <sub>3</sub> , 50 g KAl(SO <sub>4</sub> ) <sub>2</sub> , 50 g chloral hydrate, 1 g citric acid, add H <sub>2</sub> O to 1 l
2x Laemmli buffer (Sigma)	4 % SDS, 20 % glycerol, 10 % 2-mercaptoethanol, 0.004 % bromphenol blue and 0.125 M Tris HCl, pH approx. 6.8.
6x Laemmli buffer	1.2 g SDS, 6 mg bromphenol blue, 4.7 ml glycerol, 1.2 ml Tris 0.5 M (pH 6.8), 0.93g DTT, add to 10 ml
10x PBS (phosphate buffered saline)	2 g KCl, 82 g NaCl, 5.72g Na <sub>2</sub> HPO <sub>4</sub> x 2 H <sub>2</sub> O, 2 g KH <sub>2</sub> PO <sub>4</sub> , add H <sub>2</sub> O to 1 l
1x PBS	1:10 dilution of 10x PBS in deionized water, calibrate to pH 7.4
PBST (phosphate buffered saline with Tween 20)	1 ml Tween 20 (0.1 %) add to 1 l 1x PBS (pH 7.4)
Ponceau S solution	0.1 g Ponceau S, 5 ml acetic acid, ad 100 ml H <sub>2</sub> O
RIPA lysis buffer	50 mM Tris-HCl (pH 7.4), 150 mM NaCl, 2 mM EDTA, 1 % NP-40, 0.1 % SDS, add fresh: 1 mM NaF, 1 mM Na <sub>3</sub> VO <sub>4</sub> and 5 µl/ml protease inhibitor cocktail
10x SDS-PAGE buffer	250 mM Tris, 1.92 M glycine, 1 % SDS in H <sub>2</sub> O
1x SDS-PAGE buffer	1:10 dilution of 10x SDS-PAGE buffer in deionized water
Serum blocking solution	5 % donkey serum in PBS 10 % goat serum in PBS
Solubilization buffer	8 M urea, 2 % CHAPS, 0.6 % DTT, 0.5 % IPG buffer
10x TBS (tris buffered saline)	78.80 g/l Tris-HCl (500 mM), 87.66 g/l NaCl (150 mM), add H <sub>2</sub> O to 1 l
1x TBS	1:10 dilution of 10x transfer buffer in deionized water, calibrate to pH 7.4
1x TBST (tris buffered saline with Tween 20)	1 ml Tween 20 (0.1 %) add to 1 l 1x TBS (pH 7.4)
10x Transfer buffer	3 g/l Tris base (25 mM), 14.4 g/l glycin (192 mM), 20 % methanol, add H <sub>2</sub> O to 1 l
1x Transfer buffer	1:10 dilution of 10x transfer buffer in deionized water

## 2 MATERIALS AND METHODS

Buffers for protein preparation and immunodetection	Composition
0.1 % Trypsin solution	dissolve 1 tablet trypsin (1mg) in 1 ml deionized water

### 2.1.6 Antibodies

Table 10. List of monoclonal (m) or polyclonal (p) primary and secondary antibodies used for western blot (WB), immunohistochemistry (IHC), immunofluorescence (IF) and ELISA (E).

Antibody (against)	Host	m/p	Dilution	Provider
$\alpha$ -clusterin	goat	p	1:200 (IHC)	Santa Cruz Biotechnology, Heidelberg, Germany
$\alpha$ -tubulin	mouse	m	1: 5000 (WB)	Sigma-Aldrich, Taufkirchen, Germany
GAPDH	rabbit	p	1:20,000 1:10,000 (WB)	Sigma-Aldrich, Taufkirchen, Germany
glucagon receptor	rabbit	p	1:50 (IF)	Acris Antibodies GmbH, Herford, Germany
NGAL	goat	p	1:150 (IHC)	R&D Systems GmbH, Wiesbaden-Nordenstadt, Germany
NGAL	mouse	m	1:400 (E)	AntibodyShop A/S, Gentofte, Denmark
NGAL, biotinylated	mouse	m	1:4000 (E)	AntibodyShop A/S, Gentofte, Denmark
PCNA (PC10)	mouse	m	1:400 (IHC)	Santa Cruz Biotechnology
thiostatin	chicken		1: 5000 (WB)	ICL Inc., Dunn Laborotechnik GmbH, Asbach, Germany
TIMP-1	rabbit	p	1:400 (IHC)	Acris Antibodies GmbH, Herford, Germany
chicken IgY-Biotin	goat	p	1:200 (IHC)	Santa Cruz Biotechnology, Heidelberg, Germany
chicken IgY-HRP	goat	p	1:5000 (WB)	Santa Cruz Biotechnology
goat IgG-Biotin	donkey	p	1:200 (IHC)	Santa Cruz Biotechnology, Heidelberg, Germany
goat IgG-HRP	donkey	p	1:5000 (WB)	Santa Cruz Biotechnology
mouse IgG-Biotin	goat	p	1:200 (IHC)	Santa Cruz Biotechnology
mouse IgG2a-Biotin	goat	p	1:200 (IHC)	Santa Cruz Biotechnology, Heidelberg, Germany
mouse IgG-HRP	goat	p	1:5000 (WB)	Santa Cruz Biotechnology
mouse IgM-Biotin	goat	p	1:200 (IHC)	Santa Cruz Biotechnology
rabbit IgG-Biotin	goat	p	1:200 (IHC)	Vector/Linaris, Wertheim, Germany
rabbit-IgG-Cy3	goat	p	1:700 (IF)	Jackson ImmunoResearch Laboratories, West Grove, USA
rabbit IgG-HRP	goat	p	1:2500 1:5000 (WB)	Santa Cruz Biotechnology, Heidelberg, Germany

### 2.1.7 Oligonucleotides

Table 11. Sequence of forward (FW) and reverse (RV) primers used for qRT-PCR based on SYBR® Green I detection method. All primers were purchased from Biomers.net (Ulm, Germany).

Gene	Name	Acc. No.	Primer (5'-3')
Clu	clusterin	M64723	FW: CACTACGGGCTCTGAGCTT RV: ACGTCCATGGCCTGTTGAG
NGAL	neutrophil gelatinase-associated lipocalin	NM_130741	FW:TCTGGGCCTCAAGGATAACAAC RV: AGACAGGTGGGACCTGAACCA
PON1	paraoxonase-1	NM_032077.1	FW: GGGAAATACGTTGGATATGTC RV: ATATCGTTGATGCTAGGCAG
Kng1/1	T-kininogen	NM_001009628.1	FW: TTCACTACTCCCAAGAAATGCT RV: AGCAACCACCTGTGATGTTG
18S rRNA	nuclear ribosomal RNA small subunit	XR_086349.1	FW: GTAACCCGTTGAACCCATT RV: CCATCCAATCGGTAGTAGCG

Table 12. Sequence of forward and reverse primers used for TaqMan®-based qRT-PCR. All primers were purchased from Biomers.net (Ulm, Germany).

Gene	Name	Acc. No.	Primer (5'-3')
GCGR	glucagon receptor	NM_172092.1	FW: CCAGTGCCACCACAACCTA RV: AGTTCTGTTGCAGACCAGCTC
GAPDH	glycerine aldehyde-3-phosphate-dehydrogenase	XM_001055208.1	FW: AGCTTGTCATCAACGGGAAA RV: TCGCCCCATTTGATGTTAGT
18S rRNA	nuclear ribosomal RNA small subunit	M11188.1	FW: AATCAGTTATGGTTCCTTTGTCTG RV: GCTCTAGAATTACCACAGTTATCCAA

Table 13. Sequence of four siRNAs targeting glucagon receptor (GCGR) pooled in ON-TARGETplus SMARTpool siRNA purchased from Thermo Scientific Dharmacon (Lafayette, Colorado, US).

Gene	NM-No.	Target sequence (ON-TARGETplus SMARTpool)
glucagon receptor (GCGR)	NM_172091	1. AGUGGAAGCUCUAUAGUGA
		2. GGACCAGCAAUGACAAUUAU
		3. GCAGCUACCAGGUGAUGUA
		4. GCACUAUGCUGAUUACAAG

### 2.1.8 Software

Table 14. List of software used for analysis, visualization and interpretation of data.

Software	Provider
2100 Expert Software	Agilent Technologies, Waldbronn, Germany
ChemBioOffice 2010	CambridgeSoft Corporate, Cambridge, USA
Gene Chip® Operating Software (GCOS)	Affymetrix, Santa Clara, USA
GraphPad Prism 5	GraphPad Software Inc., San Diego, USA
ImageJ	Open Source
Ingenuity Pathway Analysis	Ingenuity Systems Inc., Redwood City, USA
LightCycler® 480 Software	Roche Diagnostics GmbH, Mannheim, Germany
Nanodrop 2000c Analysis Software	ThermoFisher Scientific GmbH, Dreieich, Germany
PerlPrimer	Open Source
Partek Genomics Suite 6.5	Partek Incorporated, St. Louis, USA
Cluster and TreeView	Eisen Lab, Berkeley, USA

## 2.2 *In vivo* studies

### 2.2.1 Standardized study design of the InnoMed Predictive Toxicology Project

All samples from rats treated with drug candidates (BAY16, EMD335823, BI-3) that previously failed during development, in part due to hepatotoxicity, were obtained from short term toxicity studies performed within the frame of the InnoMed PredTox project. All animal studies were conducted by project partners in accordance with European or national animal welfare regulations using a harmonized study protocol [97, 98, 105].

Briefly, male Wistar rats (8-10 weeks old) with a body weight of 170 g to 200 g were kept at a constant 12-h light/12-h dark cycle. Food and water were provided ad libitum. Animals were distributed into 3 dose groups (n = 5 per group and time-point) and dosed with a vehicle, a low and a high dose of BAY16 ((+)-(1R)-1-[4-(4-fluorophenyl)-2,6-diisopropyl-5-propyl-pyridin-3-yl]ethanol), EMD335823 (1-(2-trifluoromethoxyphenyl)-2-nitroethanone) or BI-3 (3-Pyrrolidineacetic acid, 5-[[[4'-[imino[(methoxycarbonyl) amino]methyl] [1,1'-biphenyl]-4-yl]oxy]methyl]-2-oxo-, methyl ester,(3S-trans)) by oral gavage for 1, 3 or 14 days, followed by necropsy after an overnight fasting period (Figure 9).

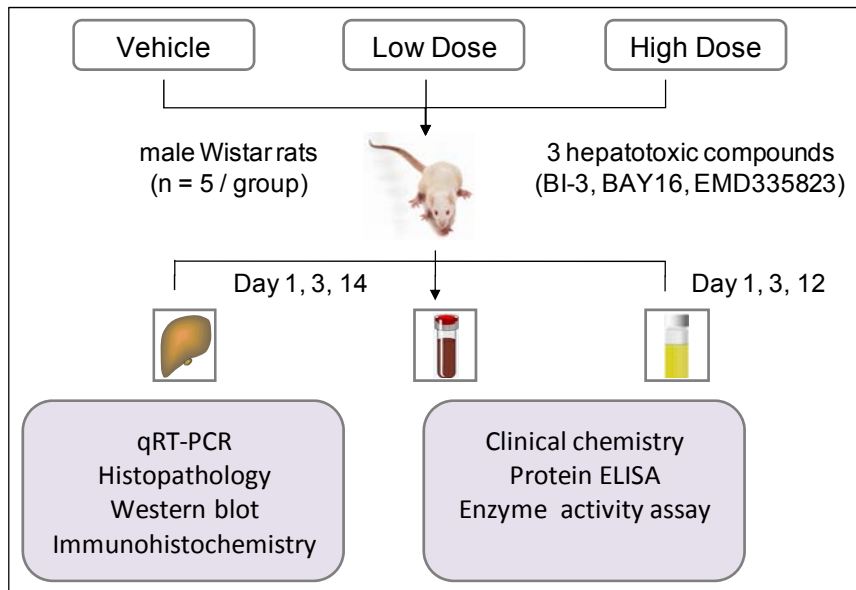


Figure 9. Scheme of the *in vivo* studies conducted as part of the PredTox project. The purpose of this work was to identify and validate potential candidate biomarkers after single and repeated administration of three hepatotoxic compounds in rats using various techniques.

Doses for treatment were selected on the basis of previously conducted pharmacological, pharmacokinetic and toxicological experiments. The low dose was chosen in a way that it is between the no observable adverse effect level (NOAEL) and the lowest observed adverse effect level (LOAEL). The high dose levels were selected with the aim to induce toxic effects after 14 days of treatment, measured by clinical chemistry and/or histology (Table 15). After 1, 3 and 12 days of dosing, 16 h urine samples were collected from animals treated for a total of 14 days, aliquoted and stored at  $-80^{\circ}\text{C}$  until use. Blood samples were collected from all animals at the time of necropsy. Blood or serum, and urine samples were used to measure routine hematology and clinical chemistry parameters according to standard operating procedures at the participating companies. At necropsy, organs (liver, kidney) were removed, aliquoted, fixed in formalin or flash frozen in liquid nitrogen and stored at  $-80^{\circ}\text{C}$ .

## 2 MATERIALS AND METHODS

Table 15. Treatment schedule. Animals were treated with either BAY16, EMD335823 or BI-33 for up to 14 days.

Animal No.	Treatment	Dose levels BAY16 [mg/kg/d]	Dose levels EMD335823 [mg/kg/d]	Dose levels BI-3 [mg/kg/d]	Total No. of doses	Necropsy day
01-05	Vehicle	0	0	0	1	2
06-10	Low Dose	20	15	100	1	2
11-15	High Dose	100	350	1000	1	2
16-20	Vehicle	0	0	0	3	4
21-25	Low Dose	20	15	100	3	4
26-30	High Dose	100	350	1000	3	4
31-35	Vehicle	0	0	0	14	15
36-40	Low Dose	20	15	100	14	15
41-45	High Dose	100	350	1000	14	15

### 2.2.2 Clinical examination

The following hematology and clinical chemistry parameters were measured in urine, blood and/or serum according to standard operating procedures by the participating companies conducting the animal experiments:

Serum: glucose, total cholesterol, triglycerides, blood urea nitrogen (BUN), creatinine, aspartate aminotransferase (AST), alanine aminotransferase (ALT), alkaline phosphatase (ALP),  $\gamma$ -glutamyltransferase (GGT), lactate dehydrogenase (LDH), creatinine kinase (CK), total bilirubin, total protein, albumin, globulin, sodium, potassium, chloride, calcium, inorganic phosphorus.

Urine: color, turbidity, bilirubin, urobilinogen, glucose, protein, urine volume, specific gravity, pH, creatinine, potassium, chloride, calcium, inorganic phosphorus.

Blood: red and white blood cells, hemoglobin, hematocrit, mean cell hemoglobin (MCH), mean cell hemoglobin concentration (MCHC), mean cell volume (MCV), platelet count, neutrophils, lymphocytes, eosinophils, basophils, monocytes.

At necropsy, a middle section (approximately 5 mm) of the left lateral lobe of the liver, and a sagittal section of the kidney were fixed in 10 % phosphate buffered formalin for histopathological examination. Sections (3-4 mm) were embedded in paraffin blocks, sectioned, stained with hematoxylin and eosin and examined by light microscopy by the respective study pathologist. Histopathological peer review was performed by an independent veterinary pathologist. Based on the peer review, histopathological findings involving hepatocyte cell death/necrosis, bile duct mitosis/hyperplasia and bile duct inflammation were summarized into a single histopathology score. Lesions were scored

as no lesion (0), minimal (1), mild (2), moderate (3) and severe (4). One section from the middle part of both kidneys was also fixed in formalin and used for histopathology.

### 2.2.3 Construction of tissue microarrays

Tissue microarrays (TMAs) were constructed as part of the PredTox project from the partners of the University College Dublin [186]. Each tissue microarray consists of paraffin blocks in which separate tissue cores of all 45 animals per study are assembled in array fashion to allow simultaneous histopathological analysis (Figure 10). Four randomly selected liver cores were used for the construction of four separate TMAs to ensure that all cores represent the entire liver tissues sections. Kidney TMAs were constructed with duplicate cores taken from the outer and inner cortex, corticomedullary junction, medullary and papillary regions. Liver and kidney sections (5  $\mu$ m) were cut from the TMA block using a microtome, and mounted onto glass slides. These slides were dried overnight at 45 °C and stored at room temperature until use.

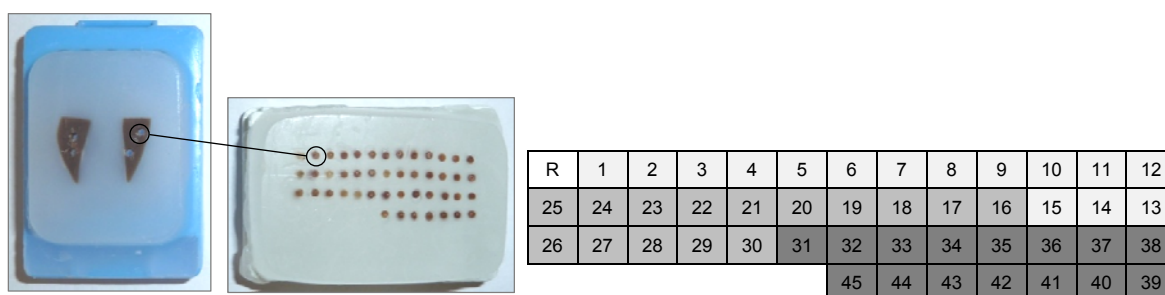


Figure 10. Schematic of liver tissue paraffin block, TMA including standard layout of cores from all 45 animals used in each study, along with a reference (R). Color coding according to days of treatment based on 1 d (light grey), 3 d (middle grey) and 14 d (dark grey).

## 2.3 *In vitro* studies

This study follows up from the previous *in vivo* studies conducted within the frame of the InnoMed PredTox project and utilizes siRNA technology in primary rat hepatocyte cultures to specifically knockdown the expression of the pharmacological target of the compound BAY16 to identify gene expression changes associated with the toxicological vs. pharmacological action of BAY16. Following successful silencing of the glucagon receptor (GCGR), the pharmacological target of BAY16, both conventional endpoints of toxicity and gene expression profiles were assessed in response to drug treatment to determine if interference with the pharmacological target plays a role in the toxic response to the drug, and to narrow down those molecular changes that are associated with toxicity, and not the

pharmacological action of the drug (Figure 11). The use of primary hepatocytes of rat enabled the modeling of the *in vivo* events observed in the Wistar rat.

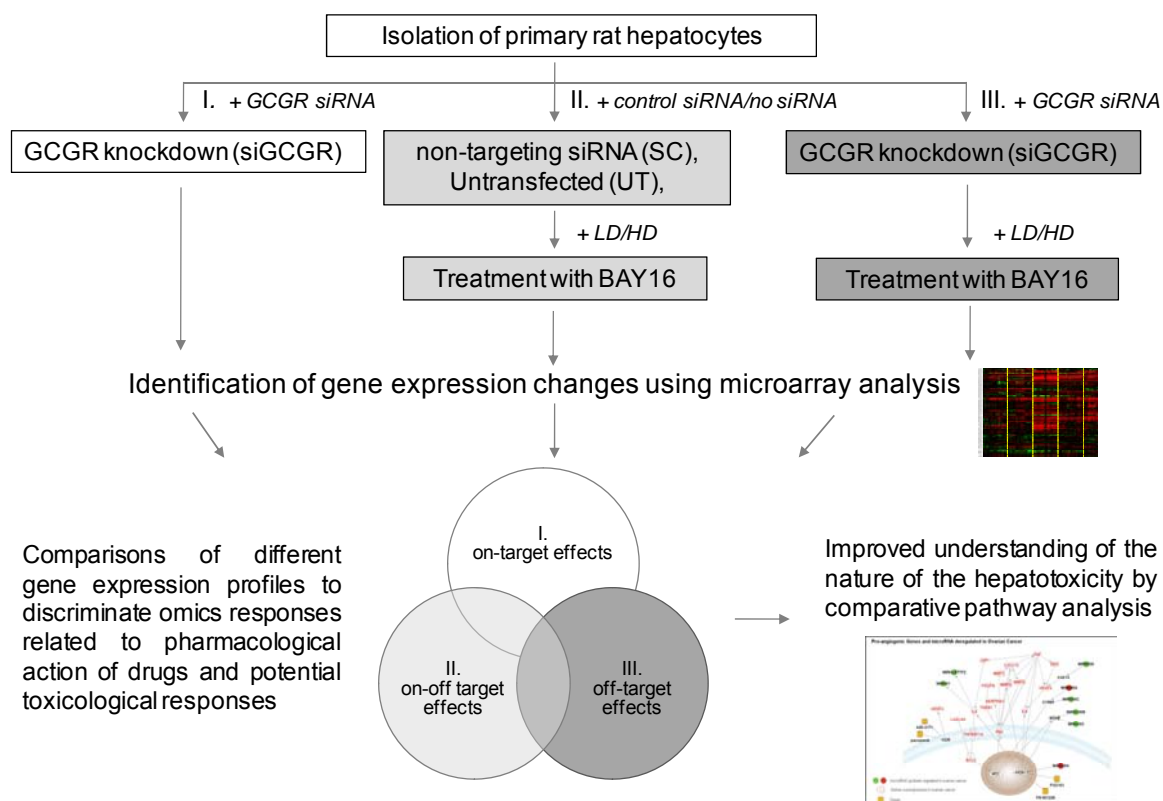


Figure 11. Overview of the workflow of *in vitro* experiments. Alterations in gene expression induced by BAY16 were determined with or without gene silencing of the pharmacological target GCGR to gain more insight into the molecular mechanism underlying the induction of hepatotoxic effects observed in male Wistar rats.

### 2.3.1 Isolation of primary rat hepatocytes

Male Wistar rats, weighing 250 g to 350 g, were used for isolation of hepatocytes. The rats were housed under standard conditions (20 °C, 12 h light/dark cycle) and had free access to food and water. All buffers were prepared as described in 2.1.5 and sterilized by filtration through a 0.22 µM filter. The perfusion buffers 1 and 2 were heated to 37 °C in a water bath before use.

Rat hepatocytes were prepared by a modified two-step *in situ* collagenase perfusion method [187, 188]. For the liver perfusion, the rats were anesthetized by intraperitoneal injection with Ketanest (100 mg/kg bw) and Rompun (15 mg/kg bw). The rats were placed in the supine position on the operating table and the abdomen was opened through a midline incision. The *Vena gastrica dextra* was then ligated to prevent outflow of perfusate into the gaster. The portal vein was cannulated using a 21-gauge injection needle. The cannula was connected to a peristaltic pump via flexible tubing, prefilled with warm



perfusion buffer 1. During the first step of perfusion the liver was flushed with calcium-free perfusion buffer 1 containing EGTA with a flow rate of 50 ml/min for 2 min followed by a reduction of the flow rate to approximately 25-40 ml/min for another 3 min. The abdominal *inferior vena cava* was cut open to remove all blood and calcium from the liver and to allow the outflow of the perfusate. Cell-cell interaction was disrupted by chelation of calcium with EGTA resulting in loss of adhesion functions of cadherins. The color of the liver changed from dark red to yellow-brown. In the second step, the liver was perfused with warm perfusion buffer 2 containing CaCl<sub>2</sub> and collagenase Liberase TM at a flow rate of 50 ml/min for 2 min, followed by reduced flow for 1-3 min for degradation of extracellular matrix proteins to release cells. Disruption of the extracellular matrix through proteolytic cleavage of collagens by Liberase TM leads to release of hepatocytes from the liver tissues. The collagenase perfusion was stopped when the liver tissue showed a reticular pattern on its surface indicating loosening of connective tissues. The liver was excised and transferred to 40 ml of ice cold washing buffer containing 2 % BSA to inhibit the Liberase TM enzyme activity. The liver capsule was carefully dissected and the separated cells were released by gentle rubbing of the liver surface around the inside of a beaker. Finally, the liver cell suspension was filtered through sterile cotton gauze, collected in a 50 ml-sterile tube and centrifuged at 50 x g at 4 °C for 2 min. The cells were washed three times in wash buffer by centrifugation at 50 x g for 2 min.

### 2.3.2 Trypan Blue exclusion test

Cell viability and cell number of freshly isolated rat hepatocytes was determined using trypan blue exclusion. This assay is based on the principle that live cells with intact cell membranes are not stained, whereas membranes of non-viable or dead cells are permeable for the dye and thus dead cells show blue staining.

100 µl of 0.4 % Trypan blue solution was diluted with 900 µl sterile PBS, mixed well with 50 µl cell suspension for 30 sec at RT and immediately loaded into the Neubauer-Chamber. The stained and unstained cells were counted in all 8 fields each consisting of 16 squares using a light microscope and a manual metal counter. Viability and total number of cells were calculated as follows:

$$\% (Viability) = \frac{\text{Number of stained cells}}{\text{Total number of cells}} \times 100$$

$$\text{Cells / ml} = \text{Cells} \times 21 (\text{Dilution Factor}) \times 10^4$$

High viability of isolated hepatocytes is required to promote cell attachment and survival as well as their functionality and structural integrity. Hence, only cell suspensions with a viability > 85 % were used.

### 2.3.3 Culture conditions of hepatocytes

All experimental procedures were performed under sterile conditions. The day before isolation of hepatocytes, culture plates were coated and culture media were prepared as described in 2.1.5. The 6-well or 24-well plates for monolayer culture were coated by adding a sterile rat tail collagen I solution (6.25  $\mu\text{g}/\text{cm}^2$ ) and then air-dried under the laminar flow overnight (Table 16). In brief, 10 mg collagen I lyophilisate were dissolved in 10 ml of sterile-filtered 0.2 % (v/v) acetic acid. The 1.0 mg/ml collagen stock solution was diluted 1:10 with ice-cold acetic acid resulting in a final collagen concentration of 100  $\mu\text{g}/\text{ml}$ . The cultivation of primary hepatocytes onto collagen surface increases the adhesion of cells and promotes the growth to a confluent layer by mimicking *in vivo* environment.

The cell pellet was resuspended with prewarmed serum-supplemented culture medium to a final concentration of  $1 \times 10^6$  cells/ml. For monolayer culture, hepatocytes were seeded at a density of  $1 \times 10^5$  cells/ $\text{cm}^2$  onto collagen-coated plates and allowed to attach for 4 h in a 5 %  $\text{CO}_2$  incubator at 37 °C (Table 16). The cultures were then carefully washed with warm PBS to remove unattached or dead cells and subsequently maintained in serum-free medium containing ITS+1 and dexamethasone for 20 h in a humidified atmosphere at 37 °C and 5 %  $\text{CO}_2$ . Medium was replaced daily with fresh maintenance medium.

Table 16. Culture condition for primary rat hepatocytes.

Cell culture vessel	100 $\mu\text{g}/\text{ml}$ collagen solution	Number of cells per well/dish	Media volume per well/dish
24 well plate	125 $\mu\text{l}$ per well	$0.2 \times 10^6$	500 $\mu\text{l}$ per well
6 well plate	600 $\mu\text{l}$ per well	$1.0 \times 10^6$	1.5 ml per well

### 2.3.4 Transfection of siRNA duplex

Primary rat hepatocytes were transfected with synthetic ON-TARGET $plus$  siRNA for gene knockdown using the lipid transfection reagent DharmaFECT 1 (DF1) purchased from ABgene according to the manufacturer's recommendations. The principle of intracellular delivery of nucleic acid using cationic lipid reagents is based on the formation of a complex between the positively charged lipids and negatively charged siRNA. The

encapsulation of siRNA with liposome facilitates the cellular delivery of siRNA by passive diffusion through the bilayer cell membrane.

To optimize transfection conditions for hepatocytes cultured in a 6-well plate format, the lipid-mediated transfection was performed with 50 nM siRNA of glucagon receptor (GCGR), 50 nM non-targeting negative control siRNA or 50 nM GAPDH positive control siRNA in triplicate and three independent experiments. SMARTpool siRNA (in 2.1.7 in Table 13) consisting of four siRNA duplexes targeting different sequences of the same mRNA of GCGR enhances the efficiency of gene silencing. In addition to GCGR siRNA, a GAPDH positive control siRNA was used to monitor transfection efficiency in all experiments. The mRNA knockdown was calculated relative to cells transfected with non-targeting siRNA (scrambled, SC), which also serves as control for non-sequence specific effects on gene expression. Furthermore, hepatocytes in 24-well plate were transfected with siRNA of GCGR at a concentration range of 6.25 nM to 100 nM to assess the cell viability after knockdown of GCGR.

All experimental procedures were performed in a laminar flow cell culture hood using sterile techniques. Each vial containing lyophilized siRNA was diluted to 20  $\mu$ M stock solutions with 1x siRNA buffer, aliquoted and stored at -20 °C until use. One day after seeding, hepatocytes were washed with warm PBS and then incubated with 500  $\mu$ l (24-well) or 1500  $\mu$ l (6-well) of medium mixture per well consisting of 50 nM siRNA and lipid-based transfection reagent DF1 at 37 °C and 5 % CO<sub>2</sub> for 24 h. Therefore, 2  $\mu$ M siRNA dissolved in RNase-free sterile 1x siRNA buffer and DF1 reagent were diluted with Opti-MEM serum-free medium in two separate tubes and then incubated for 5 min at RT (Table 17). Subsequently, the contents of both tubes were combined and incubated for 20 min at RT to allow formation of siRNA-lipid complexes. Finally, the culture medium was replaced with transfection medium followed by addition of siRNA/DF1 mixtures (Table 17).

Table 17. Volumes for transfecting 50 nM siRNA in various plating format for gene knockdown in primary rat hepatocytes.

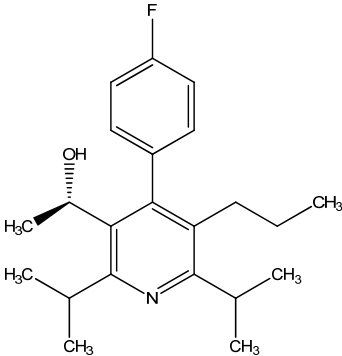
Plate	Tube 1 [ $\mu$ l/well]		Tube 2 [ $\mu$ l/well]		Tube 1 + 2 [ $\mu$ l/well]	Medium V [ $\mu$ l]	Total V [ $\mu$ l]
	2 $\mu$ M siRNA	Opti-MEM	DF1	Opti-MEM			
24	12.5	37.5	1.5	48.5	100	400	500
6	37.5	112.5	4.5	145.5	300	1200	1500

### 2.3.5 Treatment with compound BAY16

Forty eight hours after seeding, the SC or siGCGR cells were treated with either a vehicle control (0.5 % DMSO) or two concentrations of the GCGR antagonist BAY16, which has been shown to induce hepatotoxic effects in Wistar rats (Table 18). To obtain optimal

concentrations for treatment of hepatocytes, cytotoxicity of BAY16 was tested using two cell viability assays (see chapters 2.3.6 and 2.3.7) to define a low concentration, which does not affect cell viability (no observed effect concentration, NOEC) and a high concentration resulting in approximately 50 % cell death (lethal concentration, LC50). The hepatocytes were incubated with BAY16 dissolved in 0.5 % DMSO at various concentrations ranging from 10  $\mu\text{M}$  to 100  $\mu\text{M}$  for 24 h in a humidified atmosphere at 37 °C and 5 %  $\text{CO}_2$ .

Table 18. General characteristics of BAY16.

<b>Characteristics</b>	
Chemical name	(+)-(1R)-1-[4-(4-fluorophenyl)-2,6-diisopropyl-5-propylpyridin-3-yl]ethanol
Molecular formula	$\text{C}_{22}\text{H}_{30}\text{FNO}$
Structural formula	
Molecular mass (g/mol)	343.49
Appearance	white powder
Vehicle	0.5 % DMSO in medium (attachment)

### 2.3.6 WST-1 assay

The assessment of cell viability in response to treatment with BAY16 was carried out in both 24-well and 6-well plate format using the WST-1 assay. This colorimetric assay is based on the reduction of tetrazolium salt WST-1 by mitochondrial dehydrogenases of viable cells to a soluble formazan dye (Figure 12). The conversion of WST-1 into colored formazan correlates with the number of metabolically active cells. Thus, the absorbance may be used as an indicator for cytotoxicity. After 24 h incubation with several concentrations of BAY16, 500  $\mu\text{l}$  (24-well) or 1.5 ml (6-well) of WST-1 reagent (1/10<sup>th</sup> volume) in serum-free DMEM/F-12 media (attachment) was added to each well and incubated for 3 h at standard culture conditions. Following incubation, 100  $\mu\text{l}$  of each well was transferred into a 96-well plate in duplicate and the absorbance was measured at 450 nm against a blank sample without cells using a microplate photometer SpectraMax

340. Cell viability was evaluated independently in three experiments, each carried out in duplicate, and expressed as mean values relative to vehicle controls.

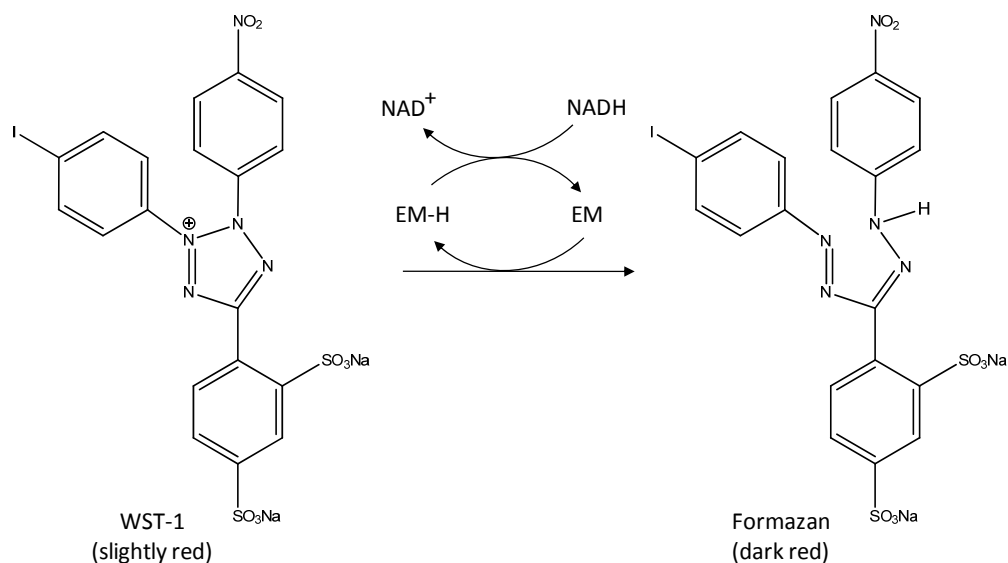


Figure 12. Reduction of the tetrazolium salt WST-1 (4-[3-(4-iodophenyl)-2-(4-nitrophenyl)-2H-5-tetrazolio]-1,3-benzene disulfonate) to the colored dye formazan. The reaction is catalyzed by NADH produced in mitochondria via electron transport and presence of an electron mediator (EM) (modified from assay manual).

### 2.3.7 CellTiter-Glo<sup>®</sup> Luminescent cell viability assay

Another assay widely used to evaluate cytotoxicity is the CellTiter-Glo<sup>®</sup> Luminescent Cell Viability Assay. This method is based on the bioluminescence measurement of ATP from viable cells catalyzed by Firefly luciferase (Figure 13). The level of ATP correlates directly with the number of metabolically active cells because cells undergoing apoptosis or necrosis lose their ability to produce ATP due to loss of membrane integrity. The assay was performed by addition of a CellTiter-Glo<sup>®</sup> Reagent mix of substrate and buffer directly to hepatocytes, leading to cell lysis, inhibition of endogenous ATPases, and ATP content determination.

This assay was carried out in 24-well plates to assess if siRNA-mediated gene silencing of GCGR may cause cytotoxicity in primary rat hepatocytes. In addition to the WST-1 assay, the cytotoxicity of BAY16 was also determined by measuring the ATP level. The lyophilized CellTiter-Glo<sup>®</sup> Substrate was dissolved in 10 ml CellTiter-Glo<sup>®</sup> Buffer, aliquoted and stored at -80 °C after use. After 24 h incubation with siRNA or BAY16, 100 µl of CellTiter-Glo<sup>®</sup> Reagent were mixed with 100 µl of serum-free DMEM/F-12 media (attachment) per well and hepatocytes were subsequently lysed by 10 min incubation at RT with moderate shaking. Three 50 µl aliquots of each supernatant were transferred into

a white opaque 96-well plate and bioluminescence was measured by multimode plate reader LB Mithras 940. The background luminescence value (reagent mixture without cells) was subtracted from all sample values.

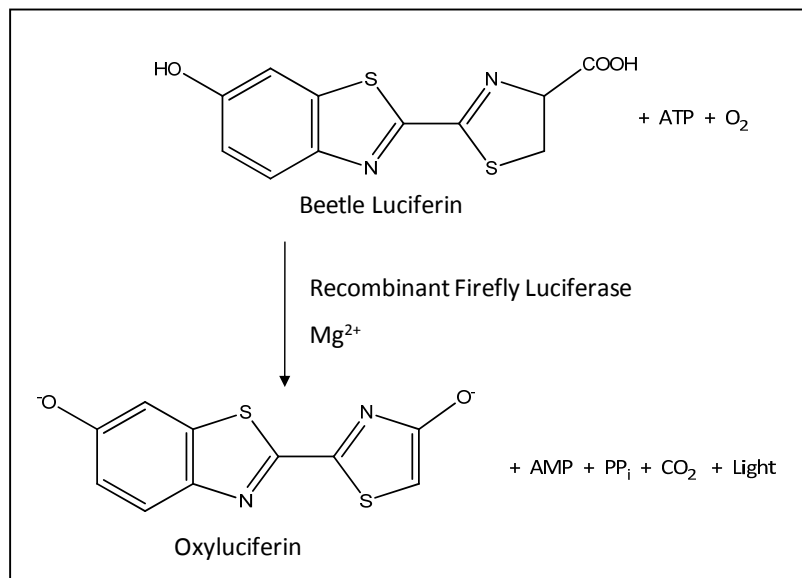


Figure 13. Firefly luciferase catalyzes the ATP-dependent oxidative decarboxylation of luciferin mediated by the presence of Mg<sup>2+</sup> and molecular oxygen. This enzymatic reaction results in the emission of light, which is directly proportional to the number of viable cells (modified from assay manual).

## 2.4 Molecular biological methods

### 2.4.1 Isolation of total RNA from tissues

RNA was extracted from frozen livers and kidneys using the RNeasy Mini Kit including on-column DNA digestion (RNase-Free DNase Set) purchased from Qiagen. The principle of this RNA isolation kit is based on the selective binding of RNA to a silica-gel membrane combined with the speed of microspin column technology. The procedure involves the lysis of the cells with a denaturing guanidine isothiocyanate-containing buffer (RLT buffer), ethanol precipitation of RNA, wash steps (RW1 buffer, RPE buffer) and elution of purified RNA.

Sterile tubes, RNase-free filter tips and DEPC water were always used when working with RNA on a purified lab bench to prevent contamination with RNase. Tissue samples of approximately 100 mg were homogenized in 2 ml RLT buffer containing β-mercaptoethanol (10 μl/ml) using a Teflon-glass manual homogenizer. The tissue homogenate was transferred to a 2-ml tube and centrifuged for 10 min at 5000 g and 4 °C. 350 μl of the lysate was then transferred to a new 1.5-ml microcentrifuge tube, and 350 μl of 70 % ethanol was added and mixed well by pipetting up and down. The sample was applied to an RNeasy mini column placed in a 2-ml tube, centrifuged for 15 sec at 8000 g. After discarding the supernatant, the RNA was washed with 350 μl RW1 buffer, centrifuged as above and the flow-through was discarded. In order to eliminate genomic

DNA using the RNase-Free DNase Set, 80  $\mu$ l of freshly prepared DNase I incubation mix composed of 10  $\mu$ l DNase I stock solution and 70  $\mu$ l RDD buffer were directly added to the column membrane. After 15 min incubation at RT, the column membrane was washed with 50  $\mu$ l of RW1 buffer and centrifuged for 15 sec at 8000 g followed by two wash steps with 500  $\mu$ l RPE buffer including centrifugation at 8000 g for 1 min and 2 min, respectively. The column was centrifuged again using a new collection tube to dry the membrane and eliminate any carryover of wash buffer. At the end of this procedure, the RNA was eluted into a new 1.5-ml tube by addition of 30  $\mu$ l RNase-free water on the column and centrifugation for 1 min.

#### **2.4.2 Isolation of total RNA from rat hepatocytes**

The isolation of RNA from rat hepatocytes was conducted using the RNeasy Mini Kit. Before cell lysis, the medium was aspirated and the hepatocytes were washed with 2 ml sterile PBS. After washing, the cells were lysed directly in the cell culture plate by addition of 230  $\mu$ l RLT buffer. The cells were scraped using a sterile rubber policeman, and the lysate of three technical replicates was pooled by transfer to one QIAshredder spin column. The lysates were homogenized by centrifugation for 2 min at full speed. The QIAshredder was discarded, and 690  $\mu$ l of 70 % ethanol was mixed well with the homogenized lysates. Two 690  $\mu$ l aliquots of the sample were successively loaded onto the RNeasy spin silica membrane and centrifuged at 8000 g for 15 sec. In contrast to the *in vivo* protocol, the flow-throughs were collected in a new 2-ml microcentrifuge tube and stored at -20 °C until use for protein preparation. Purification and elution of the RNA were then performed as described in chapter 2.4.1.

#### **2.4.3 RNA quantification and quality control**

The concentration and purity of isolated nucleic acid was measured by UV absorption at 260 nm and 280 nm using the Nanodrop™ ND-2000c (UV-spectrophotometer). The ratio between these two values is used to assess the purity of RNA and should be in the range of 1.8-2.0. If the 260/280 ratio value is lower than 1.8, this may indicate the presence of proteins, which absorb at 280 nm. The absorbance was measured by pipetting 2  $\mu$ l undiluted RNA sample directly onto a measurement pedestal. Using the Lambert-Beer law and the extinctions coefficient, the RNA concentration was calculated as follows:

$$c = (A * \epsilon) / b$$

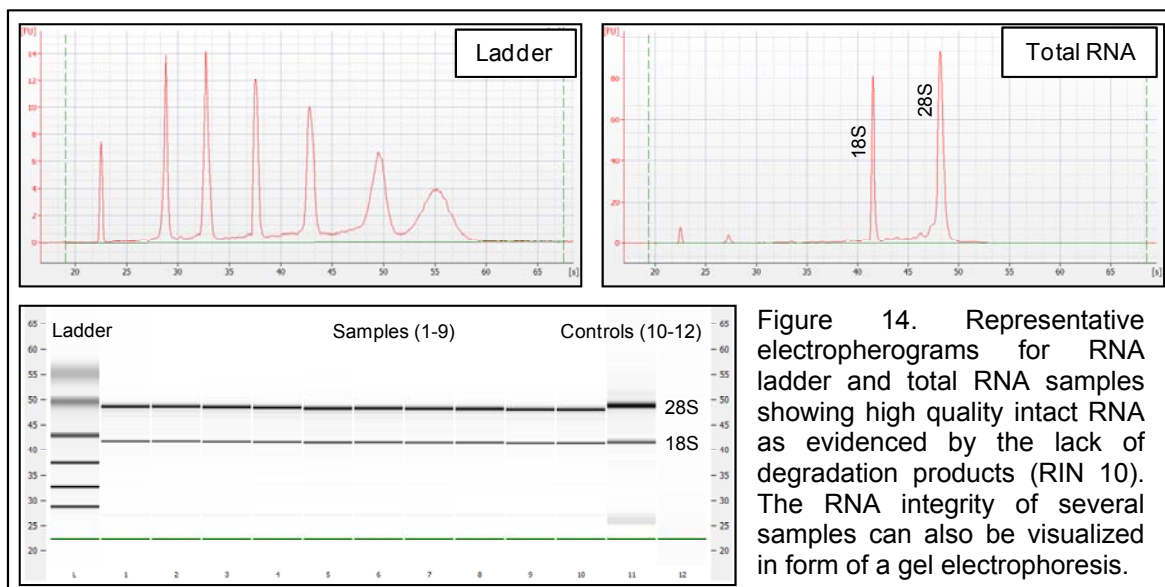
c = the nucleic acid concentration (M)

A = the absorbance (AU)

$\epsilon$  = the wavelength-dependent extinction coefficient (40 ng cm/ $\mu$ L for RNA)

b = the pathlength in cm

For microarray experiments, the quality of RNA isolated from primary rat hepatocytes was also checked with the RNA 6000 Nano LabChip Kit on the Agilent bioanalyzer according to the manufacturer's instructions. The principle of this method is based on microcapillary electrophoresis with fluorescence detection that is used to separate nucleic acids according to their size. The sample integrity is determined by the entire electrophoretic trace of the RNA sample including the presence or absence of degradation products, and is calculated as RNA Integrity Number (RIN). The RIN value can range from 10 to 1, whereby RIN 10 indicates intact RNA and RIN 1 describes totally degraded RNA. The RIN values of all RNA samples used for microarray studies were > 9.5 (Figure 14).



#### 2.4.4 cDNA synthesis and qRT-PCR using SYBR<sup>®</sup> Green

Quantitative real-time PCR (qRT-PCR) is the gold standard for sensitive determination of gene expression. Prior to the polymerase chain reaction (PCR), the mRNA strand is converted into cDNA by the enzyme reverse transcriptase that synthesizes the strand complementary to the mRNA sequence by addition of deoxynucleoside triphosphates (dNTPs) onto a random primer or oligo dT primer annealed to the RNA template. The general principle of PCR is based on the exponential amplification of short DNA sequences involving denaturation of duplex DNA, annealing of the primers to a target



specific sequence of the DNA template and extension of the primer using dNTPs. The target product molecules are then detected by measuring the fluorescence caused by use of SYBR<sup>®</sup> Green I dye that intercalates into double stranded DNA during the amplification. The crossing point at which the fluorescence signal is significantly above the background in a log-linear phase is known as the  $C_t$  (threshold cycle) value. The number of this threshold cycle is inversely proportional to the expression level of the gene of interest. Relative quantification can be performed by the  $\Delta\Delta C_t$  method which includes normalization of the target gene to a housekeeping gene (HKG, reference gene) in the sample, and then calculation of the fold change in gene expression compared to a control as follows [189]:

$$\Delta C_t = C_t (\text{target}) - C_t (\text{HKG})$$

$$\Delta\Delta C_t = \Delta C_t (\text{treated}) - \Delta C_t (\text{control})$$

$$\text{Ratio} = 2^{-\Delta\Delta C_t}$$

If the fold change is higher or less than 1, then the expression of the target gene is up-regulated or down-regulated, respectively, compared to controls. The use of this calculation method requires that the efficiency of PCR assays for both target and endogenous HKG are similar because differences in the amplification rate lead to incorrect gene expression data. An optimal PCR run has an efficiency of 2, meaning that the amount of DNA product doubles at every PCR cycle. For this reason, the efficiency of each PCR run was always measured using standard curves for non-differentially expressed HKG (18S rRNA) and differentially regulated target gene to guarantee equal amplification efficiency.

The reverse transcription procedure was carried out using the Verso<sup>™</sup> cDNA Kit purchased from Thermo Fisher. For all liver and kidney samples, 1  $\mu\text{g}$  of total RNA was dissolved in RNase-free water at a final volume of 11  $\mu\text{l}$  and incubated with 1  $\mu\text{l}$  random hexamer primer (400 ng/ $\mu\text{l}$ ) at 70 °C for 5 min in a thermal cycler. Afterwards, the reaction tubes were immediately placed on ice and briefly centrifuged. The first strand synthesis was carried out by addition of 8  $\mu\text{l}$  of master mix (Table 19) to each sample and incubation at 42 °C for 30 min following heat inactivation of the enzyme at 95 °C for 2 min.

Three non amplification controls (NAC) that contains pooled RNA samples for each time point (15 x 0.7  $\mu\text{l}$  for 1, 3 and 14 d) and all reagents of the cDNA master mix without the Verso enzyme were further prepared to ensure that RNA samples were free of genomic DNA. The NAC served as negative control in the qRT-PCR, because the presence of an amplified PCR product is an indicator for DNA contamination in the RNA samples.

## 2 MATERIALS AND METHODS

---

After reverse transcription, the cDNA was diluted with 80  $\mu$ l DEPC-H<sub>2</sub>O and stored at -20 °C. The transcribed RNA was then used as template for real-time PCR to quantify the expression of NGAL, T-kininogen (thioostatin), clusterin and PON1.

Table 19. Preparation of cDNA master mix.

Component	Amount
Water incl. 1 $\mu$ g RNA + Primer	11 + 1 $\mu$ l
5x cDNA Buffer	4 $\mu$ l
dNTP Mix	2 $\mu$ l
RT Enhancer	1 $\mu$ l
Verso Enzyme Mix	1 $\mu$ l

Table 20. Master mix with SYBR green I.

Component	Amount
2x Master Mix	10 $\mu$ l
FW Primer [14 $\mu$ M]	0.15 $\mu$ l
RV Primer [14 $\mu$ M]	0.15 $\mu$ l
H <sub>2</sub> O	7.7 $\mu$ l

PCR primers for NGAL and clusterin as well as T-kininogen were as previously described [190, 191]. All other forward and reverse gene-specific primers were designed by PerlPrimer software (PON1, GAPDH, GCGR, 18S rRNA) as described in 2.1.7 in Table 11. The mRNA expression of NGAL, clusterin, T-kininogen and PON1 was determined in livers and kidneys of rats treated with BAY16, EMD335823 and BI-3 for 1, 3 and 14 days. For the quantification of these genes, 2  $\mu$ l of diluted cDNA and 18  $\mu$ l master mix (Table 20) were added into each well of a white 96-well PCR plate, mixed gently by pipetting up and down and centrifuged briefly to remove air bubbles in the mixture. The real-time PCR was carried out on a Roche LightCycler480 using the following cycling conditions: 95 °C for 15 min, 45 cycles of 95 °C for 15 sec, 60 °C for 30 sec, and 72 °C for 30 sec. Melting curve analysis was performed immediately after amplification by heating to 95 °C to control specificity of PCR products because SYBR<sup>®</sup> Green binds to all double stranded DNA including primer dimers and contaminating DNA. During this heating process, the dissociation of the PCR product at a specific melting temperature ( $T_m$ ) determined by the length, sequence and guanine-cytosine content can be used to distinguish specific and unspecific amplification products.

All samples were measured in duplicate and normalized against the HKG 18S rRNA. For each PCR run, two standard curves each for target gene and HKG were generated using a two-fold serial dilution to calculate the efficiency of the PCR reaction. The relative quantification of gene expression was determined by the  $\Delta\Delta C_t$  method, and data are presented as mean fold mRNA expression change relative to controls (n=5).

### 2.4.5 cDNA synthesis and qRT- PCR using hydrolysis probes

To evaluate the efficiency of *in vitro* gene silencing of the GCGR by siRNA-mediated transfection in rat hepatocytes, the knockdown of gene expression compared to control siRNA was determined by real-time PCR using hydrolysis probe technology (Roche Universal Probe Library = UPL). The UPL probes are short hydrolysis probes, labeled at the 5' end with fluorescein (FAM) and at the 3' end with a dark quencher dye. In contrast to detection of PCR products using the intercalating dye SYBR<sup>®</sup> Green, the hydrolysis probes hybridize to their complementary sequences in the target amplicon, thereby enhancing specificity of the PCR assay. The 5' nuclease activity of the polymerase cleaves the probe during the amplification using a target-specific primer, resulting in the release of the reporter from the quencher (Figure 15). Thus, the reporter dye is no longer suppressed by the quencher and emits a fluorescence signal when excited.

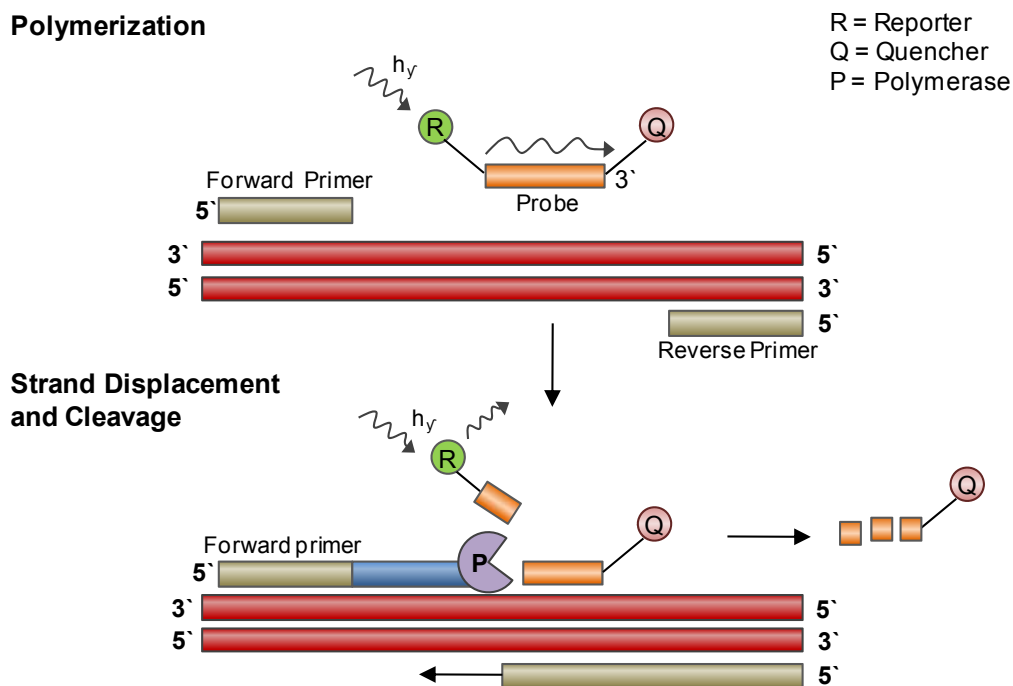


Figure 15. Mechanism of TaqMan or hydrolysis probe assays. A fluorophore-labeled probe annealed to a specific sequence in the gene of interest. The probe is degraded by the polymerase during the PCR and release of the reporter fluorophore resulting in fluorescence emission (modified from [192]).

1  $\mu$ g total RNA in 11  $\mu$ l RNase-free water was reversely transcribed using reagents of the Transcriptor First Strand cDNA Synthesis Kit (Table 21). After preincubation of RNA with 2  $\mu$ l hexamer primers for 10 min at 65  $^{\circ}$ C, 7  $\mu$ l master mix (buffer, inhibitor, dNTPs, TR transcriptase) was added to generate the first strand cDNA in a thermal cycler with the following conditions: priming at 25  $^{\circ}$ C for 10 min, transcription at 55  $^{\circ}$ C for 30 min and heat

## 2 MATERIALS AND METHODS

---

inactivation of the enzyme at 85 °C for 5 min The synthesized cDNA was also diluted with 80 µl DEPC-H<sub>2</sub>O and stored at -20 °C until use.

Table 21. Reagents of cDNA synthesis kit.

<b>Component</b>	<b>Amount</b>
Water incl. 1 µg RNA	11 µl
Hexamer Primer	2 µl
Buffer	4 µl
RNase Inhibitor	0.5 µl
dNTP Mix	2 µl
TR Transcriptase	0.5 µl

Table 22. Preparation of PCR master mix.

<b>Component</b>	<b>Amount</b>
2x Probes Master Mix	10 µl
FW Primer [20 µM]	0.2 µl
RV Primer [20 µM]	0.2 µl
Sonde [10 µM]	0.1 µl
H <sub>2</sub> O	7.5 µl

The target specific primer pairs for GCGR, GAPDH, 18S rRNA and the probes were designed using Universal ProbeLibrary Assay Design Center from Roche (sequences are provided in 2.1.7 in Table 12). The assay was performed according to the manufacturer's recommendations to achieve optimal assay conditions. Briefly, 2 µl of diluted RNA sample was mixed with 18 µl master mix (Table 22) and the PCR reaction was performed in the LightCycler 480 System using the following parameters: preincubation at 95 °C for 10 min, 45 cycles of amplification at 95 °C for 10 sec, 60 °C for 15 sec, and 72 °C for 1 sec Changes in gene expression in comparison to controls were calculated using the  $\Delta\Delta C_t$  method as described in 2.4.4.

### 2.4.6 Microarray experiments

The DNA microarray technology provides a high-throughput method for the investigation of expression level of thousand of genes simultaneously. The analysis of whole genome expression profile in rat hepatocytes after treatment with BAY16 in the presence or absence of the pharmacological target GCGR was performed using Affymetrix GeneChip® Rat Genome 230 2.0 Arrays comprised of more than 31,000 probe sets.

During the production of such in situ-synthesized arrays, 20 to 25 bp long oligonucleotides (probes) representing a single gene are directly synthesized onto the surface of a quartz wafer using photolithography technology, including multiple probes per gene to increase the specificity and sensitivity of gene expression analysis. For construction of gene chips, the array is exposed to UV light that passes through a lithographic mask filter, so that photolabile protecting group can be eliminated [193]. A single nucleotide linked with a light-sensitive protecting group is then chemically coupled to the free binding site of the

wafers surface (Figure 16). This process is repeated until the sequence of the oligonucleotides is complete.

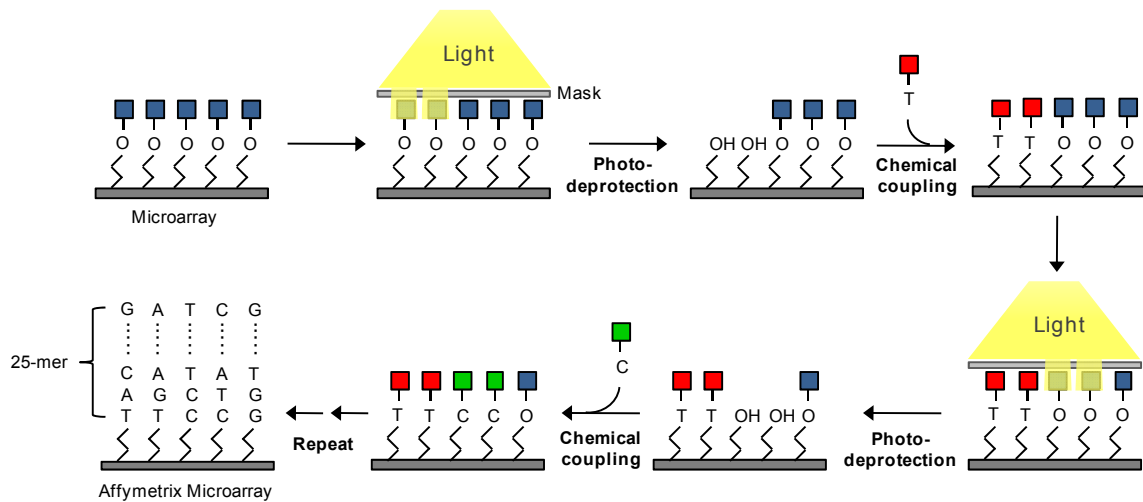


Figure 16. Construction of Affymetrix GeneChip oligonucleotide microarrays using photochemical reaction (based on [194]).

The principle of microarray analysis is based on hybridization of labeled mRNA or cDNA sample complementary to the probe on the gene chips [195]. To achieve this, total RNA has to be isolated from the sample and reverse transcribed into double stranded cDNA which serves as template for the synthesis of labeled aRNA (amplified antisense RNA or cRNA) by reverse transcription using biotin-conjugated nucleotides. The aRNA is decomposed into fragments of 35 to 200 nucleotides using a magnesium acetate buffer to eliminate secondary structure of aRNA that may be responsible for nonspecific binding to oligonucleotide probes on microarrays. After fragmentation, the labeled aRNA is hybridized to the gene chip by hydrogen bonding between probe and target oligomer sequence. The chip is stained with a fluorescence molecule (streptavidin-phycoerythrin) that binds to the biotin of the labeled aRNA. The fluorescent signal is detected with a confocal laser scanner, and the changes in intensity values of two probes generated from treated and control sample are considered as difference in gene expression level of a specific target (Figure 17).

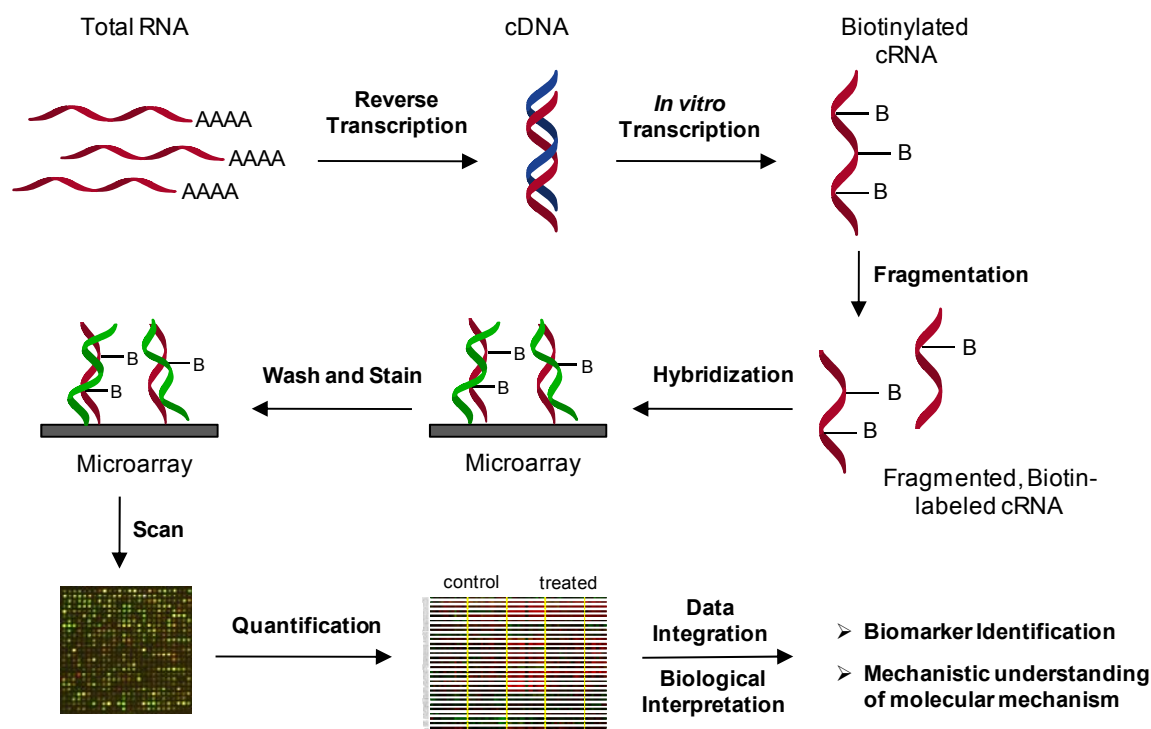


Figure 17. Workflow for conducting and analyzing microarray experiments using Affymetrix Gene Chips<sup>®</sup>.

#### 2.4.6.1 Preparation of labeled aRNA

The RNA amplification, biotin labeling and the fragmentation of aRNA was carried out using GeneChip<sup>®</sup> 3' IVT Express Kit under nuclease-free conditions. For the first-strand cDNA synthesis, 100 ng of total RNA was mixed with 2  $\mu$ l of diluted Poly-A RNA control (1:500,000 dilution) and nuclease-free water was added to make a final volume of 5  $\mu$ l. Each sample was then incubated with 5  $\mu$ l first-strand mix (4  $\mu$ l first-strand buffer and 1  $\mu$ l enzyme mix) for 2 h at 42 °C in the thermocycler. After the incubation, the single stranded cDNA samples were placed on ice while the thermocycler was cooled to 16 °C. The second strand cDNA was synthesized by incubating the samples for 1 h at 16 °C followed by 10 min at 65 °C in a thermal cycler after addition of 20  $\mu$ l of second strand master mix (Table 23).

Table 23. Preparation of second-strand master mix.

Component	Amount
Nuclease-free water	13 $\mu$ l
Second-strand buffer mix	5 $\mu$ l
Second-strand enzyme mix	2 $\mu$ l

Table 24. Preparation of IVT master mix.

Component	Amount
IVT Biotin label	4 $\mu$ l
IVT Labeling buffer	20 $\mu$ l
IVT Enzyme mix	6 $\mu$ l

The double stranded cDNA was used as a template to generate biotin-labeled aRNA for hybridization to rat genome array. Therefore, each 30  $\mu$ l cDNA sample was mixed with the same volume of IVT master mix (Table 24) and incubated for 16 h at 40 °C. The aRNA was then purified to remove salts, enzymes, inorganic phosphates and unincorporated nucleotide triphosphates using magnetic bead-based technology. To this end, the wash buffer was prepared by adding 8 ml of 100 % ethanol to the aRNA Wash Solution Concentrate. In the meanwhile, the aRNA elution solution was preheated to 55 °C in a heating block. Each aRNA sample was then gently mixed with 60  $\mu$ l aRNA binding mix containing 10  $\mu$ l RNA binding beads and 50  $\mu$ l binding buffer concentrate in a well of a U-bottom plate, 120  $\mu$ l of 100 % ethanol was subsequently added and thoroughly mixed by shaking for 2 min at 400 rpm. The plate was placed on the magnetic stand for 5 min until all the beads were captured at the bottom of the wells. The supernatant was discarded by careful aspiration followed by three washing steps. Briefly, after addition of 100  $\mu$ l wash buffer and shaking for 1 min at 800 rpm, RNA binding beads were capture by incubation on the magnetic stand and the supernatant was discarded as described above. Prior to elution of aRNA, the plate was dried vigorously for 1 min at 1100 rpm to eliminate any remaining ethanol from the beads. Finally, purified aRNA was eluted with 50  $\mu$ l preheated aRNA elution solution.

The concentration of aRNA was determined by measuring the absorbance at 260 nm using a Nanodrop 2000c spectrophotometer. To ensure successful hybridization, the aRNA concentration should be at least 500 ng/ $\mu$ l. For fragmentation of aRNA, 15  $\mu$ g aRNA was made up to 32  $\mu$ l with nuclease-free water and mixed with 8  $\mu$ l 5x Fragmentation buffer and incubated at 94 °C for 35 min.

#### **2.4.6.2 Hybridization and microarray processing**

The hybridization and staining of Affymetrix gene chips was performed using GeneChip® Hybridization, Wash and Stain Kit according to the manufacturer's instructions. In brief, 12.5  $\mu$ g fragmented aRNA were mixed with hybridization master mix (Table 25) and incubated at 99 °C for 5 min followed by 45 °C for 5 min and centrifuged at 14,000 rpm for 5 min. Meanwhile, the Affymetrix Gene Chip® Rat Expression Arrays 230 2.0 were filled with 200  $\mu$ l of ready-to-use pre-hybridization buffer and mixed at 45 °C for 10 min with rotation. The pre-hybridization buffer was removed and replaced with 200  $\mu$ l hybridization cocktail, and the chips were hybridized in a hybridization oven with 60 rpm rotation for 16 h.

Table 25. Hybridization master mix including aRNA for Rat 230 2.0 Array (Hybridization cocktail).

<b>Component</b>	<b>Amount</b>
3 nM Control Oligonucleotide B2	4.2 $\mu$ l
20x Hybridization control (bioB, bioC, bioD, cre)	12.5 $\mu$ l
2 x Hybridization Mix	125 $\mu$ l
DMSO	25 $\mu$ l
Nuclease-free water	50 $\mu$ l
fragmented, labeled aRNA	12.5 $\mu$ g to a final volume of 250 $\mu$ l

After hybridization, washing and staining of the probe arrays was carried out in an automatic Fluidics Station 450 using reagents provided in the GeneChip® Hybridization, Wash and Stain Kit. Three bottles filled with approximately 500 ml of wash buffer A, B and fresh deionized water were placed to the station. For each sample chips, three 1.5 ml tubes containing 600  $\mu$ l staining cocktail 1, staining cocktail 2 and 800  $\mu$ l array holding buffer (AHB) were also placed into the stain holder positions of the Fluidics Station. The precast protocol including initial wash steps with buffer A and B was selected. The gene chips were removed from the oven and the hybridization cocktail was removed from the array and replaced by wash buffer A. The washing and staining processes were initiated by placing the arrays in the sample holder. Finally, scanning of arrays was performed using a Gene Chip® Scanner 7G at 570 nm and resolution of 3  $\mu$ m operated by the GCOS software which was also used for further data extraction.

### 2.4.6.3 Data extraction and analysis

After performing microarray experiments, data were extracted using the Microarray Analysis Suite 5.0 software from Affymetrix (MAS 5.0). Signal intensities were obtained by scaling all hybridized gene chips to a target intensity of 500 and transformed to  $\log_2$  intensity values. The normalized data was then imported into Partek Genomic Suite v6.5 for further statistical analysis and visualization of microarray gene expression data. The fold change in the expression of each gene was calculated as a ratio by dividing mean normalized intensity values for all replicates of treated groups versus corresponding untreated control group (Table 26). Statistical significance of the values was tested by one-way analysis of variance (ANOVA) with a probability-value (p-value) less than 0.01. A significance level of 0.01 means that there is a probability of 1 % that difference between control and treated group is due to change alone. All genes with a fold change of at least 1.5 and a p-value of <0.01 were considered as significantly differentially expressed and



used for further biological and functional analysis by Partek Genomic Suite v6.5 and Ingenuity Pathway Analysis (IPA).

Table 26. The following samples were subjected to gene expression profiling using Affymetrix Rat GeneChip RAE 230plus.

siRNA	BAY16		
	0 $\mu$ M	25 $\mu$ M	75 $\mu$ M
50 nM non-targeting siRNA (scrambled, SC)	3	3	3
50 nM GCGR siRNA (siGCGR)	3	3	3
no siRNA (untransfected, UT)	3	3	3
Total number of samples	9	9	9

## 2.5 Biochemical methods

### 2.5.1 Protein preparation from tissue

Proteins of frozen liver or kidney tissues (~ 200 mg) were extracted using 1 ml RIPA lysis buffer, which was supplemented with phosphatase inhibitors NaF and Na<sub>3</sub>VO<sub>4</sub> to block serine/threonine and tyrosine kinases, and protease inhibitor cocktail just before use (Table 9 in 2.1.5). The RIPA buffer contains sodium deoxycholate as ionic detergent which is widely used for the isolation of membrane proteins. The tissues were homogenized on ice using an Ultra Turrax at low speed at 4 °C and then centrifuged at 8000 g for 5 min.

The protein concentration of the lysate was determined using the DC Assay method from Bio-Rad. This colorimetric assay is based on the reduction of cupric ions (Cu<sup>2+</sup>) to cuprous ions (Cu<sup>+</sup>) by reacting with peptide bonds in an alkaline medium. The production of cuprous ions is followed by the reduction of Folin-Ciocalteu reagent (a mixture of phosphomolybdic acid and phosphotungstic acid), resulting in formation of a blue color complex that can be measured spectrophotometrically at 750 nm [196]. The amount of color produced is directly proportional to the amount of protein/peptide in the sample. Therefore, homogenized liver and kidney tissue samples were diluted in RIPA buffer at 1:100 or 1:50, respectively. An aliquot of 20  $\mu$ l was mixed with 100  $\mu$ l of a copper-containing solution by vortexing, followed by addition of 800  $\mu$ l of Folin-Ciocalteu reagent. After incubation for 15 min at RT and transfer into a plastic cuvette, the absorbance was measured at 750 nm. The protein concentration was determined using a BSA standard curve at a concentration of 0.2 to 1.5 mg/ml.

### **2.5.2 Protein preparation from rat hepatocytes**

The simultaneous extraction of nucleic acid and protein from the same experiments allows a direct correlation between genomic and proteomic data. The column based RNA extraction technique provides a simple and reliable method for concomitant protein extraction [197]. For this, the precipitated through-flow from the column-based RNA isolation was centrifuged at 14,000 rpm for 30 min to pellet the proteins. The supernatant was carefully decanted and the pellet was washed three times in ice cold acetone by incubation at -20 °C for 30 min followed by centrifuging at full speed for 15 min. The washed protein pellet was dried under laminar flow and resuspended in solubilization buffer (Table 9 in 2.1.5) that contains urea and 3-((3-cholamidopropyl)-dimethylammonio)-1-propanesulfonate (CHAPS) to unfold proteins, dithiothreitol (DTT) to cleave disulfide bonds, CHAPS to solubilize proteins as well as carrier ampholyte (IPG buffer) to enhance the protein solubility. The protein pellet was solubilized at 4 °C overnight. Accurate quantification of these soluble proteins can be difficult because many of the detergents or reductants such as CHAPS or DTT are incompatible with commonly used protein assays. For this reason, the proteins were quantified using the 2D-Quant kit following the manufacturer's instructions. In contrast to the DC assay measuring protein-bound complexes, the proteins binds specific to copper and unbound copper is measured with a colorimetric agent. The procedure involves the formation of a precipitate generated from the sample using two precipitation buffers. After centrifugation, the protein pellet was resuspended in 500 µl alkaline copper solutions. After addition of 1 ml of color reagent solution which reacts with unbound cupric ions, the absorbance was measured at 480 nm. The protein concentration was calculated using BSA standard curve at a concentration of 10 to 50 µg/ml.

### **2.5.3 Protein separation by SDS polyacrylamid gel electrophoresis**

Separation of protein samples was carried out under denaturing conditions using sodium dodecyl sulfate (SDS) polyacrylamide gel electrophoresis (PAGE). SDS denaturates secondary and non-disulfide linked tertiary structures of proteins by adding negative charge to each protein in proportion to its mass. Thus negatively charged proteins are separated based on their molecular size, whereby smaller proteins move faster than larger proteins through the pores of polyacrylamide gel during the electrophoretic run.

Prior to electrophoresis, the sandwich gel was freshly prepared by mixing ingredients of stacking and separating gel (Table 27). The polymerization of the gel is initiated by TEMED and APS. First the separating gel was poured to 3 cm from the top of the gel caster plate and overlaid with isopropanol to remove air bubbles. After polymerization, the

isopropanol was rinsed and the stacking gel solution was layered on top of the separating gel. The 10- or 15-well comb was carefully inserted into the stacking gel before gel was polymerized. The gel was then used for SDS-PAGE or stored wrapped in wet paper towels overnight at 4 °C.

Table 27. Composition of stacking and separating gels.

Component	Stacking Gel (6 %)	Separating Gel (8 %)
Acrylamide/Bisacrylamide (37.5 : 1)	800 µl	5.3 ml
0.5 M Tris (pH 6.8)	125 µl	-
1.5 M Tris (pH 8.8)	-	5.0 ml
H <sub>2</sub> O	4.0 ml	9.2 ml
10 % SDS	50 µl	200 µl
10 % APS	50 µl	200 µl
TEMED	5 µl	20 µl

Protein lysates of liver tissues or hepatocytes were mixed with 2x concentrate or 6x concentrate of Laemmli sample buffer (Table 9 in 2.1.5) consisting of SDS, glycerol, Tris-HCl, bromphenol blue dye and either β-mercaptoethanol or DTT to a final concentration of 2 µg/µl, and boiled for 5 min at 95 °C [198]. The reducing agents DTT or β-mercaptoethanol are used to remove tertiary and quaternary structure by breaking intra and inter-molecular disulfide bonds, and bromophenol blue serves as a marker dye to enable visualization of the migration of proteins. Addition of glycerol increases the density of the sample to be loaded onto gel, which is used to prevent outflow from the wells.

The gel cassette was placed in the electrophoresis chamber and filled with 1x SDS-PAGE running buffer before loading 5 µl samples (10 µg) and 5 µl prestained molecular weight marker into gel wells. The separation of proteins was performed by applying an electric field of 75 V and 100 mA for approximately 90 min, causing the molecules to migrate across the gel towards the anode.

#### 2.5.4 Protein detection by western blot analysis and immune detection

Immunoblotting (Western blotting) is a commonly used technique to detect a specific protein immobilized on a PVDF or nitrocellulose membrane using polyclonal or monoclonal antibodies. After separation of the proteins by SDS-PAGE, the proteins can be transferred from the gel onto a membrane using a Tris-glycine-methanol transfer buffer [199]. Methanol is used to strip complexed SDS from the protein molecules and enhance protein binding capacity to the membrane. After blocking of nonspecific binding sites of

the membrane, the target protein is recognized by a specific primary antibody and a secondary horseradish peroxidase (HRP)-conjugated antibody which binds directly to the primary antibody. This complex can be detected by chemiluminescence reaction in which HRP catalyzes the oxidation of the substrate luminol, resulting in emission of light.

After SDS-Page, the separated proteins were transferred onto nitrocellulose (NC) membranes at 100 V for 75 minutes at 4 °C using 1x transfer buffer (Table 9 in 2.1.5). The transfer of proteins from a gel to a membrane was accomplished by laying a gel upside down on top of filter paper, then a membrane on top of the gel with a stack of filter paper on top of the membrane (Figure 18). Furthermore, foam pads were placed between chambers to reduce vibration during the process of protein transfer. All blotting pads were placed in 1x transfer buffer for 10 min to equilibrate before blotting.

Prior to immunodetection, the protein bands were visualized by reversible staining of the membrane with Ponceau S solution for 1 min to assess the efficiency of the transfer. After successful blotting, membranes were blocked in 5 % nonfat dry milk in TBST buffer (blocking buffer, Table 9 in 2.1.5) for 1 h at RT following incubation with chicken anti-thiostatin diluted 1:5000, rabbit anti-GAPDH diluted 1:10,000 or 1:20,000 or mouse anti- $\alpha$ -Tubulin diluted 1:5000 in blocking buffer overnight at 4 °C or 1 h at RT (Table 10 in 2.1.6). After several washing steps with TBST for 15 min to remove unbound antibody, the membrane was incubated with HRP-conjugated antibodies at a dilution of 1:5000 in blocking buffer for 1 h at RT, followed by subsequent washing step. Immunodetections of proteins was performed by incubating the membrane with 1.5 ml of a 1:1 mixture of ECL reagents 1 and 2 (ECL™ Western Blotting Detection kit, Table 4 in 2.1.2) for 1 min. The protein bands were visualized by autoradiography after exposure to a light-sensitive hyperfilm. Densitometric analysis was performed using the Bio-Rad Gel Doc 2000 system.

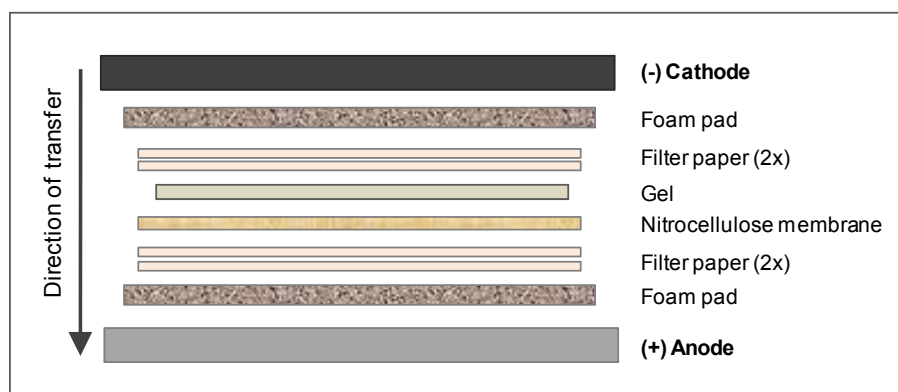


Figure 18. Transfer system of electroblotting. The proteins in the gel are transferred and immunobilized on NC membrane.

### 2.5.5 Immunofluorescence

Reduced GCGR expression by siRNA-mediated gene silencing was further confirmed at the protein level by immunofluorescence. The visualization of a specific protein by indirect immunofluorescence staining utilizes an unlabeled primary antibody that recognizes the target antigen and a fluorophore-conjugated secondary antibody, such as Cy3 (cyanine), which binds to the immunoglobulin F<sub>C</sub> fragment of the primary antibody. The subcellular localization and differences in the expression of the GCGR was analyzed using a Leica TCS confocal laser scanning microscopy. Cy3 is excited with a maximum at 550 nm and emits at 570 nm in the red part of the spectrum.

Briefly, freshly isolated hepatocytes were seeded at a density of  $1 \times 10^6$  cells per well onto collagen-coated coverslips in 6-well plates for 24 h. Following transfection with GCGR-specific siRNA, cells were washed in PBS for 5 min, fixed in 10 % neutral buffered formalin for 10 min and then permeabilized by treatment with 0.5 % Triton X-100 for 5 min at RT. Triton X-100, a nonionic detergent, is widely used to permeabilize the cell membrane to facilitate penetration of antibodies into the fixed hepatocytes. After washing twice with PBS, nonspecific binding sites were blocked with 1 % BSA in PBS at RT for 45 min. Cells were incubated with 100  $\mu$ l/coverslip of anti-rabbit polyclonal antibody for GCGR (1:50 dilution in 1 % BSA/PBS) overnight at 4 °C and 100  $\mu$ l/coverslip anti-rabbit IgG Cy3-conjugated antibody (1:700 dilution) for 1h at RT in the dark. Between each incubation step, the cells were washed three times in PBS for 15 min, and once in deionized water to remove unbound antibodies. The coverslips were mounted with Vectashield mounting medium containing 4',6-diamidino-2-phenylindole (DAPI) as a nuclear counterstain and stored at 4 °C until analysis using confocal microscopy.

### 2.5.6 Immunohistochemical analyses

Immunohistochemical staining of paraffin-embedded tissue sections is a simple method to detect specific proteins and to determine their cellular distribution and localization, based on the use of a specific antibody against the target antigen. The procedure of immunostaining includes deparaffinization, rehydration, pretreatment with antigen retrieval solutions and several blocking steps, incubation with primary and secondary antibodies and visualization of the antigen-antibody-complex using colorimetric detection.

The process of antigen retrieval is commonly used to unmask epitopes site of antigens, leading to improved detection of many target proteins. To achieve this, the tissue slides are pretreated with heating citrate buffer solution and/or digestion with trypsin, resulting in cleavage of protein crosslinks which are formed during tissue fixation in formalin solution

[200, 201]. Because the liver and kidney contain high levels of endogenous peroxidase, biotin and avidin, incubation of tissue sections with several blocking agents are necessary to suppress non-specific background staining during the avidin-biotin complex (ABC) detection system [202]. This colorimetric detection method is based on the high affinity of avidin or streptavidin to biotin, because avidin has four active binding sites for biotin, which can be used to form a bridge between the biotin-labeled peroxidase molecule and the biotinylated secondary antibody [203]. The HRP enzyme of this complex can catalyze the oxidation of a chromogenic substrate 3,3'-diaminobenzidine (DAB) to a insoluble brown precipitate in the presence of hydrogen peroxide which can be visualized by light microscopy (Figure 19).

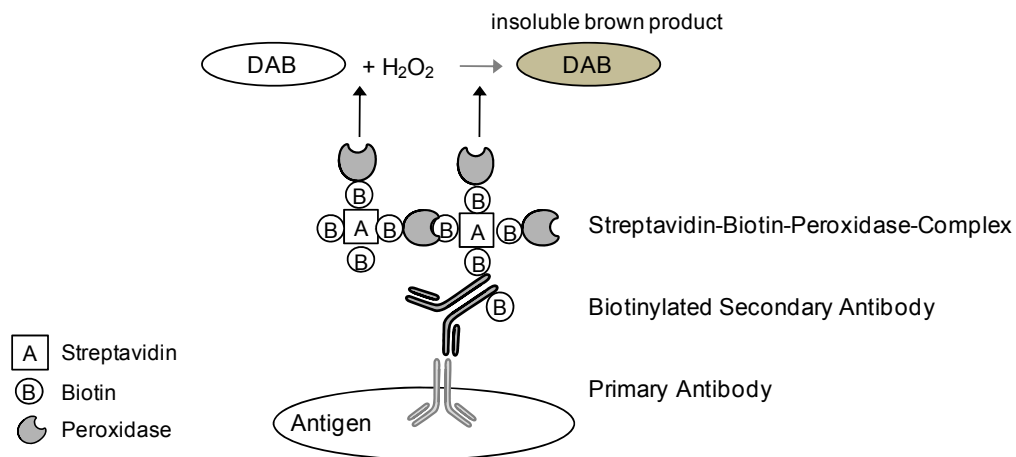


Figure 19. Principle of immunohistochemical analysis of proteins in paraffin-embedded tissues. A biotin-conjugated secondary antibody is used to detect a primary antibody bound to a specific epitope of the target antigen. The streptavidin peroxidase complex reacts with the biotin of the secondary antibody. The enzyme of this complex catalyzes the substrate DAB to form a brown colored reaction product (modified from [204]).

+Liver and kidney sections (5  $\mu$ m) were prepared from tissue microarray blocks [186] and mounted onto glass slides. Tissues were deparaffinized in Roti-Histol for 4 min thrice and rehydrated in decreasing concentrations of ethanol (3x 100% EtOH for 2 min, 1x 70 % EtOH for 2 min), and washed in PBS. Heat-induced antigen retrieval was achieved by pressure cooking in 10 mM citrate buffer, pH 6.0 for 4 min (Table 9 in 2.1.5). For detection of NGAL and Timp-1, tissues were treated with 0.1 % trypsin for 2 min at 37 °C. After washing in PBS, sections were blocked with 5 % donkey serum for 1 h. The endogenous peroxidase was subsequently blocked by incubation with 3 % H<sub>2</sub>O<sub>2</sub> in PBS for 10 min, followed by two additional blocking steps with 0.001 % avidin/PBS and 0.001 % biotin/PBS for 15 min, respectively. Between all blocking steps, sections were washed several times with PBS. Then, slides were incubated with either 1.3  $\mu$ g/ml goat anti-NGAL,

2 µg/ml goat anti-clusterin α diluted in 5 % donkey serum in PBS or 0.5 µg/ml mouse anti-PCNA, 2.5 µg/ml rabbit anti-Timp-1 diluted in 5 % goat-serum overnight at 4 °C in a humidified chamber. After three washes, tissues were incubated with the biotinylated secondary antibody (donkey anti-goat IgG; goat anti-mouse IgG2a, goat anti-rabbit IgG) diluted 1:200 in PBS for 1 h at RT and subsequently washed with PBS. The sections were then incubated with avidin-biotin-HRP solution (VECTASTAIN Elite ABC Kit) for 30 min before staining was performed using chromogenic substrate DAB. The DAB working solution (DAB Peroxidase Substrate Kit) was always freshly prepared by mixing 5 ml distilled water with 2 drops buffer solution, 5 drops DAB stock solution and 2 drops H<sub>2</sub>O<sub>2</sub>. The tissue slides were developed with DAB solution for 1-2 min until brown color is visible. Sections were then counterstained with Mayer's hematoxylin for 5 min and washed in running water for 5 min to stain nuclei. This blue nuclear staining was followed by counterstaining with eosin solution, which is used to visualize the cytoplasm and extracellular matrix in form of a pink staining. The sections were finally dehydrated by incubating in 70 % ethanol for 1 min and in 100 % ethanol four times for 2 min. After two purification steps in Roti®-Histol for 3 min, the slides were permanently embedded in Eukitt mounting medium and protein expression was analyzed by light microscopy.

### 2.5.7 Quantification of proteins by ELISA

The principle of a double antibody sandwich ELISA is based on the reaction of a capture antibody attached to the surface of a polystyrene microtiter plate with the target protein present in the sample followed by binding of a secondary biotinylated antibody at the bound antigen (Figure 20). The combination of two monoclonal antibodies that recognize two different non-overlapping epitopes of the antigen is used to increase the sensitivity and specificity of the assay. The indirect detection method can be performed using the streptavidin-HRP system by covalent binding of the streptavidin to the biotin conjugates of the secondary antibody. The addition of TMB (3,3',5,5'-tetramethylbenzidine) as the most commonly used colorimetric substrate for HRP detection in ELISA results in blue color development when TMB is oxidized during the enzymatic degradation of H<sub>2</sub>O<sub>2</sub> by HRP. The enzyme-substrate reaction can be stopped by addition of sulfuric acid, resulting in a color change to yellow which can be measured spectrophotometrically at a wavelength of 450 nm. The concentration of the target protein in the sample is determined by comparing the optical density of the samples to those of known standards, the estimated values must be multiplied by their respective dilution factors. Urinary target concentrations are normalized to urinary creatinine to correct for differences in urine volume.

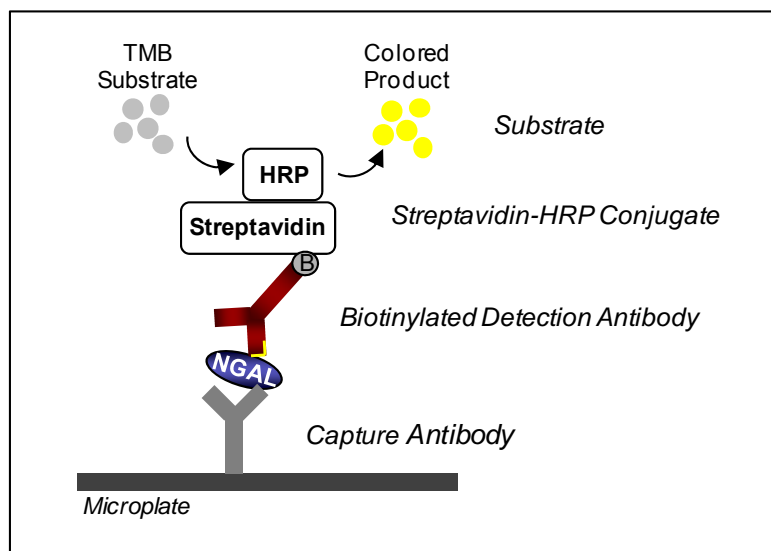


Figure 20. Principle of in-house sandwich ELISA for quantification of NGAL in rat serum and urine.

### 2.5.7.1 Development and validation of the rat NGAL ELISA

For quantification of rat NGAL in urine and serum, a sandwich enzyme-linked immunosorbent assay (ELISA) was developed using two monoclonal antibodies purchased from BioPorto Diagnostics (Figure 20). Nunc-Immuno™ Maxisorp microtitre plates were coated with 50  $\mu$ l per well of purified mouse anti-NGAL (2.5  $\mu$ g/ml) in carbonate buffer at 4 °C overnight (coating buffer, Table 9 in 2.1.5). Plates were washed twice with wash solution PBST using a manual 12 channel washer (Nunc-Immuno™ Washer 12) and unspecific binding sites were subsequently blocked by adding 200  $\mu$ l per well of 1 % BSA/PBS for 2 h at RT. After washing with PBST twice, 100  $\mu$ l of diluted urine (1:1600 or 1:6400), serum (1:400 or 1:800) or standards (recombinant rat NGAL in a concentration range of 0-5,000 pg/ml) were added to the plates in duplicate and incubated for 2 h at RT. All dilutions of standards, samples and biotin-conjugated antibody were prepared in 1 % BSA/PBS solution (pH 7.4). Following several washing steps with PBST, bound antigens were detected by addition of 100  $\mu$ l biotinylated anti-NGAL antibody diluted 1:4000 for 90 min and afterwards 50  $\mu$ l streptavidin-HRP solution for 30 min at RT. The peroxidase activity was determined by 30 min incubation with 100  $\mu$ l per well of TMB substrate reagent and the reaction was stopped with 100  $\mu$ l of 1 M sulfuric acid. The absorbance was measured by a microplate reader at 450 nm versus 650 nm as a reference for normalization of turbidity of the sample.

Assay validation is the evaluation of a test method to determine if the results of an experiment are accurate, reliable and reproducible. General principles and practices of process validation such as design, selection, development and performance



characteristics have been published by official agencies like the Food and Drug Administration and the International Committee on Harmonisation.

In-house validation of this assay required a series of inter- and intra-related processes and was evaluated by measuring the sensitivity, specificity, reference range, reproducibility, recovery, and dilutional linearity. The lower limit of detection (LLD) is the lowest NGAL concentration that can be reliably detected from the assay blank. The LLD was 78 pg/ml and the coefficient of variation (CV) was < 15 % (n = 6; P < 0.001 by Student's *t*-test). This assay is specific for rat NGAL protein and does not detect mouse and human NGAL. The range of the assay was determined by establishing a standard curve from 5,000, 2,500, 1,250, 625, 312.5, and 156.3 pg/ml. The % CV of each standard was calculated in six independent experiments and was less than 12 %. Intra- (n = 8) and interassay (n = 4) CV for three urine samples was less than 5.4 % and 9.4 %, respectively, and for three plasma samples < 6.2 % and < 8.2 %, respectively. The recovery rate of NGAL ranged from 101 to 132 % in urine and from 103 to 105 % in plasma of rats spiked with 0, 200 and 400 ng/ml recombinant NGAL protein. Furthermore, NGAL concentration was measured in two rat urine and plasma samples by diluting the samples in the range of 1:200, 1:400, 1:800, and 1:1600 (n = 2). Variation of the results was estimated by multiplying the reading with the dilution factor and ranged from 94 to 110 % CV and 91 to 117 % CV in urine and plasma samples, respectively.

#### **2.5.7.2 Thiostatin ELISA**

Quantification of urinary and serum thiostatin was carried out using a commercially available anti-rat sandwich ELISA according to the manufacturer's instructions. In brief, 100 µl of diluted samples (1:20,000) or standards containing thiostatin calibrator at a concentration range from 6.25 ng/ml to 400 ng/ml were transferred directly into the pre-coated microplate wells in duplicate. After incubation for 1 h and washing, 100 µl of diluted HRP anti-thiostatin conjugate was added to form complexes with the previously bound thiostatin present in the sample, afterwards each well was incubated with 100 µl of TMB substrate solution for 10 min. The blue color developed during the oxidation of TMB turns into yellow when the enzymatic reaction is stopped by addition of 100 µl 0.3 M sulfuric acid. The intensity of the color is directly proportional to the thiostatin concentration in the samples. The absorbance was measured by a microplate reader SpectraMax 190 at 450 nm. Results from ELISA assays were calculated using standard curves fitted with a four-parameter logistic regression and expressed as µg/ml serum or relative to urinary creatinine (ng/mg creatinine).

### 2.5.7.3 Clusterin ELISA

Urinary and serum clusterin was assayed by the Rat Clusterin ELISA Kit. In brief, serum and urine samples were diluted 1:2000 and 1:10 with dilution buffer, respectively. The recombinant rat clusterin in a concentration range of 2-128 ng/ml was used to generate a standard curve using the four-parameter logistic curve fit. For the ELISA, 100  $\mu$ l of standards and diluted samples assayed in duplicate were incubated in microtiter plate wells pre-coated with polyclonal anti-rat clusterin antibody for 1 h by moderate shaking at 300 rpm. After washing with 350  $\mu$ l wash solution thrice, 100  $\mu$ l of biotin-labeled antibody was added to each well followed by addition of 100  $\mu$ l streptavidin-HRP conjugate. Between each step, the plate was incubated and subsequently washed as described above. 100  $\mu$ l of TMB substrate was pipetted into each well and incubated for 20 min, resulting in a blue colored solution. The color development was stopped by adding 100  $\mu$ l of 0.2 M sulfuric acid solution before reading the absorbance with a spectrophotometer at 450 nm.

### 2.5.8 PON1 activity assay

PON1 enzyme activity in serum was determined by a fluorometric assay (EnzChek<sup>®</sup> Paraoxonase Assay Kit) based on enzymatic hydrolysis of a fluorogenic organophosphate analog by PON1. To this end, 10  $\mu$ l diluted serum (1:50), 10  $\mu$ l diluted positive control (1:25) or 10  $\mu$ l negative control (buffer) were mixed with 50  $\mu$ l reaction buffer per well. Each sample was measured in triplicate in a black 96-well microplate that reduces background fluorescence and minimizes well-to-well crosstalk during the measurement. A standard curve in a concentration range from 50  $\mu$ M to 0.39  $\mu$ M (1:2 dilution) was prepared by adding 100  $\mu$ l fluorescence reference standards (1/100<sup>th</sup> volume) directly into the wells that contains 100  $\mu$ l buffer. The plate was then preheated at 37 °C in an incubator. Afterwards, the enzymatic hydrolysis of the organophosphates was initiated by adding 50  $\mu$ l substrate working solution to each well containing controls and 100  $\mu$ l substrate working solution to wells containing samples and standards, respectively. The increase in fluorescence intensity was measured every minute for a time period of 60 min using a Berthold fluorescence plate reader Mithras LB940 at excitation/emission maxima 360/450 nm. The amount of fluorescence product formed in the serum samples may be converted to units of PON1 by the following definition: 1 unit (U) of paraoxonase generates 1 nmol of fluorescent product per minute at 37 °C.

### 3 ASSESSMENT OF CANDIDATE BIOMARKERS OF DRUG INDUCED LIVER INJURY IN PRECLINICAL TOXICITY STUDIES

This section has in part been published in Adler et al. 2010 [205]. According to Elsevier copyright, an author can use the article in full or in part in a dissertation without asking permission (<http://libraryconnect.elsevier.com/lcp/0403/lcp0403.pdf>).

#### 3.1 Background

Drug-induced liver toxicity is a major problem during drug development and the main cause for drug withdrawals from the market [8]. Assessment of drug hepatotoxicity and differentiation between various types of hepatic injury has been based primarily on determination of hepatic enzymes in blood, most notably alanine aminotransferase (ALT), aspartate aminotransferase (AST), alkaline phosphate (ALP) and  $\gamma$ -glutamyltranspeptidase (GGT) as indicators of hepatocellular and cholestatic liver injury, respectively. However, elevated levels of some of these conventional clinical markers in the blood are also found in other pathological conditions. Abnormal enzyme levels reveal only severe tissue injury and may not represent sensitive indicators of subtle toxic change. Hence, the need for identification and validation of additional novel biomarkers of hepatotoxicity with the ability to detect early signs of liver injury to improve safety assessment of drug candidates in preclinical studies has long been recognized. Despite application of new omics profiling strategies and world-wide efforts in the field of biomarker discovery, only few new candidate markers of hepatotoxicity have emerged. These include PON1, an antioxidant enzyme implicated in detoxification of organophosphates and prevention of low-density lipoprotein oxidation, which has been shown to be modulated in serum and plasma in response to hepatic damage [116], and clusterin, which was recently identified as part of a gene expression signature predictive of acute liver injury [104]. Clusterin is a glycoprotein synthesized and released by a variety of cells and tissues in response to injury, suggesting that determination of clusterin in body fluids may represent a sensitive non-invasive means to detect tissue injury, including hepatotoxicity. Similar to clusterin, transcriptomics results from previous *in vivo* toxicity studies conducted within the frame of the InnoMed PredTox project indicated that NGAL, a 25 kDa secreted glycoprotein, which is used as a urinary marker of renal injury [148, 206], was consistently upregulated in livers of rats following treatment with compounds associated with hepatotoxicity [97]. In addition, proteomics based on two-dimensional polyacrylamide gel electrophoresis (2D-PAGE) of urinary proteins demonstrated an increase in urinary thiostatin protein concentrations in dosed animals

compared to controls after treatment with two hepatotoxic drug candidates randomly selected for these analyses (Innomed data).

Based on these findings, the present *in vivo* investigations were conducted as part of the InnoMed PredTox project to assess the performance of PON1, clusterin, NGAL and thiostatin as potential non-invasive markers of drug-induced liver toxicity, as compared to routine clinical chemistry parameters. Specifically, we were interested to determine the ability of these biomarker candidates to detect or even predict hepatotoxicity in the form of hepatocellular necrosis and/or bile duct damage induced by three drug candidates. Thus, serum PON1 activity and release of clusterin, NGAL and thiostatin into serum or urine were analyzed following 1, 3, and 14 day treatment of male Wistar rats with low and a high doses of the glucagon receptor antagonist BAY16 ((+)-(1R)-1-[4-(4-fluorophenyl)-2,6-diisopropyl-5-propyl-pyridin-3-yl]ethanol), the aldose reductase inhibitor EMD335823 (1-(2-trifluoromethoxyphenyl)-2-nitroethanone) and the platelet fibrinogen receptor antagonist BI-3 (3-Pyrrolidineacetic acid, 5-[[[4'-[imino[(methoxycarbonyl)amino]methyl][1,1'-biphenyl]-4-yl]oxy]methyl]-2-oxo-, methyl ester,(3S-trans))). These analyses were supplemented by gene expression, protein expression and localizations studies in the target organ to link biomarker concentrations in serum and urine to their expression and localization in the liver to provide anchoring to the target organ and site of injury. In addition to testing the specificity of the biomarker response, a second aim of this investigation was to compare the sensitivity of these novel candidate markers with traditional clinical chemistry parameters.

## 3.2 Results

### 3.2.1 Biomarker responses to BAY16 in relation to traditional endpoints of toxicity

#### 3.2.1.1 Clinicopathological and histopathological observations

In this study, male Wistar rats were exposed to 20 mg/kg bw and 100 mg/kg bw of BAY16 for 1, 3 and 14 days by oral gavage. Changes in clinical chemistry parameters indicative of hepatotoxicity were observed only after treatment with the high dose. Liver enzyme activities of AST, ALT, ALP, GGT as well as bilirubin levels were significantly increased as early as day 3 (Table 28). ALT and AST are released into the circulation due to disruption of hepatocellular membrane, indicating cell necrosis, whereas elevated levels of bilirubin, GGT and ALP correlate with obstruction to bile secretion and serve as markers for cholestasis and hepatobiliary injury [84]. Changes in hepatic enzymes were accompanied by reduced food intake and body weight in high dose rats (animal no. 41-45) relative to controls (12 % by the end of treatment). After treatment with 100 mg/kg bw for 2 weeks,

hematologic examinations revealed a decrease of both hemoglobin and hematocrit and increase in neutrophil and thrombocyte counts, which could indicate an inflammatory response to drug treatment (Table 28).

Table 28. Overview of clinical chemistry data obtained from rats treated with low and high dose of BAY16 for up to 14 days. Data are presented as mean  $\pm$  standard deviation (n = 5). Statistical analysis was performed by ANOVA and Dunnett's post hoc test (\* p < 0.05, \*\*p < 0.01, \*\*\*p < 0.001).

	Day	BAY16		
		0 mg/kg	20 mg/kg	100 mg/kg
<b>Urine</b>				
Creatinine [mg/16h]	1	2.2 $\pm$ 1.0	1.9 $\pm$ 1.2	2.9 $\pm$ 0.6
	3	2.8 $\pm$ 0.3	3.3 $\pm$ 0.3	2.1 $\pm$ 1.0
	12	4.0 $\pm$ 0.4	4.3 $\pm$ 0.3	3.5 $\pm$ 0.4
Protein [mg/mg creatinine]	1	2.3 $\pm$ 1.2	2.6 $\pm$ 0.4	1.9 $\pm$ 0.5
	3	2.4 $\pm$ 0.6	2.5 $\pm$ 1.0	0.3 $\pm$ 0.8 **
	12	2.5 $\pm$ 1.1	2.1 $\pm$ 0.9	3.0 $\pm$ 2.2
<b>Serum</b>				
Creatinine [mg/dl]	1	0.58 $\pm$ 0.03	0.57 $\pm$ 0.02	0.57 $\pm$ 0.03
	3	0.57 $\pm$ 0.03	0.54 $\pm$ 0.02	0.63 $\pm$ 0.03
	14	0.64 $\pm$ 0.02	0.60 $\pm$ 0.02	0.63 $\pm$ 0.04
Blood urea nitrogen (BUN) [mg/dl]	1	39 $\pm$ 7	36 $\pm$ 4	32 $\pm$ 5
	3	40 $\pm$ 5	38 $\pm$ 2	39 $\pm$ 5
	14	34 $\pm$ 19	39 $\pm$ 3	47 $\pm$ 5
$\gamma$ -Glutamyltransferase (GGT) [U/l]	1	1.6 $\pm$ 1.1	2.0 $\pm$ 0.0	3.0 $\pm$ 2.7
	3	3.0 $\pm$ 3.2	0.8 $\pm$ 1.5	10.6 $\pm$ 6.0 *
	14	1.0 $\pm$ 0.0	2.6 $\pm$ 2.1	39.0 $\pm$ 24.5 *
Total protein [g/l]	1	62 $\pm$ 2	60 $\pm$ 2	59 $\pm$ 2 *
	3	60 $\pm$ 2	60 $\pm$ 2	64 $\pm$ 2 **
	14	65 $\pm$ 1	66 $\pm$ 2	71 $\pm$ 1 ***
Aspartate aminotransferase (AST) [U/l]	1	84 $\pm$ 6	80 $\pm$ 20	141 $\pm$ 92
	3	73 $\pm$ 21	90 $\pm$ 17	400 $\pm$ 196 **
	14	63 $\pm$ 11	60 $\pm$ 3	90 $\pm$ 13 **
Alkaline phosphatase (ALP) [U/l]	1	272 $\pm$ 41	281 $\pm$ 46	267 $\pm$ 62
	3	246 $\pm$ 21	243 $\pm$ 39	433 $\pm$ 57 ***
	14	244 $\pm$ 26	231 $\pm$ 8	293 $\pm$ 39 *
Alanine aminotransferase (ALT) [U/l]	1	51 $\pm$ 12	52 $\pm$ 5	77 $\pm$ 46
	3	50 $\pm$ 11	50 $\pm$ 11	346 $\pm$ 108 ***
	14	65 $\pm$ 7	64 $\pm$ 3	101 $\pm$ 26 **
Bilirubin [mg/dl]	1	0.07 $\pm$ 0.02	0.05 $\pm$ 0.01	0.50 $\pm$ 0.79
	3	0.10 $\pm$ 0.01	0.10 $\pm$ 0.01	3.53 $\pm$ 1.36 ***
	14	0.13 $\pm$ 0.01	0.11 $\pm$ 0.01	0.36 $\pm$ 0.05 ***
Triglycerides [mg/dl]	1	40 $\pm$ 14	49 $\pm$ 27	58 $\pm$ 27
	3	45 $\pm$ 24	37 $\pm$ 13	157 $\pm$ 28 ***
	14	73 $\pm$ 17	76 $\pm$ 23	44 $\pm$ 9
<b>Blood</b>				
Neutrophiles [10 <sup>9</sup> /l]	1	0.66 $\pm$ 0.21	0.52 $\pm$ 0.12	1.49 $\pm$ 0.95
	3	0.56 $\pm$ 0.10	0.42 $\pm$ 0.10	2.25 $\pm$ 0.53 ***
	14	0.57 $\pm$ 0.14	0.40 $\pm$ 0.09	1.24 $\pm$ 0.54 *

All morphological features involving hepatocyte cell death/necrosis, bile duct mitosis/hyperplasia and bile duct inflammation were summarized into a single histopathological score (Table 29).

No marked differences in histopathological findings were found between the liver of rats dosed with 20 mg/kg bw and controls. Initial histopathological changes in the liver characterized by necrotic epithelium of bile duct surrounded by inflammatory cells and connective tissue were observed following a single gavage of 100 mg/kg, which was scored as minimal to mild (Table 29). The severity scores of bile duct necrosis and bile duct hyperplasia accompanied by periportal inflammation were increased after three days of treatment with 100 mg/kg bw BAY16 (Table 29). Furthermore, minimal to mild necrosis and hypertrophy of hepatocytes were observed. Although single cell death was occasionally noted in some of the low dose animals at day 1 and 3, similar observations were made in control animals and thus these changes were considered as background and not compound-related. Repeated administration of high dose for 14 days resulted in extensive hyperplasia of bile ducts with moderate periportal fibrosis, whereas necrotic and inflammatory lesions in bile ducts were no longer visible (Table 29). Foci of necrotic hepatocytes forming cyst-like structures filled with erythrocytes, inflammatory cells and/or necrotic hepatocytes and single cell necrosis were detected in all high dose rats at the last time point. In these rats, hepatocyte mitosis could also be observed, which may indicate regenerative cell proliferation in the liver. No treatment-induced changes were found in the kidneys at any of the 3 time points.

Table 29. Summary of histopathological changes in the livers of Wistar rats treated with BAY16 for 1, 3 and 14 days. Numbers in parenthesis indicate the number of affected animals in each group (n = 5). Abbreviations: -  $\triangleq$  lesion not observed; +  $\triangleq$  minimal, ++  $\triangleq$  mild, +++  $\triangleq$  moderate and  $\triangleq$  ++++ high severity of lesion.

Histopathological change	BAY16		
	0 mg/kg	20 mg/kg	100 mg/kg
1 d			
Hepatocyte cell death	+ (2/5)	+ (4/5)	-
Bile duct inflammation	-	-	+ (2/5), ++ (2/5)
Bile duct epithelial cell mitosis /hyperplasia	-	-	+ (4/5)
<b>Summary score</b>	<b>+ (2/5)</b>	<b>+ (4/5)</b>	<b>+ (2/5), ++ (2/5)</b>
3 d			
Hepatocyte cell death	+ (3/5)	+ (3/5)	+ (1/5), ++ (3/5)
Bile duct inflammation	-	-	++ (2/5), +++ (3/5)
Bile duct epithelial cell mitosis /hyperplasia	-	-	+++ (5/5)
<b>Summary score</b>	<b>+ (3/5)</b>	<b>+ (3/5)</b>	<b>+++ (5/5)</b>
14 d			
Hepatocyte cell death	+ (1/5)	-	+ (2/5), ++ (1/5), +++ (2/5)
Bile duct inflammation	-	-	-
Bile duct epithelial cell mitosis /hyperplasia	-	-	++++ (5/5)
<b>Summary score</b>	<b>+ (1/5)</b>	<b>-</b>	<b>++++ (5/5)</b>

### 3.2.1.2 Gene expression of biomarkers

Oral administration of BAY16 (100 mg/kg bw) which caused marked liver damage after 3 and 14 days of treatment resulted in a significant increase in the hepatic expression of NGAL, T-kininogen and clusterin mRNAs. Results obtained from qRT-PCR showed an 89-fold up-regulation of NGAL mRNA at day 3 and 69-fold up-regulation at day 14 in livers of high dose rats as compared to controls (Figure 21a). Although effects were not statistically significant at day 1, clear overexpression of NGAL occurred in 4/5 animals showing mild or no histopathological finding. Similar results were found in the expression of T-kininogen, with a statistically significant increase in T-kininogen mRNA (8-fold) in high dose animals compared to untreated rats at day 1 (Figure 21b). Importantly, upregulation of NGAL and T-kininogen was found at a time point at which conventional clinical chemistry parameters were not altered, suggesting that induction of these genes related to acute phase response occurred before clear hepatotoxic effects could be detected by clinical chemistry.

Significantly overexpression of clusterin was also noted in high dose-rats before signs of BAY16-induced hepatotoxicity became apparent, but the response was much lower than for NGAL or thiostatin expression (Figure 21c). In contrast, no alterations in PON1 expression were evident in livers of treated rats throughout the study (Figure 21d).

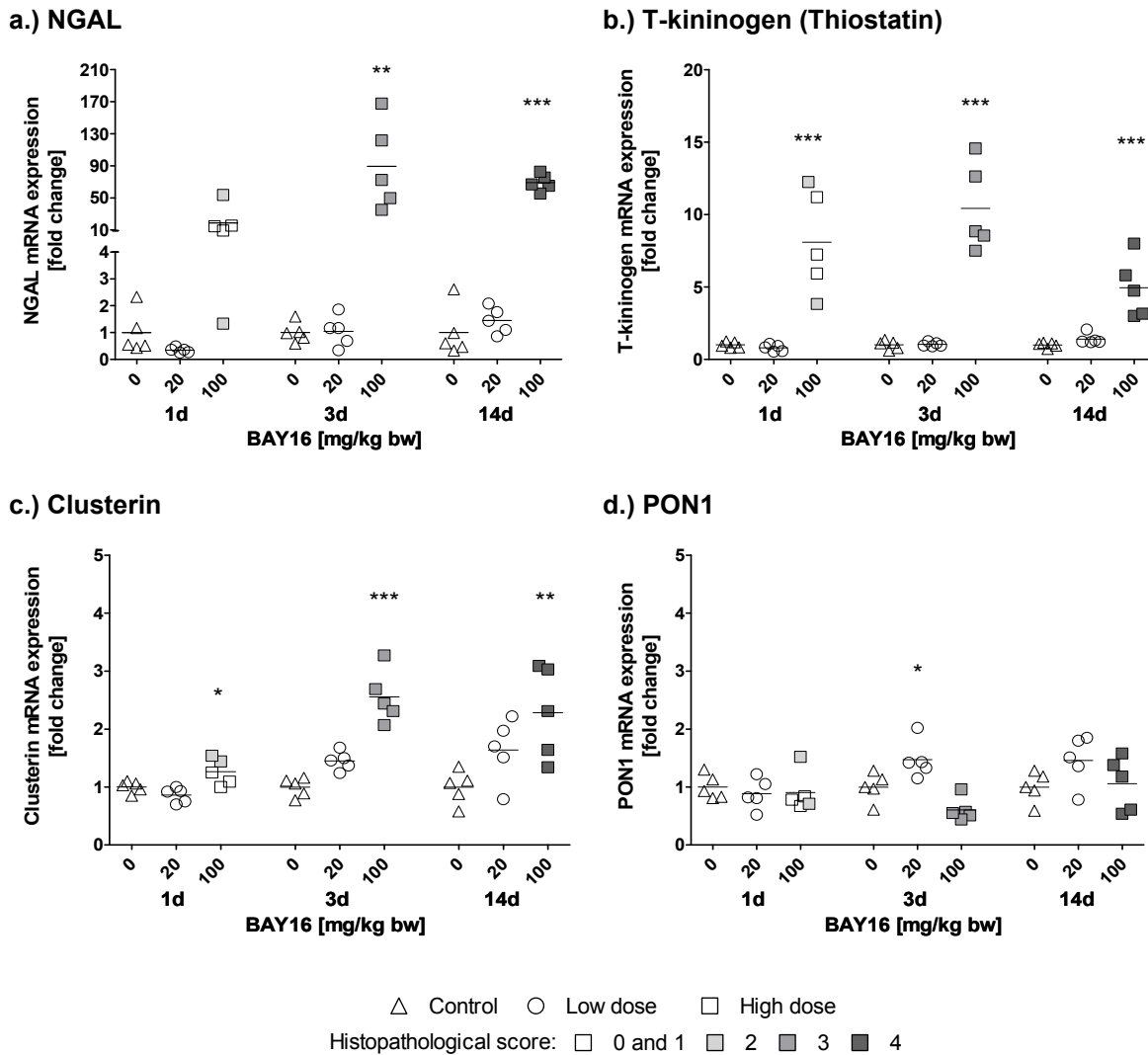


Figure 21. Changes in gene expression of candidate markers in liver of rats after administration of 20 mg/kg bw and 100 mg/kg bw BAY16. Data are presented as fold change of individual animals compared to the mean of the corresponding controls, color coded according to their histopathological score of the liver injury (n = 5 per group). Mean values of 5 individual animals per dose group are indicated by a black line. Statistical analysis was performed by ANOVA and Dunnett's post hoc test (\* p < 0.05, \*\*p < 0.01, \*\*\*p < 0.001).

Analysis of gene expression in the non-target organ kidney showed a slight increase in T-kininogen mRNA in affected animals at day 1 and day 3, although the basal level of transcription and the transcriptional response was much less pronounced as compared to the liver. In contrast, no changes in NGAL, clusterin and PON1 expression were evident (Table 30).



Table 30. Changes in gene expression of candidate markers in kidney of rats after administration of a low and a high dose of BAY16. Data are presented as mean  $\pm$  standard deviation (n.d. = not detectable).

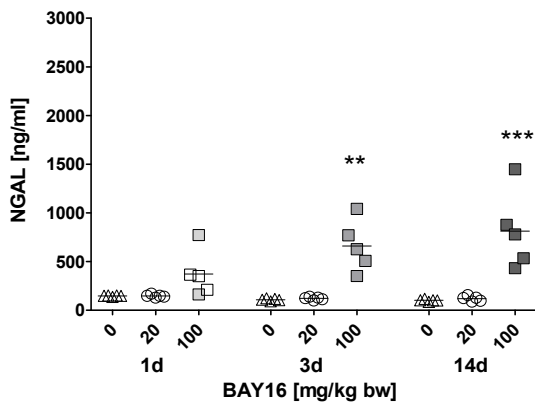
Gene title	Days of treatment	Fold deregulation		
		BAY16 [mg/kg bw]		
		0	20	100
NGAL	1	1.0 $\pm$ 0.2	1.0 $\pm$ 0.4	1.1 $\pm$ 0.3
	3	1.0 $\pm$ 0.5	1.5 $\pm$ 0.6	2.0 $\pm$ 0.7
	14	1.0 $\pm$ 0.4	0.6 $\pm$ 0.2	1.0 $\pm$ 0.4
T-kininogen	1	1.0 $\pm$ 0.4	1.4 $\pm$ 0.8	7.4 $\pm$ 6.3
	3	1.0 $\pm$ 0.7	1.6 $\pm$ 1.1	5.9 $\pm$ 3.8
	14	1.0 $\pm$ 0.9	0.8 $\pm$ 0.6	1.1 $\pm$ 0.8
Clusterin	1	1.0 $\pm$ 0.4	0.7 $\pm$ 0.3	1.3 $\pm$ 0.3
	3	1.0 $\pm$ 0.5	1.3 $\pm$ 0.5	1.0 $\pm$ 0.3
	14	1.0 $\pm$ 0.5	0.9 $\pm$ 0.5	1.2 $\pm$ 0.5
PON1	1	1.0 $\pm$ 2.2	n.d.	0.6 $\pm$ 1.4
	3	1.0 $\pm$ 0.5	4.1 $\pm$ 6.8	n.d.
	14	1.0 $\pm$ 1.4	0.2 $\pm$ 0.5	2.1 $\pm$ 2.9

### 3.2.1.3 Detection and quantification of biomarkers in serum and urine

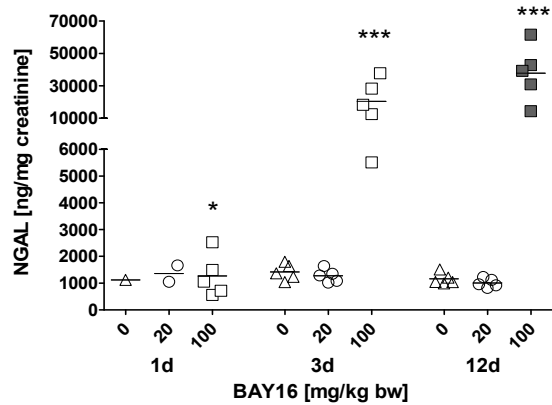
#### *ELISA assay*

Following tissue injury, hepatic enzymes and acute phase proteins may be released into blood or urine. The quantitative analysis of NGAL, T-kininogen and clusterin using ELISA assays demonstrated no significant changes in serum protein concentrations in response to 20 mg/kg bw BAY16 (Figure 22). The present data were consistent with the absence of histopathological alterations at this dose. In contrast, administration of 100 mg/kg bw BAY16 resulted in a significant increase in serum NGAL protein, evident even 1 day after administration of a single dose (Figure 22a). The release of NGAL into serum was accompanied by a pronounced increase in urinary NGAL protein concentration after 3 and 12 days (> 16-fold and 37-fold, respectively) (Figure 22a, b). In addition, serum levels of NGAL were found to correlate well with hepatic NGAL gene expression and with the severity of liver injury. Similar effects were observed on the concentration of thiostatin in serum, which was accompanied by enhanced urinary excretion and a significant up-regulation of T-kininogen mRNA in the liver (Figure 22c, d). Furthermore, a marked increase in serum clusterin was detected in all high dose animals after 3 and 14 days (Figure 22e), consistent with clusterin mRNA overexpression in the target organ. Although analysis of clusterin in urine of rats treated with BAY16 revealed increased urinary levels in 2/5 high dose animals (no. 41, 42), alterations in the target organ or in serum were not well reflected by urinary concentrations of clusterin (Figure 22f).

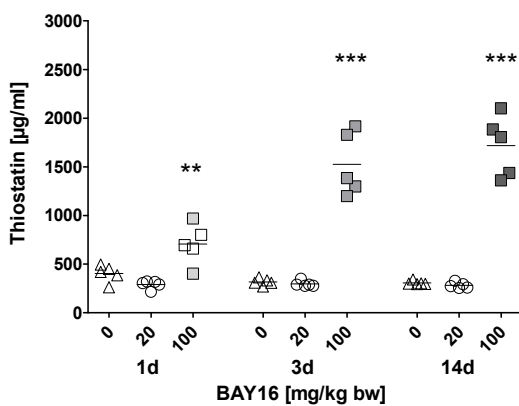
a.) Serum NGAL



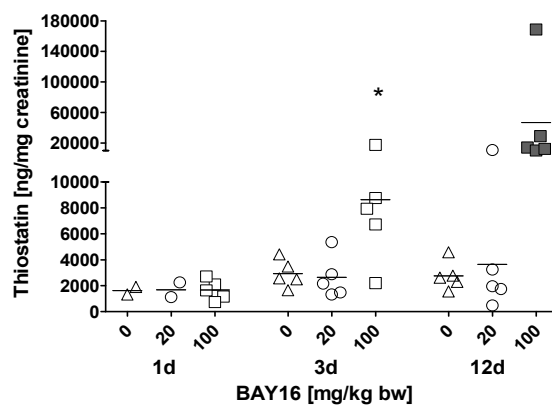
b.) Urinary NGAL



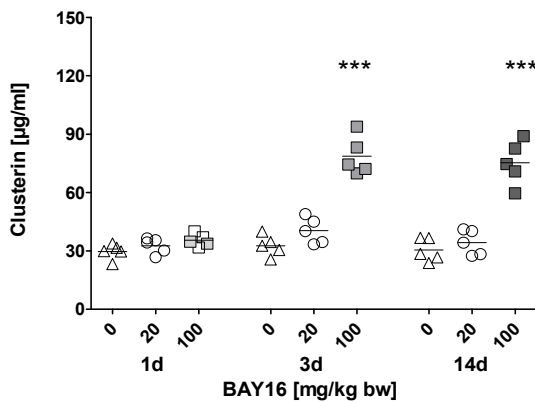
c.) Serum Thiostatin



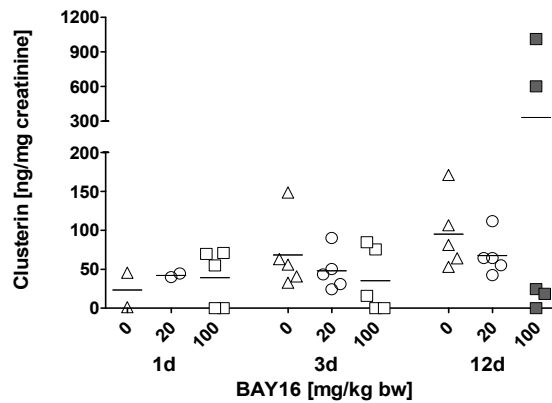
d.) Urinary Thiostatin



e.) Serum Clusterin



f.) Urinary Clusterin



△ Control ○ Low dose □ High dose  
 Histopathological score: □ 0 and 1 ■ 2 ■ 3 ■ 4

Figure 22. Determination of NGAL, thiostatin and clusterin in serum and urine of rats receiving BAY16 at oral doses of 0, 20 and 100 mg/kg bw for 1, 3 and 14 days. Data are presented as individual animals, color coded according to histopathology scores for liver damage. Mean values of 5 individual animals per dose group are indicated by a black line. For urinary markers after 1 and 3 days of treatment, no corresponding histopathology readouts are available as histopathology at these time-points was performed from groups of rats treated in parallel. Statistical analysis was performed by ANOVA and Dunnett's post hoc test (\* p < 0.05, \*\*p < 0.01, \*\*\*p < 0.001).

*Western blot of thiostatin*

Expression of thiostatin was further analyzed at the protein level to confirm T-kininogen (thiostatin) gene expression changes found in the liver of high-dose animals. In good agreement with upregulation of T-kininogen mRNA in rat liver, western blot analysis revealed increased levels of thiostatin protein in livers of affected high dose animals compared to untreated controls (Figure 23). These findings suggest that changes in protein concentration in urine or serum may be attributed to liver injury in rats treated with 100 mg/kg bw BAY16.

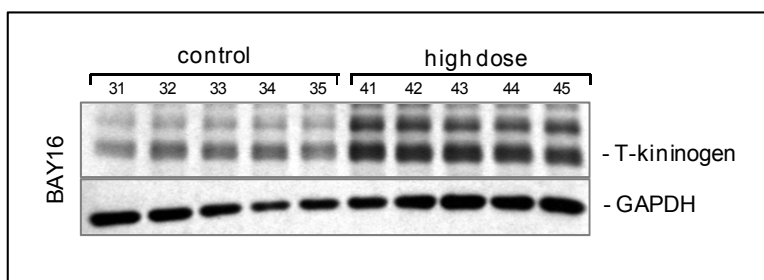


Figure 23. Western blot analysis of thiostatin protein expression in livers of Wistar rats treated with 100 mg/kg bw BAY16 for 14 days (n = 5), confirming increased thiostatin expression in all affected high dose animals as compared to untreated rats.

*PON1 activity assay*

Previous studies suggested that serum PON1 activity may be reduced in response to liver injury and may, therefore, serve as an indicator of hepatotoxicity [116-118]. Results obtained by the fluorogenic enzyme activity assay showed no significant differences in serum PON1 activity between controls and treated animals in response to BAY16, despite the marked histopathological alterations observed in animals given 100 mg/kg bw BAY16 for 3 and 14 days (Table 31).

Table 31. Enzymatic activity of PON1 in serum of rats treated with BAY16 for 1, 3 and 14 days (C = 0 mg/kg bw, LD = 20 mg/kg bw, HD = 100 mg/kg bw). PON1 activities are presented as mean  $\pm$  standard deviation (n=5). Statistical analysis was performed by ANOVA and Dunnett's post hoc test (\* p < 0.05, \*\*p < 0.01, \*\*\*p < 0.001).

Compound	Days of treatment	Serum PON1 Activity [Unit/ml]		
		C	LD	HD
BAY16	1	17.8 $\pm$ 6.6	18.6 $\pm$ 6.9	13.3 $\pm$ 4.1
	3	13.5 $\pm$ 6.9	20.1 $\pm$ 7.5	24.7 $\pm$ 9.6
	14	19.5 $\pm$ 4.2	19.1 $\pm$ 6.5	12.6 $\pm$ 2.0

#### 3.2.1.4 Immunolocalization of putative biomarkers

Results obtained by gene expression analysis and quantitative ELISA were subsequently confirmed by immunohistochemical staining of NGAL and clusterin in the liver and kidney of rats dosed with BAY16. The distribution and cellular localization of the biomarker is required to understand the functional role of protein during progression of liver injury. Commercially available antibodies against thiostatin were not suitable for immunohistochemical analysis, and we were therefore not able to discriminate between hepatocellular and hepatobiliary localization of thiostatin. In addition to immunostaining of NGAL and clusterin, immunohistochemical localization of proteins encoded by candidate marker genes identified in preliminary microarray analyses within the PredTox project [97] was performed to further confirm mRNA changes. Based on these transcriptomics data and histopathology scores, several genes involved in acute phase responses, degeneration, regeneration, and inflammation were identified that appear to be associated with the observed histopathological changes within studies BAY16, EMD335823 and BI-3. From the list of modulated genes, two markers related to proliferation and regeneration, such as PCNA and Timp-1 were selected. The proliferating cell nuclear antigen (PCNA) is an auxiliary protein of DNA polymerases  $\delta$  in eukaryotic cells [207] and can be used as a marker for cells in S phase of the cell cycle [208, 209].

In good agreement with the absence of hepatotoxic effects in animals treated with 20 mg/kg bw BAY16, no positive immunohistochemical staining of NGAL or clusterin was detected in liver tissues. In contrast, immunolocalization of both proteins in liver sections of high dose rats demonstrated increased expression in hepatocytes and biliary epithelial cells in areas associated with inflammatory and necrotic processes (Figure 24). The degree of bile duct injury was well reflected by NGAL staining in liver sections of affected high dose animals.

Treatment with 100 mg/kg bw BAY16 for 3 and 14 days resulted in enhanced proliferation of hepatocytes and biliary cells, as demonstrated by positive nuclear PCNA staining, consistent with increased hepatic PCNA gene expression and the site of liver lesions (Figure 24).

Tissue inhibitor of metalloproteinases-1 (Timp-1), which is known to inhibit the proteolytic activity of matrix metalloproteinases, was mainly detected within the biliary epithelium in the liver of both controls and BAY16-treated rats, but no differences in the pattern of Timp-1 immunostaining was visible (Figure 24). This finding suggests that the time-dependent increase in Timp-1 mRNA expression may be due to bile duct hyperplasia characterized by increased number of biliary epithelial cells, rather than due to an increased Timp-1 mRNA expression per cell.

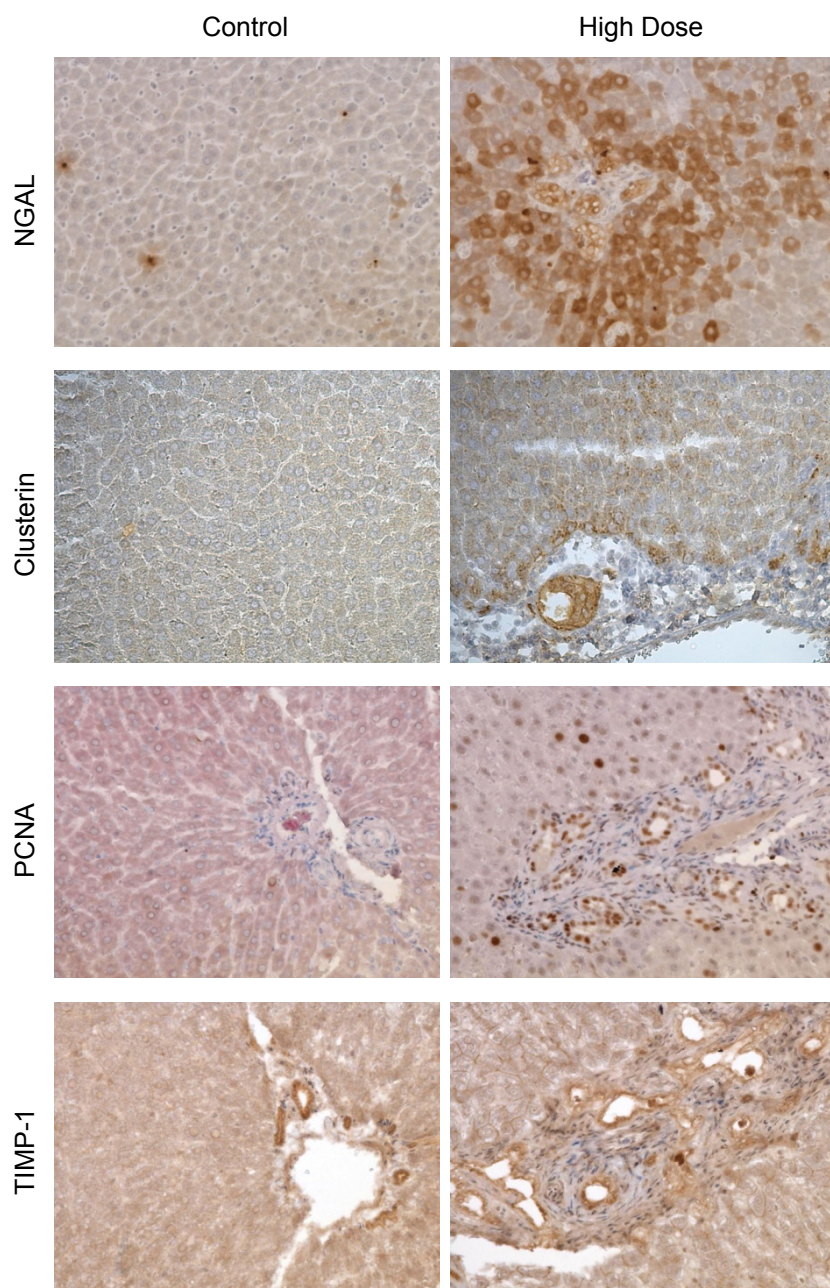


Figure 24. Immunohistochemical analysis of NGAL, clusterin, PCNA and Timp-1 in liver tissues of rats treated with BAY16. A marked induction of NGAL and clusterin both in hepatocytes and bile duct epithelial cells correlates with the degree and site of liver injury. Enhanced proliferation of both cell types occurred in response to BAY16 as shown by PCNA staining. In contrast, no differences in staining intensity of Timp-1 within the biliary epithelium were visible in liver sections.

To further understand the causes of the dramatical increase in urinary NGAL concentration despite lack of nephrotoxic effects in animals treated with BAY16, immunohistochemical analysis was also performed in kidney tissues. Interestingly, despite the absence of both histopathological alterations and changes in the expression of NGAL in kidneys from this study, increased immunoreactivity against NGAL was observed in proximal tubule cells in the outer cortex and papilla of high dose animals as compared to controls (Figure 25).

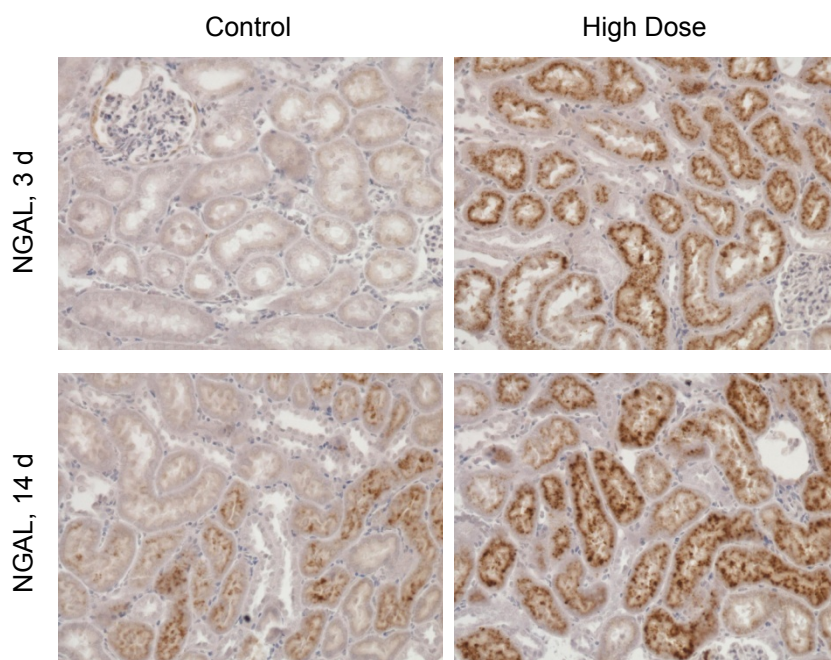


Figure 25. Expression of NGAL in kidney sections of rats treated with BAY16. Despite absence of histopathological alterations, NGAL was found in vesicles at the apical side of proximal tubule cells in the cortex as early as day 1, consistent with glomerular filtration and tubular reabsorption of NGAL present in serum.

### 3.2.1.5 Summary

The drug candidate BAY16, a glucagon receptor antagonist was originally synthesized to decrease hepatic glucose production mediated by inhibition of glucagon-stimulated glycogenolysis and gluconeogenesis in patients with type 2 diabetes mellitus. Based on previous knowledge of its toxicity to the liver, this compound was selected for assessment of novel biomarkers of drug-induced hepatotoxicity using a wide range of molecular biology and biochemical methods.

Oral administration of 100 mg/kg bw BAY16 to male Wistar rats has resulted in a time- and dose-dependent increase of acute phase proteins NGAL and T-kininogen in the serum, urine and liver. Changes in gene and protein expression of both markers correlated with the severity of BAY16-induced liver damage and were detected at an earlier time point than the conventional diagnostic markers of liver injury, ALT, AST and ALP. These observations indicate that both protein markers might be able to detect hepatotoxicity before clinical symptoms became evident. Enhanced serum and urine levels of NGAL as well as hepatic NGAL mRNA expression might be attributed to increased numbers of neutrophils found in the blood of high dose animals at day 3 and day 14, indicating recruitment of neutrophils in the liver that may be involved in initiation of inflammatory processes as a response to tissue injury [210].

Besides being expressed in neutrophils, NGAL is also released by injured renal tubular cells in the urine and serves therefore as a reliable and early non-invasive marker for acute kidney injury [132, 211, 212]. It is interesting that high NGAL concentrations were found in the urine and kidney of BAY16-treated rats in the absence of renal injury. This

results might be explained by the fact that NGAL with a low molecular weight of 25kDa may be freely filtered in the glomeruli of healthy kidneys, bound to the scavenger-receptor megalin, expressed abundantly and specifically on the brush borders of proximal tubules, and taken up by endocytosis and stored in lysosomes [138]. Immunohistochemical analysis in healthy kidney of rats showed that NGAL is localized in vesicles at the apical site of the proximal tubules in the outer cortex, suggesting glomerular filtration and tubular reabsorption of NGAL released into serum at the site of injury. Based on this observation, it appears that the high level of NGAL in urine is indeed unrelated to kidney injury but may have occurred as a result of liver injury and physiological NGAL handling of the kidney.

While our results demonstrate that overexpression of thiostatin and secretion into serum and urine may represent an immediate response to liver injury, it is important to note that slight changes in gene expression were also observed in kidneys of affected animals, although the transcriptional response in the kidney was much less pronounced as compared to the liver. Therefore we can assume that this effect is not responsible for the observed rise in urine and serum thiostatin level.

Changes in serum clusterin concentration were also associated with the histopathological findings in rat liver, whereby urinary clusterin did not correlate well with the degree of liver injury. Clusterin, a secretory heterodimeric disulphide-linked glycoprotein, may be cleaved into its alpha and beta chain, which may be able to pass the glomerulus [213] and is also known to be released into urine in response to kidney injury [214, 215]. Overall, these findings suggest that serum clusterin, but not urinary clusterin, may serve as minimally invasive indicator of liver injury.

Although the activity of serum PON1 has been reported to be reduced in rats after liver damage [115, 117], no decrease in PON1 activity could be detected in rats showing marked histopathological changes in the liver caused by 100 mg/kg bw BAY16, suggesting that serum PON1 may not present a universal marker of drug-induced hepatotoxicity.

Immunolocalization studies of biomarkers generally reflected histopathological changes but did not provide an indication of toxicity at earlier time points or at lower doses than histopathology.

### **3.2.2 Biomarker responses to EMD335823 in relation to traditional endpoints of toxicity**

#### **3.2.2.1 Histopathological and clinicopathological observations**

High variability of histopathological changes was observed in livers of rats after oral administration of 15 mg/kg bw or 350 mg/kg bw of EMD335823 for 1, 3 and 14 days.

Marked hepatotoxic effects in the bile duct, including bile duct epithelial cell death, bile duct inflammation and hyperplasia, were found in 3 of 5 animals (42, 44 and 45) receiving a dose of 350 mg/kg/d EMD 335823 over a period of 14 days (Table 32). Clinical signs of toxicity in animal 42 and 45 were characterized by initial weight loss after 5-8 days, as well as ventral recumbency and scabs on the nose or genital region during the remainder of the treatment period. These two animals showed the most severe biliary lesions in addition to massive multifocal liver cell necrosis (Table 32). No toxicologically relevant histopathological findings could be detected in the kidney of rats during the entire treatment period.

Table 32. Summary of histopathological changes in the livers of Wistar rats treated with EMD335823 for 1, 3 and 14 days. Numbers in parenthesis indicate the number of affected animals in each group (n = 5). Abbreviations: -  $\triangleq$  lesion not observed; +  $\triangleq$  minimal, ++  $\triangleq$  mild, +++  $\triangleq$  moderate and  $\triangleq$  ++++ high severity of lesion.

Histopathological change	EMD335823		
	0 mg/kg	15 mg/kg	350 mg/kg
1 d			
Hepatocyte cell death	-	-	-
Bile duct inflammation	-	-	-
Bile duct epithelial cell mitosis /hyperplasia	-	-	-
<b>Summary score</b>	-	-	-
3 d			
Hepatocyte cell death	-	-	-
Bile duct inflammation	-	-	-
Bile duct epithelial cell mitosis /hyperplasia	-	-	-
<b>Summary score</b>	-	-	-
14 d			
Hepatocyte cell death	-	-	++++ (2/5)
Bile duct inflammation	-	-	++++ (3/5)
Bile duct epithelial cell mitosis /hyperplasia	-	-	+ (2/5), +++(2/5)
<b>Summary score</b>	-	-	<b>+ (1/5), ++++ (3/5)</b>

In good agreement with the severity of hepatic lesions, alterations in conventional clinical chemistry parameters such as ALT, AST, GGT, ALP and bilirubin indicative of hepatotoxicity were restricted to animals no. 42 and 45 (Table 33). The number of neutrophils was significantly decreased at day 3, but significantly increased after 14 days of treatment with EMD335823, potentially reflecting the inflammatory response. In addition, elevated serum creatinine levels were measured in the high dose group at all time points, although no signs of kidney injury were seen by histopathology.



### 3 ASSESSMENT OF CANDIDATE BIOMARKERS OF DILI

Table 33. Alterations in clinical chemistry parameters following treatment with 0, 15 and 350 mg/kg/d EMD335823. Data are presented as mean  $\pm$  standard deviation (n = 5). Statistical analysis was performed by ANOVA and Dunnett's post hoc test (\* p < 0.05, \*\*p < 0.01, \*\*\*p < 0.001).

	Day	EMD335823			
		0 mg/kg	15 mg/kg	350 mg/kg	
<b>Urine</b>					
Creatinine [mg/16h]	1	3.7 $\pm$ 0.4	3.7 $\pm$ 0.7	4.3 $\pm$ 0.9	
	3	4.2 $\pm$ 0.9	4.1 $\pm$ 0.6	5.0 $\pm$ 1.2	
	12	5.4 $\pm$ 0.9	5.1 $\pm$ 0.3	5.3 $\pm$ 0.6	
Protein [mg/mg creatinine]	1	0.7 $\pm$ 0.3	0.7 $\pm$ 0.5	1.0 $\pm$ 0.2	
	3	0.9 $\pm$ 0.7	0.9 $\pm$ 0.3	1.3 $\pm$ 0.8	
	12	0.6 $\pm$ 0.3	0.5 $\pm$ 0.1	1.7 $\pm$ 1.9	
<b>Serum</b>					
Creatinine [mg/dl]	1	0.24 $\pm$ 0.01	0.24 $\pm$ 0.02	0.30 $\pm$ 0.01	***
	3	0.25 $\pm$ 0.01	0.23 $\pm$ 0.02	0.30 $\pm$ 0.02	***
	14	0.28 $\pm$ 0.02	0.28 $\pm$ 0.02	0.38 $\pm$ 0.14	
Blood urea nitrogen (BUN) [mg/dl]	1	72 $\pm$ 7	73 $\pm$ 5	87 $\pm$ 12	*
	3	83 $\pm$ 16	90 $\pm$ 14	71 $\pm$ 9	
	14	90 $\pm$ 20	107 $\pm$ 11	106 $\pm$ 34	
$\gamma$ -Glutamyltransferase (GGT) [U/l]	1	0.0 $\pm$ 0.0	0.0 $\pm$ 0.0	0.0 $\pm$ 0.0	
	3	0.0 $\pm$ 0.0	0.0 $\pm$ 0.0	0.0 $\pm$ 0.0	
	14	0.0 $\pm$ 0.0	0.0 $\pm$ 0.0	37 $\pm$ 61	
Total protein [g/l]	1	60 $\pm$ 2	58 $\pm$ 1	60 $\pm$ 4	
	3	61 $\pm$ 1	60 $\pm$ 2	54 $\pm$ 2	***
	14	60 $\pm$ 1	57 $\pm$ 2	57 $\pm$ 5	
Aspartate aminotransferase (AST) [U/l]	1	119 $\pm$ 32	110 $\pm$ 11	120 $\pm$ 15	
	3	124 $\pm$ 13	115 $\pm$ 21	134 $\pm$ 35	
	14	106 $\pm$ 20	125 $\pm$ 13	293 $\pm$ 282	
Alkaline phosphatase (ALP) [U/l]	1	226 $\pm$ 59	221 $\pm$ 36	202 $\pm$ 36	
	3	158 $\pm$ 33	153 $\pm$ 30	146 $\pm$ 35	
	14	164 $\pm$ 41	155 $\pm$ 49	216 $\pm$ 90	
Alanine aminotransferase (ALT) [U/l]	1	70 $\pm$ 9	71 $\pm$ 10	64 $\pm$ 8	
	3	53 $\pm$ 10	56 $\pm$ 5	68 $\pm$ 15	
	14	51 $\pm$ 10	43 $\pm$ 7	220 $\pm$ 253	
Bilirubin [mg/dl]	1	0.06 $\pm$ 0.01	0.06 $\pm$ 0.01	0.07 $\pm$ 0.02	
	3	0.10 $\pm$ 0.03	0.10 $\pm$ 0.02	0.08 $\pm$ 0.02	
	14	0.08 $\pm$ 0.02	0.08 $\pm$ 0.01	0.89 $\pm$ 1.10	
Triglycerides [mg/dl]	1	164 $\pm$ 74	125 $\pm$ 43	54 $\pm$ 25	*
	3	40 $\pm$ 8	48 $\pm$ 18	46 $\pm$ 13	
	14	48 $\pm$ 10	43 $\pm$ 14	87 $\pm$ 83	
Glucose [mg/dl]	1	112 $\pm$ 6	118 $\pm$ 22	123 $\pm$ 13	
	3	83 $\pm$ 30	95 $\pm$ 16	91 $\pm$ 11	
	14	95 $\pm$ 24	80 $\pm$ 5	82 $\pm$ 2	
<b>Blood</b>					
Neutrophiles [10 <sup>9</sup> /l]	1	1.32 $\pm$ 0.18	1.06 $\pm$ 1.15	0.44 $\pm$ 0.44	
	3	1.31 $\pm$ 0.12	0.88 $\pm$ 0.47	0.47 $\pm$ 0.09	**
	14	0.97 $\pm$ 0.13	0.95 $\pm$ 2.06	2.06 $\pm$ 0.80	**

## 3.2.2.2 Gene expression of biomarkers

As expected, changes in gene expression between vehicle-treated controls and high dose rats were restricted to individual animals showing clear signs of hepatotoxicity after 14 days of treatment with EMD335823. Strong overexpression of NGAL (~640-fold in rat no. 42; ~150-fold in rat no. 45, respectively) and thiostatin (~40-fold in rat no. 42; ~30-fold in rat no. 45, respectively) were detected in affected animals, whereas a moderate up-regulation of clusterin was seen only in rat no. 42 (Figure 26a, b, c). Quantification of PON1 mRNA determined by qRT-PCR showed no alteration in PON1 expression between the controls and EMD335823-treated animals (Figure 26d). In contrast to BAY16, differences in expression of NGAL, T-kininogen and clusterin in the liver did not precede the onset of clinical signs of hepatotoxicity.

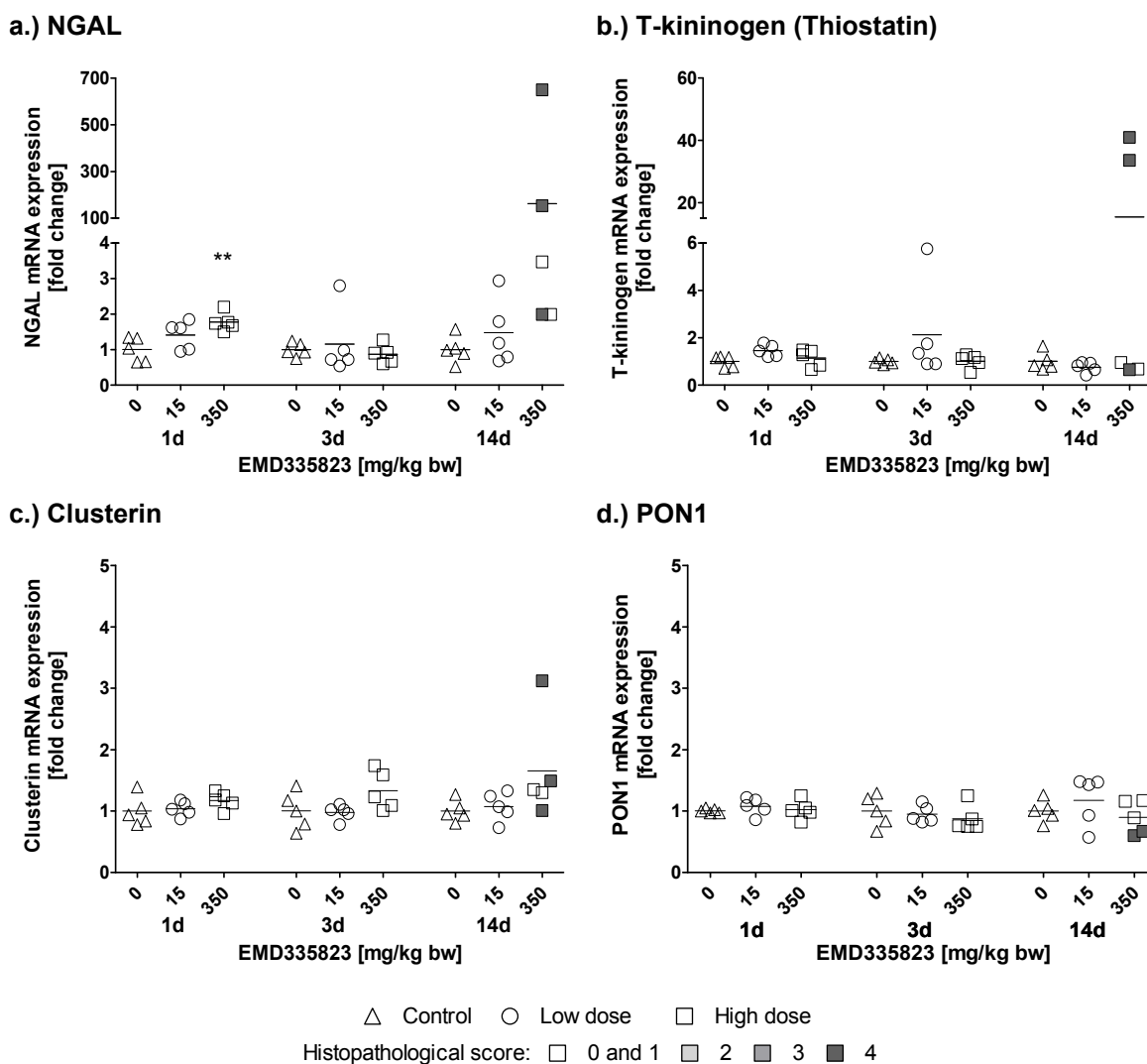


Figure 26. Expression of marker candidates in livers of rats administered with EMD335823 in a doses of 15 mg/kg bw and 350 mg/kg bw for 1, 3 and 14 days. Data are presented as fold change of individual animals compared to the mean of the corresponding controls, color coded according to their histopathological score of liver injury (n = 5 per group). Mean values of 5 animals per dose group are indicated by a black line. Statistical analysis was performed by ANOVA and Dunnett's post hoc test (\* p < 0.05, \*\*p < 0.01, \*\*\*p < 0.001).

The analysis of candidate marker genes in the kidney as a non-target organ of EMD335823 toxicity revealed no increase in the expression of clusterin and PON1, although a slight upregulation in NGAL and T-kininogen mRNA was detected in affected animals 42 and 45 (Table 34). However, the basal expression level of T-kininogen ( $c_t$ -value  $\sim 30$ ) in the kidney was much less pronounced than in the liver ( $c_t$ -value  $\sim 18$ ).

Table 34. Changes in gene expression of candidate markers in kidney of rats after administration of 15 and 350 mg/kg bw EMD335823. Data are presented as mean  $\pm$  standard derivation.

Gene title	Days of treatment	Fold deregulation		
		EMD335823 [mg/kg bw]		
		0	15	350
NGAL	1	1.0 $\pm$ 0.4	0.7 $\pm$ 0.2	0.7 $\pm$ 0.2
	3	1.0 $\pm$ 0.3	0.7 $\pm$ 0.4	1.5 $\pm$ 0.4
	14	1.0 $\pm$ 0.7	1.4 $\pm$ 0.3	1.9 $\pm$ 1.6 <sup>1</sup>
T-kininogen	1	1.0 $\pm$ 0.5	1.0 $\pm$ 1.1	0.7 $\pm$ 0.9
	3	1.0 $\pm$ 0.7	1.0 $\pm$ 1.1	2.1 $\pm$ 2.4
	14	1.0 $\pm$ 0.5	2.5 $\pm$ 1.1	14.2 $\pm$ 20.6 <sup>1</sup>
Clusterin	1	1.0 $\pm$ 0.5	0.7 $\pm$ 0.3	0.5 $\pm$ 0.1
	3	1.0 $\pm$ 0.3	0.8 $\pm$ 0.5	1.7 $\pm$ 0.5
	14	1.0 $\pm$ 0.4	1.7 $\pm$ 0.3	1.4 $\pm$ 0.8
PON1	1	1.0 $\pm$ 0.5	0.9 $\pm$ 1.1	0.6 $\pm$ 1.0
	3	1.0 $\pm$ 1.2	0.9 $\pm$ 0.2	2.8 $\pm$ 2.4
	14	1.0 $\pm$ 0.5	2.2 $\pm$ 1.0	1.7 $\pm$ 0.8

<sup>1</sup> increased gene expression restricted to animals no. 42 and 45

### 3.2.2.3 Detection and quantification of biomarkers in serum and urine

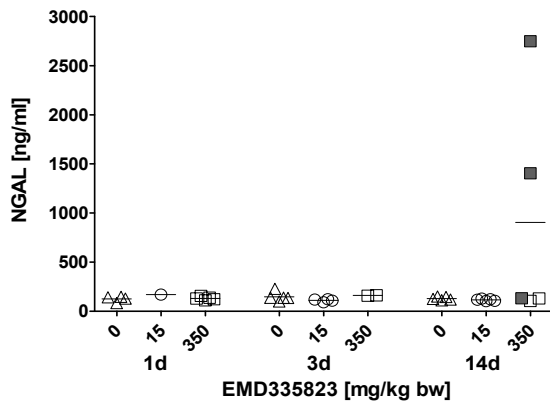
#### *ELISA assay*

Overexpression of hepatic NGAL in the liver was associated with a dramatic increase in serum NGAL protein specifically in those high dose animals, in which marked histopathological changes were seen. NGAL measurement revealed a 23-fold increase in serum of rat no. 42 and a 12-fold increase in rat no. 45, accompanied by enhanced urinary excretion of NGAL (> 90-fold and 50-fold, respectively) (Figure 27a, b). Similar changes in serum and urinary thiostatin were observed in affected animal no. 42 and 45, correlating with hepatic mRNA expression of thiostatin (Figure 27c, d).

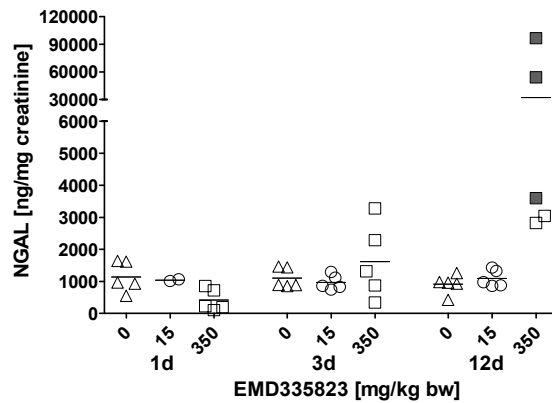
In contrast to NGAL and thiostatin, there were no significant alterations in serum clusterin concentration, despite an increase in mRNA expression (Figure 26c) and urinary clusterin in individual high dose animals (Figure 27e, f).

### 3 ASSESSMENT OF CANDIDATE BIOMARKERS OF DILI

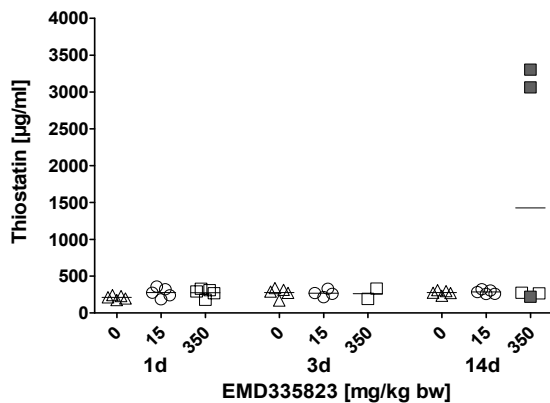
a.) Serum NGAL



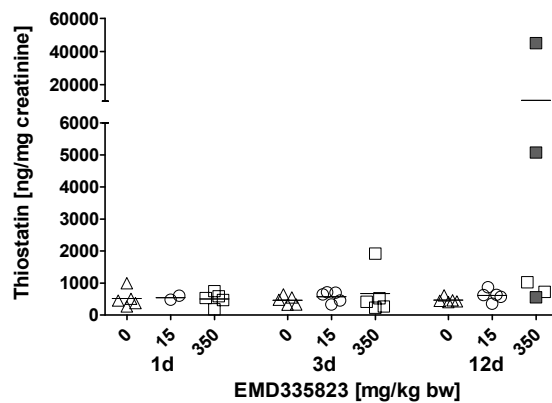
b.) Urinary NGAL



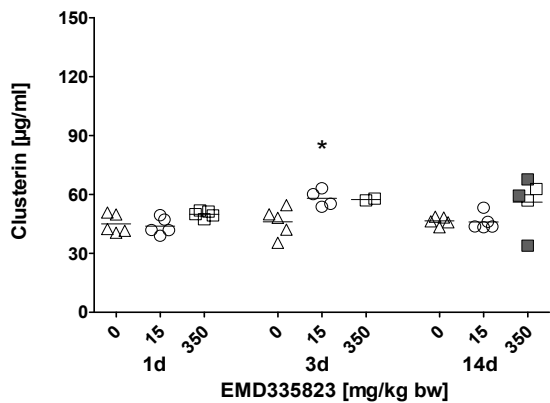
c.) Serum Thiostatin



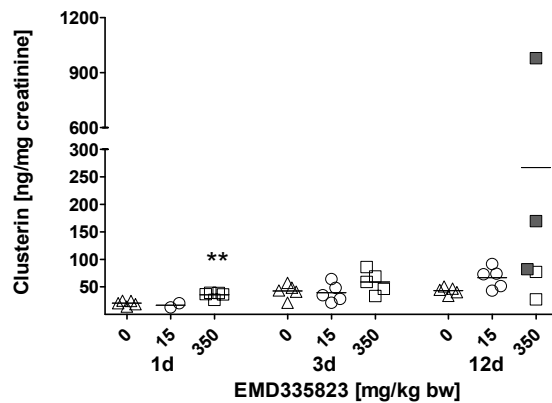
d.) Urinary Thiostatin



e.) Serum Clusterin



f.) Urinary Clusterin



△ Control ○ Low dose □ High dose  
 Histopathological score: □ 0 and 1 □ 2 ■ 3 ■ 4

Figure 27. Changes in the concentration of putative biomarker candidates in serum and urine following treatment with EMD335823. Data are presented as individual animals, color coded according to histopathology scores for liver damage. For urinary markers after 1 and 3 days of treatment, no corresponding histopathology readouts are available as histopathology at these time-points was performed from groups of rats treated in parallel. Mean values of 5 individual animals per dose group are indicated by a black line. Statistical analysis was performed by ANOVA and Dunnett's post hoc test (\*  $p < 0.05$ , \*\*  $p < 0.01$ , \*\*\*  $p < 0.001$ ).

*Western blot of thiostatin*

Immunoblot analysis of liver homogenates of rats treated with 0 or 350 mg/kg bw for 14 days demonstrated an increase in protein expression of rat thiostatin, a 68 kDa glycoprotein cysteine proteinase inhibitor, in animals no. 42 and 45. Thus, a good correlation between thiostatin serum levels and mRNA and protein expression in the target organ of affected animals was evident.

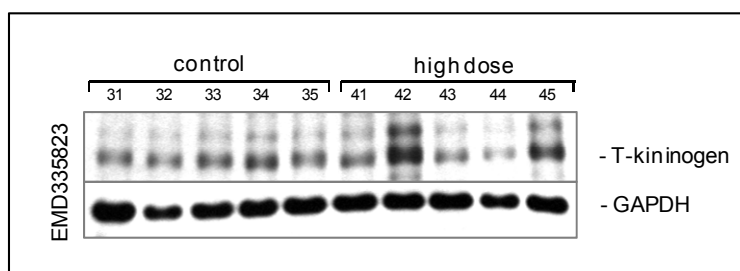


Figure 28. Overexpression of thiostatin in livers of Wistar rats treated with 350 mg/kg bw for 14 days (n=5), demonstrating an increase in the amount of protein particularly in affected high dose animals as compared to controls.

*PON1 activity assay*

The activity of PON1 was significantly reduced in serum of rats treated with 350 mg/kg bw EMD335823 after 3 and 14 days although no histopathological alterations were observed in response to EMD335823 at day 3 (Table 35). Changes in PON1 enzyme activity were not associated with down-regulation of mRNA expression in the liver.

Table 35. PON1 activity in rats administered with EMD335823 over a period of 1, 3 and 14 days (C = 0 mg/kg bw, LD = 15 mg/kg bw, HD = 350 mg/kg bw). PON1 activities are presented as mean  $\pm$  standard deviation (n=5). Statistical analysis was performed by ANOVA and Dunnett's post hoc test (\* p < 0.05, \*\*p < 0.01, \*\*\*p < 0.001).

Compound	Days of treatment	Serum PON1 Activity [Unit/ml]		
		C	LD	HD
EMD335823	1	31.2 $\pm$ 4.7	31.3 $\pm$ 4.2	29.7 $\pm$ 3.2
	3	36.4 $\pm$ 6.4	29.1 $\pm$ 2.2	8.1 $\pm$ 0.6 <sup>1</sup> ***
	14	27.0 $\pm$ 1.7	27.7 $\pm$ 4.4	18.7 $\pm$ 6.3 *

<sup>1</sup> Samples from only two high dose animals (no. 26, 27) were available on day 3.

**3.2.2.4 Immunolocalization of putative biomarkers**

Immunohistochemical staining in liver TMAs showed a marked induction of NGAL and clusterin only in single animals 42 and 45, localized predominantly in hepatocytes and biliary cells in regions of liver with marked histopathological changes (Figure 29a).

Similar to results obtained after treatment with BAY16, strong immunoreactivity against NGAL was also observed in kidney tubule cells in individual high dose animals at day 14, in which marked hepatotoxicity but no signs of kidney injury were evident (Figure 29b).

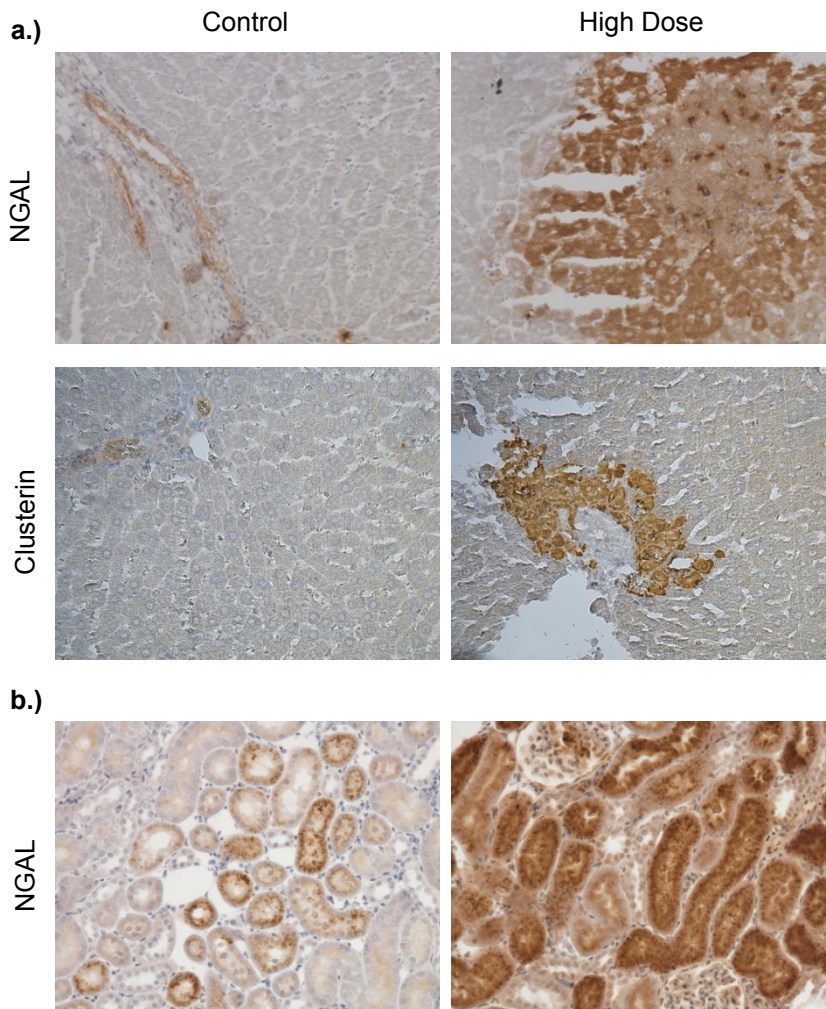


Figure 29.  
(a) Localization of NGAL and clusterin in liver tissue of individual high dose animals after treatment with EMD335823 for 14 days. (b) Vesicular immunostaining of NGAL in proximal tubule cells in kidney sections after treatment with EMD335823.

#### 3.2.2.5 Summary

The pharmacological action of EMD335823 involves inhibition of the enzyme aldose reductase (AR), which prevents, delays or even reverses diabetic changes in the lens, kidney, and nerves. The AR catalyzes the reduction of glucose to sorbitol, the first reaction in the polyol pathway of glucose metabolism. Activation of the polyol pathway due to increased aldose reductase activity is one of several mechanisms that have been implicated in the development of various secondary complications of diabetes. The accumulation of sorbitol under hyperglycemic conditions causes osmotic imbalance leading to cell swelling retinopathy and neuropathy. AR is also involved in detoxification of reactive aldehydes which are formed during lipid peroxidation, such as 4-hydroxy-trans-2-nonenal, acrolein, crotonaldehyde and their corresponding glutathione (GSH) conjugates

[216]. The impaired detoxification of toxic lipid peroxidation products through inhibition of AR by EMD335823 may provide an explanation for the observed damage to cellular macromolecules and is presumed to be responsible for liver injury.

Investigation of putative biomarkers for hepatotoxicity have shown that both NGAL and thiostatin levels in urine and serum generally reflected the onset and degree of liver injury induced by 350 mg/kg bw EMD335823 in individual animals, but changes in protein concentration were not consistently increased before clinical or histopathological changes occurred. Similarly to the results obtained from immunohistochemical analysis of NGAL in kidneys of rats administered with BAY16, strong vesicular brown staining of NGAL was also seen in kidney tubule cells of affected rats, thus confirming that its urinary concentration may be influenced by the release of NGAL into serum due to liver injury and subsequent renal processing. Based on the absence of renal damage as well as the upregulation of NGAL mRNA in the liver (650-fold), it has been suggested that NGAL is not specific for kidney injury and that the presence of NGAL in urine of rats treated with EMD335823 may have occurred as a result of glomerular filtration and tubular reabsorption of NGAL produced by the liver in response to toxic injury.

Results obtained in this study confirm decreased PON1 activity in response to liver injury after 14 days of treatment with 350 mg/kg bw EMD335823, but the lower activity of PON1 observed in rats without evidence of hepatotoxic effects at day 3 indicate that PON1 is not suitable as a reliable biomarker of drug-induced hepatotoxicity. Changes in clusterin expression were also found to be inconsistent with clinical and histopathological findings.

### **3.2.3 Biomarker responses to BI-3 in relation to traditional endpoints of toxicity**

#### **3.2.3.1 Clinicopathological and histopathological observations**

In this study, treatment of male Wistar rats with 100 mg/kg bw and 1000 mg/kg bw of BI-3 for 1, 3 and 14 days resulted in both hepatotoxic and nephrotoxic effects including marked interanimal differences in susceptibility. Renal effects consisted of tubular changes in the form of necrosis, inflammation and dilation in one high dose animal after 3 days (no. 29) and in three animals after 14 day treatment with the high dose (no. 41, 43 and 45) [132]. In addition to kidney injury, liver damage including hepatocyte necrosis, bile duct inflammation and hyperplasia were observed in individual animals at all time points in response to BI-3 (Table 36). Slight to moderate pericholangitis associated with bile duct hyperplasia occurred in almost all animals and distribution and severity of hepatocellular vacuolation increased with time. Administration of 1000 mg/kg bw BI-3 for 14 days lead to

### 3 ASSESSMENT OF CANDIDATE BIOMARKERS OF DILI

cholestasis in all animals, hepatocellular hypertrophy (centrilobular) in 3 animals (no. 41, 42, 44) and minimal single cell necrosis in 2 rats (no. 42, 43) (Table 36).

Table 36. Summary of histopathological changes in the livers of Wistar rats treated with BI-3 for 1, 3 and 14 days. Numbers in parenthesis indicate the number of affected animals in each group (n = 5). Abbreviations: -  $\triangleq$  lesion not observed; +  $\triangleq$  minimal, ++  $\triangleq$  mild, +++  $\triangleq$  moderate and  $\triangleq$  ++++ high severity of lesion.

Histopathological change	BI-3		
	0 mg/kg	100 mg/kg	1000 mg/kg
1 d			
Hepatocyte cell death	-	++ (1/5)	+(2/5), ++ (3/5)
Bile duct inflammation	+(5/5)	+(4/5), +++ (1/5)	+(1/5), ++ (2/5), +++ (2/5)
Bile duct epithelial cell mitosis /hyperplasia	-	+(1/5)	++ (3/5)
<b>Summary score</b>	<b>+(5/5)</b>	<b>+(4/5), +++ (1/5)</b>	<b>+(1/5), ++ (2/5), +++ (2/5)</b>
3 d			
Hepatocyte cell death	-	-	-
Bile duct inflammation	+(5/5)	+(5/5)	++ (2/5), +++ (3/5)
Bile duct epithelial cell mitosis /hyperplasia	-	-	++ (1/5), +++ (4/5)
<b>Summary score</b>	<b>+(5/5)</b>	<b>+(5/5)</b>	<b>++ (1/5), +++ (4/5)</b>
14 d			
Hepatocyte cell death	++ (1/5)	-	+(2/5)
Bile duct inflammation	+(5/5)	+(1/5), ++ (4/5)	+++ (4/5)
Bile duct epithelial cell mitosis /hyperplasia	-	+(1/5)	++ (1/5), +++ (4/5)
<b>Summary score</b>	<b>+(5/5)</b>	<b>+(1/5), ++ (4/5)</b>	<b>+++ (5/5)</b>

Measurement of liver enzymes in serum showed elevated level of AST, ALT and ALP with maximal effects occurring in rats with histopathological changes in the liver after treatment with 1000 mg/kg bw BI-3 (Table 37). At the same time, an increase in serum creatinine and BUN indicative of impaired kidney function was observed in the high-dose group, although this effect were not statistically significant due to interanimal variability. A marked decrease in body weight (20 % compared to controls) associated with reduced food intake was recorded in high dose animals (1000 mg/kg bw) at the end of the 14-day dosing period. At this time point, an increase in the number of neutrophils was observed in individual high-dose animals, especially in rats 41 and 43.



### 3 ASSESSMENT OF CANDIDATE BIOMARKERS OF DILI

Table 37. Summary of clinical parameters in serum and urine of rats treated with BI-3 for up to 14 days. Data are presented as mean  $\pm$  standard deviation (n = 5). Statistical analysis was performed by ANOVA and Dunnett's post hoc test (\* p < 0.05, \*\*p < 0.01, \*\*\*p < 0.001).

	Day	BI-3		
		0 mg/kg	100 mg/kg	1000 mg/kg
<b>Urine</b>				
Creatinine [mg/16h]	1	7.9 $\pm$ 1.3	8.5 $\pm$ 0.8	6.8 $\pm$ 1.6
	3	8.1 $\pm$ 1.5	8.9 $\pm$ 1.3	6.3 $\pm$ 1.1
	12	7.7 $\pm$ 1.2	7.7 $\pm$ 2.0	5.5 $\pm$ 1.8
Protein [mg/mg creatinine]	1	0.5 $\pm$ 0.1	0.5 $\pm$ 0.1	0.7 $\pm$ 0.6
	3	0.5 $\pm$ 0.1	0.7 $\pm$ 0.2	1.1 $\pm$ 0.9
	12	0.7 $\pm$ 0.6	1.1 $\pm$ 0.9	0.6 $\pm$ 0.4
<b>Serum</b>				
Creatinine [mg/dl]	1	0.51 $\pm$ 0.03	0.46 $\pm$ 0.03	0.47 $\pm$ 0.03
	3	0.52 $\pm$ 0.04	0.45 $\pm$ 0.04 *	0.48 $\pm$ 0.04
	14	0.52 $\pm$ 0.07	0.53 $\pm$ 0.05	0.65 $\pm$ 0.32
Blood urea nitrogen (BUN) [mg/dl]	1	49 $\pm$ 6	53 $\pm$ 17	46 $\pm$ 9
	3	50 $\pm$ 7	48 $\pm$ 7	67 $\pm$ 19
	14	45 $\pm$ 6	60 $\pm$ 6	110 $\pm$ 72
$\gamma$ -Glutamyltransferase (GGT) [U/l]	1	0.0 $\pm$ 0.0	0.0 $\pm$ 0.0	1.7 $\pm$ 1.4 **
	3	0.0 $\pm$ 0.0	0.0 $\pm$ 0.0	1.6 $\pm$ 2.4
	14	0.0 $\pm$ 0.0	0.0 $\pm$ 0.0	1.6 $\pm$ 1.3 **
Total protein [g/l]	1	59 $\pm$ 1	58 $\pm$ 2	61 $\pm$ 2
	3	59 $\pm$ 1	58 $\pm$ 3	56 $\pm$ 3
	14	58 $\pm$ 2	55 $\pm$ 2	45 $\pm$ 6 ***
Aspartate aminotransferase (AST) [U/l]	1	193 $\pm$ 37	167 $\pm$ 38	298 $\pm$ 195
	3	190 $\pm$ 25	172 $\pm$ 22	215 $\pm$ 43
	14	157 $\pm$ 19	151 $\pm$ 27	144 $\pm$ 40
Alkaline phosphatase (ALP) [U/l]	1	182 $\pm$ 25	149 $\pm$ 32	513 $\pm$ 289 *
	3	197 $\pm$ 47	177 $\pm$ 36	425 $\pm$ 77 ***
	14	114 $\pm$ 11	116 $\pm$ 13	262 $\pm$ 90 **
Alanine aminotransferase (ALT) [U/l]	1	31 $\pm$ 5	28 $\pm$ 14	169 $\pm$ 185
	3	24 $\pm$ 4	22 $\pm$ 2	43 $\pm$ 14 **
	14	24 $\pm$ 4	28 $\pm$ 10	24 $\pm$ 4
Triglycerides [mg/dl]	1	64 $\pm$ 33	64 $\pm$ 22	73.8 $\pm$ 11
	3	65.6 $\pm$ 25	79 $\pm$ 27	36 $\pm$ 15
	14	87.4 $\pm$ 22	86 $\pm$ 6	51 $\pm$ 18
Glucose [mg/dl]	1	147 $\pm$ 11	132 $\pm$ 23	152 $\pm$ 20
	3	144 $\pm$ 20	143 $\pm$ 8	122 $\pm$ 6 *
	14	148 $\pm$ 14	163 $\pm$ 4	128 $\pm$ 47
<b>Blood</b>				
Neutrophiles [10 <sup>9</sup> /l]	1	1.04 $\pm$ 0.40	0.91 $\pm$ 0.10	1.56 $\pm$ 0.25 *
	3	1.30 $\pm$ 0.15	1.21 $\pm$ 0.50	1.47 $\pm$ 0.54
	14	1.30 $\pm$ 0.20	1.54 $\pm$ 0.94	4.11 $\pm$ 4.23

3.2.3.2 Gene expression of biomarkers

Analysis of gene expression using qRT-PCR technology demonstrated upregulation of NGAL mRNA in livers of individual animals at all time points, although these effects were not statistically significant due to high variability between rats treated with the high dose of BI-3 (Figure 30a). Significant dose-dependent changes in mRNA expression of T-kininogen were evident as early as 1 day after administration with 1000 mg/kg BI-3 (Figure 30b). Compared to NGAL, the induction of T-kininogen correlated well with the degree of hepatic injury. No-treatment related effects on the expression of clusterin and PON1 in the liver were detected throughout the study (Figure 30c, d).

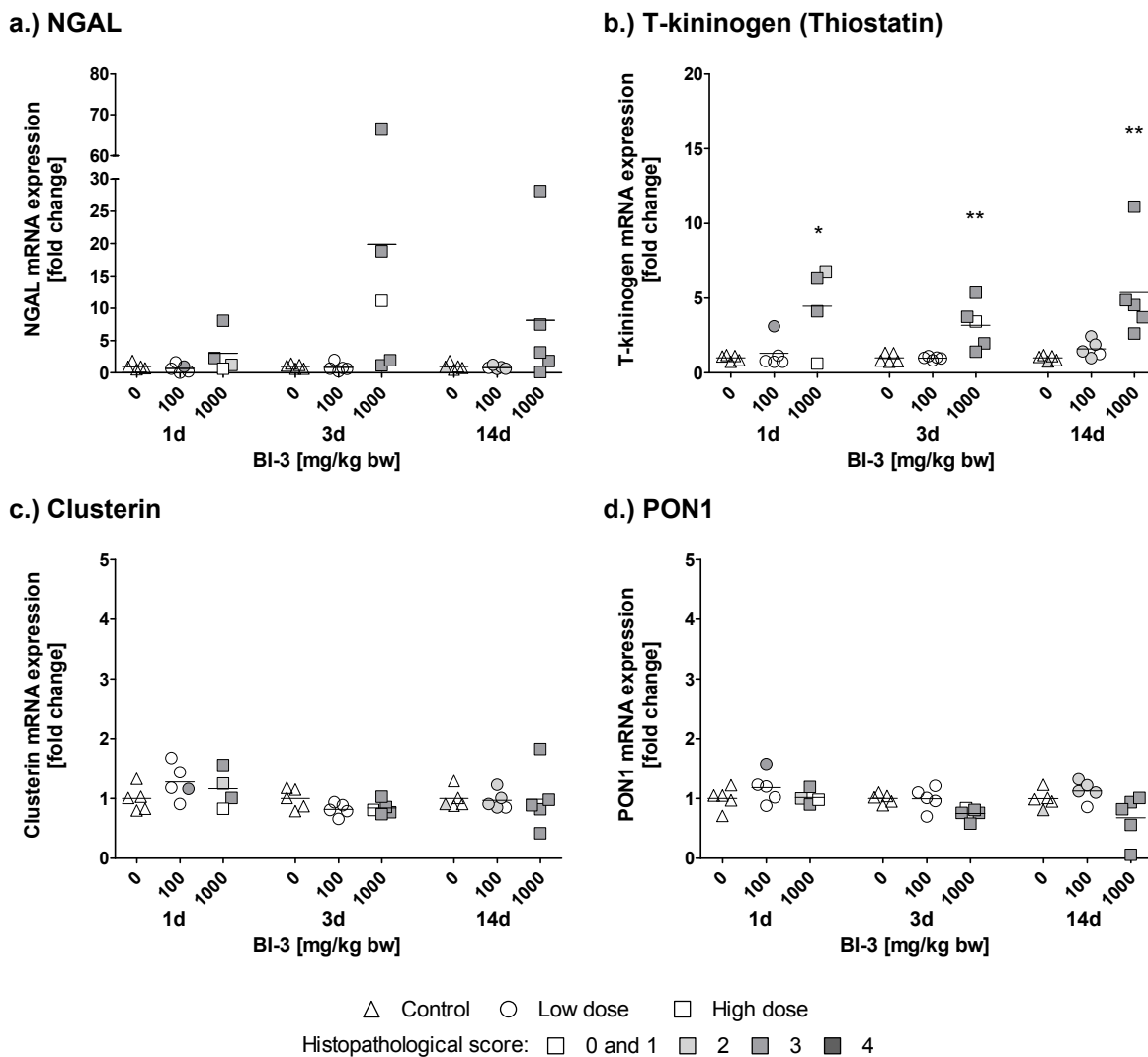


Figure 30. Fold changes in mRNA expression of markers candidates relative to controls in liver of male rats repeatedly dosed with 100 (low dose) and 1000 mg/kg bw BI-3 (high dose) for 1, 3 or 14 days. Data are presented as fold change of individual animals compared to the mean of the corresponding controls, color coded according to their histopathological score of liver injury (n = 5 per group). Mean values of 5 animals per dose group are indicated by a black line. Statistical analysis was performed by ANOVA and Dunnett's post hoc test (\* p < 0.05, \*\*p < 0.01, \*\*\*p < 0.001).

It is important to point out that clusterin and NGAL mRNA levels were increased in kidneys of animals after treatment with 1000 mg/kg bw BI-3 for 14 days as a result of BI-3-induced nephrotoxicity [132] (Table 38). Modulation of T-kininogen mRNA expression was also found in the kidney of high dose-rats, but this increase was mainly caused by the high variations due to low basal level of T-kininogen transcription in this organ (Table 38). As expected, no changes in renal PON1 gene expression were detected in this study.

Table 38. Changes in gene expression of candidate markers in kidney of rats after administration of 100 mg/kg bw and 1000 mg/kg bw BI-3. Data are presented as mean  $\pm$  standard deviation (n.d. = not detectable).

Gene title	Days of treatment	Fold deregulation		
		BI-3 [mg/kg bw]		
		0	100	1000
NGAL	1	1.0 $\pm$ 0.6	0.8 $\pm$ 0.7	0.7 $\pm$ 0.4 <sup>1</sup>
	3	1.0 $\pm$ 0.4	1.0 $\pm$ 0.4	1.5 $\pm$ 1.5 <sup>1</sup>
	14	1.0 $\pm$ 0.3	1.7 $\pm$ 0.3	81.6 $\pm$ 151.4 <sup>1</sup>
T-kininogen	1	1.0 $\pm$ 0.4	2.7 $\pm$ 2.4	5.3 $\pm$ 5.2 <sup>2</sup>
	3	1.0 $\pm$ 1.1	0.8 $\pm$ 0.3	13.7 $\pm$ 15.0 <sup>2</sup>
	14	1.0 $\pm$ 1.0	1.0 $\pm$ 0.5	30.5 $\pm$ 46.6 <sup>2</sup>
Clusterin	1	1.0 $\pm$ 0.4	1.1 $\pm$ 0.5	1.0 $\pm$ 0.4 <sup>1</sup>
	3	1.0 $\pm$ 0.2	1.0 $\pm$ 0.3	2.8 $\pm$ 4.4 <sup>1</sup>
	14	1.0 $\pm$ 0.4	1.3 $\pm$ 0.3	39.2 $\pm$ 43.1 <sup>1</sup>
PON1	1	1.0 $\pm$ 0.8	n.d.	2.2 $\pm$ 0.7
	3	1.0 $\pm$ 1.1	n.d.	1.9 $\pm$ 0.7
	14	1.0 $\pm$ 2.2	n.d.	n.d.

<sup>1</sup> from [132]

<sup>2</sup> increased gene expression due to high variations between animals and low basal level of transcription

### 3.2.3.3 Detection and quantification of biomarkers in serum and urine

#### *ELISA assay*

Elevated excretion of NGAL into urine occurred in individual high-dose rats (no. 41, 43 and 42) after 14 days of treatment with BI-3 (Figure 31b). In contrast, NGAL was undetectable in both urine and serum of animal 45, correlating well with the lack of changes in NGAL mRNA expression in kidney and liver. In rats no. 41 and 42, urinary concentration of NGAL were increased as early as day 1, however, changes were not statistically significant due to high variability in between animals of this group (Figure 31b). Levels of NGAL in serum were only affected in individual rats following 14 days treatment with the high dose (Figure 31a).

In contrast to NGAL, levels of thiostatin in serum appeared to reflect liver injury and hepatic thiostatin (T-kininogen) mRNA expression better than measurement of urinary thiostatin, with statistically significant changes in serum occurring within 1 day of administration of a single dose (Figure 31c, d).

Increased concentrations of clusterin were observed in urine and serum of individual animals in response to 1000 mg/kg bw BI-3, despite absence of changes in mRNA liver expression (Figure 31e, f). Changes in the level of urinary clusterin were found in high dose at day 3 and 14, particularly in animals 41, 43, and are thus consistent with over-expression of clusterin in kidneys of these animals. It thus appears that the kidney as a further target of BI-3 toxicity may also be a source of clusterin and that elevated serum or urinary clusterin may be associated with kidney injury rather than hepatotoxicity.

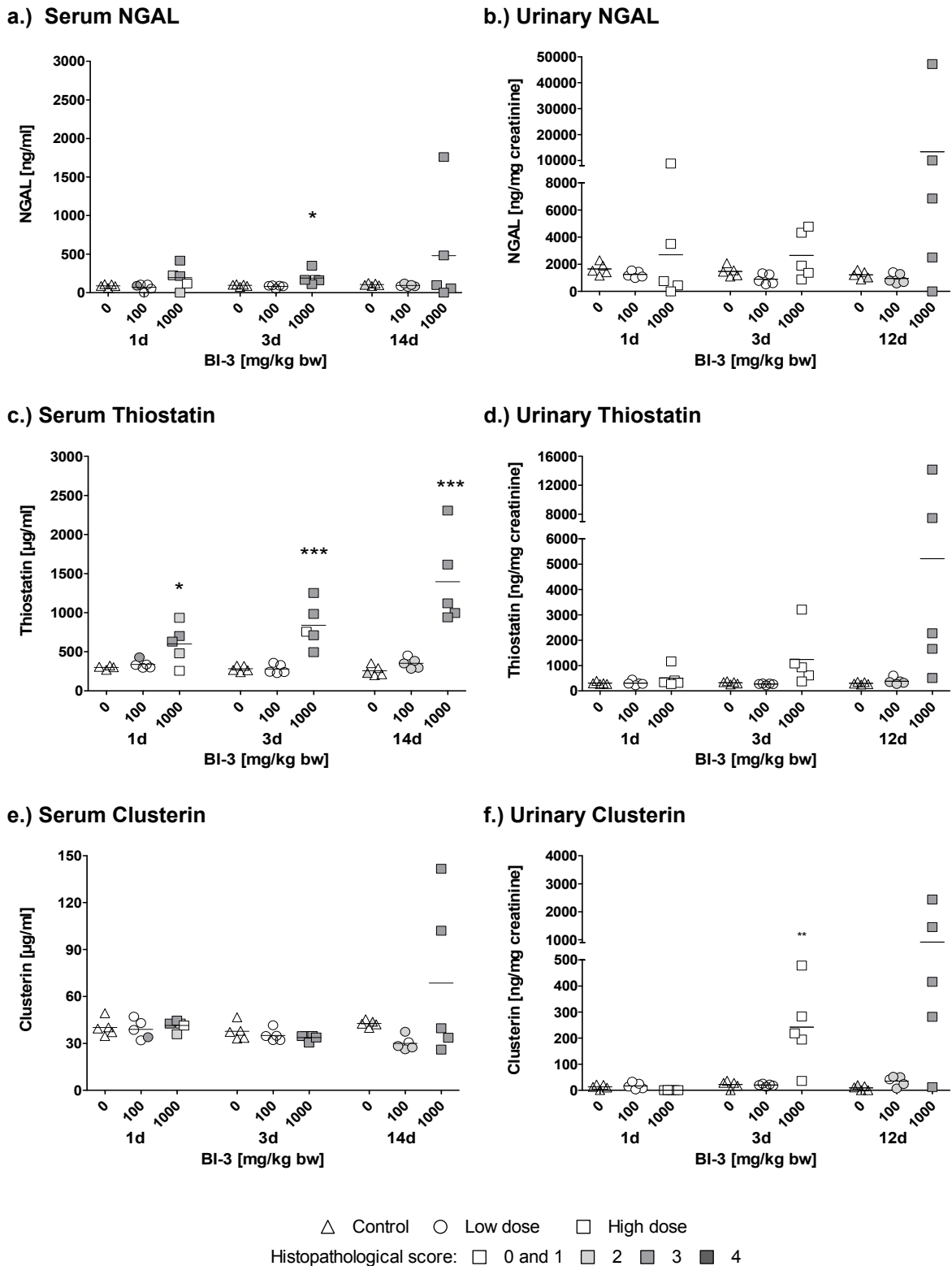


Figure 31. Protein expression of NGAL, thioistatin and clusterin in serum and urine of rats orally treated with 0, 100 and 1000 mg/kg bw BI-3. Data are presented as individual animals, color coded according to histopathology scores for liver damage. For urinary markers after 1 and 3 days of treatment, no corresponding histopathology readouts are available as histopathology at these time-points was performed from groups of rats treated in parallel. Mean values of 5 individual animals per dose group are indicated by a black line. Statistical analysis was performed by ANOVA and Dunnett's post hoc test (\* p < 0.05, \*\*p < 0.01, \*\*\*p < 0.001).

*Western blot of thiostatin*

Consistent with results obtained by qRT-PCR and sandwich ELISA, alteration in the protein expression of thiostatin in liver homogenates was detected in high dose rats 41 and 43 (Figure 32).

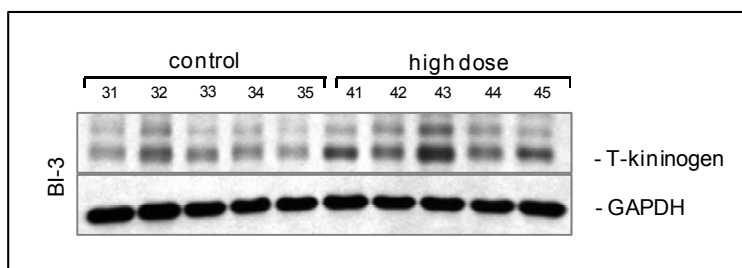


Figure 32. Protein expression of thiostatin in livers of rats treated with 0 and 1000 mg/kg bw BI-3 for 14 days (n=5).

*PON1 activity assay*

A dose-dependent decrease in PON1 activity was found in serum of rats treated with BI-3 for 14 days, whereas PON1 activity appeared to increase after single administration of a high dose of BI-3 (Table 39).

Table 39. Enzymatic activity of serum PON1 in male Wistar rats following treatment with BI-3 (C = control, LD = low dose, HD = high dose). PON1 activities are presented as mean  $\pm$  standard deviation (n = 5). \* p < 0.05, \*\* p < 0.01, \*\*\* p < 0.001 (ANOVA + Dunnett's post hoc test).

Compound	Days of treatment	Serum PON1 Activity [Unit/ml]		
		C	LD	HD
BI-3	1	30.3 $\pm$ 4.5	40.6 $\pm$ 14.1	62.2 $\pm$ 23.9 *
	3	45.3 $\pm$ 19.9	25.4 $\pm$ 4.6	27.3 $\pm$ 18.9
	14	43.4 $\pm$ 25.4	19.9 $\pm$ 5.2	10.9 $\pm$ 3.8 **

**3.2.3.4 Immunolocalization of putative biomarkers**

Immunohistochemical analysis of NGAL on liver TMAs showed no clear alterations in NGAL protein expression after treatment with BI-3 for 3 days, despite changes at the mRNA level (Figure 33). However, the quality of the TMAs was poor and some tissue pieces easily detached from the slides so that later time-points could not be assessed. As NGAL gene expression was induced in both liver and kidney, it is not possible to determine whether the increase in serum and urine NGAL observed in individual animals is related to liver or kidney injury or both.

Although, increased immunoreactivity of clusterin was found in liver sections of affected

rats treated with BI-3, no changes in clusterin mRNA were observed in rat liver in contrast to the kidney (Figure 33).

Increased nuclear staining of PCNA indicated enhanced proliferation of hepatocytes and biliary cells in tissues from high dose animals after 14 days (Figure 33).

Consistent with immunohistochemical staining of Timp-1 in liver TMAs of rats treated with BAY16, Timp-1 was also localized in biliary cells, but no increase in protein expression per cell were observed in livers of high-dose animals (Figure 33). This observation suggests that enhanced expression of Timp-1 mRNA may be due to bile duct hyperplasia [97].

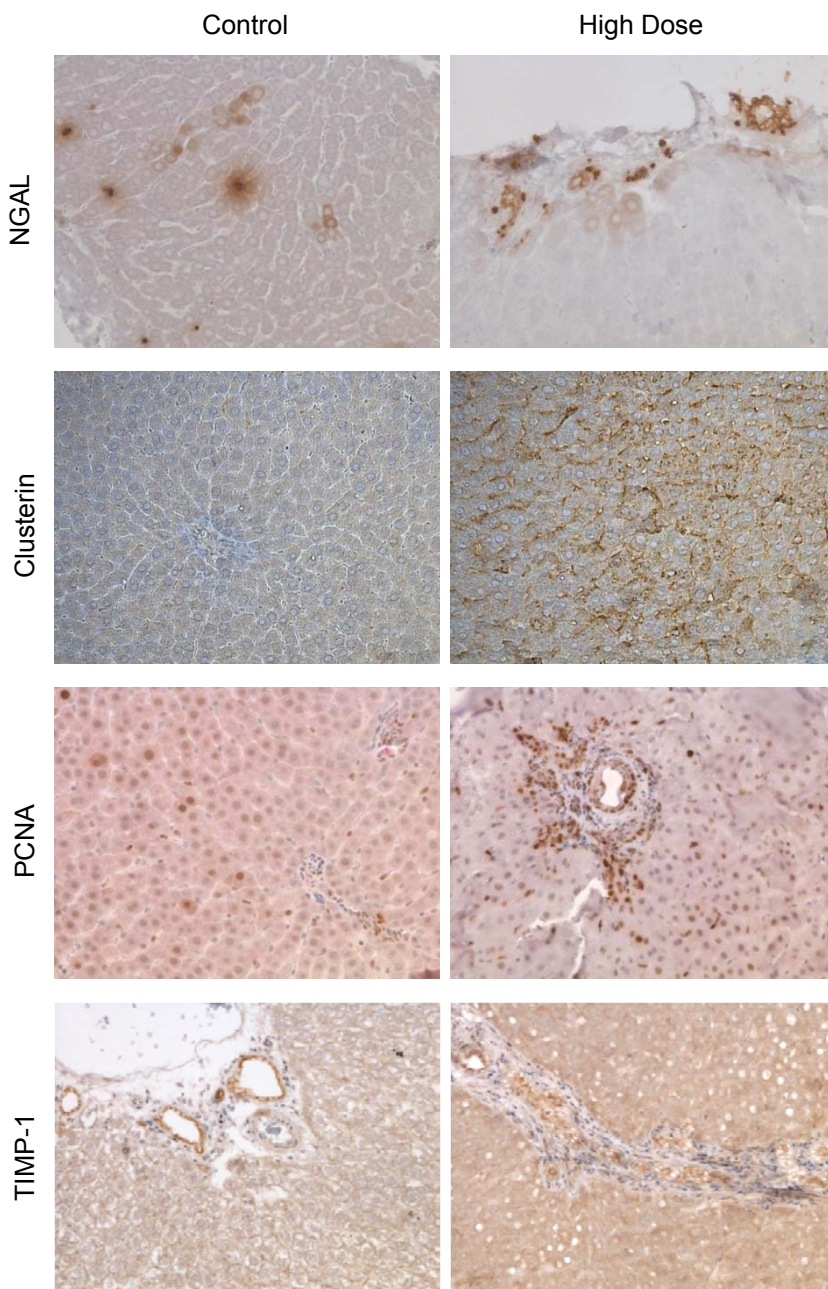


Figure 33. Subcellular distribution, localization and expression of proteins in liver sections of male Wistar rats after administration of 0 and 1000 mg/kg bw BI-3 for 3 and 14 days.

#### **3.2.3.5 Summary**

The drug candidate BI-3, a non-peptide platelet fibrinogen receptor antagonist, was synthesized to inhibit the aggregation of platelets by blocking fibrinogen binding to its receptor and was designed as a new therapeutic agent for the treatment of thromboembolic disease. A preclinical study conducted within the frame of the PredTox project showed that oral administration of 100 mg/kg and 1000 mg/kg bw BI-3 for 1, 3 and 14 days caused dose- and time-dependent histopathological effects in livers and kidneys of male Wistar rats [97, 106, 132, 205]. During evaluation of urinary and serum proteins as non-invasive biomarkers for liver injury, the occurrence of nephrotoxic effects must be considered in this study.

Due to the fact that NGAL mRNA both in liver and kidney of treated rats were up-regulated, it can be assumed that the increase of NGAL in urine and serum may originate from tissue injury in both organs induced by 1000 mg/kg bw BI-3. This is in contrast to BAY16 and EMD335823, where marked NGAL gene expression changes occurred exclusively in the liver as the target organ of toxicity. Release of thiostatin into serum following exposure to BI-3 at a high dose as early as day 1 is due to upregulation within the liver and correlated with histopathological alterations. However, the rise of urinary thiostatin occurred after 2 weeks, and may also be caused by increased mRNA expression in the kidney in response to renal injury, especially in rat 45. Thus, thiostatin does not appear to be specific for liver injury but may serve as a non-invasive, general marker of tissue injury. Previous studies have demonstrated an enhanced expression of clusterin protein and mRNA in the kidney of affected high-dose animals after 14 days of treatment with BI-3 [132], whereas no changes in the clusterin mRNA level could be detected in the liver. The observed induction of serum and urinary clusterin in the present study may be primarily attributed to the nephrotoxic effect caused by BI-3. Therefore, it can be concluded that the use of clusterin as a non-invasive biomarker of hepatotoxicity is limited. Although serum PON1 activity was significantly lower in rats given 1000 mg/kg bw BI-3 for 14 days than in control rats, single administration of BI-3 resulted in an increase of enzyme activity. Results from this study show that the activity of PON1 is not consistently decreased in response to liver injury and therefore not suitable as an universal marker for detection of hepatotoxicity.

#### **3.2.4 Evaluation of candidate biomarkers using ROC analyses**

In a cross-study analysis, receiver operating characteristic (ROC) analysis was used to determine the ability of the biomarker candidates to discriminate animals without evidence of liver toxicity from those with hepatocyte and bile duct damage. The area under the ROC



curve (AUC), which serves as a measure for the diagnostic accuracy of biomarkers, is described by calculating the sensitivity and specificity [217]. Sensitivity is the probability that a truly diseased individual is correctly categorized and specificity is the probability that a nondiseased individual is identified. For example, an AUC value of 0.90, which would represent an excellent biomarker, means that 90 % of all samples are correctly classified as either healthy or diseased groups, whereas an AUC of 0.50 means that classification is random. Due to the large background variability observed between all three studies conducted at different sites, all values were normalized to corresponding controls prior to ROC analysis using the GraphPad Prism 5 software package. The statistical analysis revealed thiostatin (T-kininogen) as the most sensitive serum marker (AUC 0.92) and marker gene (AUC 0.90) (Figure 34). Moreover, serum thiostatin, but not NGAL, clusterin or PON-1, was found to be a better indicator of drug-induced hepatobiliary injury than the conventional parameters ALP, ALT, and AST (AUC 0.71-0.85).

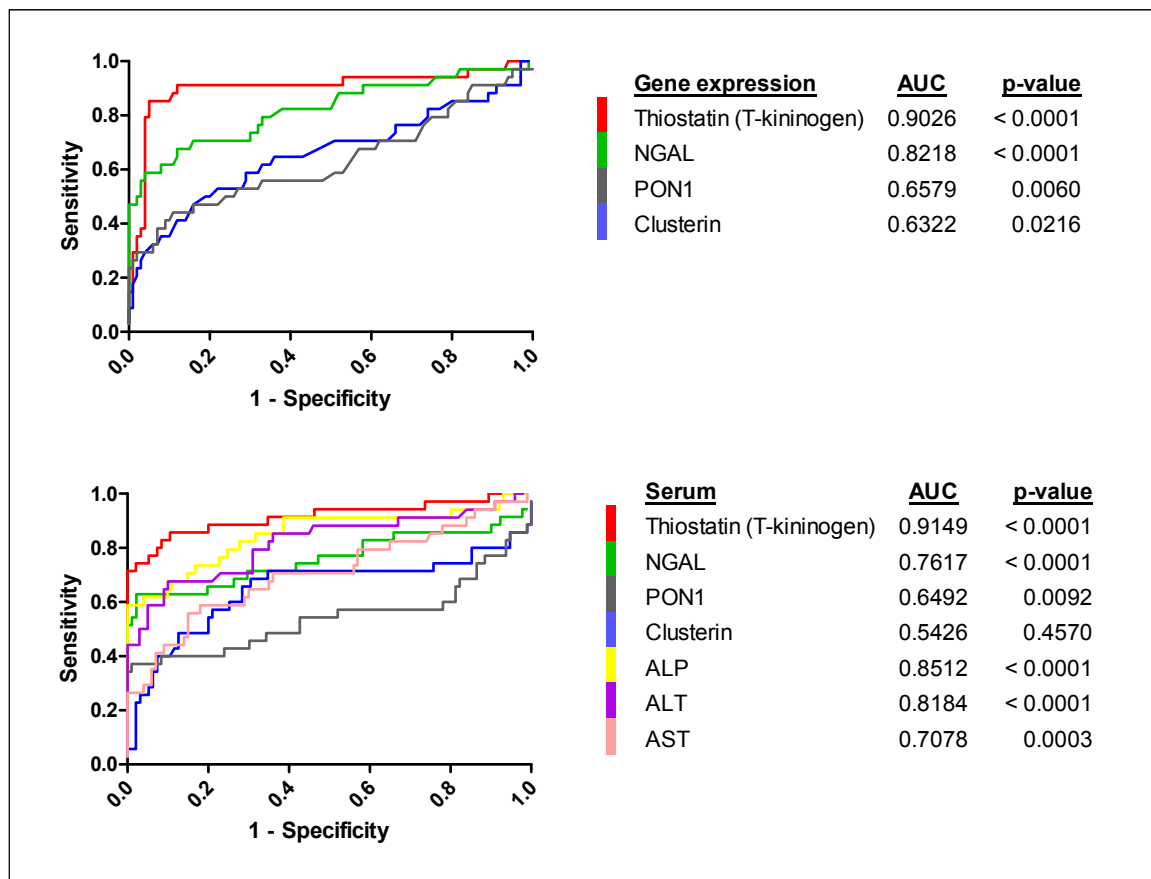


Figure 34. Receiver-operator characteristics (ROC) curves for candidate biomarker gene and serum biomarkers compared to traditional clinical chemistry parameters. Analysis was performed using normalized data of all animals of the three studies with a corresponding histopathological readout. For calculation of the ROC curve, data obtained from rats with a hepatocyte and bile duct damage histopathology score > 1 was considered as positive (diseased group), and control as well as treated rats with no clear signs of liver injury (histopathology score < 1) was considered as negative (healthy group).

## **3.3 Discussion**

### **3.3.1 NGAL as a non-invasive marker of acute tissue injury**

NGAL is an acute phase protein expressed by neutrophils and a variety of epithelial cells during inflammation and tissue injury [142, 146, 147, 218]. Previous studies demonstrated increased hepatic NGAL mRNA expression in mice chronically exposed to ethanol [219], under conditions of oxidative stress [220] and in acute endotoxemia [221]. Moreover, gene expression profiling in liver of rats administered model hepatotoxicants, like acetaminophen, carbon tetrachloride, dimethylnitrosamine, and thioacetamide, identified NGAL gene expression as significantly altered more than 2.0-fold by all four chemicals [222]. Increased NGAL expression in injured hepatocytes was found in rats after treatment with carbon tetrachloride and in bile duct ligation induced liver injury [223]. Consistent with these findings, upregulation of NGAL was observed in livers of rats suffering from drug-induced hepatobiliary injury in the present study. Importantly, increased rates of transcription in the target organ were also associated with a rise of NGAL in serum and urine, suggesting that measurement of NGAL in body fluids may provide a diagnostic tool to assess drug toxicity. Urinary excretion of NGAL has previously been regarded as an early biomarker of acute kidney injury [138, 149, 206, 224-227]. However, this and other reports demonstrating increased urinary NGAL accompanied by enhanced immunoreactivity against NGAL in the kidney tubule epithelium in the absence of histopathological signs of nephrotoxicity, suggest that a rise in urinary excretion of NGAL may not be specific for kidney injury but may also occur as a result of increased transcription in response to systemic inflammation or tissue damage at other sites, and subsequent renal handling of NGAL [228]. Indeed, it is known that the low molecular weight lipocalins may be freely filtered in the glomeruli, bound to the scavenger-receptor megalin, which is expressed specifically at the brush borders of proximal tubules, taken up by endocytosis and stored in lysosomes [229].

### **3.3.2 Thiostatin as a sensitive marker of hepatotoxicity**

Thiostatin (T-kininogen) is a rat-specific 56 kDa glycoprotein and major acute phase protein which is synthesized primarily in liver and released into plasma during acute inflammatory conditions, e.g. in response to endotoxemia [152, 153]. While it has not been previously associated with drug-induced liver toxicity, proteomics profiling conducted as part of the InnoMed PredTox project recently identified thiostatin as being elevated in urine of rats suffering from hepatobiliary injury induced by treatment with EMD335823 and BI-3 (unpublished data). To further assess the sensitivity and time- and dose-dependency of the response, we used an ELISA assay to quantify thiostatin in urine and serum along

with the determination of its mRNA expression in the target organ. ELISA analyses confirmed increased urinary excretion of thioistatin in response to 14-day treatment with EMD335823 and BI-3, and revealed elevated thioistatin levels at earlier time points than previously examined. In addition, hepatobiliary toxicity caused by a further drug candidate not previously investigated, BAY16, was also found to cause a marked rise in urinary thioistatin. However, modulation of urinary thioistatin occurred late, compared to the corresponding transcriptional changes and histopathological alterations. Therefore, we speculated that thioistatin in serum may be a more suitable marker of hepatotoxicity than thioistatin excretion into urine. Indeed, statistically significant changes in serum thioistatin were evident as early as day 1 after treatment with BAY16 and BI-3 and, while in good agreement with liver pathology, preceded alterations in the activity of serum transaminases. In support of these observations, ROC analysis confirmed serum thioistatin as a better diagnostic marker of drug-induced hepatobiliary injury than conventional clinical chemistry parameters. To date, little is known regarding the function of thioistatin. It has been speculated that as a potent inhibitor of cysteine proteases, thioistatin may afford protection to healthy cells against proteolytic enzymes released during inflammation and tissue damage [150, 230]. However, as the liver is known to be the primary source of plasma proteins, including thioistatin [231], it is important to note that increased hepatic expression and alterations in circulating thioistatin levels are not necessarily indicative of liver injury but may also occur in response to tissue injury at other sites, e.g. the kidney [232]. Given the sensitivity of the response, however, our results suggest that incorporation of thioistatin into the current battery of tests may enhance our ability to non-invasively diagnose drug-induced tissue damage and inflammation during preclinical safety assessment. Unfortunately, translation into the clinic may be hampered by the fact that thioistatin (T-kininogen) appears to be formed exclusively in the rat and no human equivalent has been reported to date.

#### **3.3.3 Evaluation of PON1 activity for detection of liver damage**

Reduced activity of the antioxidant enzyme PON1, most likely as a result of decreased PON1 expression and secretion by the liver, has been suggested as an early biochemical change indicative of hepatotoxicity based on an inverse correlation between hepatic and/or serum PON1 activity and liver function in human and experimental liver disease models, including chronic hepatitis and liver cirrhosis [115, 117, 118, 233]. Similarly, proteomics analysis of rat liver protein extracts identified PON1 as significantly down-regulated following treatment with acetaminophen and compound A [117, 119]. Although results from our studies demonstrated reduced serum PON1 activity in the absence of

changes at the mRNA level in response to liver injury induced by BI-3 and EMD335823, the lack of effects on PON1 activity in rats treated with BAY16, in which marked histopathological alterations were seen, suggests that serum PON1 may not represent a reliable marker of drug-induced hepatotoxicity. Moreover, while PON1 as a down regulated marker has been recommended as a valuable addition to a liver biomarker panel [234], the unexpected finding that PON1 activity (but not gene expression) appeared to increase after single administration of a high dose of BI-3 is difficult to reconcile with our expectations of a reliable biomarker. Similarly, a recent study reported increased rather than decreased hepatic and serum PON1 activity in parallel to a rise in serum ALT activity in rats given a single dose of cyclophosphamide [235]. In the absence of further data supporting the value of PON1 as a marker of drug-induced liver injury, these findings suggest that modulation of PON1 activity may at least in part depend on the compound rather than being a regular feature of drug-induced liver damage, although it seems indisputable that a considerable impairment of liver function may result in a decline in PON1 activity secondary to decreased PON1 expression.

#### **3.3.4 Expression of clusterin as a marker for liver damage**

Clusterin, which is also under evaluation as a urinary biomarker of proximal tubule injury [132, 190, 214, 215], was recently found to be significantly up-regulated in livers of rats treated with a range of hepatotoxins, including carbon tetrachloride, alpha-naphthylisothiocyanate, acetaminophen and chloroform [104]. Moreover, clusterin was among the top-scoring gene set responsible for the correct discrimination between hepatotoxic and nonhepatotoxic model compounds [104]. While these data suggested that clusterin expression and subsequent release into body fluids may serve as a promising marker of drug-induced liver injury, hepatic expression as well as concentrations of clusterin in serum did not correlate well with the histopathological changes seen in response to BI-3 and EMD335823 in the present study. The poor diagnostic value of clusterin as an indicator of drug-induced liver injury is also reflected by the small area under the ROC curve. While the significant increase in urinary excretion of clusterin observed in rats treated with BI-3 is likely related to the drug's nephrotoxic effects, it is interesting to note that elevated urinary levels were also seen in individual animals dosed with EMD335823 and BAY16, which were not associated with kidney injury. Thus, the possibility that increased urinary clusterin levels may not be as specific for kidney injury as generally assumed should be taken into consideration when applying clusterin as a novel biomarker of nephrotoxicity.

### 3.4 Conclusion

This *in vivo* study was designed to evaluate the performance of a set of non-invasive candidate markers for improved detection of drug-induced liver injury as compared to traditional hepatotoxicity clinical chemistry parameters. Thus, the potential of literature and omics derived markers, i.e., PON1, thiostatin, NGAL and clusterin, as novel preclinical markers of hepatobiliary toxicity was assessed following treatment of male Wistar rats with drug candidates that were dropped from further development, in part due to hepatotoxicity. The comprehensive analysis of candidate serum biomarkers of liver injury and corresponding transcriptional changes in the target organ provided important information regarding the ability of these candidate liver markers to accurately detect drug-induced hepatotoxicity.

Our results have shown that a rise in serum thiostatin, which was accompanied by a corresponding increase in the rate of transcription of thiostatin (T-kininogen) in the target organ and correlated well with the progressive histopathological changes, may provide a more sensitive - albeit not necessarily specific - indicator of drug-induced liver damage than current clinical chemistry parameters, i.e. serum transaminases and alkaline phosphatase. While data obtained from this study suggest that thiostatin may be a promising marker of inflammation and tissue damage in toxicity studies in rats, further evaluation of its sensitivity and specificity is needed.

In contrast, NGAL, PON1 and clusterin were not consistently altered and thus only provide limited additive information to the traditional liver enzymes in detecting drug-induced hepatotoxicity. Further analysis demonstrated that increased protein levels of NGAL in kidney and/or urine are not as specific for kidney injury as generally assumed, but may also occur in response to inflammation and tissue damage at other organs, e.g. the liver. Our data suggest that serum NGAL may serve as an early, sensitive and minimally invasive indicator of inflammatory responses.

Immunolocalization studies showed good agreement with gene expression and histopathological changes, providing mechanistic insight into the initiation and progression of toxic injury but did not provide an indication of hepatotoxicity at earlier time points or at lower doses than histopathology.

# 4 APPLICATION OF TOXICOGENOMICS TO IMPROVE MECHANISTIC UNDERSTANDING OF DRUG-INDUCED HEPATOTOXICITY

## 4.1 Background

DNA microarray technology is the most commonly used technique to analyze the expression of thousand of genes simultaneously. Over the last decades, the assessment of toxicant-induced gene expression profiles by Affymetrix microarray has become a valuable tool in the field of toxicology both to gain a better insight into molecular events underlying mechanism of toxicity and to identify reliable markers of toxicity [96, 236]. A large number of toxicogenomics studies have been carried out to investigate liver injuries caused by a variety of drugs *in vivo* and *in vitro* to generate mechanistic hypotheses or develop predictive models of DILI [101, 104, 155-157, 237-239]. In addition, previous transcriptomics studies conducted within the frame of the InnoMed PredTox project were performed to characterize changes in gene expression in response to several hepatotoxic drug candidates, which may be involved in molecular events leading to the observed toxicities [97, 98]. The analysis of such expression profiles enables identification of differentially expressed genes that may play a key role in various molecular pathways, such as lipid metabolism, fatty acid  $\beta$ -oxidation, mitochondrial homeostasis and ATP production, biotransformation and transport of xenobiotics or oxidative stress [240-243]. Alterations in the expression level of these genes and their encoded protein products may be directly associated with mechanisms leading to hepatotoxicity, or indirectly via regulation of other cell signaling pathways. On the other hand, induction of genes involved in cell proliferation or inflammation may represent regenerative processes which occur in response to tissue damage caused by a cytotoxic effect of the drug on liver cells.

The complexity of different interacting pathways involved in the onset and progression of hepatotoxicity make it difficult to identify the initial molecular events which might be primarily responsible for drug-induced liver injury. Furthermore, mechanistic interpretation of genomics data generated from pharmacologically active compounds can be very difficult, especially if the toxicity occurs in the same organ in which the pharmacological target is present, because changes in expression pattern may represent a combination of therapeutic, adaptive and toxic changes induced by a drug. To reveal relevant molecular mechanism indicative of drug-induced hepatotoxicity, which may be associated with specific pathological features of cholestasis, steatohepatitis, fibrosis or cirrhosis, gene expression changes related to the drug's toxicity need to be differentiated from those that may result from the pharmacological mode of action of a given drug.

#### 4.1.1 Selection of BAY16 as model compound for studying hepatotoxicity

Toxic effect of several drug candidates on the liver of rats were characterized using transcriptomics, metabolomics and proteomics in short-term *in vivo* toxicity studies within the frame of the PredTox project. One of these compounds was BAY16, a glucagon receptor (GCGR) antagonist, which was designed to be used as a therapeutic agent for treatment of type 2 diabetes mellitus. Recent studies indicate that genetic disruption of GCGR signaling increases the susceptibility to hepatosteatosis and hepatocellular injury [244, 245]. Based on these observations, and the fact that the toxicity of BAY16 occurred in the same organ in which the pharmacological target is present, we were interested to investigate whether modulation of the GCGR by BAY16 plays a role in the toxic response in the liver and if it is possible to discriminate gene expression changes related to the pharmacological action from those relevant to the drug's toxicity.

The pathophysiology in patients with type 2 diabetes is characterized by postprandial hyperglycemia due to impaired glucagon suppression as a consequence of insulin resistance or deficiency [246]. Insulin and glucagon are pancreatic hormones that work synergistically to control blood glucose concentrations. An enhanced blood glucose level is related to increased insulin secretion that stimulates glucose uptake and metabolism by activation of glycolysis [247-249]. Glucagon is a 29 amino acid polypeptide released from pancreatic  $\alpha$ -cells in response to hypoglycemia [250]. As a counterregulator to insulin, glucagon increases hepatic glucose levels through induction of glucose synthesis from non-carbohydrate sources, such as pyruvate, amino acid and glycerol (gluconeogenesis) or stimulation of glycogen degradation (glycogenolysis) by activation of the GCGR during periods of fasting [251] (Figure 35). The GCGR is a member of the family B receptors within the G-protein coupled superfamily of seven-transmembrane receptors [252]. Activation of the GCGR is associated with elevated intracellular cAMP concentrations caused by stimulation of adenylate cyclase [253-255]. Increased insulin levels inhibit glucagon release from  $\alpha$ -cells under physiological conditions, but a resistance to the action of insulin on cells or a deficiency observed in patients with type 2 diabetes mellitus is associated with reduced suppression of glucose production.

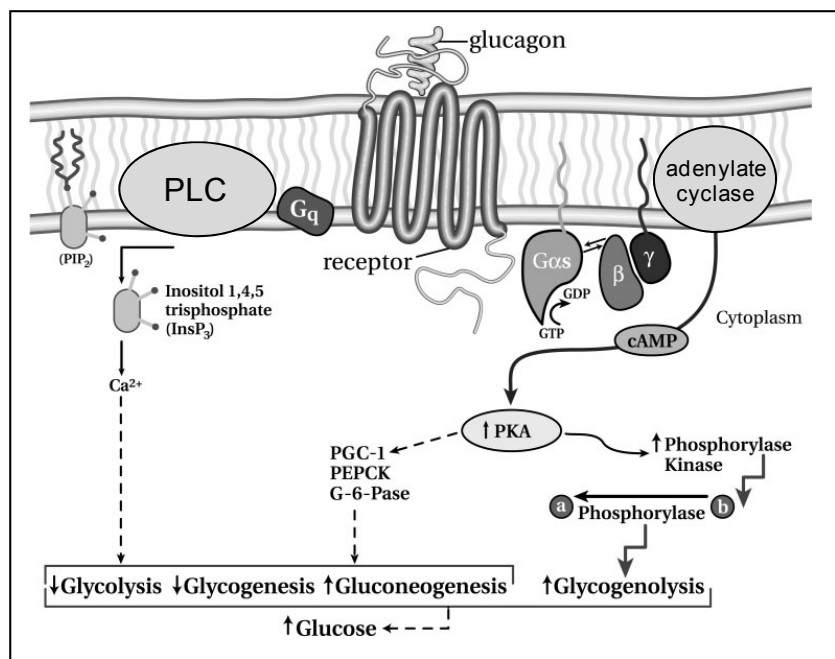


Figure 35. Schematic illustration of glucagon-mediated intracellular signaling cascades (from [251], permission granted by American Physiological Society).

There is evidence suggesting that hyperglucagonemia plays a key role in the initiation of hyperglycemic conditions in diabetic subjects. Hence, new therapeutic approaches focus on the reduction of glucagon secretion or inhibition of GPCR activity to decrease hepatic glucose overproduction in diabetic animals and humans [256]. In recent years, many different classes of competitive and non-competitive GPCR antagonists have been developed such as the triarylimidazoles (Merck) [257], alkylidene hydrazides (Agouron) [258], NNC 25-2504 (Novo Nordisk) [259], 5-Hydroxyalkyl-4-phenylpyridines (Bayer) [260] and Bay 27-9955 (Bayer) [261].

Several studies have shown that exogenous glucagon-induced glucose elevation was successfully blocked by antagonizing the GPCR using peptidyl and non-peptidyl molecules in mice [262] and in human [261]. Moreover, Liang et al. reported that suppression of *GPCR* mRNA expression using antisense oligonucleotides (ASO) leads to reduced levels of blood glucose, triglyceride and free fatty acid and improved glucose tolerance in diabetes (db/db) mice [263]. The improvement of glucose homeostasis has also been observed in *GPCR* knockout mice (*GPCR*<sup>-/-</sup>) showing normal glycemia in the presence of very large glucagon plasma levels, whereas insulin level were unchanged compared to control mice [264, 265].

Despite these desirable effects on glucose metabolism by inhibition of the GPCR, several of such therapeutic candidates failed during non-clinical drug development due to undesirable side effects in the liver. Because little is known concerning the action of this drug candidate on the liver, which is the target organ of both pharmacological activity and toxicity of BAY16, dose-dependent transcriptional changes induced by BAY16 in the liver of rats after treatment with 20 and 100 mg/kg bw for 1, 3 and 14 days were investigated



by genome wide expression analysis using Affymetrix cDNA within the PredTox project [97, 98]. Transcriptomic analyses showed that BAY16 induced liver injury in the form of hepatocellular necrosis and bile duct damage is accompanied by extensive changes in the pattern of hepatic gene expression in rats treated with a toxic dose of 100 mg/kg bw BAY16 [97]. In order to better understand the molecular mechanisms responsible for the initiation of tissue injury, biological functions of deregulated genes and their roles in the liver with respect to the pharmacological modulation of the GCGR were studied. Whereas no morphological effects could be detected after treatment with a low dose of BAY16, more than 200 genes were significantly deregulated more than 1.5-fold at this dose. This included downregulation of several genes involved in gluconeogenesis, fatty acid oxidation or lipid catabolism as well as upregulation of genes involved in glycolysis [97]. The deregulation of these metabolic genes was also strongly affected by high dose treatment at day 1 and 3, and can be related to pharmacological inhibition of the GCGR. Oral administration of BAY16 at 100 mg/kg bw for 3 and 14 days leading to hepatocyte and bile duct injuries was associated with altered expression of genes linked to acute phase response, inflammation and oxidative stress, apoptosis, cell proliferation and tissue reorganization, fibrosis and response to cholestasis [97]. Although a wide range of molecular signaling networks could be identified in the liver of rats exposed to a toxic dose of BAY16, it remains uncertain whether pharmacological modulation of the GCGR by BAY16 is responsible for hepatotoxic effects or some of the gene expression changes.

Even though inhibition of GCGR represents an attractive option for the treatment of type 2 diabetes, several studies have demonstrated that disruption of glucagon signaling was also associated with unexpected phenotypes in mice, including elevated plasma cholesterol levels and increased pancreas weight resulting from  $\alpha$ -cells hyperplasia [264-267]. It has been shown that GCGR<sup>-/-</sup> mice exhibit defects in lipid synthesis,  $\beta$ -oxidation of free fatty acids and secretion of triglycerides during periods of fasting, which suggest that GCGR signaling may be necessary for the regulation of lipid metabolism [244]. This is supported by a transcriptional profiling study in GCGR<sup>-/-</sup> mice, which demonstrated that the genetic knockout of the GCGR leads to upregulation of genes involved in cholesterol and fatty acid biosynthesis, and downregulation of genes encoding enzymes of amino acids catabolic and gluconeogenetic processes [268].

Sinclair et al. found that mice lacking GCGR were more susceptible to liver injury in response to a high fat-diet, whereas administration of glucagon resulted in a lower rate of apoptosis in wild type mice and primary murine hepatocytes [245]. These observations suggest that endogenous GCGR signaling might be important for hepatocyte survival.

Thus, it is critical to examine if the mechanism of toxicity of the drug candidate BAY16 is related to its pharmacologic action and to discriminate between gene expression changes

related to pharmacological vs. toxic effects to provide a better understanding of the key events responsible for the observed toxicity.

### **4.1.2 Experimental approach to discriminate between omics responses related to pharmacological vs. toxic effects**

For a better mechanistic understanding of BAY16 induced transcriptional changes, an *in vitro* study was designed to identify genes associated with the molecular mechanism of BAY16-induced hepatotoxicity (Figure 36).

The first aim of this study was to identify dose-dependent *in vitro* gene expression profiles in response to BAY16 by identifying transcriptional changes in primary rat hepatocytes after treatment with a low and a high dose of BAY16 (untransfected cells, UT) using Affymetrix GeneChip® Rat Genome 230 2.0 Arrays (Figure 36). Furthermore, these effects were compared with BAY16-induced effects observed in the liver of rats, which have already been performed by Ellinger-Ziegelbauer and colleagues as part of the PredTox project [97]. To achieve this, we isolated primary rat hepatocytes from the liver of male Wistar rats, the same strain of rats which was used in the previous preclinical studies within the PredTox project. The comparative transcriptional analysis was also used to evaluate the relevance of primary hepatocytes as an *in vitro* system for studying effects of this compound.

To determine the importance of GCGR-mediated signaling for hepatocytes survival and to select genes modulated by the pharmacological target of BAY16 (on-target effects), as a second aim of this work, both the effects on cell viability and changes in gene expression profiles were studied in primary rat hepatocytes after inhibition of the GCGR mRNA expression by siRNA-mediated gene silencing (siGCGR). The cells were therefore transfected with siRNA targeting GCGR, followed by analysis of downstream effects on gene expression using cDNA microarrays (Figure 36). The expression pattern of silenced hepatocytes was normalized to cells transfected with negative control siRNA (scrambled, SC) to ensure that the observed biological responses were not caused by the transfection procedure itself.

Another objective of this study was to discriminate between those components of the transcriptional response that may result from the pharmacological modulation of the glucagon receptor caused by BAY16 and those that are truly related to BAY16-induced toxicity. This includes a comparative assessment of gene expression changes in non-targeting (SC) and GCGR-targeting (siGCGR) siRNA transfected hepatocyte cultures after exposure to a low and high dose of BAY16 (Figure 36). Normalization of treated hepatocytes to corresponding untreated control group controls for effects induced by lipid-mediated transfection. Changes in the transcriptional response to BAY16 in GCGR-

expressing hepatocytes (SC) may occur due to both on-target effects caused by blocking of the pharmacological target and off-target effects that are characterized by non-specific interaction of the drug. In contrast, effects induced by BAY16 in cells lacking GCGR (siGCGR) may occur independently of GCGR inhibition and would therefore be considered critically involved in the off-target mediated mechanism of BAY16 hepatotoxicity. The comparison of these two datasets may be used to identify molecular events that are induced if no interference with the pharmacological target GCGR has occurred. The experimental design of this study enables us to investigate whether modulation of the pharmacological target of BAY16 plays a role in the toxic response to the drug.

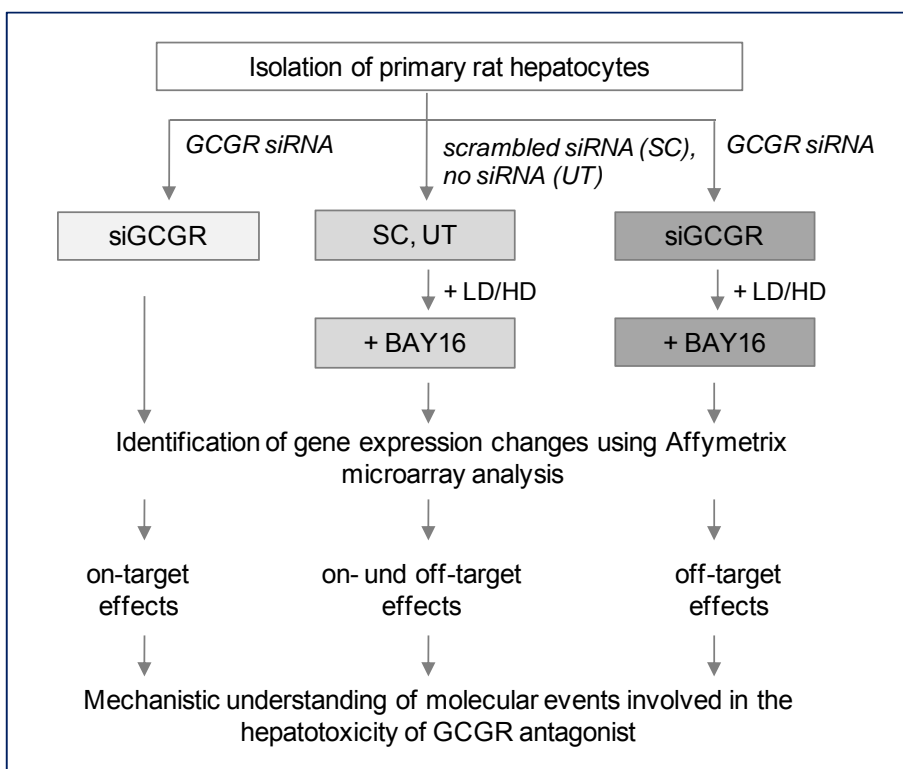


Figure 36. Design of *in vitro* study used for application of toxicogenomics to improve mechanistic understanding of molecular events leading to hepatotoxicity of the GCGR antagonist BAY16.

## 4.2 Effect of BAY16 *in vitro*

To investigate dose-dependent effects of BAY16 using toxicogenomics *in vitro*, the cytotoxic effect of BAY16 on primary rat hepatocytes were initially examined using two cell viability assays and visual inspection by microscopy. The transcriptional profile in primary hepatocytes was then analyzed in cells exposed to two different concentrations of BAY16 for 24 h using cDNA Affymetrix microarrays. The aim of this part of this work was to identify molecular mechanisms that were influenced by alterations in the expression of genes in response to a non-toxic and a toxic dose of BAY16. For a comprehensive

understanding of these mechanisms, the effects observed from *in vitro* investigations were considered in regard to knowledge derived from previous *in vivo* toxicity study.

### 4.2.1 Results

#### 4.2.1.1 Evaluation of BAY16 cytotoxicity in primary rat hepatocytes

Freshly isolated hepatocytes with a viability of more than 85 % were incubated for 24 h to adapt to the cell culture environment. For optimal conditions for the *in vitro* experiments, the primary rat hepatocytes were cultured on collagen monolayers for up to 72 h. After isolation, the cells were incubated with serum-containing medium to enhance the attachment on the bottom of the culture dishes for 4 h. It is known that serum improves the ability of hepatocytes to attach onto the surface of culture dishes [269]. Morphological observations of hepatocytes revealed that cells exhibit their polygonal shape and established cell-cell contacts already after 4 h (Figure 37). During the following 20 h, the hepatocytes formed a confluent monolayer under serum-free conditions and acquired more cuboidal cell morphology (Figure 37). In general, the hepatocytes displayed clear cytoplasm with multiple nuclei, well-defined cytoplasmic membrane and canaliculi-like structures. After 72 h, the hepatocytes spread out and the cytoplasm was more granulated. These findings are consistent with morphological alterations observed in hepatocytes cultured in a monolayer system [78]. Because the cultivation of this system was no longer than 72 h, this aspect does not impact on further investigations.

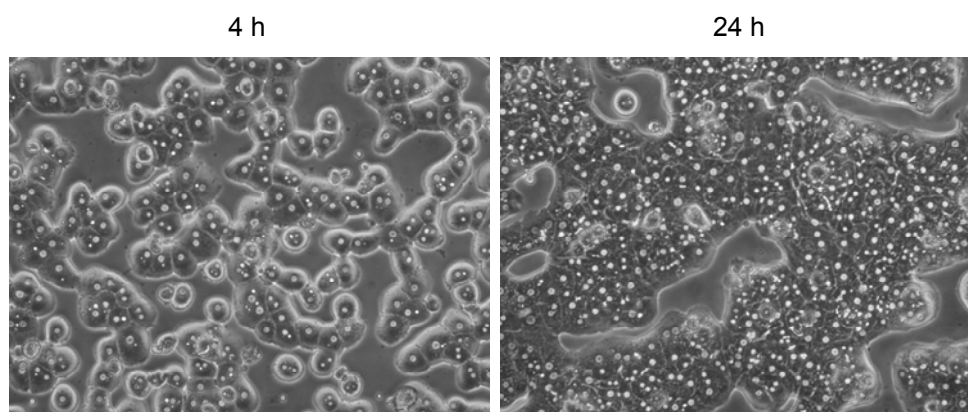


Figure 37. Morphological development of cultured rat hepatocytes 4 h and 24 h after isolation using two-step *in situ* collagenase perfusion method [187, 188].

To evaluate the cytotoxic effect of BAY16 on rat hepatocytes, two different cell viability tests measuring ATP levels (CellTiter-Glo<sup>®</sup> assay) and mitochondrial activity (WST-1 assay) were performed 24 h after cell seeding. A series of multiple concentrations of

BAY16 was tested in triplicate in three independent experiments in hepatocytes seeded in 24-well plates at a density of  $0.2 \times 10^6$  cells per well. Results obtained from the CellTiter-Glo<sup>®</sup> assay revealed a significant concentration-dependent cytotoxicity at concentrations exceeding 25  $\mu\text{M}$  after 24 h exposure to BAY16 (Figure 38a). The same trend was also observed with the WST-1 assay. However, significantly reduced cell viability in hepatocytes was evident at a concentrations  $> 40 \mu\text{M}$  BAY16 (Figure 38a).

Cell culture conditions can affect the sensitivity of hepatocytes exposed to the external stimulus. Thus, in subsequent experiments, the effect of BAY16 on cell viability of hepatocytes was also assessed in cells seeded in 6-well coated plates at a density of  $1.0 \times 10^6$  cells per well which represent the same culture conditions that were used for further experiments to determine gene expression profiles by Affymetrix microarray. The final concentrations for BAY16 were selected based on the results of this assay, whereby the low concentration of 25  $\mu\text{M}$  BAY16 did not affect cell viability (95 %) while the number of viable cells was reduced by 50 % at a high concentration of 75  $\mu\text{M}$  BAY16 compared with the 0.5 % DMSO-treated control group (Figure 38b).

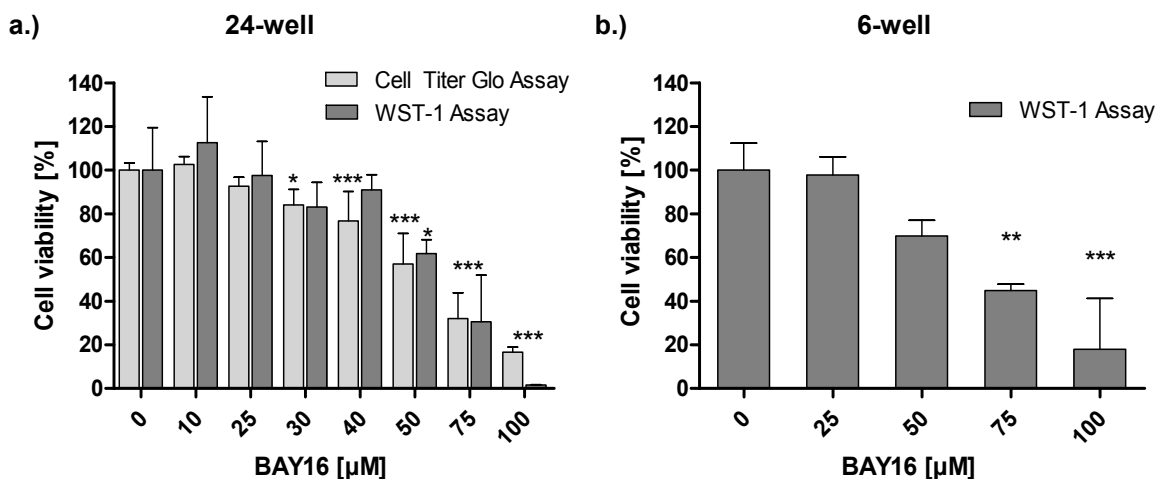


Figure 38. Cell viability of rat hepatocytes after treatment with BAY16 for 24 h cultured in 24-well plate (a) and 6-well plate (b). Data are presented as mean  $\pm$  standard deviation ( $n = 3$ ). Statistical analysis was performed by ANOVA and Dunnett's post hoc test (\*  $p < 0.05$ , \*\* $p < 0.01$ , \*\*\* $p < 0.001$ ).

In addition to both assays, cells were also examined by light microscopy to assess morphological changes of rat hepatocytes after 24 h exposure to 25  $\mu\text{M}$  and 75  $\mu\text{M}$  BAY16. Light microscopy observations showed no clear differences in morphology and cell viability between untreated controls and hepatocytes exposed to 25  $\mu\text{M}$  of BAY16 (Figure 39). These findings were consistent with data from viability assays, demonstrating that a single administration of 25  $\mu\text{M}$  of BAY16 for 24 h did not affect the survival rate of hepatocytes relative to control. However, marked cytotoxic effects, reflected by changes in

morphology, were seen in hepatocytes treated with 75  $\mu$ M of BAY16. These alterations included rounded and floating cells as well as cells with disrupted cell membrane accompanied by release of granular cytoplasm (Figure 39).

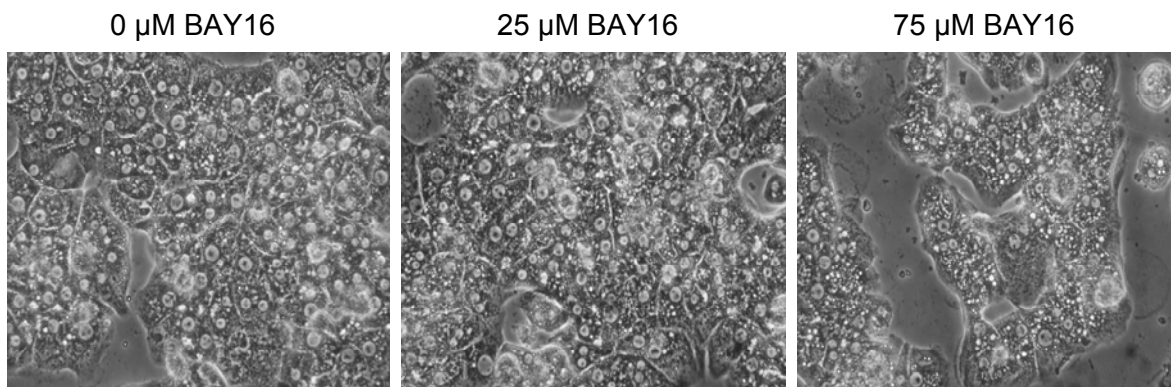


Figure 39. Effect of 0  $\mu$ M, 25  $\mu$ M and 75  $\mu$ M of BAY16 after 24 h in rat hepatocytes cultured as monolayer in 6-well plates. Light microscopic visualization showed a dose-dependent increase of cell degeneration after treatment with the high concentration of BAY16.

#### 4.2.1.2 Gene expression profile induced by BAY16 *in vitro* and comparison with existing *in vivo* data

In order to compare dose-dependent changes in the mRNA expression level in response to BAY16 exposure *in vitro* with existing preclinical toxicogenomics data obtained from the PredTox project, freshly isolated primary rat hepatocytes were treated with BAY16 at doses of 0  $\mu$ M, 25  $\mu$ M and 75  $\mu$ M for 24 h before analyzing changes in gene expression. The *in vivo* study design was described previously in chapter 2.2.1. For clarification, the higher concentration used for *in vivo* or *in vitro* experiments are named “high” and the lower concentration are named “low”.

As a first step in the analysis of transcriptional profiling, the complete dataset of MAS5 normalized intensity values (>31,000 values) for all samples of *in vivo* and *in vitro* experiments were used for principal component analyses (PCA) to visualize variations in the expression pattern between different treatment conditions. The PCA is based on a mathematical algorithm that reduces a multidimensional dataset to a two or three dimensional space [270]. The 3D scatter plot of the *in vivo* data showed that all five biological replicates of control and low dose (20 mg/kg bw BAY16) animals clustered together, which in turn demonstrated a high *in vivo* reproducibility due to a small variability between replicates as well as a similarity in the gene expression pattern between these two groups (Figure 40a). The expression profile in the liver of rats after treatment with the low dose for 1 day did not differ from those treated repeatedly with the same dose over a period of 3 days, while the genomic profiles of the control and low dose animals at day 14

were grouped together at a small distance. The similarity in the gene expression pattern within the controls and low dose animals can be attributed to the absence of toxic effects at this dose. In contrast, a clear separation of the transcriptional signature of high dose animals (100 mg/kg bw BAY16) from the control and low dose group were seen at all time points, which correlates well with the histopathological observations in the liver (Figure 40a).

The cluster analysis of *in vitro* samples showed that the expression profiles of hepatocytes exposed to 75  $\mu$ M BAY16 was different from the controls and low concentration group. However these effects were restricted to two of three replicates, indicating a higher inter- and intravariability within this study (Figure 40b).

Overall, the PCA analysis indicated that treatment with 75  $\mu$ M and 100 mg/kg bw of BAY16 resulted in different expression pattern both *in vitro* and *in vivo*, whereby higher variability was found within *in vitro* studies.

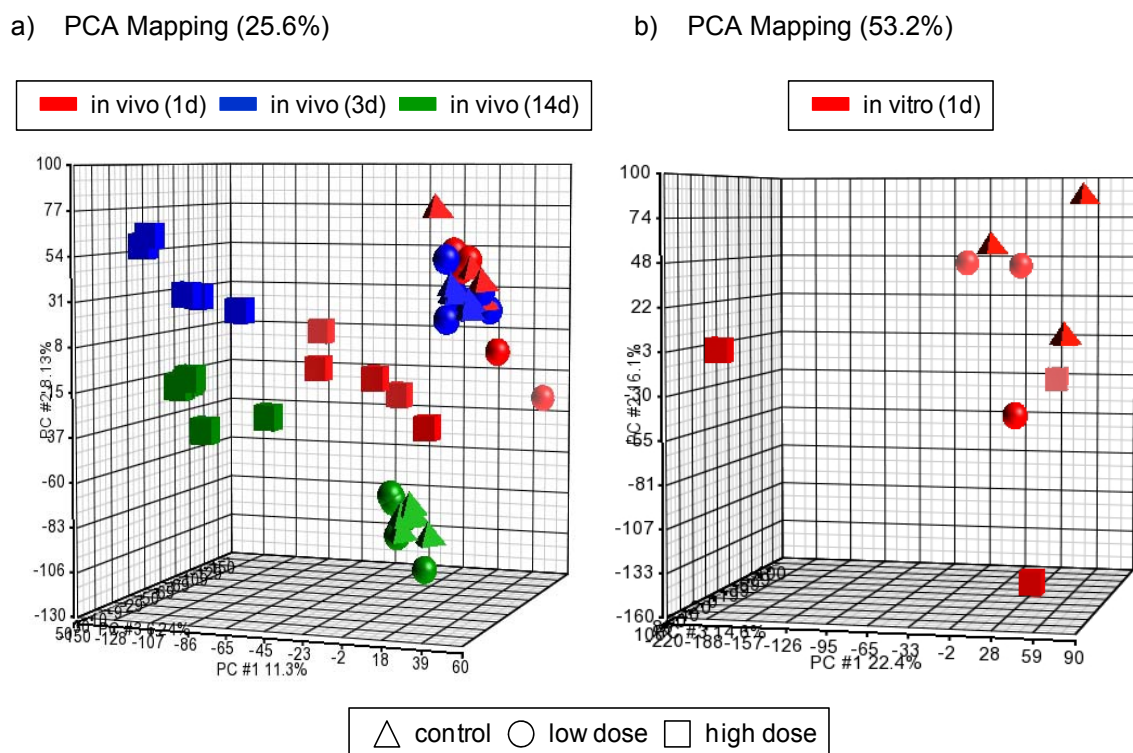


Figure 40. PCA 3D scatter plot of gene expression pattern of all biological replicates of *in vivo* (n=5) (a) and *in vitro* studies (n=3) (b) was performed using Partek Genome Suite 6.5. Samples are colored according to time point of BAY16 treatment. The PCA represents a total variation in the gene expression profiles of 25.6 % and 53.2 % *in vivo* and *in vitro*, respectively.

To further investigate dose-dependent effects of BAY16, we identified differentially expressed genes using ANOVA by the Partek GS v6.5 software. The fold change in the expression of genes induced by BAY16 *in vitro* and *in vivo* relative to controls were

calculated by dividing the average intensity value for all biological replicates of treated group by the average value of the corresponding control. In general, all genes with a p-value < 0.01 (one-way ANOVA) and a fold-change of at least 1.5 were considered to be statistically significant and differentially expressed.

Based on these criteria, 345 and 606 genes were found to be significantly altered in their mRNA level in primary rat hepatocytes after incubation with 25  $\mu$ M and 75  $\mu$ M for 1 d (Figure 41). Marked dose-dependent 8-fold increases in the number of deregulated genes were observed in the liver of rats administered with a high dose of 100 mg/kg bw BAY16 compared to low dose at each time point (Figure 41). The highest numbers of significantly modulated genes were found on day 3 and 14 correlating with the degree of liver injury, indicating that BAY16-induced hepatotoxic effects were accompanied by extensive alteration in the gene expression. In contrast to *in vivo*, the cytotoxic effects observed with high concentration of BAY16 in primary rat hepatocytes were not reflected by a large increase in the number of modulated genes.

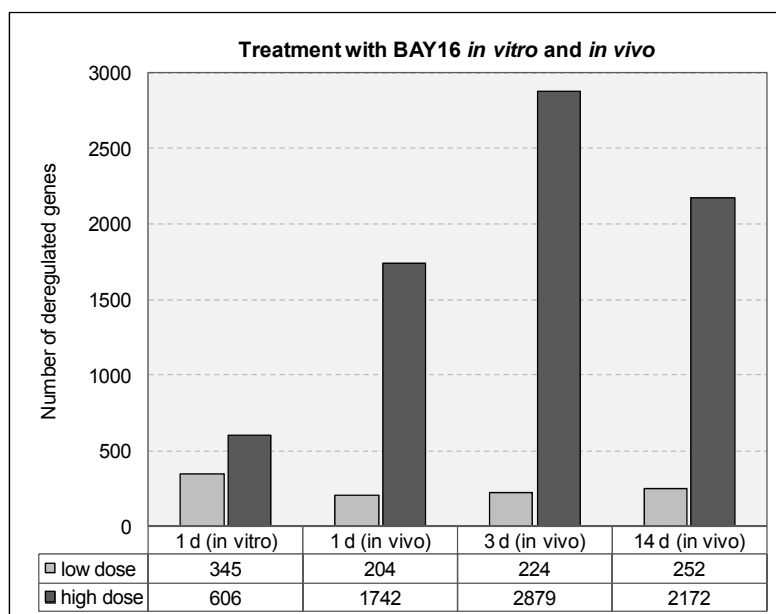


Figure 41. Number of genes significantly deregulated by treatment with BAY16 *in vitro* (low dose = 25  $\mu$ M BAY16, high dose = 75  $\mu$ M BAY16) and *in vivo* (low dose = 20 mg/kg bw BAY16, high dose = 100 mg/kg bw BAY16).

To compare concentration-dependent significant differences in the expression pattern in primary rat hepatocytes with time-dependent differences observed in the liver of rats, a union list of all 5408 deregulated genes ( $p < 0.01$ , Fold change 1.5) were used for hierarchical clustering. Cluster analysis is a widely used statistical method to sort genes or several conditions (e.g. treated vs. untreated, tumor vs. non-tumor) in the dataset according to their similarities or dissimilarities in the expression profiles [271, 272]. The principle is based on the measurement of the distance between two clusters and can be calculated by several algorithms that define the type of distance-measurement [272]. All



genes in our dataset were hierarchically clustered using the Euclidean distance with an average linkage method to calculate the distance between two clusters as mean distance between all data in the cluster [272].

The clustering results were displayed as a heatmap, in which overexpressed (red), downregulated (green) and not significantly changed (black) genes were grouped according to their expression values across the different experimental conditions. Results obtained *in vitro* showed that there were slightly more genes downregulated after incubation with the high dose of BAY16 *in vitro*, indicating that transcriptional responses to toxic concentration of BAY16 were generally associated with decreased gene expression in primary rat hepatocytes (Figure 42). In contrast, clustering of differentially expressed genes in the liver of rats treated with BAY16 *in vivo* revealed marked dose- and time-dependent modulation of genes that were either overexpressed or repressed by 100 mg/kg bw of BAY16. The high-dose effect of BAY16 on the expression of genes after 24 h was more pronounced in livers of rats than in cultured primary rat hepatocytes. These findings suggest differences in the intensity of transcriptional changes between whole liver and isolated hepatocytes, which can be attributed to the limited number of cell types in the *in vitro* system and the cellular responses *in vivo*.

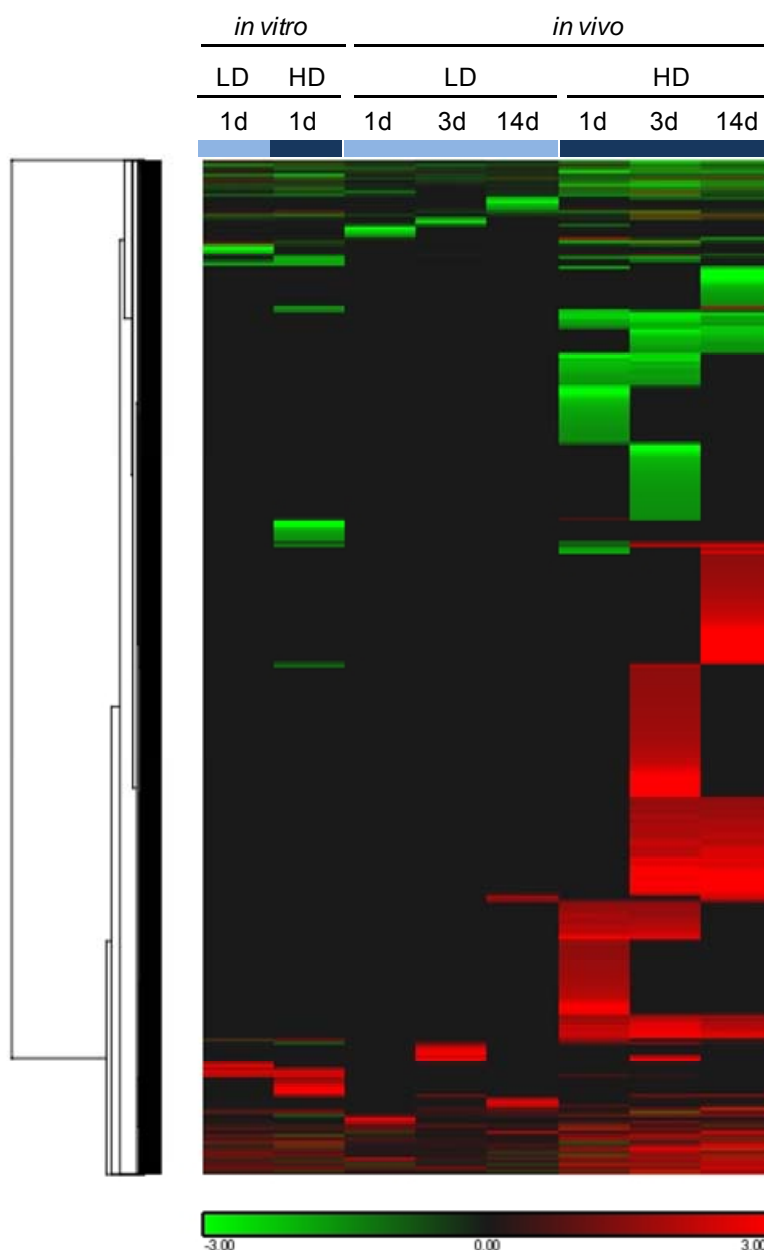


Figure 42. Heatmap generated by hierarchical clustering of all significantly deregulated genes using Partek GS 6.5. Each row indicates a single gene, and each column represents the average fold change for different treatment conditions (n=3 *in vitro*, n=5 *in vivo*). Red color indicates up-regulated, black indicates no significant change, and green color indicates down-regulated genes. Abbreviations: *in vitro* (LD = 25 µM BAY16, HD = 75 µM BAY16) and *in vivo* (LD = 20 mg/kg bw BAY16, HD = 100 mg/kg bw BAY16).

#### 4.2.1.3 Pathway analysis of transcriptional changes induced by BAY16 *in vitro* and comparison with *in vivo*

To better understand transcriptional changes induced by BAY16 in primary rat hepatocytes, all significantly deregulated genes with at least 1.5-fold change and a p-value of <0.01 were used for further biological interpretation using Ingenuity Pathway Analysis (IPA) software tool. The aim of this analysis was to identify signaling pathways enriched in the gene lists by categorization of genes according to their biological function. Thus, identification of possible affected pathways can provide further information regarding molecular processes that may contribute to the toxicity of BAY16. Therefore, the *in vitro* and *in vivo* gene lists were uploaded separately into IPA and analyzed using a

specific IPA database named “TopTox List” that focuses on toxicity of compounds, including mechanism of toxicity and drug metabolism, as well as pathological endpoints associated with drug treatment. Using the software tool, the Fischer’s exact test was performed to calculate the probability ( $p\text{-value} \leq 0.05$ ) that an association between the genes from the microarray dataset and the pathway exists. For the calculation of the  $p$ -value for each category, the number of Pathway Eligible molecules in the pathway and its size, the total number of genes in the uploaded dataset and the total number of genes from the uploaded dataset which was assigned to a pathway were considered. The most enriched pathways were ranked according to their  $p$ -value, based on the results obtained in response to the high concentration of BAY16.

##### *Significantly enriched pathways identified by IPA ToxList*

The analysis revealed a high overlap of the top-ranked pathways between the low and high concentration of BAY16 in primary rat hepatocytes. Interestingly, RXR (retinoid X receptor) nuclear receptor-mediated pathways were associated with six of the top fifteen most significantly affected pathways, which included activation of the pregnane X receptor (PXR), the constitutive androstane receptor (CAR) and the farnesoid X receptor (FXR) via dimerization with RXR (Figure 43). The pathways named “LPS/IL-1 mediated inhibition of RXR function”, “PXR/RXR activation” and “CAR/RXR activation” showed overlapping gene sets. The induction of these nuclear receptors leads to transcriptional regulation of genes involved in xenobiotic, fatty acid and cholesterol metabolism. Similarly modulated pathways were identified in the liver of rats, but only at the highest dose level of BAY16.

It is important to note that alterations in the cholesterol biosynthesis were only observed at the highest concentration of BAY16 *in vitro*, indicating a clear concentration-dependent effect of BAY16 (Figure 43). This finding correlated with transcriptional changes observed in the liver of rats. These data suggest that there is a link between toxic effects of BAY16 and deregulation of cholesterol metabolism in both *in vitro* and *in vivo* models.

GSH depletion, oxidative stress and Nrf2-mediated stress response were more pronounced in rat hepatocytes after incubation with the lower concentration of BAY16 and seem to be an early effect of BAY16 induced transcriptional changes *in vitro*.

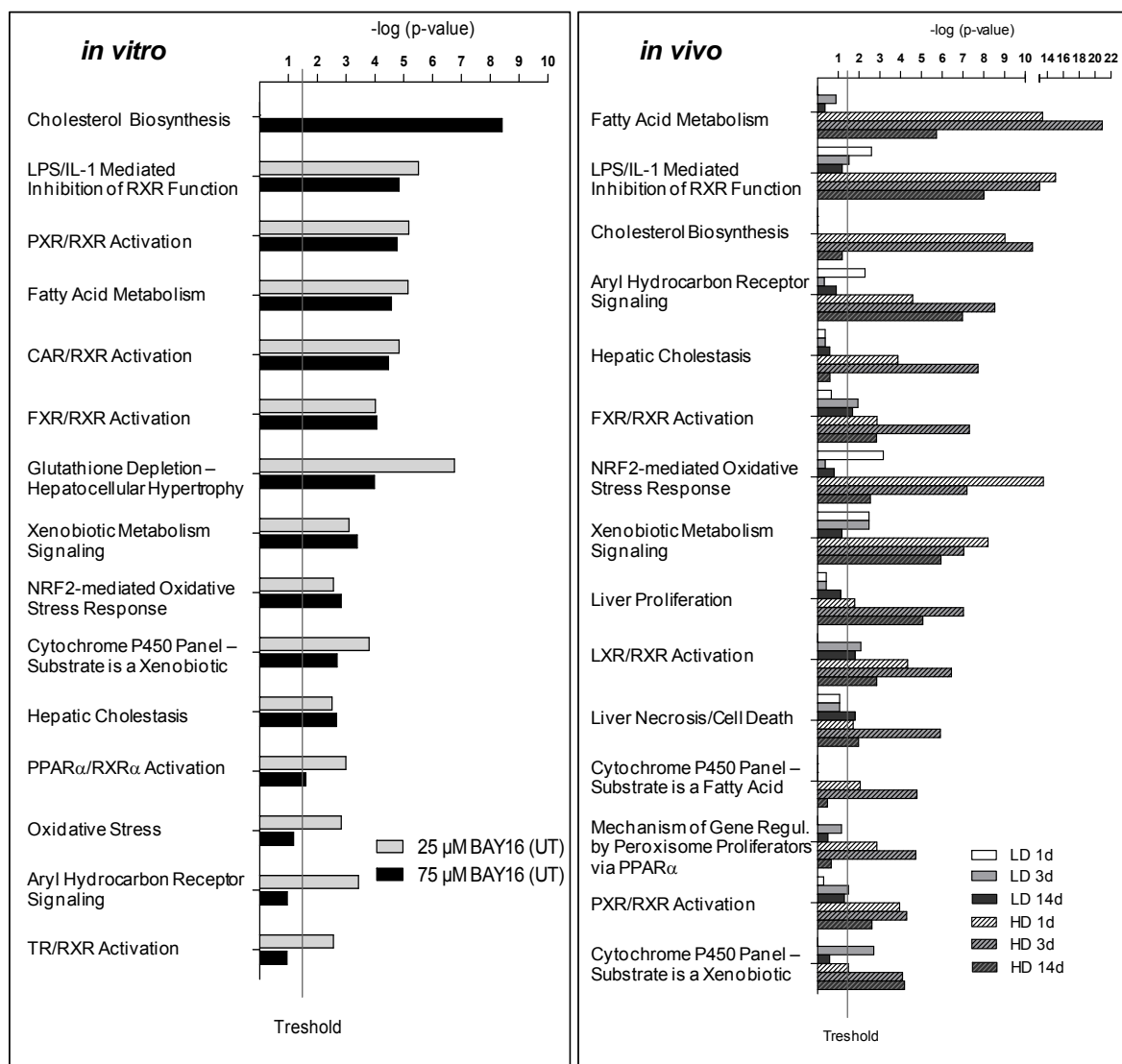


Figure 43. Top significant Tox pathways (IPA) associated with BAY16-mediated effects in rat hepatocytes (*in vitro*) and liver of rats (*in vivo*).

#### Comparative analysis of affected pathways induced by a high dose of BAY16 *in vitro* and *in vivo* (3 d)

All genes whose expression was influenced by 75  $\mu\text{M}$  of BAY16 *in vitro* were compared with significantly deregulated genes induced by 100 mg/kg bw of BAY16 for 3 d *in vivo* in order to assess the relevance of primary rat hepatocytes for studying effect of this compound. The 3-day time point was chosen because most of the histopathological changes, demonstrating early signs of toxicity, were caused by BAY16 after this treatment period. A Venn diagram showed that 193 genes were commonly regulated, whereas 413 genes were found to be deregulated only *in vitro* but not *in vivo* (Figure 44). Among the 193 commonly expressed genes, 35 genes were upregulated and 58 genes were downregulated (Figure 44). For a better understanding of the functional role of commonly

and uniquely deregulated genes, we identified the most enriched pathways using the IPA analysis tool.

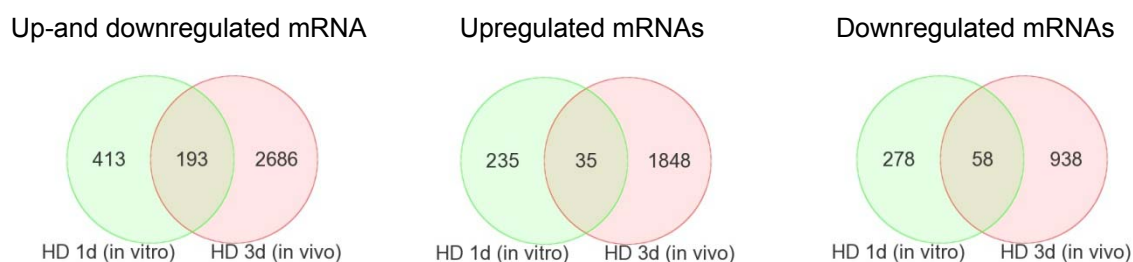


Figure 44. Venn diagram representing the number of commonly or uniquely differentially expressed genes among *in vitro* and *in vivo*.

Pathways that included commonly upregulated and downregulated genes were involved in xenobiotic metabolism and lipid transport via activation of nuclear receptor CAR, PXR, and FXR (Table 40). Five genes contributing to oxidative stress and GSH metabolism were increased in the expression by both *in vitro* and *in vivo* BAY16 treatment. The most significant pathway commonly regulated by BAY16 was cholesterol biosynthesis, but all genes involved in this functional category were oppositely expressed *in vitro* and *in vivo*. Similar effects were observed in the transcriptional mRNA level of genes which are associated with fatty acid and PPAR $\alpha$ /RXR $\alpha$  activation (Table 40).

Table 40. Significant Tox pathways commonly regulated by a toxic dose of BAY16 *in vitro* (1 d) and *in vivo* (3 d).

Tox Pathways	$-\log$ (p-value)	Ratio	Genes
<b>Commonly upregulated genes (35 genes)</b>			
CAR/RXR Activation	8.9	0.17	GADD45B, UGT2B4, GSTA5, CYP2B6, CCND1
Glutathione Depletion - Hepatocellular Hypertrophy	4.1	0.25	UGT2B4, CYP2B6
Oxidative Stress	3.9	0.05	GSTA5, GGT1, GSS
FXR/RXR Activation	3.3	0.03	UGT2B4, SREBF1, VLDLR
LPS/IL-1 Mediated Inhibition of RXR Function	2.1	0.01	SREBF1, GSTA5, CYP2B6
<b>Commonly downregulated genes (58 genes)</b>			
Cytochrome P450 Panel - Substrate is a Sterol	3.2	0.14	CYP17A1, CYP8B1
PXR/RXR Activation	3.1	0.04	CPT1A, HMGCS2, SLCO1B3
LPS/IL-1 Mediated Inhibition of RXR Function	2.5	0.02	CPT1A, SULT1C2, HMGCS2, SLCO1B3
FXR/RXR Activation	1.7	0.02	SLCO1B3, CYP8B1
<b>Common genes that were oppositely deregulated (100 genes)</b>			
Cholesterol Biosynthesis	14.5	0.50	MVD, SQLE, DHCR7, PMVK, ACAT2, IDI1, MVK, HMGCS1
Fatty Acid Metabolism	5.6	0.06	HADHB, ACAT2, CYP2C9, ACAA1, ACOX1, ACAA2, CYP51A1
PPAR $\alpha$ /RXR $\alpha$ Activation	3.7	0.03	GPD1, CYP2C9, ACAA1, NR0B2, ACOX1, CD36
FXR/RXR Activation	3.0	0.05	IL18, NR0B2, SLC10A2, IL36B
Hepatic Cholestasis	2.2	0.03	IL18, NR0B2, SLC10A2, IL36B

To identify differences in the signaling pathways between *in vitro* and *in vivo*, all not commonly deregulated genes were analyzed using IPA. The results showed that similar pathways were affected by BAY16 *in vivo* vs. *in vitro* including metabolic, cellular and transport processes, although there was no correlation between two gene lists (Table 41). The significant induction of proliferative and apoptotic or necrotic processes was only observed in rat liver, and may be an indicator for regenerative processes due to BAY16-mediated injury on the hepatocytes and biliary epithelium.

Table 41. Most significantly enriched functional categories based on genes uniquely regulated by BAY16 *in vitro* (413 genes) and *in vivo* (2686 genes).

Category [in vitro]	p-value	Genes	Category [in vivo]	p-value	Genes
Carbohydrate Metabolism	6.0E-06 - 2.2E-02	18	Lipid Metabolism	2.2E-31 - 4.2E-04	330
Drug Metabolism	6.0E-06 - 1.8E-02	13	Cell Cycle	2.6E-19 - 4.2E-04	225
Lipid Metabolism	6.0E-06 - 2.7E-02	44	Energy Production	5.5E-17 - 3.2E-04	78
Molecular Transport	6.0E-06 - 2.7E-02	61	Cell Death	7.6E-16 - 4.3E-04	327
Cellular Assembly and Organization	2.6E-05 - 2.3E-03	30	Cellular Assembly and Organization	2.0E-15 - 3.8E-04	279

#### 4.2.1.4 Functional analysis of deregulated genes

##### *Hepatic nuclear receptor-mediated changes in gene expression*

Activation of PXR and CAR resulted in increased expression of drug metabolizing cytochrome (CYP) P450 enzymes, detoxification enzymes and several drug transporter in rat hepatocytes following exposure to BAY16 (Table 42). Among this, CYP3A4 was found to be 9-fold upregulated *in vitro*, but was not significantly differentially expressed *in vivo*. Although CYP2B6 was also overexpressed in the liver, the mRNA level of CYP2C9 was decreased in comparison to *in vitro*. The incubation of hepatocytes with BAY16 leads to enhanced expression of phase II metabolizing enzymes, including SULT2A6, which is responsible for sulfation of hydroxysteroids and xenobiotics, as well as GSTA4 and GSTA5 that catalyze the conjugation of glutathione to electrophilic xenobiotics. Enhanced capacity of detoxification, especially mediated by GSTs (GSTA4/5, GSTM1/3), was already observed at the lower concentration of BAY16. The efflux transporter ABCB1 (MDR1) was upregulated, whereas organic transporter SLCO1A2 (OATP) and SLCO1B3 (OATP4) involved in the uptake of bile acids and xenobiotics were both up- and downregulated, respectively.

Overexpression of ABCB11 (BSEP) and ABCB4 (MDR3), which are indicative of FXR activation and responsible for secretion of bile acid into the canaliculi, occurred only *in vitro*. The expression of UGT2B4, which mediates glucuronidation of intermediate

metabolites, was 8-fold upregulated in hepatocytes and more than 2-fold overexpressed in the liver (Table 42). Furthermore, genes implicated in the bile salt synthesis and uptake of bile salts, like CYP8B1 and SLC10A2 (NTCP2), were inhibited in their mRNA expression by FXR-mediated induction of NROB2 (SHP, short heterodimer partner). SHP, an orphan nuclear receptor that inhibits the expression of a large number of target genes involved in bile acid synthesis, gluconeogenesis and lipid metabolism [273, 274], was the most highly upregulated genes after incubation with 25  $\mu$ M (42-fold) and 75  $\mu$ M (94-fold) of BAY16 in rat hepatocytes, but significantly downregulated after treatment with BAY16 *in vivo* (Table 42). On the other side, the expression of sterol regulatory element binding transcription factor 1 (SREBF1, SREBP-1c), which induced the expression of lipogenic enzymes, was upregulated *in vitro* and *in vivo*. In addition, an increased expression of very low density lipoprotein receptor (VLDLR), which is responsible for uptake of triglyceride-rich lipoproteins [275], was observed both *in vitro* and *in vivo*.

#### 4 TOXICOGENOMICS TO IMPROVE MECHANISTIC UNDERSTANDING OF DILI

Table 42. Significantly deregulated genes involved in nuclear receptor-mediated signaling caused by 75  $\mu$ M of BAY16 in rat hepatocytes (*in vitro*) and in liver of rats administered with 100 mg/kg bw of BAY16 for 3 d (*in vivo*).

Probe Set ID	Symbol	Gene Name	in vitro (HD 1d)		in vivo (HD 3d)	
			p-value	Fold change	p-value	Fold change
<b>LPS/IL-1 mediated inhibition of RXR function &amp; *PXR/CAR/RXR function &amp; *Xenobiotic metabolism signaling</b>						
1370464_at	ABCB1 <sup>+</sup>	ATP-binding cassette, sub-family B (MDR/TAP), member 1	3.2E-03	2.0		
1368769_at	ABCB11*	ATP-binding cassette, sub-family B (MDR/TAP), member 11	1.1E-07	3.0		
1386946_at	CPT1A*	carnitine palmitoyltransferase 1A (liver)	3.3E-03	-1.5	1.4E-10	-3.5
1371076_at	CYP2B6 <sup>+</sup>	cytochrome P450, family 2, subfamily B, polypeptide 6	9.5E-03	3.3	1.3E-03	2.5
1387328_at	CYP2C9 <sup>+</sup>	cytochrome P450, family 2, subfamily C, polypeptide 9	6.1E-04	3.0	2.6E-04	-2.3
1387118_at	CYP3A4 <sup>+</sup>	cytochrome P450, family 3, subfamily A, polypeptide 4	1.0E-15	9.2		
1372297_at	Gsta4	glutathione S-transferase, alpha 4	3.4E-04	1.6		
1368180_s_at	GSTA5 <sup>+</sup>	glutathione S-transferase alpha 5	3.4E-08	6.8	5.0E-05	1.8
1370310_at	HMGCS2*	3-hydroxy-3-methylglutaryl-CoA synthase 2	1.2E-04	-2.7	1.7E-09	-2.1
1368376_at	NR0B2*	nuclear receptor subfamily 0, group B, member 2	1.0E-07	94.9	3.9E-03	-3.0
1387094_at	SLCO1A2	solute carrier organic anion transporter family, member 1A2	1.1E-04	4.3		
1388426_at	SREBF1	sterol regulatory element binding transcription factor	1.3E-10	4.3	2.1E-03	1.7
1387006_at	Sult2a6 <sup>+</sup>	sulfotransferase family 2A, dehydroepiandrosterone (DHEA)-preferring, member 6	5.1E-03	2.6		
<b>FXR/RXR activation</b>						
1369161_at	ABCB4	ATP-binding cassette, sub-family B (MDR/TAP), member 4	2.6E-06	2.4		
1368769_at	ABCB11	ATP-binding cassette, sub-family B (MDR/TAP), member 11	1.1E-07	3.0		
1368435_at	CYP8B1	cytochrome P450, family 8, subfamily B,	1.4E-06	-7.9	5.7E-06	-8.0
1369665_a_at	IL18	interleukin 18 (interferon-gamma-inducing factor)	3.2E-04	-1.8	8.5E-03	1.6
1385842_at	IL36B	interleukin 36, beta	9.9E-04	-2.1	9.1E-04	2.0
1368376_at	NR0B2	nuclear receptor subfamily 0, group B, member 2	1.0E-07	94.9	3.9E-03	-3.0
1368745_at	SLC10A2	solute carrier family 10 (sodium/bile acid cotransporter family), member 2	5.0E-05	-3.9	3.9E-04	1.9
1387679_at	SLCO1B3	solute carrier organic anion transporter family, member 1B3	3.8E-03	-1.7	1.2E-09	-1.8
1388426_at	SREBF1	sterol regulatory element binding transcription factor 1	1.3E-10	4.3	2.1E-03	1.7
1370698_at	UGT2B4	UDP glucuronosyltransferase 2 family, polypeptide B4	5.7E-12	7.9	3.6E-07	2.5
1389611_at	VLDLR	very low density lipoprotein receptor	1.7E-04	2.8	4.6E-03	5.5

#### Alterations in cholesterol metabolism

Exposure of primary rat hepatocytes to 75  $\mu$ M BAY16 for 1 d resulted in downregulation of genes involved in the de novo cholesterol synthesis from acetyl-CoA, such as 3-hydroxy-3-methylglutaryl-CoA synthase 1 (HMGCS1), mevalonate kinase (MVK), mevalonate (diphospho) decarboxylase (MVD), isopentenyl-diphosphate delta isomerase 1 (IDI1), squalene epoxidase (SQLE), phosphomevalonate kinase (PMVK), sterol-C4-methyl oxidase-like (SC4MOL) and CYP51 (Figure 45). Interestingly, 3-hydroxy-3-methylglutaryl-CoA reductase (HMGCR), which catalyzes the rate-limiting reaction in the cholesterol



synthesis, was unchanged *in vitro*. The expression of the sterol regulatory element binding transcription factor 2 (SREBF2), which is responsible for induction of genes involved in cholesterol synthesis, was not significantly decreased. Results from previous preclinical study have shown that cholesterol-synthesis associated genes were upregulated in the liver of rats administered with 100 mg/kg bw BAY16, resulting in enhanced cholesterol level [97]. In parallel, the expression level of cholesterol efflux transporter ATP-binding cassette, sub-family G (WHITE), member 5 and member 8 (ABCG5, ABCG8), which are important for biliary transport of cholesterol, were decreased, and are likely to be associated with intracellular accumulation of cholesterol and observed cholestasis *in vivo* [97]. The effect of BAY16 on the cholesterol synthesis appears to be associated with high-dose mediated toxic effects, although differences in the transcriptional regulation between *in vivo* and *in vitro* systems were observed.

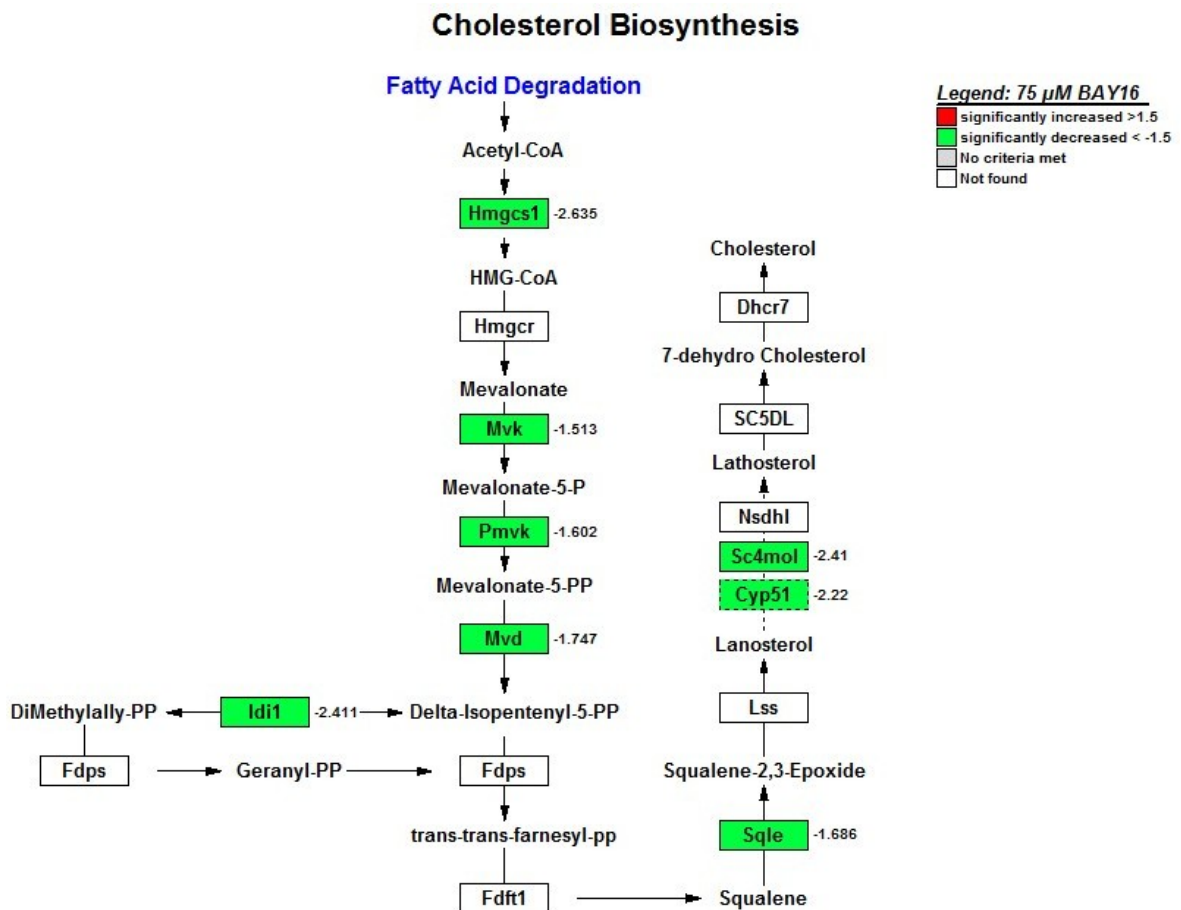


Figure 45. Decreased expression of genes involved in the synthesis of cholesterol from acetyl-CoA in primary rat hepatocytes after treatment with 75  $\mu$ M BAY16.

*Alterations in fatty acid metabolism*

Genes related to mitochondrial and peroxisomal beta-oxidation, such as acetyl-CoA acyltransferase 1 and 2 (ACAA1, ACAA2), acyl-CoA oxidase (ACOX1), hydroxyacyl-CoA dehydrogenase B (HADHB) were upregulated *in vitro*, but downregulated *in vivo* following exposure to BAY16 (Table 43). However, the rate-limiting enzyme for fatty acid oxidation, carnitine palmitoyltransferase 1A (CPT1), which transports fatty acids into mitochondria, was downregulated both *in vitro* and *in vivo* (Table 43).

Activation of the transcription factor SREBP-1c, which represent an insulin-mediated action, resulted in increased mRNA expression of genes involved in lipogenesis like fatty acid synthase (FASN), acyl-CoA synthetase long-chain family member 1 (ACSL1), stearoyl-CoA desaturase (delta-9-desaturase) (SCD) in hepatocytes exposed to BAY16. However these effects were more pronounced in the low dose of BAY16 and thus appear to be an early event in pharmacologically mediated metabolic effects (Appendix 1).

Table 43. Effect of BAY16 on the expression of genes involved in fatty acid metabolism.

Probe Set ID	Symbol	Gene Name	in vitro (HD 1d)		in vivo (HD 3d)	
			p-value	Fold change	p-value	Fold change
<b>Fatty acid metabolism</b>						
1387783_a_at	ACAA1	acetyl-CoA acyltransferase 1	3.8E-04	1.7	1.6E-10	-2.0
1380504_at	ACAA2	acetyl-CoA acyltransferase 2	1.8E-05	2.4	7.2E-12	-4.4
1372462_at	ACAT2	acetyl-CoA acetyltransferase 2	1.0E-03	-2.3	1.0E-04	2.4
1367680_at	ACOX1	acyl-CoA oxidase 1, palmitoyl	2.8E-05	2.0	2.1E-15	-2.5
1378260_at	ADH1C	alcohol dehydrogenase 1C (class I), gamma	8.3E-03	-2.2	2.5E-04	-2.4
1392384_s_at	AKR1D1	aldo-keto reductase family 1, member D1 (delta 4-3-ketosteroid-5-beta-reductase)	8.1E-03	1.9		
1386946_at	CPT1A	carnitine palmitoyltransferase 1A (liver)	3.3E-03	-1.5	1.4E-10	-3.5
1387020_at	CYP51A1	cytochrome P450, family 51, subfamily A, polypeptide 1	1.9E-04	-1.8	5.0E-07	2.6
1367694_at	HADHB	hydroxyacyl-CoA dehydrogenase/3-ketoacyl-CoA thiolase/enoyl-CoA hydratase (trifunctional protein), beta subunit	4.5E-06	1.6	3.6E-15	-2.0

*Expression of genes involved in oxidative stress*

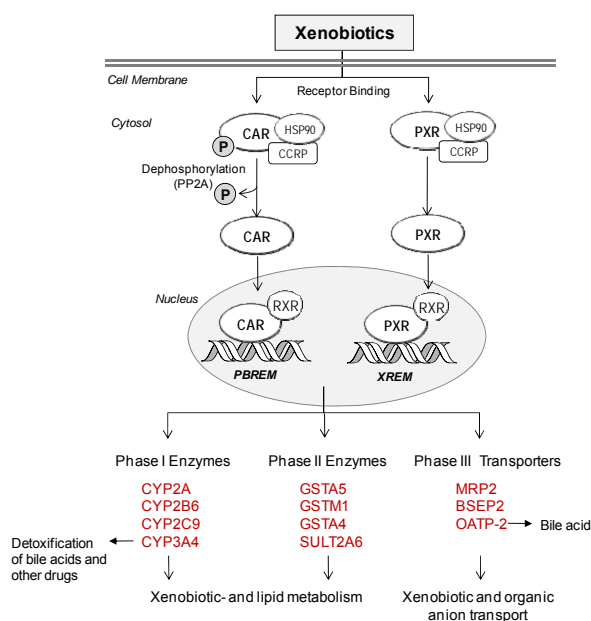
Overexpression of glutathione synthetase (GSS, 1.5-fold), glutathione reductase (GSR, 2.3-fold) and P450 cytochrome oxidoreductase (POR, > 3-fold) suggest that there is an increased demand for GSH after exposure to BAY16 *in vitro*. GSR is involved in the resynthesis of GSH by catalyzing reduction of GSSG to GSH [276, 277]. The protein encoded by GSS is involved in the de novo synthesis of GSH by catalyzing ATP-dependent conversion of gamma-L-glutamyl-L-cysteine to glutathione [278].

#### 4.2.2 Discussion

The results of this study have shown that increased nuclear receptor activity, including PXR, CAR and FXR, which serves to detoxify and eliminate xenobiotics, steroids and bile acids by induction of CYPs, GSTs, UGT, SULT and efflux transporters, represent an early molecular response to BAY16 in primary rat hepatocytes (Figure 46). A broad range of substances and drugs are known to activate PXR, such as steroid hormones, statins, calcium-channel inhibitors, antidiabetic and anticancer drugs [279-281]. Although no information regarding biotransformation of BAY16 is available, it is conceivable that transcriptional induction of metabolizing proteins regulated by PXR/RXR or CAR/RXR may contribute to elimination of BAY16. Beside its role in drug metabolism, PXR and CAR also mediate clearance of steroid hormones, bilirubin and bile acids [282, 283]. On the other hand, FXR has been primarily implicated in the regulation of metabolic pathways, such as bile acids, cholesterol, lipid and glucose metabolism [284, 285]. The modulation of FXR target genes by BAY16 is likely to result in suppression of bile acid synthesis, increase of biliary detoxification and secretion, and inhibition of bile acid import into hepatocytes (Figure 5, Figure 46). In cholestatic conditions where intracellular bile acid levels rise, FXR is directly activated by these bile acids, like cholic acid, deoxycholic acid and chenodeoxycholic acid, which in turn represents a feedback regulation in order to avoid the accumulation of potentially toxic bile acids inside cells [286]. Results from previous metabolomics studies *in vivo* have demonstrated that bile acid and cholesterol levels were increased in response to 100 mg/kg bw of BAY16 in the liver and serum of rats, leading to bile duct injury and hepatic cholestasis at day 3 [97]. Cholesterol is the precursor of the bile acid and steroid biosynthesis [287, 288]. Although the formation of bile acids was not quantified *in vitro*, increased expression of genes involved in cholesterol catabolism and bile acid synthesis, including aldo-keto reductase family 1, member D1 (AKR1D1), cytochrome P450, family 39, subfamily a, polypeptide 1 (CYP39A1) and 24-dehydrocholesterol reductase (DHCR24), were found to be upregulated at the lower concentration of BAY16. It should be noted that the key enzyme of the bile acid synthesis, CYP7A1, was more than 4-fold increased at mRNA level *in vitro*, but this gene did not match our stringent statistical criteria for identifying deregulated genes (p-value 0.0105 and 0.0202). Hence, it could conceivably be hypothesized that an early event in BAY16-induced molecular alterations involves the stimulation on sterol and bile acid synthesis, although there is no evidence for increased cholesterol production. When the export of bile acids is impaired due to drug-mediated effects on transporters then toxic bile acids may accumulate in the cells, resulting in the progression of cholestatic liver damage [49, 289].

An important observation in the current study is the marked downregulation of genes coding for enzymes associated with cholesterol synthesis *in vitro* at the toxic high concentration of BAY16. This is in contrast to previously conducted *in vivo* studies, which clearly show a link between hepatotoxic effects of BAY16 and increases in cholesterol biosynthesis [97]. Cholesterol is able to inhibit its own synthesis in response to high intracellular cholesterol levels [290]. Since BAY16 has been linked to high cholesterol and bile acid levels, it is tempting to speculate that the reduced cholesterol biosynthesis *in vitro* may be a compensatory mechanism to bile acid accumulation. Further examinations of transcriptional changes induced by 75  $\mu\text{M}$  of BAY16 in hepatocytes at an earlier time points may provide more insight concerning this issue and, moreover, may be useful to explain the differential responses of BAY16 on cholesterol synthetic processes. On the other hand, it should be taken into account that cholesterol metabolism is regulated by several metabolic states.

#### a.) Receptor mediated regulation of detoxication



#### b.) Role of FXR in bile acid homeostasis

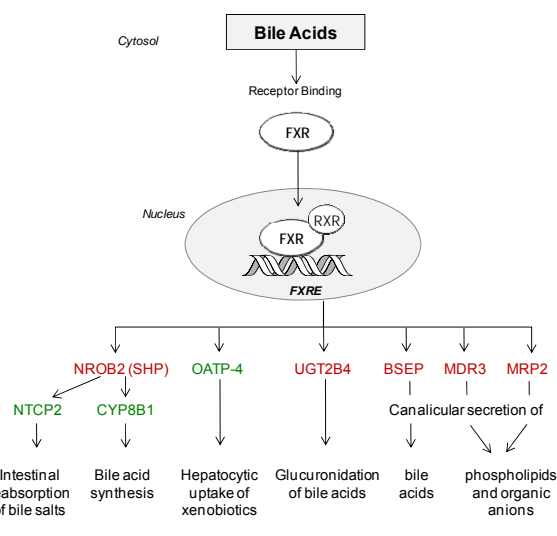


Figure 46. Overview of receptor mediated regulation of detoxification and homeostasis of xenobiotics and bile acids. Treatment with BAY16 in rat hepatocytes resulted in PXR/RXR or CAR/RXR-mediated up-regulation of genes that metabolize xenobiotics, lipids and bile acids and promote their excretion. In parallel, FXR/RXR increased expression of genes involved in canicular secretion and glucuronidation of bile acids while accumulation of bile acids was suppressed by inhibition of intestinal reabsorption and production. Red indicates gene was upregulated and green indicates gene was downregulated by BAY16 treatment.

Looking at the differentially expressed genes and the mechanisms, it is obvious that Bay16 affected fatty acid metabolism and energy homeostasis. Our results show that overexpression of SREBP-1c leads to induction of lipogenic enzymes, especially at the lower concentration of BAY16, and therefore promote the synthesis of fatty acids. It is well established that insulin stimulates the transcription of SREBP-1c via the nuclear activity of LXR [291, 292]. As counterregulator of the insulin signaling pathways, glucagon has been reported to repress hepatic lipid synthesis and increase  $\beta$ -oxidation of free fatty acids [244, 293]. In GCGR<sup>-/-</sup> mice, the increased hepatic triglyceride secretion, leading to accumulation of intracellular free fatty acids, may promote the development of hepatic steatosis [244].

A consequence of enhanced de novo lipid synthesis is the increased formation of malonyl-CoA, which inhibits CPT-1, the rate-limiting enzyme of mitochondrial  $\beta$ -oxidation [294]. This would explain the observed dose-dependent downregulation of CPT-1 while simultaneously other genes involved in peroxisomal and mitochondrial oxidation of fatty acids were upregulated *in vitro*. These transcriptional findings are consistent with those of Yang et al. in GCGR knockout mice [268]. Increased fatty acid oxidation has also been reported in mice lacking GCGR under fasting conditions [244]. In contrast, a reduced expression of genes involved in mitochondrial  $\beta$ -oxidation has been observed in the liver of rats treated with BAY16. The reason for the difference between these *in vivo* findings and our *in vitro* results remains unclear.

Another important observation in this study relates to GSH metabolism during the incubation of hepatocytes with both concentrations of BAY16. GSH is one of the most important intracellular antioxidant, which is involved in redox cycling and scavenging of free radicals [295]. The strong induction of GSTs (GSTA4/5, GSTM1/3) indicates a reaction to oxidative stress within the hepatocytes. GSTA's are the main enzymes for the detoxification of lipid peroxidation products [296], whereas GSTMs are mainly responsible for the detoxification of electrophilic metabolites [297, 298]. Thus, the increasing need for GSH, indicated through increased expression of GSS and GSR, might be attributable to drug metabolism, increased fatty acid and triglyceride synthesis, as suggested by the data derived from gene expression profiling.

It is surprising that the clear toxic effect of BAY16 on the viability of hepatocytes is not reflected by more pronounced transcriptional changes compared to non-toxic concentration. In contrast, significant induction of genes related to proliferation and cell death has been observed in the liver of BAY16-treated rats, and may be an indicator for regenerative processes due to BAY16-mediated injury on the hepatocytes and biliary epithelium. There are several possible explanations for the discrepancy in the observed transcriptional response to BAY16 between the primary rat hepatocytes and the liver of

rats. An explanation might be the lack of systemic effects in the *in vitro* cell culture system consisting of one single cell type of the whole liver. It has long been recognized that clinical manifestation of drug-induced organ toxicity may require systemic, multiple organ interaction [299]. Damage to hepatocytes in the liver is often associated with the recruitment of inflammatory cells which stimulates immune response by the release of cytokines and chemokines, leading to further liver injury [300]. The fact that inflammatory response in the liver is mainly mediated by Kupffer cells, explains the lack of inflammatory response on *in vitro* system.

In summary, BAY16-mediated effects revealed altered expression of genes associated with xenobiotic metabolism, transport processes, increased fatty acid synthesis and bile acid synthesis and downregulation of cholesterol synthesis *in vitro*. Although most of the observed molecular mechanisms via activation of nuclear receptors demonstrate regulatory action to prevent hepatocytes for enhanced levels of xenobiotics or endogenous produced lipids, cholesterol or bile acids, it remains uncertain whether these processes are impaired for a prolonged treatment period *in vitro*.

### **4.3 Effect of GCGR gene silencing by siRNA-mediated transfection *in vitro***

In order to further investigate whether modulation of the pharmacological target of BAY16 plays a role in the toxic response to BAY16, we assessed the effect of siRNA-mediated knockdown of the GCGR on the viability of primary rat hepatocytes. For a better understanding of the nature of toxicity of BAY16, the gene expression profile was analyzed in cells lacking GCGR using cDNA microarrays to discriminate between molecular changes related to pharmacologic and/or toxic effects induced by BAY16-mediated inhibition of GCGR.

#### **4.3.1 Results**

##### **4.3.1.1 Efficiency of GCGR knockdown in primary rat hepatocytes**

To determine whether the inhibition of GCGR function may be linked to decreased cell viability in rat hepatocytes, the *GCGR* mRNA was degraded via RNAi, resulting in inhibition of protein translation. One day after seeding, the cells were transfected with GCGR siRNA at concentrations ranging from 6.25 nM to 100 nM for 24 h, and knockdown efficiency was quantified by TaqMan qRT-PCR. The mRNA expression of GCGR in silenced cells (siGCGR) was normalized to cells transfected with control siRNA (SC). The results showed a strong reduction of GCGR mRNA expression by approximately 80 %

compared to controls (Figure 47). This effect was stable over a period of at least 48 h so that the GCGR expression was effectively silenced during subsequent treatment with BAY16.

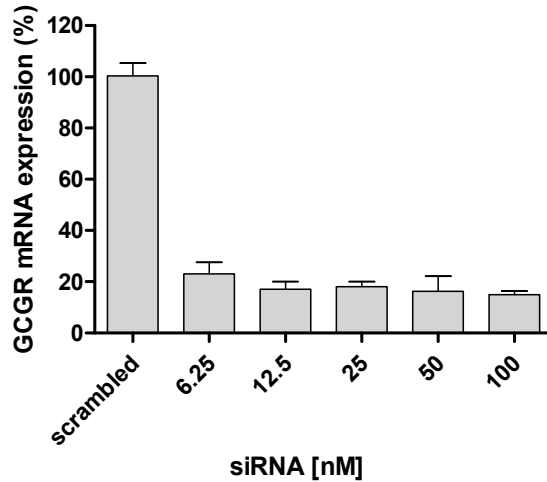


Figure 47. Suppression of GCGR gene expression after transfection with siRNA GCGR for 24 h. Data are presented as mean  $\pm$  standard deviation (n=3).

The GCGR knockdown was also verified at the protein level 48 h after transfection using immunodetection. Immunofluorescence labeling with anti-GCGR and Cy3-anti-rabbit-IgG resulted in a strong staining at the membrane of untransfected hepatocytes visualized by confocal laser scanning fluorescence microscopy (Figure 48a). Reduced membrane staining was detected in GCGR-silenced cells (Figure 48b). Quantification of fluorescence intensity between cytosol and membrane showed a statistically significant decrease in GCGR protein expression in transfected hepatocytes related to untransfected cells (Figure 48c). This demonstrates that siRNA-mediated knockdown of GCGR leads to translational repression of the receptor and, consequently, a lower rate of protein synthesis. The red fluorescence signal was changed to green using ImageJ to obtain a better graphic visualization of the effects.

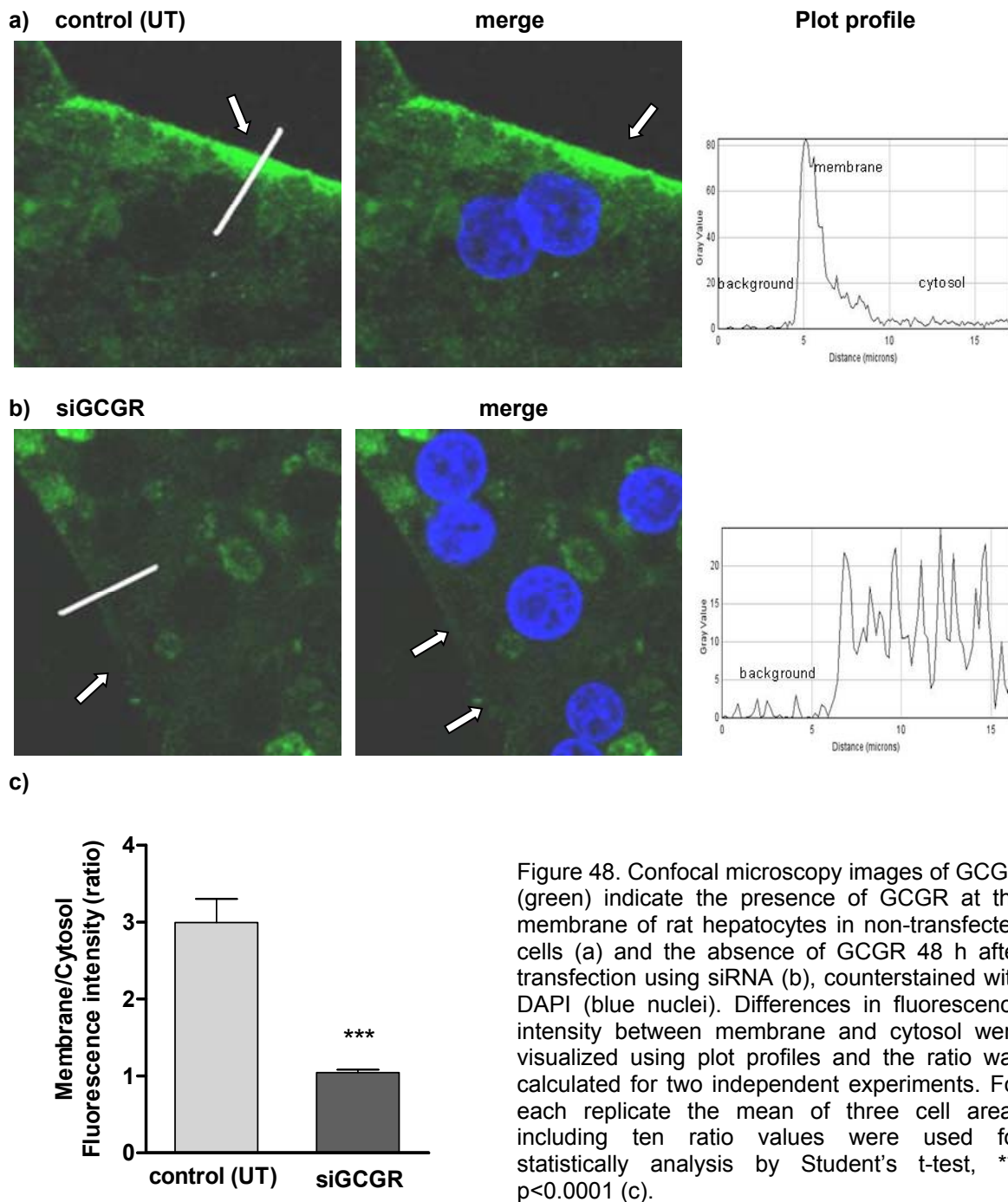


Figure 48. Confocal microscopy images of GCGR (green) indicate the presence of GCGR at the membrane of rat hepatocytes in non-transfected cells (a) and the absence of GCGR 48 h after transfection using siRNA (b), counterstained with DAPI (blue nuclei). Differences in fluorescence intensity between membrane and cytosol were visualized using plot profiles and the ratio was calculated for two independent experiments. For each replicate the mean of three cell areas including ten ratio values were used for statistically analysis by Student's t-test, \*\*\* p<0.0001 (c).

#### 4.3.1.2 Effect of GCGR knockdown on cell viability

To investigate if disruption of GCGR signaling is associated with cytotoxic effects on hepatocytes, the cell viability of silenced cells was assessed using the CellTiter-Glo<sup>®</sup> Luminescent assay. The suppression of GCGR mRNA expression by siRNA did not affect the viability of hepatocytes compared to cells transfected with control siRNA (SC) (Figure 47). Morphological examination of the cells by light microscope confirmed these findings. These results demonstrate that disruption of GCGR signaling alone does not cause



cytotoxicity in hepatocytes, suggesting that BAY16 toxicity is not mediated by inhibition of GCGR function.

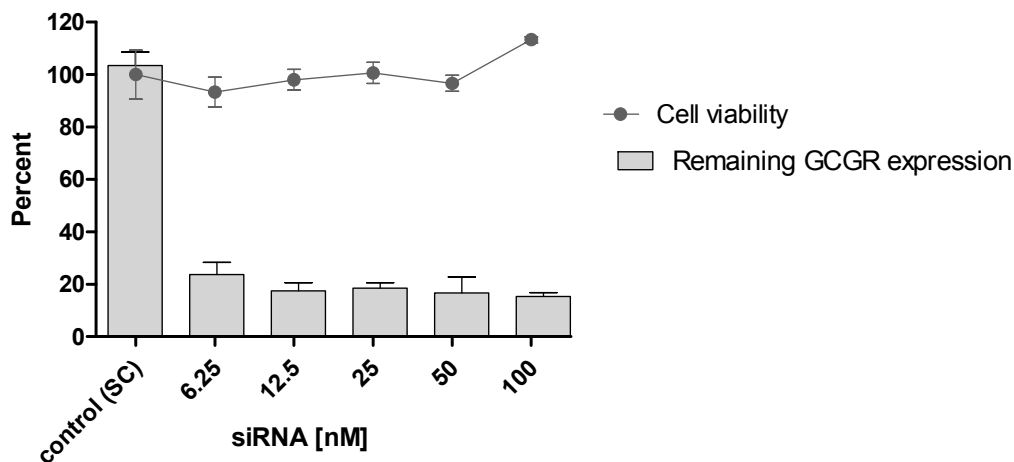


Figure 49. Cell viability of primary rat hepatocytes after gene silencing of GCGR. Data are presented as mean  $\pm$  standard deviation (n=3).

#### 4.3.1.3 Transcriptional changes induced by gene silencing of *GCGR*

In order to reveal relevant molecular mechanisms indicative of BAY16-induced hepatotoxicity, we filtered out all genes modulated by the pharmacological target of BAY16 to narrow down those molecular changes that are associated with toxicity and not the pharmacological action of the drug. To identify downstream signaling effects accompanied exclusively by the suppression of the GCGR, the gene expression profile was analyzed in rat hepatocytes after siRNA-mediated knockdown of GCGR using Affymetrix cDNA microarray.

The difference in the expression level of genes in hepatocytes lacking GCGR were calculated as fold changes in mRNA levels relative to hepatocytes transfected with non-targeting control siRNA (SC). Using ANOVA ( $p$ -value  $< 0.01$ ), a total number of 244 genes were found to be significantly differentially expressed at least 1.5-fold after GCGR gene silencing. Among them, 116 genes were upregulated and 128 genes were downregulated. All modulated genes were uploaded in the IPA software tool for further biological and functional interpretation.

No statistically significant toxicological pathways were identified by categorization of deregulated genes according to their biological function using IPA ToxList analysis. These findings correlated with the normal morphology and normal viability rate of hepatocytes after gene silencing of the GCGR. The canonical pathway analysis revealed altered

expression of genes associated with interferon signaling, antimicrobial and inflammatory response (Table 44). It is generally known that transfection using siRNA in mammalian cells can stimulate innate immune response via Toll-like receptor pathways, leading to overexpression of interferons and inflammatory chemokines [180, 301, 302]. Most of the upregulated genes found in this study (e.g. interferon regulatory factor 7, interferon-induced protein with tetratricopeptide repeats 3, 2',5'-oligoadenylate synthetase 1, 40/46kDa and chemokine (C-C motif) ligand 5) appear to be linked to unspecific off-target effects that occur through binding of the siRNA to its target mRNA and its degradation (Table 45).

Table 44. Top three of significantly enriched canonical pathways (cp) according to IPA analysis software associated with gene silencing of *GCGR* in rat hepatocytes. The ratio is calculated by dividing the number of genes from the *in vitro* study that categorized in this cp by the total number of genes existing in the cp.

Canonical pathways associated with inhibition of the GCGR receptor via siRNA	p-value	No. Genes	Ratio	Genes
Interferon signaling	5.9E-09	8	0.22	IFIT3, IFI35, IRF9, OAS1, MX1, PSMB8, STAT1, STAT2
Activation of IRF (interferone regulatory factor) by cytosolic pattern recognition receptors	8.8E-07	8	0.11	DHX58, DDX58, IFIT2, IRF7, IRF9, STAT1, STAT2, ISG15
Role of pattern recognition receptors in recognition of bacteria and viruses	2.1E-03	5	0.06	CCL5, DDX58, EIF2AK2, IRF7, OAS1

The gene expression of *GCGR* was downregulated by 4.9-fold in si*GCGR*-transfected hepatocytes, confirming knockdown of the *GCGR* for more than 80% in comparison to controls. No metabolic processes were significantly affected by gene silencing of the *GCGR*, although the complete ablation of the hepatic *GCGR* function in mice (*GCGR* knockout mice) is associated with alterations in metabolic processes [268]. The expression of *GCGR*-target genes, such as phosphoenolpyruvate carboxykinase (*PEPCK*), glucose-6-phosphatase (*G6P*) and peroxisome proliferator-activated receptor gamma coactivator-1 (*PGC-1*), transcriptionally regulated via protein kinase A (*PKA*), was not significantly decreased in response to *GCGR* gene silencing *in vitro*. In contrast, a marked decrease in the expression of cAMP-regulated genes, such as cAMP-regulated phosphoprotein, 21kDa (7.5-fold), adenylylase cyclase 6 (*ADCY6*), protein phosphatase 2A (6.7-fold) were detected.

Table 45. Categorization of significantly deregulated genes (cutoff 1.5,  $p < 0.05$ ) involved in inhibition of siGCGR via siRNA relative to SC (n=3).

Probe Set ID	Symbol	Gene Title	p-value	Fold Change
<b>Interferone signaling / Antimicrobial and immune response</b>				
1369983_at	CCL5	chemokine (C-C motif) ligand 5	1.3E-05	102.0
1374551_at	IFI35	interferon-induced protein 35	3.9E-03	1.6
1376908_at	IFIT3	interferon-induced protein with tetratricopeptide repeats 3	1.8E-04	24.5
1383564_at	IRF7	interferon regulatory factor 7	8.1E-06	15.6
1383448_at	IRF9	interferon regulatory factor 9	2.3E-05	3.1
1382314_at	ISG15	ISG15 ubiquitin-like modifier	6.0E-06	23.2
1369202_at	MX1	myxovirus (influenza virus) resistance 1, interferon-	1.3E-05	20.8
1371152_a_at	OAS1	2',5'-oligoadenylate synthetase 1, 40/46kDa	5.1E-06	29.4
1387354_at	STAT1	signal transducer and activator of transcription 1, 91kDa	4.7E-04	2.1
1389571_at	STAT2	signal transducer and activator of transcription 2, 113kDa	4.5E-03	1.8

### 4.3.2 Discussion

Genetic disruption of GCGR signaling has been reported to increase the susceptibility to experimentally induced hepatocellular injury, whereas administration of glucagon leads to a reduction of Jo2-induced apoptosis in wild type mice [245]. Thus, it has been proposed that glucagon-mediated GCGR signaling is linked with anti-apoptotic action, probably via cAMP-mediated activation of adenylate cyclase [245]. This raises the question whether modulation of GCGR expression could be associated with cytotoxic effects on hepatocytes and that the reduction of glucagon action by pharmacological inhibition of the GCGR might be responsible for the hepatotoxic effects of the GCGR antagonist BAY16.

Although primary cells are generally known to be difficult to transfect [303], we were able to successfully downregulate the expression of GCGR through lipid-mediated transfection with siRNA targeted against rat GCGR mRNA by 80 % compared to controls. The results obtained from cytotoxicity assays show that the knockdown of GCGR does not affect the viability of rat hepatocytes. It can therefore be assumed that partial ablation of the GCGR signaling without a toxic stimulus has no consequences on the survival of hepatocytes. It is therefore likely that interference of the drug candidate BAY16 with its pharmacological target GCGR is not primarily responsible for the hepatotoxic effects of Bay16 *in vitro* or in rats during preclinical studies. However, it should be considered that our findings reflect responses to gene silencing of GCGR while pharmaceutical inhibition of GCGR is mediated via a direct interference of BAY16 with its receptor at the protein level.

The lack of toxicity in silenced hepatocytes correlated with the absence of toxicological relevant gene expression changes. We did not find an association between deregulated metabolic pathways and suppressed GCGR signaling. In general, activation of intracellular signaling via cAMP-PKA and PLC/Ca<sup>2+</sup>/PKC by binding of glucagon at the

GCGR are involved in production of glucose through induction of gluconeogenesis and glycogenolysis [251, 255, 304]. The observed downregulation of adenylate cyclase, phosphoprotein 21kDa and protein phosphatase 2A in rat hepatocytes seems to be a consequence of suppressed GCGR signaling *in vitro*, which indicates a specific receptor-mediated on-target effect. However, the reduced cAMP-signaling has no effect on the expression of gluconeogenic enzymes. In contrast, a previous *in vivo* study demonstrated that reduced GCGR expression by ASO resulted in decreased expression of genes encoding for glycogenolytic and gluconeogenic enzymes, e.g. glucose-6-phosphatase (G6P), phosphoenolpyruvate carboxykinase (PECK) in Sprague Dawley rats [267]. The glucagon-induced glycogenolysis was also inhibited by antagonizing the GCGR in human hepatocytes after supplementation of glucagon that mimics the physiological condition in the liver [305]. It is therefore likely that differences in the transcriptional responses to metabolic processes between primary rat hepatocytes in our study and other published studies occurred because silenced hepatocytes cultured under normal conditions were not exposed to glucagon. Mice with a genetic deletion of the GCGR (GCGR<sup>-/-</sup> mice) showed improved glucose tolerance, but exhibit elevated plasma glucagon and cholesterol levels [264, 265]. Investigations of transcriptional profiling in GCGR<sup>-/-</sup> mice compared to wild type mice show that the GCGR knockout is associated with metabolic alterations, including increased cholesterol and fatty acid biosynthesis, as well as reduced amino acid catabolism and gluconeogenesis in the liver [268]. An interpretation of our results obtained *in vitro* in relation to the deregulated metabolic processes in GCGR<sup>-/-</sup> mice is complicated, because enhanced circulating levels of glucagon was also shown to induce compensatory mechanisms, including cellular hyperplasia of pancreatic cells and impaired  $\beta$ -cell function [264, 306]. Specific receptor-mediated on-target effects on the expression of few genes, including downregulation of CYP3A4 and upregulation of SREBF2, which is involved in the induction of cholestatic enzymes, were considered for further discrimination between on- and off-target mediated effects of BAY16. The strong induction of non-specific off-target effects of siRNA targeting GCGR, including stimulation of the immune response via Toll-like receptor pathways, which leads to overexpression of interferons and inflammatory chemokines, arises from the siRNA processing and mRNA degradation [180, 301, 302]. Similar effects were observed in response to transfection with non-targeting siRNA, but to a lesser extent, because of the lack of target mRNA degradation. The difference in the transcriptional response to these unspecific siRNA-mediated effects between control siRNA and GCGR siRNA explains why so many genes were found to be upregulated in GCGR-silenced cells despite normalization to control siRNA.

Taken together, neither survival rate nor specific molecular pathways were affected by suppressed GCGR mRNA expression in rat hepatocytes without toxic stimulus. Thus, it

can be assumed that the toxicity of BAY16 in the liver of rats occur independent of its therapeutic effect.

#### 4.4 Discrimination of gene expression changes induced by BAY16 in the presence and absence of the GCGR

To gain more insight into off-target mediated mechanisms of BAY16-induced hepatotoxicity, we compared the gene expression profiles after treatment with BAY16 in hepatocytes lacking GCGR (siGCGR) with cells expressing the GCGR (SC). Thus, the cells were either transfected with 50 nM of control siRNA (SC) or 50 nM of siRNA targeting GCGR for 24 h and were then incubated with 0  $\mu$ M, 25  $\mu$ M or 75  $\mu$ M of BAY16 for further 24 h before analyzing transcriptional changes using cDNA microarrays.

##### 4.4.1 Results

###### 4.4.1.1 Morphological examination

Light microscopy observations showed no clear differences in morphology and cell viability between untreated controls and hepatocytes exposed to 25  $\mu$ M of BAY16 in the presence (SC) and absence (siGCGR) of the receptor, respectively. Morphological features in hepatocytes after incubation with 75  $\mu$ M of BAY16, indicating an increased rate of cell degeneration, occurred independent of GCGR expression and thus appear to be a receptor-independent effect of BAY16.

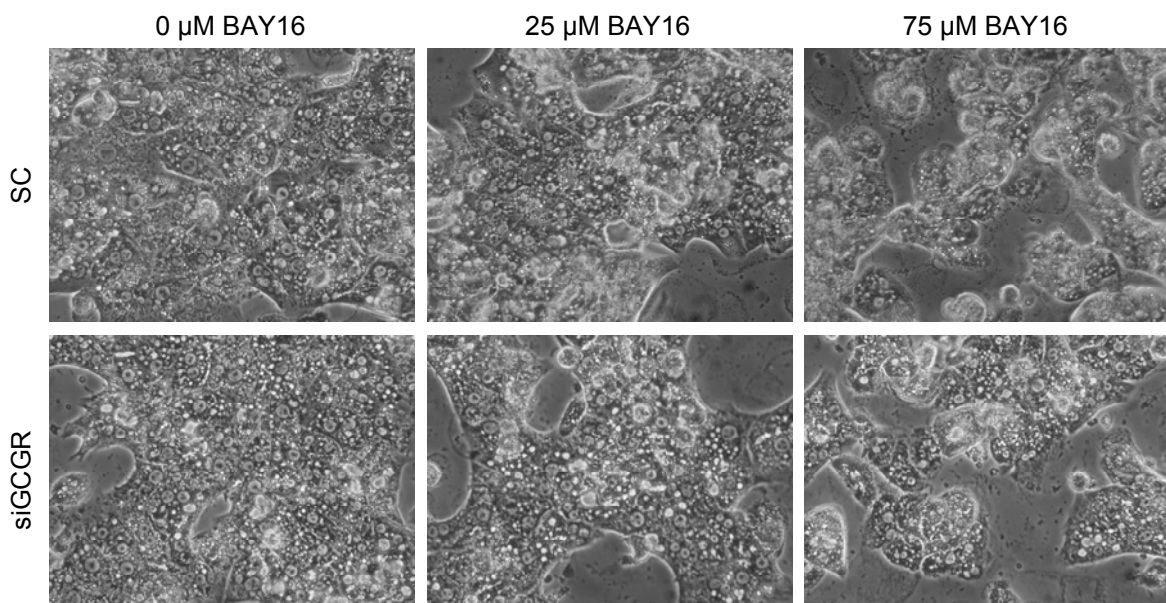


Figure 50. Effect of BAY16 in primary rat hepatocytes transfected either with control siRNA (SC) or GCGR-targeting siRNA (siGCGR). Morphological changes in cells exposed to BAY16 appear to be a receptor-independent dose-related effect of BAY16.

#### 4.4.1.2 Comparison of gene expression profile

All intensity values derived from the cDNA microarray analysis were used for PCA analysis to find differences between the transcriptional changes induced by BAY16 in hepatocytes in the presence (SC, UT) or absence of the GCGR (siGCGR). The visualization of the gene expression pattern showed a clear separation of controls from the low and high concentration group, whereas no marked differences in the gene expression profile between the SC, UT and siGCGR groups were visible (Figure 51). The Cluster analysis revealed a high variability between the three biological replicates of all groups.

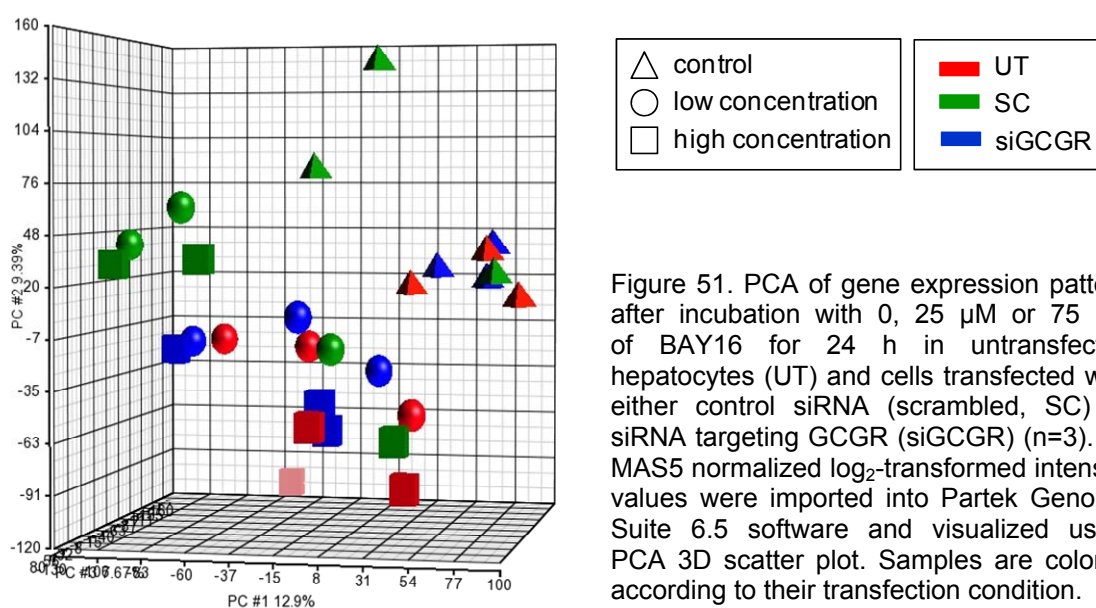


Figure 51. PCA of gene expression pattern after incubation with 0, 25  $\mu$ M or 75  $\mu$ M of BAY16 for 24 h in untransfected hepatocytes (UT) and cells transfected with either control siRNA (scrambled, SC) or siRNA targeting GCGR (siGCGR) (n=3). All MAS5 normalized  $\log_2$ -transformed intensity values were imported into Partek Genome Suite 6.5 software and visualized using PCA 3D scatter plot. Samples are colored according to their transfection condition.

Using 1-way ANOVA, a total number of 420 and 623 genes were at least 1.5-fold up- or downregulated after incubation with 25  $\mu$ M and 75  $\mu$ M of BAY16 in the presence of GCGR, respectively (Figure 52). In contrast, 418 and 498 genes were differentially expressed by a low and high concentration of BAY16 in the absence of its pharmacological target (siGCGR) (Figure 52). These data show that the number of deregulated genes induced by BAY16 does not differ between GCGR-silenced and non-silenced hepatocytes (UT, SC).

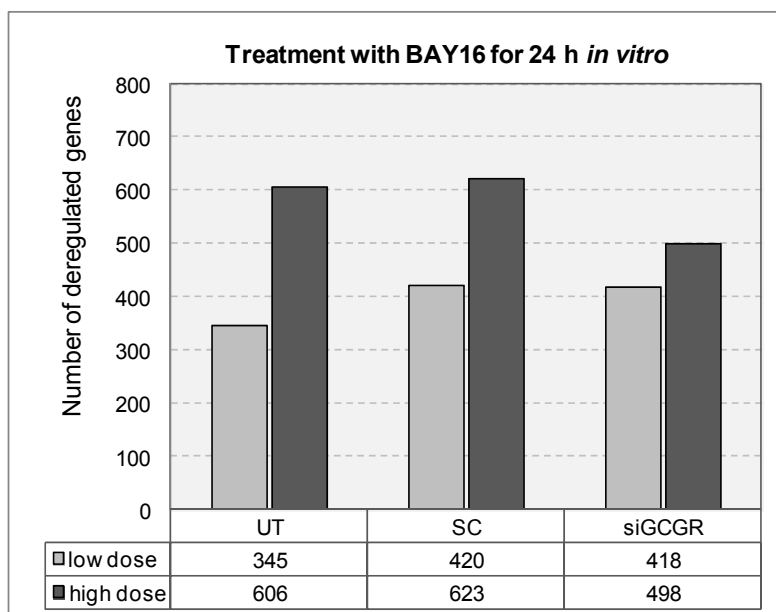


Figure 52. Number of deregulated genes *in vitro* after exposure to 25  $\mu$ M (low dose) and 75  $\mu$ M (high dose) of BAY16 in the presence (UT, SC) and absence (siGCGR) of GCGR.

#### 4.4.1.3 Comparative pathway analysis and biological interpretation of transcriptional response related to BAY16-induced hepatotoxicity

Pathway mapping of transcriptional changes induced by 25  $\mu$ M or 75  $\mu$ M of BAY16 using IPA ToxList revealed a high overlap of top-ranked pathways between siGCGR-silenced and non-silenced hepatocytes. These indicated, amongst others, liver cholestasis and steatosis as significantly enriched Tox function (Table 46), and xenobiotic metabolism, nuclear receptor activation and fatty acid metabolism as significantly enriched Tox pathways (Figure 53).

Table 46. Top three of significantly enriched Top Tox function according to IPA analysis software associated with off-target effects of BAY16 in rat hepatocytes. The ratio is calculated by dividing the number of genes from the *in vitro* study that categorized in this Tox function by the total number of genes existing in the Tox function.

Top Tox function associated with BAY16	p-value	Ratio	Genes with highest p-value
Cholestasis	2.77E-10	0.27	SCD, PAH, SLC10A1, ABCB11, SLC01A2, GGT1, ABCC2, NR0B2, ABCB4, AKR1D1, SREBF1, SLC10A2, ACSL1, MGST3
Steatosis	2.04E-07	0.11	SCD, GPD1, CPT1A, INSIG1, ACOX1, MAT1A, ABCB11, PDE4B, CCND1, POR, INSIG2, FABP5, SREBF1, NFE2L1
Necrosis/Cell death	8.03E-04	0.06	ADM, SCD, GADD45B, NR0B2, DDIT3, CDKN1A, USP2, CCND1, NFE2L1, IRF1, BCL2L1

Gene expression changes indicate an increased demand for GSH as the most significant event in hepatocytes incubated with 25  $\mu$ M of BAY16. This effect appears to be induced independent of the presence or absence of GCGR. The reduced expression of genes

involved in cholesterol biosynthesis was more pronounced in untransfected (UT) than in transfected (SC, siGCGR) hepatocytes exposed to high concentration of BAY16 (Figure 53). Most of the phase I (CYP3A4, CYP2B6, CYP2C6), phase II (GSTAs, UGT2B6, SULT) and phase III enzymes (MDR1, MDR3, BSEP, OATP, NTCP2), which are transcriptionally regulated via activation of PXR, CAR and FXR, were modulated receptor-independently. It can therefore be assumed that these effects are likely to occur compound-specific rather than target-specific. Stimulation of peroxisomal  $\beta$ -oxidation, and fatty acid biosynthesis as well as FXR-mediated regulation of bile acid homeostasis were observed in all groups, irrespective of the presence or absence of GCGR.

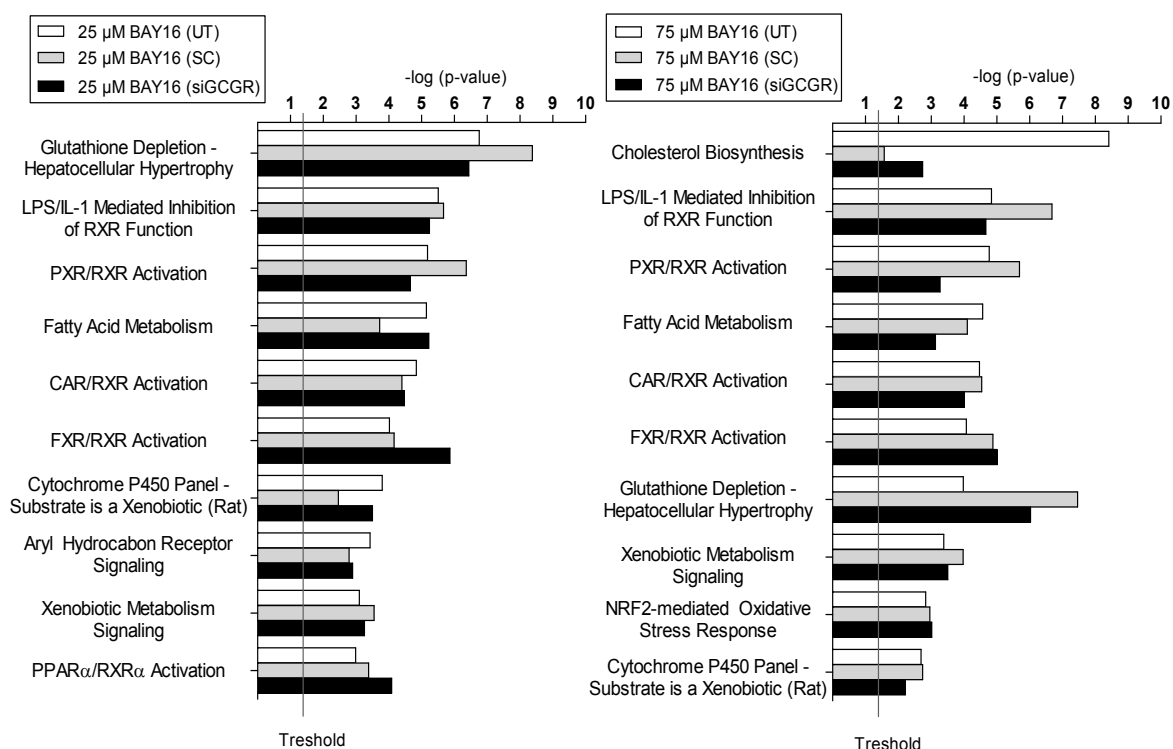


Figure 53. Top ten of significantly affected Tox pathways associated with BAY16-mediated effects occurred in rat hepatocytes in the presence (UT, SC) and absence (siGCGR) of GCGR.

In order to characterize the molecular events associated with BAY16 toxicity in the absence of its pharmacological target, we compared alterations in gene expression affected by 75  $\mu$ M of BAY16 in the presence (SC) and absence of the GCGR (siGCGR). There was a poor overlap between genes that are deregulated upon knockdown of GCGR (siGCGR) and genes associated with pharmacological modulation of the GCGR by BAY16 (HD 1d SC). Analysis of gene overlap between both groups revealed 6 upregulated and 9 downregulated genes, but these genes were not functionally relevant for BAY16-mediated toxicity (Figure 54). It is clear that there is a difference between inhibition of the GCGR at the mRNA level and protein level, but the small overlap of genes



suggests that the majority of changes in gene expression caused by BAY16 occur independently of the pharmacological modulation of the receptor.

The fact that on-target effects, e.g. changes induced by gene silencing of GCGR, were controlled for by normalization of data obtained in siGCGR hepatocytes exposed to BAY16 (HD 1d siGCGR) with control siRNA, explains why the expression profiles of siGCGR and HD 1d siGCGR show no significant overlap, apart from one downregulated gene (Figure 54). The lack of overlapping genes demonstrates that all observed effects in HD 1d siGCGR may be seen as off-targets effects caused by BAY16.

The comparative analysis of transcriptional changes induced by BAY16 in the presence (HD 1d SC, on-off target effects) and absence (HD 1d siGCGR, off-target effects) of the GCGR showed that 269 genes were commonly deregulated (Figure 54, Figure 53). The high overlap of genes included those involved in nuclear-receptor mediated signaling pathways, such as xenobiotic metabolism and lipid metabolism (Figure 53). All these BAY16-mediated molecular mechanisms thus appear to be linked to off-target effects that may occur through non-specific interaction of BAY16 with cellular targets other than the GCGR.

A total number of 354 genes, which were altered by BAY16 only in the presence of GCGR (HD 1d SC), might be related to on-target effects and secondary adaptive responses to inhibition of the receptor at the protein level (HD 1d, SC) (Figure 54).

On the other hand, 229 genes were differentially expressed only in the absence of GCGR after exposure to BAY16 (HD 1d, siGCGR) (Figure 54). The functional analysis of these genes may provide more insight into those molecular changes that are associated with toxicity and not the pharmacological action of BAY16.

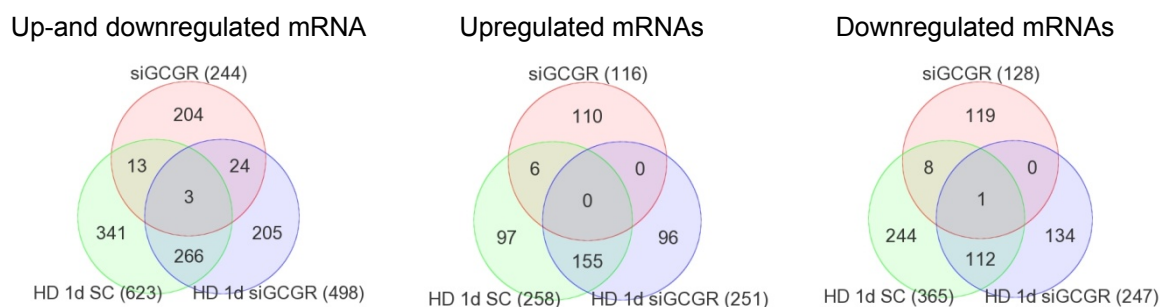


Figure 54. Venn diagram showing the number of deregulated genes associated with GCGR knockdown (on-target effects, siGCGR), and changes in gene expression induced by 75  $\mu$ M BAY16 in GCGR-silenced cells (HD 1d, siGCGR, off-target) and non-silenced cells (HD 1d, SC, on- and off-target).

Pathways represented by the 354 up- and downregulated genes which may be associated with both pharmacological inhibition of the GCGR and secondary adaptive responses of BAY16 involved LXR/RXR activation, decreased mitochondrial permeability, hepatic cholestasis and fatty acid metabolism (Table 47). LXR activation resulted in decreased expression of proinflammatory cytokines, such as interleukin 1 alpha (IL1A, 7-fold) and interleukin 18 (IL-18, 2-fold), increased expression of lipogenic key enzymes (FASN, acetyl-coenzyme A carboxylase alpha (ACACA)) and decreased expression of CD36 molecule and lecithin cholesterol acyltransferase (LCAT). CD36 has been implicated in the uptake and intercellular transport of fatty acids and cholesterol esters [307, 308]. Downregulation of LCAT, which catalyzes esterification of free cholesterol and promotes its transport in high density lipoprotein, leads to impaired transport of cholesterol [309]. The functional categorization of 205 genes, which were modulated by BAY16 only in the absence of the receptor, revealed a decreasing activity of the thyroid hormone receptor TR/RXR, associated with stimulation of lipogenesis and inhibition of cholesterol de novo synthesis. The TR receptor plays a role in the differentiation, growth and regulation of metabolic pathways [310]. The sterol regulatory element binding transcription factor 2 (SREBF2), a transcriptional regulator of cholesterol biosynthesis, was decreased in its mRNA expression (1.8-fold).

Table 47. Gene ontology analysis of genes associated with on- and off-target effects (SC) and off-target effects induced by 75  $\mu$ M (HD) of BAY16 in hepatocytes in the presence (SC) and absence (siGCGR) of the GCGR.

Category [high dose SC]-354 genes	p-value	Ratio	Genes	Category [high dose siGCGR]- 205 genes	p-value	Ratio	Genes
<b>ToxList</b>							
LXR/RXR Activation	2.5E-04	0.09	7	TR/RXR Activation	2.0E-03	0.06	5
Decreases Permeability Transition of Mitochondria and Mitochondrial Membrane	2.4E-03	0.40	2	Cholesterol Biosynthesis	1.2E-02	0.13	2
Hepatic Cholestasis	8.3E-03	0.05	7				
Fatty Acid Metabolism	1.4E-02	0.05	6				

#### 4.4.2 Discussion

For a better mechanistic interpretation of genomics data derived from pharmacologically active compounds, gene expression changes related to the toxicity need to be differentiated from those that may result from the pharmacological mode of action of a drug. Thus, the aim of this study was to discriminate between those components of the transcriptional response that may result from inhibition of the glucagon receptor and those that are truly related to the hepatotoxicity of BAY16 by comparative assessment of gene

expression changes in control vs. siRNA transfected hepatocyte in response to BAY16 treatment.

The categorization of deregulated genes according to their functional role shows that most pathways affected by BAY16 occurred regardless of the presence of GCGR. Results obtained in this study are consistent with our previous observations in untransfected hepatocytes revealing a link between BAY16 and the strong induction of nuclear-receptor mediated pathways.

Decreased receptor activity of TR/RXR and reduced cholesterol synthesis were identified as secondary off-target effects of BAY16 in GCGR-silenced hepatocytes, but both events were also found to be affected by BAY16 in GCGR-expressing hepatocytes.

The remaining 200 genes, which were found to be modulated only in GCGR-silenced cells after incubation with BAY16, could not be significantly assigned to specific IPA ToxList pathways. Categorization of genes according to their molecular and cellular function revealed connective tissue development processes, energy production and molecular transport.

Comparing siGCGR vs. siGCGR+BAY16 demonstrate that SREBF2 was upregulated in untreated GCGR-silenced hepatocytes, whereas lower mRNA levels of SREBF2 were detected in BAY16-treated silenced cells. This important observation suggests that inhibition of cholesterol synthetic processes by downregulation of SREBF2 is receptor-independent and directly linked to high concentration of BAY16. However, significantly fewer cholesterol-related genes were modulated in transfected cells compared to untransfected cells (UT) despite downregulation of SREBF2. Thus, it can be concluded that multiple mechanism are involved in the transcriptional regulation of cholesterol homeostasis.

The similarity of BAY16 induced molecular changes between SC and siGCGR indicate that the underlying mechanism of BAY16-induced hepatotoxicity is not primarily due to the pharmacological action of the drug, but seems more likely to be attributed to chemical properties of the drug.

### **4.5 Conclusions**

The inhibition of the GCGR activity for decreasing hepatic glucose overproduction represents a new therapeutic approach for the treatment of type 2 diabetes [256]. Despite intensive pharmaceutical research efforts to develop small molecule GCGR antagonists [256], the development of suitable compounds remains a big challenge due to a lack of long-term efficacy of the molecules to lowering the glucose levels in the blood [311]. This may be partly attributed to elevated glucagon levels resulting from oversecretion of

glucagon as a compensatory response to the reduced glucagon receptor signaling [311, 312]. The non-peptidyl glucagon receptor antagonist BAY27-9955 at a dose of 200 mg has been shown to effectively block glucagon-induced glucose elevation by antagonizing the GCGR in humans [261]. However, there is no report about long-term follow-up studies of this drug candidate in diabetic patients. It remains unclear why this compound was not further developed.

To improve the research and development of drug candidates, it is essential to understand the mechanism of drug toxicity in order to redesign safe and effective analogues. Toxicogenomics is widely used to gain insight into drug-mediated molecular changes but often difficult to interpret as gene expression changes may represent a combination of toxic, adaptive and pharmacological properties of the drug. To reveal relevant information about the underlying mechanism of a drug's toxicity, it may be valuable to discriminate between pharmacological and toxicological molecular responses. Due to the fact that BAY16-induced hepatotoxicity is accompanied by extensive hepatic genes expression changes in rats and insufficient knowledge about the action of GCGR antagonist of BAY16 exist, we examined if the toxic effect of BAY16 is associated with the pharmacology or occur independently of the therapeutic effects.

The genetic suppression of the GCGR had no toxic effects on the morphology and viability in primary rat hepatocytes. Based on these findings, it can be assumed that BAY16-mediated inhibition of the GCGR signaling is not primarily responsible for the hepatotoxicity of BAY16 in rats. However, it should be considered that inhibition of the GCGR by gene silencing maybe have different consequences than inhibition of GCGR function due to exposure with BAY16. Although no effects on the transcription of critical genes were observed after knockdown of the GCGR alone, hepatocytes exposed to BAY16 showed altered genes involved in xenobiotic metabolism, cholesterol and bile acid transport and synthesis, fatty acid de novo synthesis and oxidative stress. Comparative analysis of BAY16-mediated gene expression profiles in the presence and absence of GCGR showed that these pathways were independent of inhibition of GCGR by BAY16, and thus represent off-target compound-related effects. BAY16-induced hepatotoxicity is not primarily due to the pharmacological action of the drug, but seems more likely to be due to the chemical properties of the drug and interaction with cellular targets other than the GCGR. Further follow-up studies in GCGR<sup>-/-</sup> mice can be used to confirm that the toxicity of BAY16 is independent of GCGR inhibition.

These effects include molecular mechanisms related to suppressed bile acid synthesis, increased biliary detoxification and secretion, decreased bile acid import into hepatocytes, upregulation of fatty acid synthesis and xenobiotic metabolizing enzymes. All these observed effects, which are regulated by nuclear receptor signaling, suggest that

hepatocytes attempt to initiate detoxifying and eliminating processes in order to protect themselves from accumulation of fatty acids, bile acids, cholesterol or drug intermediates. Genes identified as secondary off-target effects of BAY16 in GCGR-silenced hepatocytes also relate to metabolic processes. Although low concentration of BAY16 did not cause any morphological changes compared to controls, both low and high concentration of BAY16 resulted in deregulation of genes involved in the same pathways, apart from high-concentration-mediated inhibition of cholesterol synthesis. Some of these effects are known to contribute to liver injury, especially oxidative stress and xenobiotic metabolizing processes [72, 313]. It was demonstrated that acetaminophen at a dose without morphologically sign of toxicity induced similar gene expression changes as a toxic dose of acetaminophen [96]. It is known that acetaminophen-induced liver injury is attributed to formation of a toxic metabolite N-acetyl-p-benzoquinone imine that can covalently bind to proteins, leading to increase of oxidative stress, which is accompanied by mitochondrial injury and ATP depletion [160, 161, 314]. However, no information of biotransformation of BAY16 is available.

Results from previous metabonomics and transcriptomics studies have demonstrated that bile acid and cholesterol levels were increased in response to BAY16 in the liver of rats, as consequence of cholestatic injury [97]. The mechanism underlying downregulation of genes related to cholesterol biosynthesis *in vitro* remains unclear and needs to be further investigated. However, the fact that gene expression changes induced by BAY16 *in vitro* revealed cholestasis and hepatocyte necrosis as significantly enriched Tox functions suggest that *in vitro* transcriptomics may be predictive of the cholestatic type of liver injury induced by BAY16 *in vivo*. Because BAY16 induced cell death in hepatocytes at a concentration of 75  $\mu$ M for 24 h despite absence of biliary epithelia cells in a culture model, hepatocytes can be considered as primary target cells of BAY16-induced liver injury in the rat. Early expression changes associated with oxidative stress, observed both *in vivo* and *in vitro*, might be caused by the formation of a reactive metabolite.

In several cases of drug-induced cholestatic injuries, reactive metabolites are excreted into the bile via canicular transporters, such as BSEP [168, 315], and directly or indirectly inhibit biliary transport, resulting in intrahepatic accumulation of toxic bile acids and subsequent hepatocyte necrosis [64]. It might thus be hypothesized that hepatobiliary injury induced by BAY16 in rats may be due to downregulation of biliary transport efflux resulting from increased clearance of a reactive metabolite. This hypothesis needs to be further investigated.

Taken together, effects of BAY16 on the expression of genes *in vitro* appear to be compound-specific and not GCGR mediated and have characteristics of pathological phenotypes associated with cholestasis and steatosis. Thus, there is a good correlation

between *in vitro* data and histopathological features in the rat liver despite differences in the transcriptional regulation of genes. However, results obtained from this study show that the utilization of siRNA-mediated gene silencing *in vitro* to specifically knockdown the expression of the pharmacological target of selected drugs provide additional information regarding the underlying mechanism of a drug's toxicity.

## 5 SUMMARY

The high failure rate of new drug candidates in preclinical or clinical studies due to hepatotoxicity represents a considerable problem in the drug development. Hence, there is an urgent need to develop new approaches for early and reliable prediction of drug-induced hepatotoxicity that enables a better identification of drug candidates with high potential for toxicity at early stages of drug development. Therefore, the aim of this work was to improve the prediction of drug-induced liver injury in preclinical studies through evaluation of more reliable and sensitive biomarkers of hepatotoxicity and a better understanding of the underlying mechanistic basis for drug-induced toxicity.

First, the ability of a set of potential markers (NGAL, thiostatin, clusterin, PON1) to detect early signs of liver injury was assessed in rats treated with drug candidates that were dropped from further development, in part due to toxic adverse effects in the liver. In summary, PON1 and clusterin were not consistently altered in response to liver injury and thus provide no additive information to the traditional liver enzymes in detecting drug-induced hepatotoxicity. In contrast, thiostatin and NGAL were increased in serum and urine of treated animals in a time- and dose-dependent manner. These changes correlated well with mRNA expression in the target organ and generally reflected the onset and degree of drug-induced liver injury. Receiver-operating characteristics analyses supported serum thiostatin, but not NGAL, as a better indicator of drug-induced hepatobiliary injury than conventional clinical chemistry parameters, such as ALP, ALT and AST. Although thiostatin, an acute phase protein expressed in a range of tissues, may not be specific for liver injury, our results indicate that thiostatin may serve as a sensitive, minimally-invasive diagnostic marker of inflammation and tissue damage in preclinical safety assessment.

In the second part of this work, combined application of genomics profiling technology and RNAi to inhibit the pharmacological target of a drug candidate BAY16, a glucagon receptor (GCGR) antagonist, was used to determine if interference with the pharmacological target plays a role in the toxic response to BAY16, and to narrow down those molecular changes that are associated with toxicity, and not the pharmacological action of BAY16. In contrast to Bay 16, which was found to be cytotoxic at concentrations of 75  $\mu$ M, silencing of the glucagon receptor did not affect cell viability in primary rat hepatocytes. Thus, it can be concluded that hepatotoxicity of Bay 16 was not related to the drugs inhibitory effect on the glucagon receptor *in vitro* and *in vivo*. These findings were supported by the fact that most of BAY16-induced changes in gene expression occurred independently of the pharmacological modulation of GCGR. These off-target effects include altered xenobiotic metabolism, oxidative stress, increased fatty acid

synthesis, and alterations in cholesterol and bile acid metabolic processes. Although it was not possible to draw a final conclusion about the mechanism of BAY16 hepatotoxicity, changes in these molecular mechanisms appear contribute to progression of hepatic injury. With regard to drug safety assessment in preclinical studies, the utilization of siRNA technology *in vitro* represents a new approach to improve mechanistic understanding of the nature of drug's toxicity, being either chemically mediated or due to primary or secondary pharmacological mode of action.



## 6 ZUSAMMENFASSUNG

Das häufige Scheitern neuer Arzneistoffkandidaten aufgrund von Lebertoxizität in präklinischen und klinischen Studien stellt ein erhebliches Problem in der Entwicklung von neuen Arzneimitteln dar. Deshalb ist es wichtig, neue Ansätze zu entwickeln, mit deren Hilfe unerwünschte Wirkungen von Arzneimitteln früher und zuverlässiger erkannt werden können. Um die Vorhersage von Lebertoxizität in präklinischen Studien zu verbessern, wurden im Rahmen dieser Arbeit zwei wesentliche Ansätze gewählt: 1) die Evaluierung neuer Biomarker, durch die Lebertoxizität zuverlässiger und empfindlicher detektiert werden könnte und 2.) wirkmechanistische Untersuchungen mittels Toxicogenomics für ein besseres Verständnis der zugrunde liegenden Mechanismen der Arzneimittel-induzierten Toxizität.

Ein Ziel dieser Arbeit war, die Fähigkeit einiger neuer potenzieller Biomarker (NGAL, Thiostatin, Clusterin und PON1) zu bewerten, Arzneimittel-induzierte Lebertoxizität in Ratten frühzeitig zu erkennen. Die Ergebnisse zeigen, dass PON1 und Clusterin infolge eines durch die verabreichten Arzneistoffkandidaten verursachten Leberschadens nicht konsistent verändert waren. Diese beiden Marker sind daher, verglichen mit bestehenden klinisch-chemischen Markern, nicht für eine sichere Vorhersage von Arzneistoff-induzierten Leberschäden geeignet. Bei Thiostatin und NGAL zeigte sich hingegen ein zeit- und dosisabhängiger Anstieg im Serum und Urin behandelte Tiere. Diese Veränderungen, die gut mit der mRNA Expression im Zielorgan übereinstimmten, korrelierten mit dem Schweregrad der Arzneistoff-induzierten Leberschäden. Die Analyse mittels ROC zeigte, Thiostatin im Serum, nicht aber NGAL, ein besserer Indikator für Arzneimittel-induzierte hepatobiliäre Schäden ist als die routinemäßig verwendeten klinische-chemischen Marker, wie z.B. die Leberenzyme ALP, ALT und AST. Thiostatin wird jedoch als Akute-Phase-Protein in einer Vielzahl von Geweben exprimiert und kann somit nicht spezifisch als Lebermarker betrachtet werden. Dennoch zeigen unsere Ergebnisse, dass Thiostatin als sensitiver, minimal-invasiver diagnostischer Marker für Entzündungsprozesse und Gewebeschäden eine sinnvolle Ergänzung in der präklinischen Testung auf Lebertoxizität darstellt.

Im zweiten Teil dieser Arbeit wurde mittels RNA-Interferenz das pharmakologische Target des Arzneistoffkandidaten BAY16, der Glukagonrezeptor, auf mRNA-Ebene gehemmt und anhand von Genexpressionsanalysen untersucht, ob die pharmakologisch-bedingte Modulation des Glukagonrezeptors eine Rolle in der Toxizität von BAY16 spielt. Desweiteren sollten diese Arbeiten Aufschluss geben, welche molekularen Veränderungen auf die pharmakologische Wirkung des Arzneistoffs zurückzuführen sind, und daher für den Mechanismus der Toxizität möglicherweise wenig relevant sind.

Während BAY16 in Konzentrationen von 75  $\mu$ M starke zytotoxische Wirkungen aufwies, hatte die siRNA vermittelte Depletion des Glukagonrezeptors keinen Einfluss auf die Vitalität primärer Rattenhepatozyten. Daraus lässt sich ableiten, dass die Hepatotoxizität von BAY16 *in vitro* und *in vivo* nicht mit der pharmakologischen Modulation des Glukagonrezeptors assoziiert ist. Diese Ergebnisse wurden durch die Tatsache gestützt, dass die meisten der durch BAY16 induzierten Genexpressionsveränderungen unabhängig von der pharmakologischen Modulation des Glucagonrezeptors auftraten. Diese beobachteten off-target-Effekte beinhalteten Veränderungen im Fremdstoffmetabolismus, oxidativer Stress, erhöhte Fettsäuresynthese und Veränderungen im Cholesterol- und Gallensäuremetabolismus. Obwohl Veränderungen in diesen molekularen Mechanismen zum Fortschreiten eines Leberschadens beitragen können, ist es anhand dieser Daten nicht möglich einen eindeutigen Mechanismus für die Toxizität von BAY16 abzuleiten.

In dieser Arbeit konnte jedoch gezeigt werden, dass die Anwendung der siRNA-Technologie einen neuen methodischen Ansatz darstellt, um Mechanismen arzneimittelbedingter Toxizität besser verstehen zu können.

## 7 REFERENCES

1. Kola, I. and J. Landis, *Can the pharmaceutical industry reduce attrition rates?* Nat Rev Drug Discov, 2004. **3**(8): p. 711-5.
2. Schuster, D., C. Laggner, and T. Langer, *Why drugs fail--a study on side effects in new chemical entities.* Curr Pharm Des, 2005. **11**(27): p. 3545-59.
3. Zimmerman, H.J., *Hepatotoxicity : the adverse effects of drugs and other chemicals on the liver.* 2nd ed. 1999, Philadelphia ; London: Lippincott Williams & Wilkins. viii, 789 p. [16] p. of col. plates.
4. Kiyosawa, N., Y. Ando, S. Manabe, et al., *Toxicogenomic Biomarkers for Liver Toxicity.* Journal of Toxicologic Pathology, 2009. **22**(1): p. 35-52.
5. Holt, M.P. and C. Ju, *Mechanisms of drug-induced liver injury.* AAPS J, 2006. **8**(1): p. E48-54.
6. Kaplowitz, N., *Drug-induced liver injury.* Clinical Infectious Diseases, 2004. **38**: p. S44-S48.
7. Holt, M. and C. Ju, *Drug-induced liver injury.* Handb Exp Pharmacol, 2010(196): p. 3-27.
8. Ostapowicz, G. and W.M. Lee, *Acute hepatic failure: a Western perspective.* J Gastroenterol Hepatol, 2000. **15**(5): p. 480-8.
9. Fung, M., *Evaluation of the characteristics of safety withdrawal of prescription drugs from worldwide pharmaceutical markets-1960 to 1999.* Drug Information Journal, 2001. **35**(1): p. 293-317.
10. Zimmerman, H.J., *Drug-induced liver disease.* Clin Liver Dis, 2000. **4**(1): p. 73-96, vi.
11. Bjornsson, E. and R. Olsson, *Suspected drug-induced liver fatalities reported to the WHO database.* Dig Liver Dis, 2006. **38**(1): p. 33-8.
12. Ostapowicz, G., R.J. Fontana, F.V. Schiodt, et al., *Results of a prospective study of acute liver failure at 17 tertiary care centers in the United States.* Ann Intern Med, 2002. **137**(12): p. 947-54.
13. Wei, G., A. Bergquist, U. Broome, et al., *Acute liver failure in Sweden: etiology and outcome.* Journal of Internal Medicine, 2007. **262**(3): p. 393-401.
14. Bakke, O.M., M. Manocchia, F. de Abajo, et al., *Drug safety discontinuations in the United Kingdom, the United States, and Spain from 1974 through 1993: a regulatory perspective.* Clin Pharmacol Ther, 1995. **58**(1): p. 108-17.
15. Graham, D.J., L. Green, J.R. Senior, et al., *Troglitazone-induced liver failure: a case study.* Am J Med, 2003. **114**(4): p. 299-306.
16. Ikehata, K., T.G. Duzhak, N.A. Galeva, et al., *Protein targets of reactive metabolites of thiobenzamide in rat liver in vivo.* Chem Res Toxicol, 2008. **21**(7): p. 1432-42.
17. Trauner, M., M. Wagner, P. Fickert, et al., *Molecular regulation of hepatobiliary transport systems: clinical implications for understanding and treating cholestasis.* J Clin Gastroenterol, 2005. **39**(4 Suppl 2): p. S111-24.
18. Geier, A., S.K. Kim, T. Gerloff, et al., *Hepatobiliary organic anion transporters are differentially regulated in acute toxic liver injury induced by carbon tetrachloride.* J Hepatol, 2002. **37**(2): p. 198-205.

## 7 REFERENCES

---

19. Zollner, G., M. Wagner, and M. Trauner, *Nuclear receptors as drug targets in cholestasis and drug-induced hepatotoxicity*. *Pharmacol Ther*, 2010. **126**(3): p. 228-43.
20. Kaplowitz, N., *Biochemical and cellular mechanisms of toxic liver injury*. *Semin Liver Dis*, 2002. **22**(2): p. 137-44.
21. Russmann, S., G.A. Kullak-Ublick, and I. Grattagliano, *Current concepts of mechanisms in drug-induced hepatotoxicity*. *Curr Med Chem*, 2009. **16**(23): p. 3041-53.
22. Casarett, L.J., J. Doull, and C.D. Klaassen, *Casarett and Doull's toxicology : the basic science of poisons*. 7th ed. 2008, New York: McGraw-Hill. xv, 1310 p., 1 leaf of plates.
23. LaBrecque, D., *Liver regeneration: a picture emerges from the puzzle*. *Am J Gastroenterol*, 1994. **89**(8 Suppl): p. S86-96.
24. Malarkey, D.E., K. Johnson, L. Ryan, et al., *New insights into functional aspects of liver morphology*. *Toxicol Pathol*, 2005. **33**(1): p. 27-34.
25. Blouin, A., R.P. Bolender, and E.R. Weibel, *Distribution of organelles and membranes between hepatocytes and nonhepatocytes in the rat liver parenchyma. A stereological study*. *J Cell Biol*, 1977. **72**(2): p. 441-55.
26. Wisse, E., *On the endothelial cells of rat liver sinusoids*. *Bibl Anat*, 1977(16 Pt 2): p. 373-6.
27. Widmann, J.J., R.S. Cotran, and H.D. Fahimi, *Mononuclear phagocytes (Kupffer cells) and endothelial cells. Identification of two functional cell types in rat liver sinusoids by endogenous peroxidase activity*. *J Cell Biol*, 1972. **52**(1): p. 159-70.
28. Rappaport, A.M., Z.J. Borowy, W.M. Lougheed, et al., *Subdivision of Hexagonal Liver Lobules into a Structural and Functional Unit - Role in Hepatic Physiology and Pathology*. *Anatomical Record*, 1954. **119**(1): p. 11-33.
29. Si-Tayeb, K., F.P. Lemaigre, and S.A. Duncan, *Organogenesis and Development of the Liver*. *Developmental Cell*, 2010. **18**(2): p. 175-189.
30. Le Lay, J. and K.H. Kaestner, *The Fox genes in the liver: from organogenesis to functional integration*. *Physiol Rev*, 2010. **90**(1): p. 1-22.
31. Elvevold, K., B. Smedsrod, and I. Martinez, *The liver sinusoidal endothelial cell: a cell type of controversial and confusing identity*. *Am J Physiol Gastrointest Liver Physiol*, 2008. **294**(2): p. G391-400.
32. He, F.C., L. Tang, J.T. Yang, et al., *Liver Sinusoidal Endothelial Cell Lectin, LSECtin, Negatively Regulates Hepatic T-Cell Immune Response*. *Gastroenterology*, 2009. **137**(4): p. 1498-1508.
33. Knolle, P.A., F.A. Schildberg, S.L. Hegenbarth, et al., *Liver sinusoidal endothelial cells veto CD8 T cell activation by antigen-presenting dendritic cells*. *European Journal of Immunology*, 2008. **38**(4): p. 957-967.
34. Winwood, P.J. and M.J. Arthur, *Kupffer cells: their activation and role in animal models of liver injury and human liver disease*. *Semin Liver Dis*, 1993. **13**(1): p. 50-9.
35. Wake, K., *Perisinusoidal Stellate Cells (Fat-Storing Cells, Interstitial Cells, Lipocytes), Their Related Structure in and around the Liver Sinusoids, and Vitamin A-Storing Cells in Extrahepatic Organs*, in *International Review of Cytology*, J.F.D. G.H. Bourne and K.W. Jeon, Editors. 1980, Academic Press. p. 303-353.
36. Arthur, M.J., A. Stanley, J.P. Iredale, et al., *Secretion of 72 kDa type IV collagenase/gelatinase by cultured human lipocytes. Analysis of gene expression, protein synthesis and proteinase activity*. *Biochem J*, 1992. **287** ( Pt 3): p. 701-7.

37. Kim, K.Y., I. Choi, and S.S. Kim, *Progression of hepatic stellate cell activation is associated with the level of oxidative stress rather than cytokines during CCl4-induced fibrogenesis*. *Mol Cells*, 2000. **10**(3): p. 289-300.
38. Carpino, G., A. Franchitto, S. Morini, et al., *Activated hepatic stellate cells in liver cirrhosis. A morphologic and morphometrical study*. *Ital J Anat Embryol*, 2004. **109**(4): p. 225-38.
39. Hagenbuch, B. and P.J. Meier, *Molecular cloning, chromosomal localization, and functional characterization of a human liver Na<sup>+</sup>/bile acid cotransporter*. *J Clin Invest*, 1994. **93**(3): p. 1326-31.
40. Hagenbuch, B. and P.J. Meier, *The superfamily of organic anion transporting polypeptides*. *Biochim Biophys Acta*, 2003. **1609**(1): p. 1-18.
41. Trauner, M. and J.L. Boyer, *Bile salt transporters: molecular characterization, function, and regulation*. *Physiol Rev*, 2003. **83**(2): p. 633-71.
42. Pauli-Magnus, C. and P.J. Meier, *Hepatobiliary transporters and drug-induced cholestasis*. *Hepatology*, 2006. **44**(4): p. 778-87.
43. Tolson, A.H. and H. Wang, *Regulation of drug-metabolizing enzymes by xenobiotic receptors: PXR and CAR*. *Adv Drug Deliv Rev*, 2010. **62**(13): p. 1238-49.
44. Ferguson, S.S., E.L. LeCluyse, M. Negishi, et al., *Regulation of human CYP2C9 by the constitutive androstane receptor: discovery of a new distal binding site*. *Mol Pharmacol*, 2002. **62**(3): p. 737-46.
45. Maglich, J.M., C.M. Stoltz, B. Goodwin, et al., *Nuclear pregnane x receptor and constitutive androstane receptor regulate overlapping but distinct sets of genes involved in xenobiotic detoxification*. *Mol Pharmacol*, 2002. **62**(3): p. 638-46.
46. Goodwin, B., L.B. Moore, C.M. Stoltz, et al., *Regulation of the human CYP2B6 gene by the nuclear pregnane X receptor*. *Mol Pharmacol*, 2001. **60**(3): p. 427-31.
47. Lee, W.M., *Drug-induced hepatotoxicity*. *N Engl J Med*, 2003. **349**(5): p. 474-85.
48. Cullen, J.M., *Mechanistic classification of liver injury*. *Toxicol Pathol*, 2005. **33**(1): p. 6-8.
49. Hofmann, A.F., *Bile Acids: The Good, the Bad, and the Ugly*. *News Physiol Sci*, 1999. **14**: p. 24-29.
50. Norlin, M. and K. Wikvall, *Enzymes in the conversion of cholesterol into bile acids*. *Curr Mol Med*, 2007. **7**(2): p. 199-218.
51. Zollner, G. and M. Trauner, *Nuclear receptors as therapeutic targets in cholestatic liver diseases*. *Br J Pharmacol*, 2009. **156**(1): p. 7-27.
52. Parks, D.J., S.G. Blanchard, R.K. Bledsoe, et al., *Bile acids: natural ligands for an orphan nuclear receptor*. *Science*, 1999. **284**(5418): p. 1365-8.
53. Denson, L.A., E. Sturm, W. Echevarria, et al., *The orphan nuclear receptor, shp, mediates bile acid-induced inhibition of the rat bile acid transporter, ntcp*. *Gastroenterology*, 2001. **121**(1): p. 140-7.
54. Ananthanarayanan, M., N. Balasubramanian, M. Makishima, et al., *Human bile salt export pump promoter is transactivated by the farnesoid X receptor/bile acid receptor*. *J Biol Chem*, 2001. **276**(31): p. 28857-65.

## 7 REFERENCES

---

55. Kast, H.R., B. Goodwin, P.T. Tarr, et al., *Regulation of multidrug resistance-associated protein 2 (ABCC2) by the nuclear receptors pregnane X receptor, farnesoid X-activated receptor, and constitutive androstane receptor*. J Biol Chem, 2002. **277**(4): p. 2908-15.
56. Repa, J.J. and D.J. Mangelsdorf, *The role of orphan nuclear receptors in the regulation of cholesterol homeostasis*. Annu Rev Cell Dev Biol, 2000. **16**: p. 459-81.
57. Geier, A., C. Gartung, and S. Matern, *Regulationsmechanismen hepatobiliärer Transporter bei cholestatischen Erkrankungen\**. Medizinische Klinik, 2004. **99**(1): p. 7-17.
58. Trauner, M., P.J. Meier, and J.L. Boyer, *Molecular pathogenesis of cholestasis*. N Engl J Med, 1998. **339**(17): p. 1217-27.
59. Stieger, B., K. Fattinger, J. Madon, et al., *Drug- and estrogen-induced cholestasis through inhibition of the hepatocellular bile salt export pump (Bsep) of rat liver*. Gastroenterology, 2000. **118**(2): p. 422-30.
60. Byrne, J.A., S.S. Strautnieks, G. Mieli-Vergani, et al., *The human bile salt export pump: characterization of substrate specificity and identification of inhibitors*. Gastroenterology, 2002. **123**(5): p. 1649-58.
61. Watkins, P.B. and L.B. Seeff, *Drug-induced liver injury: summary of a single topic clinical research conference*. Hepatology, 2006. **43**(3): p. 618-31.
62. Tanaka, Y., L.M. Aleksunes, Y.J. Cui, et al., *ANIT-induced intrahepatic cholestasis alters hepatobiliary transporter expression via Nrf2-dependent and independent signaling*. Toxicol Sci, 2009. **108**(2): p. 247-57.
63. Dietrich, C.G., R. Ottenhoff, D.R. de Waart, et al., *Role of MRP2 and GSH in intrahepatic cycling of toxins*. Toxicology, 2001. **167**(1): p. 73-81.
64. Klaassen, C.D. and L.M. Aleksunes, *Xenobiotic, bile acid, and cholesterol transporters: function and regulation*. Pharmacol Rev, 2010. **62**(1): p. 1-96.
65. Powell, E.E., J.R. Jonsson, and A.D. Clouston, *Steatosis: co-factor in other liver diseases*. Hepatology, 2005. **42**(1): p. 5-13.
66. Anderson, N. and J. Borlak, *Molecular mechanisms and therapeutic targets in steatosis and steatohepatitis*. Pharmacol Rev, 2008. **60**(3): p. 311-57.
67. Kennedy, J.A., S.A. Unger, and J.D. Horowitz, *Inhibition of carnitine palmitoyltransferase-1 in rat heart and liver by perhexiline and amiodarone*. Biochemical pharmacology, 1996. **52**(2): p. 273-80.
68. Fromenty, B., C. Fisch, A. Berson, et al., *Dual effect of amiodarone on mitochondrial respiration. Initial protonophoric uncoupling effect followed by inhibition of the respiratory chain at the levels of complex I and complex II*. J Pharmacol Exp Ther, 1990. **255**(3): p. 1377-84.
69. Bolt, M.W., J.W. Card, W.J. Racz, et al., *Disruption of mitochondrial function and cellular ATP levels by amiodarone and N-desethylamiodarone in initiation of amiodarone-induced pulmonary cytotoxicity*. J Pharmacol Exp Ther, 2001. **298**(3): p. 1280-9.
70. Kassahun, K., K. Farrell, and F. Abbott, *Identification and characterization of the glutathione and N-acetylcysteine conjugates of (E)-2-propyl-2,4-pentadienoic acid, a toxic metabolite of valproic acid, in rats and humans*. Drug Metab Dispos, 1991. **19**(2): p. 525-35.
71. Fromenty, B. and D. Pessayre, *Impaired mitochondrial function in microvesicular steatosis. Effects of drugs, ethanol, hormones and cytokines*. J Hepatol, 1997. **26 Suppl 2**: p. 43-53.

72. Jaeschke, H., G.J. Gores, A.I. Cederbaum, et al., *Mechanisms of hepatotoxicity*. Toxicol Sci, 2002. **65**(2): p. 166-76.
73. Ulrich, R.G., J.A. Bacon, C.T. Cramer, et al., *Cultured hepatocytes as investigational models for hepatic toxicity: practical applications in drug discovery and development*. Toxicol Lett, 1995. **82-83**: p. 107-15.
74. Guillouzo, A., *Liver cell models in in vitro toxicology*. Environ Health Perspect, 1998. **106 Suppl 2**: p. 511-32.
75. Castell, J.V. and M.J. Gomez-Lechon, *Liver cell culture techniques*. Methods Mol Biol, 2009. **481**: p. 35-46.
76. Henkens, T., T. Vanhaecke, P. Papeleu, et al., *Rat hepatocyte cultures: conventional monolayer and cocultures with rat liver epithelial cells*. Methods Mol Biol, 2006. **320**: p. 239-46.
77. Tuschl, G., J. Hrach, Y. Walter, et al., *Serum-free collagen sandwich cultures of adult rat hepatocytes maintain liver-like properties long term: a valuable model for in vitro toxicity and drug-drug interaction studies*. Chem Biol Interact, 2009. **181**(1): p. 124-37.
78. Tuschl, G. and S.O. Mueller, *Effects of cell culture conditions on primary rat hepatocytes-cell morphology and differential gene expression*. Toxicology, 2006. **218**(2-3): p. 205-15.
79. Richert, L., D. Binda, G. Hamilton, et al., *Evaluation of the effect of culture configuration on morphology, survival time, antioxidant status and metabolic capacities of cultured rat hepatocytes*. Toxicol In Vitro, 2002. **16**(1): p. 89-99.
80. Davila, J.C. and D.L. Morris, *Analysis of cytochrome P450 and phase II conjugating enzyme expression in adult male rat hepatocytes*. In Vitro Cell Dev Biol Anim, 1999. **35**(3): p. 120-30.
81. Kefalas, V. and N.H. Stacey, *Use of primary cultures of rat hepatocytes to study interactive toxicity: Carbon tetrachloride and trichloroethylene*. Toxicol In Vitro, 1993. **7**(3): p. 235-40.
82. Amacher, D.E., *The discovery and development of proteomic safety biomarkers for the detection of drug-induced liver toxicity*. Toxicol Appl Pharmacol, 2010. **245**(1): p. 134-42.
83. Group, B.D.W., *Biomarkers and surrogate endpoints: preferred definitions and conceptual framework*. Clin Pharmacol Ther, 2001. **69**(3): p. 89-95.
84. Ramaiah, S.K., *A toxicologist guide to the diagnostic interpretation of hepatic biochemical parameters*. Food Chem Toxicol, 2007. **45**(9): p. 1551-7.
85. Nathwani, R.A., S. Pais, T.B. Reynolds, et al., *Serum alanine aminotransferase in skeletal muscle diseases*. Hepatology, 2005. **41**(2): p. 380-2.
86. Shteyer, E., I. Yatsiv, M. Sharkia, et al., *Serum Transaminases as a Prognostic Factor in Children Post Cardiac Surgery*. Pediatr Int, 2011.
87. Antoine, D.J., A.E. Mercer, D.P. Williams, et al., *Mechanism-based bioanalysis and biomarkers for hepatic chemical stress*. Xenobiotica, 2009. **39**(8): p. 565-77.
88. Tobiume, H., S. Kanzaki, S. Hida, et al., *Serum bone alkaline phosphatase isoenzyme levels in normal children and children with growth hormone (GH) deficiency: a potential marker for bone formation and response to GH therapy*. J Clin Endocrinol Metab, 1997. **82**(7): p. 2056-61.
89. Cooper, D.S., M.M. Kaplan, E.C. Ridgway, et al., *Alkaline phosphatase isoenzyme patterns in hyperthyroidism*. Ann Intern Med, 1979. **90**(2): p. 164-8.

## 7 REFERENCES

---

90. Chikhi, N., N. Holic, G. Guellaen, et al., *Gamma-glutamyl transpeptidase gene organization and expression: a comparative analysis in rat, mouse, pig and human species*. *Comp Biochem Physiol B Biochem Mol Biol*, 1999. **122**(4): p. 367-80.
91. Suter, L., L.E. Babiss, and E.B. Wheeldon, *Toxicogenomics in predictive toxicology in drug development*. *Chem Biol*, 2004. **11**(2): p. 161-71.
92. Lindon, J.C., E. Holmes, and J.K. Nicholson, *Metabonomics and its role in drug development and disease diagnosis*. *Expert Rev Mol Diagn*, 2004. **4**(2): p. 189-99.
93. Cunningham, M.J., *Genomics and proteomics: the new millennium of drug discovery and development*. *J Pharmacol Toxicol Methods*, 2000. **44**(1): p. 291-300.
94. Ge, F. and Q.Y. He, *Genomic and proteomic approaches for predicting toxicity and adverse drug reactions*. *Expert Opin Drug Metab Toxicol*, 2009. **5**(1): p. 29-37.
95. Nuwaysir, E.F., M. Bittner, J. Trent, et al., *Microarrays and toxicology: the advent of toxicogenomics*. *Mol Carcinog*, 1999. **24**(3): p. 153-9.
96. Cui, Y. and R.S. Paules, *Use of transcriptomics in understanding mechanisms of drug-induced toxicity*. *Pharmacogenomics*, 2010. **11**(4): p. 573-85.
97. Ellinger-Ziegelbauer, H., M. Adler, A. Amberg, et al., *The enhanced value of combining conventional and "omics" analyses in early assessment of drug-induced hepatobiliary injury*. *Toxicol Appl Pharmacol*, 2011. **252**(2): p. 97-111.
98. Suter, L., S. Schroeder, K. Meyer, et al., *EU Framework 6 Project: Predictive Toxicology (PredTox) - Overview and Outcome*. *Toxicol Appl Pharmacol*, 2010.
99. Searfoss, G.H., T.P. Ryan, and R.A. Jolly, *The role of transcriptome analysis in pre-clinical toxicology*. *Curr Mol Med*, 2005. **5**(1): p. 53-64.
100. Waters, M.D. and J.M. Fostel, *Toxicogenomics and systems toxicology: aims and prospects*. *Nat Rev Genet*, 2004. **5**(12): p. 936-48.
101. Waring, J.F., R.A. Jolly, R. Ciurlionis, et al., *Clustering of hepatotoxins based on mechanism of toxicity using gene expression profiles*. *Toxicol Appl Pharmacol*, 2001. **175**(1): p. 28-42.
102. Fielden, M.R., R. Brennan, and J. Gollub, *A gene expression biomarker provides early prediction and mechanistic assessment of hepatic tumor induction by nongenotoxic chemicals*. *Toxicol Sci*, 2007. **99**(1): p. 90-100.
103. Rohrbeck, A., G. Salinas, K. Maaser, et al., *Toxicogenomics applied to in vitro carcinogenicity testing with Balb/c 3T3 cells revealed a gene signature predictive of chemical carcinogens*. *Toxicol Sci*, 2010. **118**(1): p. 31-41.
104. Zidek, N., J. Hellmann, P.J. Kramer, et al., *Acute hepatotoxicity: a predictive model based on focused illumina microarrays*. *Toxicol Sci*, 2007. **99**(1): p. 289-302.
105. Gallagher, W.M., D. Tweats, and J. Koenig, *Omic profiling for drug safety assessment: current trends and public-private partnerships*. *Drug Discov Today*, 2009. **14**(7-8): p. 337-42.
106. Matheis, K.A., E. Com, J.C. Gautier, et al., *Cross-study and cross-omics comparisons of three nephrotoxic compounds reveal mechanistic insights and new candidate biomarkers*. *Toxicol Appl Pharmacol*, 2010.
107. Boitier, E., A. Amberg, V. Barbie, et al., *A comparative integrated transcript analysis and functional characterization of differential mechanisms for induction of liver hypertrophy in the rat*. *Toxicol Appl Pharmacol*, 2011.



108. La Du, B.N., *Pharmacogenetics of drug metabolism (Kalow, W., ed.)*, pp 51-91. 1st ed ed. 1992, New York Pergamon. xxxii, 897 p.
109. Richter, R.J., G.P. Jarvik, and C.E. Furlong, *Paraoxonase 1 (PON1) status and substrate hydrolysis*. *Toxicol Appl Pharmacol*, 2009. **235**(1): p. 1-9.
110. Mackness, M.I., S. Arrol, C. Abbott, et al., *Protection of low-density lipoprotein against oxidative modification by high-density lipoprotein associated paraoxonase*. *Atherosclerosis*, 1993. **104**(1-2): p. 129-35.
111. Aviram, M., M. Rosenblat, C.L. Bisgaier, et al., *Paraoxonase inhibits high-density lipoprotein oxidation and preserves its functions. A possible peroxidative role for paraoxonase*. *J Clin Invest*, 1998. **101**(8): p. 1581-90.
112. Rodrigo, L., A.F. Hernandez, J.J. Lopez-Caballero, et al., *Immunohistochemical evidence for the expression and induction of paraoxonase in rat liver, kidney, lung and brain tissue. Implications for its physiological role*. *Chem Biol Interact*, 2001. **137**(2): p. 123-37.
113. Deakin, S.P., S. Bioletto, M.L. Bochaton-Piallat, et al., *HDL-associated paraoxonase-1 can redistribute to cell membranes and influence sensitivity to oxidative stress*. *Free Radic Biol Med*, 2011. **50**(1): p. 102-9.
114. Kotur-Stevuljevic, J., S. Spasic, Z. Jelic-Ivanovic, et al., *PON1 status is influenced by oxidative stress and inflammation in coronary heart disease patients*. *Clin Biochem*, 2008. **41**(13): p. 1067-73.
115. Ferre, N., J. Camps, M. Cabre, et al., *Hepatic paraoxonase activity alterations and free radical production in rats with experimental cirrhosis*. *Metabolism*, 2001. **50**(9): p. 997-1000.
116. Ferre, N., J. Marsillach, J. Camps, et al., *Paraoxonase-1 is associated with oxidative stress, fibrosis and FAS expression in chronic liver diseases*. *J Hepatol*, 2006. **45**(1): p. 51-9.
117. Amacher, D.E., R. Adler, A. Herath, et al., *Use of proteomic methods to identify serum biomarkers associated with rat liver toxicity or hypertrophy*. *Clin Chem*, 2005. **51**(10): p. 1796-803.
118. Feingold, K.R., R.A. Memon, A.H. Moser, et al., *Paraoxonase activity in the serum and hepatic mRNA levels decrease during the acute phase response*. *Atherosclerosis*, 1998. **139**(2): p. 307-15.
119. Meneses-Lorente, G., P.C. Guest, J. Lawrence, et al., *A proteomic investigation of drug-induced steatosis in rat liver*. *Chem Res Toxicol*, 2004. **17**(5): p. 605-12.
120. Jenne, D.E. and J. Tschopp, *Clusterin: the intriguing guises of a widely expressed glycoprotein*. *Trends Biochem Sci*, 1992. **17**(4): p. 154-9.
121. Rosenberg, M.E. and J. Silkensen, *Clusterin: physiologic and pathophysiologic considerations*. *Int J Biochem Cell Biol*, 1995. **27**(7): p. 633-45.
122. Aronow, B.J., S.D. Lund, T.L. Brown, et al., *Apolipoprotein J expression at fluid-tissue interfaces: potential role in barrier cytoprotection*. *Proc Natl Acad Sci U S A*, 1993. **90**(2): p. 725-9.
123. Blaschuk, O., K. Burdzy, and I.B. Fritz, *Purification and characterization of a cell-aggregating factor (clusterin), the major glycoprotein in ram rete testis fluid*. *J Biol Chem*, 1983. **258**(12): p. 7714-20.

## 7 REFERENCES

---

124. Fritz, I.B., K. Burdzy, B. Setchell, et al., *Ram rete testis fluid contains a protein (clusterin) which influences cell-cell interactions in vitro*. Biol Reprod, 1983. **28**(5): p. 1173-88.
125. Trougakos, I.P. and E.S. Gonos, *Regulation of clusterin/apolipoprotein J, a functional homologue to the small heat shock proteins, by oxidative stress in ageing and age-related diseases*. Free Radic Res, 2006. **40**(12): p. 1324-34.
126. Falgarone, G. and G. Chiocchia, *Chapter 8: Clusterin: A multifacet protein at the crossroad of inflammation and autoimmunity*. Adv Cancer Res, 2009. **104**: p. 139-70.
127. Wyatt, A.R., J.J. Yerbury, P. Berghofer, et al., *Clusterin facilitates in vivo clearance of extracellular misfolded proteins*. Cell Mol Life Sci, 2011. **68**(23): p. 3919-31.
128. Markopoulou, S., E. Kontargiris, C. Batsi, et al., *Vanadium-induced apoptosis of HaCaT cells is mediated by c-fos and involves nuclear accumulation of clusterin*. The FEBS journal, 2009. **276**(14): p. 3784-99.
129. Kaisman-Elbaz, T., I. Sekler, D. Fishman, et al., *Cell death induced by zinc and cadmium is mediated by clusterin in cultured mouse seminiferous tubules*. J Cell Physiol, 2009. **220**(1): p. 222-9.
130. Zhang, H., J.K. Kim, C.A. Edwards, et al., *Clusterin inhibits apoptosis by interacting with activated Bax*. Nat Cell Biol, 2005. **7**(9): p. 909-15.
131. Dieterle, F., E. Perentes, A. Cordier, et al., *Urinary clusterin, cystatin C, beta2-microglobulin and total protein as markers to detect drug-induced kidney injury*. Nat Biotechnol, 2010. **28**(5): p. 463-9.
132. Hoffmann, D., M. Adler, V.S. Vaidya, et al., *Performance of novel kidney biomarkers in preclinical toxicity studies*. Toxicol Sci, 2010. **116**(1): p. 8-22.
133. Aigelsreiter, A., E. Janig, J. Sostaric, et al., *Clusterin expression in cholestasis, hepatocellular carcinoma and liver fibrosis*. Histopathology, 2009. **54**(5): p. 561-70.
134. Flower, D.R., *The lipocalin protein family: structure and function*. Biochem J, 1996. **318** ( Pt 1): p. 1-14.
135. Flower, D.R., A.C. North, and C.E. Sansom, *The lipocalin protein family: structural and sequence overview*. Biochim Biophys Acta, 2000. **1482**(1-2): p. 9-24.
136. Kjeldsen, L., A.H. Johnsen, H. Sengelov, et al., *Isolation and primary structure of NGAL, a novel protein associated with human neutrophil gelatinase*. J Biol Chem, 1993. **268**(14): p. 10425-32.
137. Triebel, S., J. Blaser, H. Reinke, et al., *A 25 kDa alpha 2-microglobulin-related protein is a component of the 125 kDa form of human gelatinase*. FEBS Lett, 1992. **314**(3): p. 386-8.
138. Mori, K. and K. Nakao, *Neutrophil gelatinase-associated lipocalin as the real-time indicator of active kidney damage*. Kidney Int, 2007. **71**(10): p. 967-70.
139. Nielsen, B.S., N. Borregaard, J.R. Bundgaard, et al., *Induction of NGAL synthesis in epithelial cells of human colorectal neoplasia and inflammatory bowel diseases*. Gut, 1996. **38**(3): p. 414-20.
140. Hemdahl, A.L., A. Gabrielsen, C. Zhu, et al., *Expression of neutrophil gelatinase-associated lipocalin in atherosclerosis and myocardial infarction*. Arterioscler Thromb Vasc Biol, 2006. **26**(1): p. 136-42.
141. Goetz, D.H., M.A. Holmes, N. Borregaard, et al., *The neutrophil lipocalin NGAL is a bacteriostatic agent that interferes with siderophore-mediated iron acquisition*. Mol Cell, 2002. **10**(5): p. 1033-43.

142. Flo, T.H., K.D. Smith, S. Sato, et al., *Lipocalin 2 mediates an innate immune response to bacterial infection by sequestering iron*. Nature, 2004. **432**(7019): p. 917-21.
143. Borregaard, N., O.E. Sørensen, and K. Theilgaard-Mönch, *Neutrophil granules: a library of innate immunity proteins*. Trends in Immunology, 2007. **28**(8): p. 340-345.
144. Schmidt-Ott, K.M., K. Mori, J.Y. Li, et al., *Dual action of neutrophil gelatinase-associated lipocalin*. J Am Soc Nephrol, 2007. **18**(2): p. 407-13.
145. Nilsen-Hamilton, M., Q. Liu, J. Ryon, et al., *Tissue involution and the acute phase response*. Ann N Y Acad Sci, 2003. **995**: p. 94-108.
146. Jayaraman, A., K.A. Roberts, J. Yoon, et al., *Identification of neutrophil gelatinase-associated lipocalin (NGAL) as a discriminatory marker of the hepatocyte-secreted protein response to IL-1beta: a proteomic analysis*. Biotechnol Bioeng, 2005. **91**(4): p. 502-15.
147. Cowland, J.B., T. Muta, and N. Borregaard, *IL-1beta-specific up-regulation of neutrophil gelatinase-associated lipocalin is controlled by IkappaB-zeta*. J Immunol, 2006. **176**(9): p. 5559-66.
148. Mitsnefes, M.M., T.S. Kathman, J. Mishra, et al., *Serum neutrophil gelatinase-associated lipocalin as a marker of renal function in children with chronic kidney disease*. Pediatr Nephrol, 2007. **22**(1): p. 101-8.
149. Mishra, J., Q. Ma, C. Kelly, et al., *Kidney NGAL is a novel early marker of acute injury following transplantation*. Pediatr Nephrol, 2006. **21**(6): p. 856-63.
150. Fung, W.P. and G. Schreiber, *Structure and expression of the genes for major acute phase alpha 1-protein (thioctatin) and kininogen in the rat*. J Biol Chem, 1987. **262**(19): p. 9298-308.
151. Otto, H.H. and T. Schirmeister, *Cysteine Proteases and Their Inhibitors*. Chem Rev, 1997. **97**(1): p. 133-172.
152. Urban, J., D. Chan, and G. Schreiber, *A rat serum glycoprotein whose synthesis rate increases greatly during inflammation*. J Biol Chem, 1979. **254**(21): p. 10565-8.
153. Cole, T., A. Inglis, M. Nagashima, et al., *Major acute-phase alpha(1)protein in the rat: structure, molecular cloning, and regulation of mRNA levels*. Biochem Biophys Res Commun, 1985. **126**(2): p. 719-24.
154. Kramer, J.A., J.E. Sagartz, and D.L. Morris, *The application of discovery toxicology and pathology towards the design of safer pharmaceutical lead candidates*. Nat Rev Drug Discov, 2007. **6**(8): p. 636-49.
155. Heinloth, A.N., R.D. Irwin, G.A. Boorman, et al., *Gene expression profiling of rat livers reveals indicators of potential adverse effects*. Toxicol Sci, 2004. **80**(1): p. 193-202.
156. Huang, Q., X. Jin, E.T. Gaillard, et al., *Gene expression profiling reveals multiple toxicity endpoints induced by hepatotoxicants*. Mutat Res, 2004. **549**(1-2): p. 147-67.
157. Kienhuis, A.S., M.C. van de Poll, H. Wortelboer, et al., *Parallel approach using rat-human in vitro and rat in vivo toxicogenomics predicts acetaminophen-induced hepatotoxicity in humans*. Toxicol Sci, 2009. **107**(2): p. 544-52.
158. Jollow, D.J., J.R. Mitchell, W.Z. Potter, et al., *Acetaminophen-induced hepatic necrosis. II. Role of covalent binding in vivo*. J Pharmacol Exp Ther, 1973. **187**(1): p. 195-202.
159. Mitchell, J.R., D.J. Jollow, W.Z. Potter, et al., *Acetaminophen-induced hepatic necrosis. I. Role of drug metabolism*. J Pharmacol Exp Ther, 1973. **187**(1): p. 185-94.

## 7 REFERENCES

---

160. Adamson, G.M. and A.W. Harman, *Oxidative stress in cultured hepatocytes exposed to acetaminophen*. *Biochem Pharmacol*, 1993. **45**(11): p. 2289-94.
161. Masubuchi, Y., C. Suda, and T. Horie, *Involvement of mitochondrial permeability transition in acetaminophen-induced liver injury in mice*. *J Hepatol*, 2005. **42**(1): p. 110-6.
162. Lehmann, J.M., L.B. Moore, T.A. Smith-Oliver, et al., *An antidiabetic thiazolidinedione is a high affinity ligand for peroxisome proliferator-activated receptor gamma (PPAR gamma)*. *J Biol Chem*, 1995. **270**(22): p. 12953-6.
163. Spiegelman, B.M., *PPAR-gamma: adipogenic regulator and thiazolidinedione receptor*. *Diabetes*, 1998. **47**(4): p. 507-14.
164. Wang, M., S.C. Wise, T. Leff, et al., *Troglitazone, an antidiabetic agent, inhibits cholesterol biosynthesis through a mechanism independent of peroxisome proliferator-activated receptor-gamma*. *Diabetes*, 1999. **48**(2): p. 254-60.
165. Yamamoto, Y., H. Yamazaki, T. Ikeda, et al., *Formation of a novel quinone epoxide metabolite of troglitazone with cytotoxicity to HepG2 cells*. *Drug Metab Dispos*, 2002. **30**(2): p. 155-60.
166. Kassahun, K., P.G. Pearson, W. Tang, et al., *Studies on the metabolism of troglitazone to reactive intermediates in vitro and in vivo. Evidence for novel biotransformation pathways involving quinone methide formation and thiazolidinedione ring scission*. *Chem Res Toxicol*, 2001. **14**(1): p. 62-70.
167. Tetley, J.N., J.L. Maggs, W.G. Rapeport, et al., *Enzyme-induction dependent bioactivation of troglitazone and troglitazone quinone in vivo*. *Chem Res Toxicol*, 2001. **14**(8): p. 965-74.
168. Funk, C., M. Pantze, L. Jehle, et al., *Troglitazone-induced intrahepatic cholestasis by an interference with the hepatobiliary export of bile acids in male and female rats. Correlation with the gender difference in troglitazone sulfate formation and the inhibition of the canalicular bile salt export pump (Bsep) by troglitazone and troglitazone sulfate*. *Toxicology*, 2001. **167**(1): p. 83-98.
169. Nozawa, T., S. Sugiura, M. Nakajima, et al., *Involvement of organic anion transporting polypeptides in the transport of troglitazone sulfate: implications for understanding troglitazone hepatotoxicity*. *Drug Metab Dispos*, 2004. **32**(3): p. 291-4.
170. Bae, M.A. and B.J. Song, *Critical role of c-Jun N-terminal protein kinase activation in troglitazone-induced apoptosis of human HepG2 hepatoma cells*. *Mol Pharmacol*, 2003. **63**(2): p. 401-8.
171. Bova, M.P., D. Tam, G. McMahon, et al., *Troglitazone induces a rapid drop of mitochondrial membrane potential in liver HepG2 cells*. *Toxicol Lett*, 2005. **155**(1): p. 41-50.
172. Fire, A., S. Xu, M.K. Montgomery, et al., *Potent and specific genetic interference by double-stranded RNA in *Caenorhabditis elegans**. *Nature*, 1998. **391**(6669): p. 806-11.
173. Elbashir, S.M., J. Harborth, W. Lendeckel, et al., *Duplexes of 21-nucleotide RNAs mediate RNA interference in cultured mammalian cells*. *Nature*, 2001. **411**(6836): p. 494-8.
174. Hokaiwado, N., F. Takeshita, A. Banas, et al., *RNAi-based drug discovery and its application to therapeutics*. *IDrugs*, 2008. **11**(4): p. 274-8.
175. Natt, F., *siRNAs in drug discovery: target validation and beyond*. *Curr Opin Mol Ther*, 2007. **9**(3): p. 242-7.
176. Ito, M., K. Kawano, M. Miyagishi, et al., *Genome-wide application of RNAi to the discovery of potential drug targets*. *FEBS Lett*, 2005. **579**(26): p. 5988-95.

177. Bolon, B., *Genetically engineered animals in drug discovery and development: a maturing resource for toxicologic research*. Basic Clin Pharmacol Toxicol, 2004. **95**(4): p. 154-61.
178. Choi, E., S. Lee, S.Y. Yeom, et al., *Characterization of activating signal cointegrator-2 as a novel transcriptional coactivator of the xenobiotic nuclear receptor constitutive androstane receptor*. Mol Endocrinol, 2005. **19**(7): p. 1711-9.
179. Song, E., S.K. Lee, J. Wang, et al., *RNA interference targeting Fas protects mice from fulminant hepatitis*. Nat Med, 2003. **9**(3): p. 347-51.
180. Svoboda, P., *Off-targeting and other non-specific effects of RNAi experiments in mammalian cells*. Curr Opin Mol Ther, 2007. **9**(3): p. 248-57.
181. Sledz, C.A., M. Holko, M.J. de Veer, et al., *Activation of the interferon system by short-interfering RNAs*. Nat Cell Biol, 2003. **5**(9): p. 834-9.
182. Jackson, A.L., J. Burchard, D. Leake, et al., *Position-specific chemical modification of siRNAs reduces "off-target" transcript silencing*. RNA, 2006. **12**(7): p. 1197-205.
183. Elbashir, S.M., W. Lendeckel, and T. Tuschl, *RNA interference is mediated by 21- and 22-nucleotide RNAs*. Genes Dev, 2001. **15**(2): p. 188-200.
184. Agrawal, N., P.V. Dasaradhi, A. Mohammed, et al., *RNA interference: biology, mechanism, and applications*. Microbiol Mol Biol Rev, 2003. **67**(4): p. 657-85.
185. Chendrimada, T.P., R.I. Gregory, E. Kumaraswamy, et al., *TRBP recruits the Dicer complex to Ago2 for microRNA processing and gene silencing*. Nature, 2005. **436**(7051): p. 740-4.
186. Mulrane, L., E. Rexhepaj, V. Smart, et al., *Creation of a digital slide and tissue microarray resource from a multi-institutional predictive toxicology study in the rat: an initial report from the PredTox group*. Exp Toxicol Pathol, 2008. **60**(4-5): p. 235-45.
187. Berry, M.N. and D.S. Friend, *High-yield preparation of isolated rat liver parenchymal cells: a biochemical and fine structural study*. J Cell Biol, 1969. **43**(3): p. 506-20.
188. Seglen, P.O., *Preparation of isolated rat liver cells*. Methods Cell Biol, 1976. **13**: p. 29-83.
189. Pfaffl, M.W., *A new mathematical model for relative quantification in real-time RT-PCR*. Nucleic Acids Res, 2001. **29**(9): p. e45.
190. Rached, E., D. Hoffmann, K. Blumbach, et al., *Evaluation of putative biomarkers of nephrotoxicity after exposure to ochratoxin a in vivo and in vitro*. Toxicol Sci, 2008. **103**(2): p. 371-81.
191. Hillmeister, P., K.E. Lehmann, A. Bondke, et al., *Induction of cerebral arteriogenesis leads to early-phase expression of protease inhibitors in growing collaterals of the brain*. J Cereb Blood Flow Metab, 2008. **28**(11): p. 1811-23.
192. Koch, W.H., *Technology platforms for pharmacogenomic diagnostic assays*. Nat Rev Drug Discov, 2004. **3**(9): p. 749-61.
193. Singh-Gasson, S., R.D. Green, Y. Yue, et al., *Maskless fabrication of light-directed oligonucleotide microarrays using a digital micromirror array*. Nat Biotechnol, 1999. **17**(10): p. 974-8.
194. Miller, M.B. and Y.W. Tang, *Basic concepts of microarrays and potential applications in clinical microbiology*. Clin Microbiol Rev, 2009. **22**(4): p. 611-33.

## 7 REFERENCES

---

195. Iida, K. and I. Nishimura, *Gene expression profiling by DNA microarray technology*. Crit Rev Oral Biol Med, 2002. **13**(1): p. 35-50.
196. Lowry, O.H., N.J. Rosebrough, A.L. Farr, et al., *Protein measurement with the Folin phenol reagent*. J Biol Chem, 1951. **193**(1): p. 265-75.
197. Tolosa, J.M., J.E. Schjenken, T.D. Civiti, et al., *Column-based method to simultaneously extract DNA, RNA, and proteins from the same sample*. Biotechniques, 2007. **43**(6): p. 799-804.
198. Laemmli, U.K., *Cleavage of structural proteins during the assembly of the head of bacteriophage T4*. Nature, 1970. **227**(5259): p. 680-5.
199. Towbin, H., T. Staehelin, and J. Gordon, *Electrophoretic transfer of proteins from polyacrylamide gels to nitrocellulose sheets: procedure and some applications*. Proc Natl Acad Sci U S A, 1979. **76**(9): p. 4350-4.
200. Norton, A.J., S. Jordan, and P. Yeomans, *Brief, high-temperature heat denaturation (pressure cooking): a simple and effective method of antigen retrieval for routinely processed tissues*. J Pathol, 1994. **173**(4): p. 371-9.
201. Cattoretti, G., S. Pileri, C. Parravicini, et al., *Antigen unmasking on formalin-fixed, paraffin-embedded tissue sections*. J Pathol, 1993. **171**(2): p. 83-98.
202. Wood, G.S. and R. Warnke, *Suppression of endogenous avidin-binding activity in tissues and its relevance to biotin-avidin detection systems*. J Histochem Cytochem, 1981. **29**(10): p. 1196-204.
203. Hsu, S.M., L. Raine, and H. Fanger, *Use of avidin-biotin-peroxidase complex (ABC) in immunoperoxidase techniques: a comparison between ABC and unlabeled antibody (PAP) procedures*. J Histochem Cytochem, 1981. **29**(4): p. 577-80.
204. Bratthauer, G.L., *The avidin-biotin complex (ABC) method and other avidin-biotin binding methods*. Methods Mol Biol, 2010. **588**: p. 257-70.
205. Adler, M., D. Hoffmann, H. Ellinger-Ziegelbauer, et al., *Assessment of candidate biomarkers of drug-induced hepatobiliary injury in preclinical toxicity studies*. Toxicol Lett, 2010. **196**(1): p. 1-11.
206. Mishra, J., K. Mori, Q. Ma, et al., *Neutrophil gelatinase-associated lipocalin: a novel early urinary biomarker for cisplatin nephrotoxicity*. Am J Nephrol, 2004. **24**(3): p. 307-15.
207. Miyachi, K., M.J. Fritzler, and E.M. Tan, *Autoantibody to a Nuclear Antigen in Proliferating Cells*. Journal of Immunology, 1978. **121**(6): p. 2228-2234.
208. Celis, J.E., P. Madsen, A. Celis, et al., *Cyclin (PCNA, auxiliary protein of DNA polymerase delta) is a central component of the pathway(s) leading to DNA replication and cell division*. FEBS Lett, 1987. **220**(1): p. 1-7.
209. Celis, J.E. and P. Madsen, *Increased nuclear cyclin/PCNA antigen staining of non S-phase transformed human amnion cells engaged in nucleotide excision DNA repair*. FEBS Lett, 1986. **209**(2): p. 277-83.
210. Jaeschke, H. and T. Hasegawa, *Role of neutrophils in acute inflammatory liver injury*. Liver Int, 2006. **26**(8): p. 912-9.
211. Mishra, J., C. Dent, R. Tarabishi, et al., *Neutrophil gelatinase-associated lipocalin (NGAL) as a biomarker for acute renal injury after cardiac surgery*. Lancet, 2005. **365**(9466): p. 1231-8.

212. Koyner, J.L., V.S. Vaidya, M.R. Bennett, et al., *Urinary biomarkers in the clinical prognosis and early detection of acute kidney injury*. Clin J Am Soc Nephrol, 2010. **5**(12): p. 2154-65.
213. Shannan, B., M. Seifert, K. Leskov, et al., *Challenge and promise: roles for clusterin in pathogenesis, progression and therapy of cancer*. Cell Death Differ, 2006. **13**(1): p. 12-9.
214. Hidaka, S., B. Kranzlin, N. Gretz, et al., *Urinary clusterin levels in the rat correlate with the severity of tubular damage and may help to differentiate between glomerular and tubular injuries*. Cell Tissue Res, 2002. **310**(3): p. 289-96.
215. Sieber, M., D. Hoffmann, M. Adler, et al., *Comparative analysis of novel noninvasive renal biomarkers and metabonomic changes in a rat model of gentamicin nephrotoxicity*. Toxicol Sci, 2009. **109**(2): p. 336-49.
216. Srivastava, S.K., K.V. Ramana, and A. Bhatnagar, *Role of aldose reductase and oxidative damage in diabetes and the consequent potential for therapeutic options*. Endocr Rev, 2005. **26**(3): p. 380-92.
217. Metz, C.E., *Basic principles of ROC analysis*. Semin Nucl Med, 1978. **8**(4): p. 283-98.
218. Bu, D.X., A.L. Hemdahl, A. Gabrielsen, et al., *Induction of neutrophil gelatinase-associated lipocalin in vascular injury via activation of nuclear factor-kappaB*. Am J Pathol, 2006. **169**(6): p. 2245-53.
219. Bykov, I., S. Junnikkala, M. Pekna, et al., *Effect of chronic ethanol consumption on the expression of complement components and acute-phase proteins in liver*. Clin Immunol, 2007. **124**(2): p. 213-20.
220. Roudkenar, M.H., Y. Kuwahara, T. Baba, et al., *Oxidative stress induced lipocalin 2 gene expression: addressing its expression under the harmful conditions*. J Radiat Res (Tokyo), 2007. **48**(1): p. 39-44.
221. Sunil, V.R., K.J. Patel, M. Nilsen-Hamilton, et al., *Acute endotoxemia is associated with upregulation of lipocalin 2p3/Lcn2 in lung and liver*. Exp Mol Pathol, 2007. **83**(2): p. 177-87.
222. Minami, K., T. Saito, M. Narahara, et al., *Relationship between hepatic gene expression profiles and hepatotoxicity in five typical hepatotoxicant-administered rats*. Toxicol Sci, 2005. **87**(1): p. 296-305.
223. Borkham-Kamphorst, E., F. Drews, and R. Weiskirchen, *Induction of lipocalin-2 expression in acute and chronic experimental liver injury moderated by pro-inflammatory cytokines interleukin-1beta through nuclear factor-kappaB activation*. Liver Int, 2011. **31**(5): p. 656-65.
224. Bennett, M., C.L. Dent, Q. Ma, et al., *Urine NGAL predicts severity of acute kidney injury after cardiac surgery: a prospective study*. Clin J Am Soc Nephrol, 2008. **3**(3): p. 665-73.
225. Han, W.K., G. Wagener, Y. Zhu, et al., *Urinary biomarkers in the early detection of acute kidney injury after cardiac surgery*. Clin J Am Soc Nephrol, 2009. **4**(5): p. 873-82.
226. Malyszko, J., H. Bachorzewska-Gajewska, E. Sitniewska, et al., *Serum neutrophil gelatinase-associated lipocalin as a marker of renal function in non-diabetic patients with stage 2-4 chronic kidney disease*. Ren Fail, 2008. **30**(6): p. 625-8.
227. Wagener, G., G. Gubitosa, S. Wang, et al., *Urinary neutrophil gelatinase-associated lipocalin and acute kidney injury after cardiac surgery*. Am J Kidney Dis, 2008. **52**(3): p. 425-33.

## 7 REFERENCES

---

228. Smyth, R., C.S. Lane, R. Ashiq, et al., *Proteomic investigation of urinary markers of carbon-tetrachloride-induced hepatic fibrosis in the Hanover Wistar rat*. Cell Biol Toxicol, 2009. **25**(5): p. 499-512.
229. Hvidberg, V., C. Jacobsen, R.K. Strong, et al., *The endocytic receptor megalin binds the iron transporting neutrophil-gelatinase-associated lipocalin with high affinity and mediates its cellular uptake*. FEBS Lett, 2005. **579**(3): p. 773-7.
230. Moreau, T., F. Esnard, N. Gutman, et al., *Cysteine-proteinase-inhibiting function of T kininogen and of its proteolytic fragments*. Eur J Biochem, 1988. **173**(1): p. 185-90.
231. Mann, E.A. and J.B. Lingrel, *Developmental and tissue-specific expression of rat T-kininogen*. Biochem Biophys Res Commun, 1991. **174**(2): p. 417-23.
232. Bandara, L.R., M.D. Kelly, E.A. Lock, et al., *A correlation between a proteomic evaluation and conventional measurements in the assessment of renal proximal tubular toxicity*. Toxicol Sci, 2003. **73**(1): p. 195-206.
233. Ferre, N., J. Camps, E. Prats, et al., *Serum paraoxonase activity: a new additional test for the improved evaluation of chronic liver damage*. Clin Chem, 2002. **48**(2): p. 261-8.
234. Ozer, J., M. Ratner, M. Shaw, et al., *The current state of serum biomarkers of hepatotoxicity*. Toxicology, 2008. **245**(3): p. 194-205.
235. Abraham, P. and E. Sugumar, *Increased glutathione levels and activity of PON1 (phenyl acetate esterase) in the liver of rats after a single dose of cyclophosphamide: a defense mechanism?* Exp Toxicol Pathol, 2008. **59**(5): p. 301-6.
236. Gatzidou, E.T., A.N. Zira, and S.E. Theocharis, *Toxicogenomics: a pivotal piece in the puzzle of toxicological research*. J Appl Toxicol, 2007. **27**(4): p. 302-9.
237. Uehara, T., M. Hirode, A. Ono, et al., *A toxicogenomics approach for early assessment of potential non-genotoxic hepatocarcinogenicity of chemicals in rats*. Toxicology, 2008. **250**(1): p. 15-26.
238. de Longueville, F., F.A. Atienzar, L. Marcq, et al., *Use of a low-density microarray for studying gene expression patterns induced by hepatotoxicants on primary cultures of rat hepatocytes*. Toxicol Sci, 2003. **75**(2): p. 378-92.
239. Suzuki, H., T. Inoue, T. Matsushita, et al., *In vitro gene expression analysis of hepatotoxic drugs in rat primary hepatocytes*. J Appl Toxicol, 2008. **28**(2): p. 227-36.
240. Yin, H.Q., M. Kim, J.H. Kim, et al., *Hepatic gene expression profiling and lipid homeostasis in mice exposed to steatogenic drug, tetracycline*. Toxicol Sci, 2006. **94**(1): p. 206-16.
241. Jolly, R.A., R. Ciurlionis, D. Morfitt, et al., *Microvesicular steatosis induced by a short chain fatty acid: effects on mitochondrial function and correlation with gene expression*. Toxicol Pathol, 2004. **32 Suppl 2**: p. 19-25.
242. Heijne, W.H., A.L. Slitt, P.J. van Bladeren, et al., *Bromobenzene-induced hepatotoxicity at the transcriptome level*. Toxicol Sci, 2004. **79**(2): p. 411-22.
243. McMillian, M., A.Y. Nie, J.B. Parker, et al., *A gene expression signature for oxidant stress/reactive metabolites in rat liver*. Biochem Pharmacol, 2004. **68**(11): p. 2249-61.
244. Longuet, C., E.M. Sinclair, A. Maida, et al., *The glucagon receptor is required for the adaptive metabolic response to fasting*. Cell Metab, 2008. **8**(5): p. 359-71.
245. Sinclair, E.M., B. Yusta, C. Streutker, et al., *Glucagon receptor signaling is essential for control of murine hepatocyte survival*. Gastroenterology, 2008. **135**(6): p. 2096-106.



246. Shah, P., A. Vella, A. Basu, et al., *Lack of suppression of glucagon contributes to postprandial hyperglycemia in subjects with type 2 diabetes mellitus*. J Clin Endocrinol Metab, 2000. **85**(11): p. 4053-9.
247. Saltiel, A.R. and C.R. Kahn, *Insulin signalling and the regulation of glucose and lipid metabolism*. Nature, 2001. **414**(6865): p. 799-806.
248. Khan, A.H. and J.E. Pessin, *Insulin regulation of glucose uptake: a complex interplay of intracellular signalling pathways*. Diabetologia, 2002. **45**(11): p. 1475-83.
249. Henquin, J.C., *Triggering and amplifying pathways of regulation of insulin secretion by glucose*. Diabetes, 2000. **49**(11): p. 1751-60.
250. Baetens, D., F. Malaisse-Lagae, A. Perrelet, et al., *Endocrine pancreas: three-dimensional reconstruction shows two types of islets of langerhans*. Science, 1979. **206**(4424): p. 1323-5.
251. Jiang, G. and B.B. Zhang, *Glucagon and regulation of glucose metabolism*. Am J Physiol Endocrinol Metab, 2003. **284**(4): p. E671-8.
252. Pierce, K.L., R.T. Premont, and R.J. Lefkowitz, *Seven-transmembrane receptors*. Nat Rev Mol Cell Biol, 2002. **3**(9): p. 639-50.
253. Mayo, K.E., L.J. Miller, D. Bataille, et al., *International Union of Pharmacology. XXXV. The glucagon receptor family*. Pharmacol Rev, 2003. **55**(1): p. 167-94.
254. Rodbell, M., L. Birnbaumer, S.L. Pohl, et al., *The glucagon-sensitive adenylyl cyclase system in plasma membranes of rat liver. V. An obligatory role of guanylnucleotides in glucagon action*. J Biol Chem, 1971. **246**(6): p. 1877-82.
255. Wakelam, M.J., G.J. Murphy, V.J. Hruby, et al., *Activation of two signal-transduction systems in hepatocytes by glucagon*. Nature, 1986. **323**(6083): p. 68-71.
256. Estall, J.L. and D.J. Drucker, *Glucagon and glucagon-like peptide receptors as drug targets*. Curr Pharm Des, 2006. **12**(14): p. 1731-50.
257. Chang, L.L., K.L. Sidler, M.A. Cascieri, et al., *Substituted imidazoles as glucagon receptor antagonists*. Bioorg Med Chem Lett, 2001. **11**(18): p. 2549-53.
258. Ling, A., Y. Hong, J. Gonzalez, et al., *Identification of alkylidene hydrazides as glucagon receptor antagonists*. J Med Chem, 2001. **44**(19): p. 3141-9.
259. Madsen, P., A. Ling, M. Plewe, et al., *Optimization of alkylidene hydrazide based human glucagon receptor antagonists. Discovery of the highly potent and orally available 3-cyano-4-hydroxybenzoic acid [1-(2,3,5,6-tetramethylbenzyl)-1H-indol-4-ylmethylene]hydrazide*. J Med Chem, 2002. **45**(26): p. 5755-75.
260. Ladouceur, G.H., J.H. Cook, E.M. Doherty, et al., *Discovery of 5-hydroxyalkyl-4-phenylpyridines as a new class of glucagon receptor antagonists*. Bioorg Med Chem Lett, 2002. **12**(3): p. 461-4.
261. Petersen, K.F. and J.T. Sullivan, *Effects of a novel glucagon receptor antagonist (Bay 27-9955) on glucagon-stimulated glucose production in humans*. Diabetologia, 2001. **44**(11): p. 2018-24.
262. Dallas-Yang, Q., X. Shen, M. Strowski, et al., *Hepatic glucagon receptor binding and glucose-lowering in vivo by peptidyl and non-peptidyl glucagon receptor antagonists*. Eur J Pharmacol, 2004. **501**(1-3): p. 225-34.

## 7 REFERENCES

---

263. Liang, Y., M.C. Osborne, B.P. Monia, et al., *Reduction in glucagon receptor expression by an antisense oligonucleotide ameliorates diabetic syndrome in db/db mice*. *Diabetes*, 2004. **53**(2): p. 410-7.
264. Gelling, R.W., X.Q. Du, D.S. Dichmann, et al., *Lower blood glucose, hyperglucagonemia, and pancreatic alpha cell hyperplasia in glucagon receptor knockout mice*. *Proc Natl Acad Sci U S A*, 2003. **100**(3): p. 1438-43.
265. Parker, J.C., K.M. Andrews, M.R. Allen, et al., *Glycemic control in mice with targeted disruption of the glucagon receptor gene*. *Biochem Biophys Res Commun*, 2002. **290**(2): p. 839-43.
266. Gu, W., H. Yan, K.A. Winters, et al., *Long-term inhibition of the glucagon receptor with a monoclonal antibody in mice causes sustained improvement in glycemic control, with reversible alpha-cell hyperplasia and hyperglucagonemia*. *J Pharmacol Exp Ther*, 2009. **331**(3): p. 871-81.
267. Sloop, K.W., J.X. Cao, A.M. Siesky, et al., *Hepatic and glucagon-like peptide-1-mediated reversal of diabetes by glucagon receptor antisense oligonucleotide inhibitors*. *J Clin Invest*, 2004. **113**(11): p. 1571-81.
268. Yang, J., M.L. Macdougall, M.T. McDowell, et al., *Polyomic profiling reveals significant hepatic metabolic alterations in glucagon-receptor (GCGR) knockout mice: implications on anti-glucagon therapies for diabetes*. *BMC Genomics*, 2011. **12**: p. 281.
269. Williams, G.M., E. Bermudez, and D. Scaramuzzino, *Rat hepatocyte primary cell cultures. III. Improved dissociation and attachment techniques and the enhancement of survival by culture medium*. *In Vitro*, 1977. **13**(12): p. 809-17.
270. Jolliffe, I.T., *Principal component analysis*. Springer series in statistics. 1986, New York: Springer-Verlag. 271 p.
271. Kaufman, L. and P.J. Rousseeuw, *Finding groups in data : an introduction to cluster analysis*. Wiley series in probability and mathematical statistics. Applied probability and statistics. 1990, New York ; Chichester: Wiley. xiv, 342 p.
272. Quackenbush, J., *Computational analysis of microarray data*. *Nat Rev Genet*, 2001. **2**(6): p. 418-27.
273. Boulias, K., N. Katrakili, K. Bamberg, et al., *Regulation of hepatic metabolic pathways by the orphan nuclear receptor SHP*. *EMBO J*, 2005. **24**(14): p. 2624-33.
274. Yamagata, K., H. Daitoku, Y. Shimamoto, et al., *Bile acids regulate gluconeogenic gene expression via small heterodimer partner-mediated repression of hepatocyte nuclear factor 4 and Foxo1*. *J Biol Chem*, 2004. **279**(22): p. 23158-65.
275. Takahashi, S., J. Suzuki, M. Kohno, et al., *Enhancement of the binding of triglyceride-rich lipoproteins to the very low density lipoprotein receptor by apolipoprotein E and lipoprotein lipase*. *J Biol Chem*, 1995. **270**(26): p. 15747-54.
276. Carlberg, I. and B. Mannervik, *Purification and characterization of the flavoenzyme glutathione reductase from rat liver*. *J Biol Chem*, 1975. **250**(14): p. 5475-80.
277. Morgan, K.T., H. Ni, H.R. Brown, et al., *Application of cDNA microarray technology to in vitro toxicology and the selection of genes for a real-time RT-PCR-based screen for oxidative stress in Hep-G2 cells*. *Toxicol Pathol*, 2002. **30**(4): p. 435-51.
278. Meierjohann, S., R.D. Walter, and S. Muller, *Glutathione synthetase from Plasmodium falciparum*. *Biochem J*, 2002. **363**(Pt 3): p. 833-8.

279. Drocourt, L., J.M. Pascussi, E. Assenat, et al., *Calcium channel modulators of the dihydropyridine family are human pregnane X receptor activators and inducers of CYP3A, CYP2B, and CYP2C in human hepatocytes*. Drug Metab Dispos, 2001. **29**(10): p. 1325-31.
280. Kliewer, S.A., B. Goodwin, and T.M. Willson, *The nuclear pregnane X receptor: a key regulator of xenobiotic metabolism*. Endocr Rev, 2002. **23**(5): p. 687-702.
281. Liddle, C. and B. Goodwin, *Regulation of hepatic drug metabolism: role of the nuclear receptors PXR and CAR*. Semin Liver Dis, 2002. **22**(2): p. 115-22.
282. Wagner, M., E. Halilbasic, H.U. Marschall, et al., *CAR and PXR agonists stimulate hepatic bile acid and bilirubin detoxification and elimination pathways in mice*. Hepatology, 2005. **42**(2): p. 420-30.
283. Xie, W., M.F. Yeuh, A. Radominska-Pandya, et al., *Control of steroid, heme, and carcinogen metabolism by nuclear pregnane X receptor and constitutive androstane receptor*. Proc Natl Acad Sci U S A, 2003. **100**(7): p. 4150-5.
284. Lefebvre, P., B. Cariou, F. Lien, et al., *Role of bile acids and bile acid receptors in metabolic regulation*. Physiol Rev, 2009. **89**(1): p. 147-91.
285. Lambert, G., M.J. Amar, G. Guo, et al., *The farnesoid X-receptor is an essential regulator of cholesterol homeostasis*. J Biol Chem, 2003. **278**(4): p. 2563-70.
286. Handschin, C. and U.A. Meyer, *Regulatory network of lipid-sensing nuclear receptors: roles for CAR, PXR, LXR, and FXR*. Arch Biochem Biophys, 2005. **433**(2): p. 387-96.
287. Mitropoulos, K.A., N.B. Myant, G.F. Gibbons, et al., *Cholesterol precursor pools for the synthesis of cholic and chemodeoxycholic acids in rats*. J Biol Chem, 1974. **249**(19): p. 6052-6.
288. Yokoyama, S., *Release of cellular cholesterol: molecular mechanism for cholesterol homeostasis in cells and in the body*. Biochim Biophys Acta, 2000. **1529**(1-3): p. 231-44.
289. Perez, M.J. and O. Briz, *Bile-acid-induced cell injury and protection*. World J Gastroenterol, 2009. **15**(14): p. 1677-89.
290. Goldstein, J.L., R.A. DeBose-Boyd, and M.S. Brown, *Protein sensors for membrane sterols*. Cell, 2006. **124**(1): p. 35-46.
291. Chen, G., G. Liang, J. Ou, et al., *Central role for liver X receptor in insulin-mediated activation of Srebp-1c transcription and stimulation of fatty acid synthesis in liver*. Proc Natl Acad Sci U S A, 2004. **101**(31): p. 11245-50.
292. Cagen, L.M., X. Deng, H.G. Wilcox, et al., *Insulin activates the rat sterol-regulatory-element-binding protein 1c (SREBP-1c) promoter through the combinatorial actions of SREBP, LXR, Sp-1 and NF-Y cis-acting elements*. Biochem J, 2005. **385**(Pt 1): p. 207-16.
293. Bansal, P. and Q. Wang, *Insulin as a physiological modulator of glucagon secretion*. Am J Physiol Endocrinol Metab, 2008. **295**(4): p. E751-61.
294. Browning, J.D. and J.D. Horton, *Molecular mediators of hepatic steatosis and liver injury*. J Clin Invest, 2004. **114**(2): p. 147-52.
295. Meister, A. and M.E. Anderson, *Glutathione*. Annu Rev Biochem, 1983. **52**: p. 711-60.
296. Pham, R.T., D.S. Barber, and E.P. Gallagher, *GSTA is a major glutathione S-transferase gene responsible for 4-hydroxynonenal conjugation in largemouth bass liver*. Mar Environ Res, 2004. **58**(2-5): p. 485-8.

## 7 REFERENCES

---

297. Sharma, R., Y. Yang, A. Sharma, et al., *Antioxidant role of glutathione S-transferases: protection against oxidant toxicity and regulation of stress-mediated apoptosis*. *Antioxid Redox Signal*, 2004. **6**(2): p. 289-300.
298. Jourenkova-Mironova, N., A. Voho, C. Bouchardy, et al., *Glutathione S-transferase GSTM1, GSTM3, GSTP1 and GSTT1 genotypes and the risk of smoking-related oral and pharyngeal cancers*. *Int J Cancer*, 1999. **81**(1): p. 44-8.
299. Sahu, S.C., *Hepatotoxicity : from genomics to in vitro and in vivo models*. 2007, Chichester: John Wiley & Sons. xvi, 682 p.
300. Ganey, P.E., J.P. Luyendyk, J.F. Maddox, et al., *Adverse hepatic drug reactions: inflammatory episodes as consequence and contributor*. *Chem Biol Interact*, 2004. **150**(1): p. 35-51.
301. Sioud, M., *Induction of inflammatory cytokines and interferon responses by double-stranded and single-stranded siRNAs is sequence-dependent and requires endosomal localization*. *J Mol Biol*, 2005. **348**(5): p. 1079-90.
302. Robbins, M., A. Judge, and I. MacLachlan, *siRNA and innate immunity*. *Oligonucleotides*, 2009. **19**(2): p. 89-102.
303. Gardmo, C., P. Kotokorpi, H. Helander, et al., *Transfection of adult primary rat hepatocytes in culture*. *Biochem Pharmacol*, 2005. **69**(12): p. 1805-13.
304. Li, X.C. and J.L. Zhuo, *Targeting glucagon receptor signalling in treating metabolic syndrome and renal injury in Type 2 diabetes: theory versus promise*. *Clin Sci (Lond)*, 2007. **113**(4): p. 183-93.
305. Qureshi, S.A., M. Rios Candelore, D. Xie, et al., *A novel glucagon receptor antagonist inhibits glucagon-mediated biological effects*. *Diabetes*, 2004. **53**(12): p. 3267-73.
306. Sorensen, H., M.S. Winzell, C.L. Brand, et al., *Glucagon receptor knockout mice display increased insulin sensitivity and impaired beta-cell function*. *Diabetes*, 2006. **55**(12): p. 3463-9.
307. Drover, V.A., D.V. Nguyen, C.C. Bastie, et al., *CD36 mediates both cellular uptake of very long chain fatty acids and their intestinal absorption in mice*. *J Biol Chem*, 2008. **283**(19): p. 13108-15.
308. Yue, P., Z. Chen, F. Nassir, et al., *Enhanced hepatic apoA-I secretion and peripheral efflux of cholesterol and phospholipid in CD36 null mice*. *PLoS One*, 2010. **5**(3): p. e9906.
309. Jonas, A., *Lecithin cholesterol acyltransferase*. *Biochim Biophys Acta*, 2000. **1529**(1-3): p. 245-56.
310. Brent, G.A., *Tissue-specific actions of thyroid hormone: insights from animal models*. *Rev Endocr Metab Disord*, 2000. **1**(1-2): p. 27-33.
311. Yan, H., W. Gu, J. Yang, et al., *Fully human monoclonal antibodies antagonizing the glucagon receptor improve glucose homeostasis in mice and monkeys*. *J Pharmacol Exp Ther*, 2009. **329**(1): p. 102-11.
312. Wang, M., *Metabolic syndrome : underlying mechanisms and drug therapies*. 2011, Hoboken, N.J.: Wiley. xiii, 494 p.
313. Srivastava, A., J.L. Maggs, D.J. Antoine, et al., *Role of reactive metabolites in drug-induced hepatotoxicity*. *Handb Exp Pharmacol*, 2010(196): p. 165-94.
314. Jaeschke, H. and M.L. Bajt, *Intracellular signaling mechanisms of acetaminophen-induced liver cell death*. *Toxicol Sci*, 2006. **89**(1): p. 31-41.

315. Morgan, R.E., M. Trauner, C.J. van Staden, et al., *Interference with bile salt export pump function is a susceptibility factor for human liver injury in drug development*. *Toxicol Sci*, 2010. **118**(2): p. 485-500.

### 8 ACKNOWLEDGEMENTS

An dieser Stelle möchte ich mich bei allen bedanken, die mich bei der Durchführung dieser Arbeit unterstützt und begleitet haben.

Ein besonderes Dankeschön geht an meine direkte Betreuerin PD Dr. Angela Mally für die permanente Unterstützung während der gesamten Arbeit, das mir entgegengebrachte Vertrauen, und die Möglichkeit, an verschiedenen Tagungen und Weiterbildungen teilzunehmen. Durch ihre immerwährende Gesprächsbereitschaft, ihre kritischen Fragen und zahlreichen Denkanstöße hat sie mich immer wieder auf den richtigen Weg gebracht und somit wesentlich zum Gelingen dieser Arbeit beigetragen.

Herrn Prof. Dr. Wolfgang Dekant danke ich für die Begutachtung der Arbeit. Durch die Vergabe der Diplomarbeit hat er mir die Tür zu diesem Institut geöffnet und diese Arbeit erst möglich gemacht.

Prof. Dr. Ulrike Holzgrabe als Vertreterin der Fakultät für Chemie und Pharmazie danke ich für die freundliche und bereitwillige Übernahme der Betreuung meiner Dissertation und ihre wertvollen Hinweise bei der Durchsicht dieser Arbeit.

Des Weiteren danke ich ganz herzlich Herrn Dr. Philip G. Hewitt und Frau Birte Lauer vom Institut für Toxikologie der Merck KGaA in Darmstadt für die Unterstützung bei der Isolierung der primären Rattenhepatozyten. Ohne ihre Hilfe und Fachkompetenz wäre die Etablierung des Zellkultursystems in dieser kurzen Zeit nicht möglich gewesen.

Für die gute Zusammenarbeit bei der Durchführung und Datenauswertung der Genexpressionsanalysen danke ich ganz besonders Herrn Prof. Dr. Andreas Rosenwald, Leiter des Instituts für Pathologie der Universität Würzburg, und Frau Dr. Ellen Leich. Vor allem Ellen möchte ich dafür danken, dass sie jederzeit bereit war, ihre Erfahrungen bei der Analyse der Genexpressionsdaten an mich weiterzugeben.

Ein Teil dieser Arbeit entstand im Rahmen des InnoMed-PredTox-Projektes innerhalb des „6th framework programme“ der Europäischen Union. Allen Projektpartnern danke ich für die gute Zusammenarbeit und Unterstützung während der gesamten Dauer des Projektes.

Für die hervorragende Zusammenarbeit und tatkräftige Unterstützung im Labor danke ich Ursula Tatsch, Michaela Bekthesi und Elisabeth Rüb-Spiegel. Ihr habt mit Eurer

aufmunternden und optimistischen Art nicht nur meinen Laboralltag unglaublich erleichtert.

Tinka, Sabrina, Susi, Silvia, Tobi, Patrizia, Dana, Stephi, Micha und Hannelore danke ich für Ihre Freundschaft, die vielen Aufmunterungen, fachlichen Diskussionen und die "kleinen Schwätzchen zwischendurch". Ihr habt für mich die Zeit in Würzburg unvergesslich gemacht!

Ein ganz spezielles Dankeschön geht an das „Handwerker-Team“ Antoni Romanowski und Bernd Klima, die mehr als einmal meine „Retter in der Not“ waren. Danke für die tollen Erlebnisse auf dem Parkplatz des Institutsgebäudes.

Auch bei allen anderen nicht-genannten Personen der Toxikologie Würzburg möchte ich mich herzlichst für die schöne Zeit und die tolle Atmosphäre am Institut bedanken.

Vielen lieben Dank auch an meine „Mädels“ (Pamela, Karena, Bettina, Tatjana und Marion) für die seelische und moralische Unterstützung außerhalb der Wissenschaft. Ich danke Euch für die vielen schönen Momente, die ich mit Euch erleben durfte und hoffentlich noch erleben werde.

Der wichtigste Dank richtet sich jedoch an meine Eltern Ute und Michael, die mich in allen Lebenslagen bedingungslos unterstützt und immer an mich geglaubt haben. Ohne ihr Vertrauen und Verständnis wäre diese Arbeit nie entstanden.

## 9 PUBLICATIONS

- Adler. M.**, Muller. K., Rached. E., Dekant. W. and Mally. A. (2009). Modulation of key regulators of mitosis linked to chromosomal instability is an early event in ochratoxin A carcinogenicity. *Carcinogenesis* 30. 711-9.
- Sieber. M., Hoffmann. D., **Adler. M.**, Vaidya. V. S., Clement. M., Bonventre. J. V., Zidek. N., Rached. E., Amberg. A., Callanan. J. J., Dekant. W. and Mally. A. (2009). Comparative analysis of novel noninvasive renal biomarkers and metabonomic changes in a rat model of gentamicin nephrotoxicity. *Toxicol Sci* 109. 336-49.
- Adler. M.**, Hoffmann. D., Ellinger-Ziegelbauer. H., Hewitt. P., Matheis. K., Mulrane. L., Gallagher. W. M., Callanan. J. J., Suter. L., Fountoulakis. M. M., Dekant. W. and Mally. A. (2010). Assessment of candidate biomarkers of drug-induced hepatobiliary injury in preclinical toxicity studies. *Toxicol Lett* 196. 1-11.
- Hoffmann. D., **Adler. M.**, Vaidya. V. S., Rached. E., Mulrane. L., Gallagher. W. M., Callanan. J. J., Gautier. J. C., Matheis. K., Staedtler. F., Dieterle. F., Brandenburg. A., Sposny. A., Hewitt. P., Ellinger-Ziegelbauer. H., Bonventre. J. V., Dekant. W. and Mally. A. (2010). Performance of novel kidney biomarkers in preclinical toxicity studies. *Toxicol Sci* **116**. 8-22.
- Ellinger-Ziegelbauer. H., **Adler. M.**, Amberg. A., Brandenburg. A., Callanan. J. J., Connor. S., Fountoulakis. M., Gmuender. H., Gruhler. A., Hewitt. P., Hodson. M., Matheis. K. A., McCarthy. D., Raschke. M., Riefke. B., Schmitt. C. S., Sieber. M., Sposny. A., Suter. L., Sweatman. B. and Mally. A. (2010). The enhanced value of combining conventional and "omics" analyses in early assessment of drug-induced hepatobiliary injury. *Toxicol Appl Pharmacol*. [Epub ahead of print]

### Conference presentations

- Adler. M.**, Muller. K., Rached. E., Dekant. W. and Mally. A. (2007). Modulation of the expression of genes involved in cell cycle control and progression through mitosis by ochratoxin A in vivo. 29<sup>th</sup> Mycotoxin-Workshop. Fellbach. Germany
- Adler. M.**, Muller. K., Rached. E., Dekant. W. and Mally. A. (2008). Aberrant expression of key regulators of mitosis and chromosome segregation in rat kidney following exposure to ochratoxin A. Society of Toxicology 47<sup>th</sup> Annual Meeting. Seattle. USA. *The Toxicologist*. Supplement to Toxicological Sciences
- Gautier. J.C., Mally. A., Hoffmann. D., **Adler. M.**, Betton. G., Davis. D., Bounous. D., Ennulat. D., Riefke. B., Mylecraine. L., Hoffman. D., Schuster. K., Pettit. S., Harpur. E. (2008) Use of novel biomarkers in pre-clinical renal assessment. Meeting of the Association of European Comparative Clinical Pathology. Barcelona. Spanien
- Adler. M.**, Hoffmann. D., Ellinger. H., Hewitt. P., Matheis. K., Mulrane. L., Gallagher. W.M., Suter-Dick. L., Fountoulakis. M.M., Dekant. W. und Mally. A. (2009) Assessment of candidate biomarkers of drug induced liver injury in preclinical toxicity studies. 46<sup>th</sup> Congress of the European Society of Toxicology. Dresden. Deutschland. *Toxicology Letters*. Vol. 189S



Hoffmann. D., **Adler. M.**, Rached. E., Mulrane. E., Gallagher. W.M., Callanan. J.J., Gautier. J.C., Matheis. K., Staedtler. F., Dieterle. F., Walijew. A., Hewitt. P., Ellinger. H., Vaidya. V., Clement.M., Bonventre. J.V., Dekant. W. und Mally. A. (2009) Performance of novel kidney biomarkers in preclinical toxicity studies. Society of Toxicology 48<sup>th</sup> Annual Meeting. Baltimore. USA. The Toxicologist. Supplement to Toxicological Sciences

**Adler. M.**, Muller. K., Rached. E., Dekant. W. and Mally. A. (2009). Modulation of key regulators of mitosis linked to chromosomal instability as an early event in ochratoxin A carcinogenicity. 7<sup>th</sup> Congress of the Toxicology in Developing Countries. Sun City. South Africa

Ellinger. H., Walijew. A., Schmitt. C., Hewitt. P., Matheis. K., Raschke. M., Riefke. B., Brandenburg. A., Gmuender. H., Amberg. A., Mulrane. L., Gallagher. W., Sieber. M., **Adler. M.**, Mally. A. Combined conventional and -omics evaluation of 4 hepatotoxicants with bile duct or cholestatic effects (Poster) Society of Toxicology 48<sup>th</sup> Annual Meeting. Baltimore. 2009. The Toxicologist. Supplement to Toxicological Sciences

## 10 APPENDIX

Appendix 1. List of significantly deregulated genes with at least 1.5-fold change and a p-value of < 0.01 (1-way ANOVA) after treatment with BAY16 in primary rat hepatocytes in the presence (UT, SC) or absence (siGCGR) of the GCGR or knockdown of the GCGR alone without BAY16-treatment (siGCGR+C). Abbreviations: UT = untransfected cells, SC = scrambled siRNA transfected cells, siGCGR = GCGR siRNA transfected cells, LD = 25  $\mu$ M BAY16, HD = 75  $\mu$ M BAY16, - = 0  $\mu$ M BAY16, ns = non-significant.

Symbol	Entrez gene name	Probeset ID	Fold change						
			UT		SC		siGCGR		
			LD	HD	LD	HD	LD	HD	C
A2bp1	ataxin 2 binding protein 1	1378371_at	5.1	ns	ns	ns	ns	-5.6	ns
A2ld1	AIG2-like domain 1	1392725_at	ns	ns	ns	-1.6	ns	ns	ns
Aacs	acetoacetyl-CoA synthetase	1368126_at	1.9	ns	2.2	1.8	2.2	ns	ns
Aadac	arylacetamide deacetylase (esterase)	1369492_at	ns	-2.1	-2.0	-2.0	-1.9	-2.1	ns
Aak1	AP2 associated kinase 1	1397988_at	ns	7.8	-8.8	ns	ns	ns	ns
Abca4	ATP-binding cassette, sub-family A (ABC1), member 4	1384603_at	ns	ns	ns	ns	ns	ns	2.3
Abca8a	ATP-binding cassette, sub-family A (ABC1), member 8a	1390783_at	ns	-1.9	ns	ns	ns	ns	ns
Abcb11	ATP-binding cassette, sub-family B (MDR/TAP), member 11	1368769_at	3.2	3.0	2.9	3.0	2.8	2.8	ns
Abcb1a	ATP-binding cassette, sub-family B (MDR/TAP), member 1A	1370464_at	ns	2.0	ns	2.1	ns	2.1	ns
Abcb4	ATP-binding cassette, sub-family B (MDR/TAP), member 4	1369161_at	2.4	2.4	2.7	3.0	2.6	2.8	ns
Abcc2	ATP-binding cassette, sub-family C (CFTR/MRP), member 2	1368497_at	1.9	2.3	1.6	1.9	ns	1.5	ns
Abcc5	ATP-binding cassette, sub-family C (CFTR/MRP), member 5	1387030_at	ns	ns	ns	-1.9	ns	ns	ns
Abcc6	ATP-binding cassette, sub-family C (CFTR/MRP), member 6	1368452_at	ns	ns	ns	-1.7	ns	ns	ns
Abcc8	ATP-binding cassette, sub-family C (CFTR/MRP), member 8	1369632_a_at	ns	ns	ns	ns	1.9	2.1	ns
Abcg5	ATP-binding cassette, sub-family G (WHITE), member 5	1369455_at	ns	ns	ns	ns	ns	2.5	ns
Acaa1	acetyl-Coenzyme A acyltransferase 1 /similar to 3-ketoacyl-CoA thiolase B, peroxisom	1387783_a_at	2.1	1.7	2.0	1.9	2.1	2.0	ns
Acaa2	Acetyl-Coenzyme A acyltransferase 2	1380504_at	2.4	2.4	2.1	1.8	2.1	1.9	ns
Acaa2	acetyl-Coenzyme A acyltransferase 2	1386880_at	1.9	2.1	1.6	1.7	1.8	1.8	ns
Acaca	acetyl-coenzyme A carboxylase alpha	1370893_at	1.9	1.9	2.0	2.1	ns	ns	ns
Acan	aggrecan	1387355_at	ns	-6.2	ns	ns	4.7	4.0	ns
Acap1	ArfGAP with coiled-coil, ankyrin repeat and PH domains 1	1376030_at	ns	3.7	ns	ns	ns	ns	ns
Acat1	Acetyl-coenzyme A acetyltransferase 1	1383416_at	ns	ns	ns	-1.5	ns	ns	ns
Acat2	acetyl-Coenzyme A acetyltransferase 2	1372462_at	ns	-2.3	ns	ns	ns	ns	ns
Accn2	amiloride-sensitive cation channel 2, neuronal	1371045_at	ns	ns	-5.0	ns	ns	ns	ns
Acer2	alkaline ceramidase 2	1379846_at	ns	ns	ns	ns	8.7	ns	ns
Acmsd	aminocarboxymuconate semialdehyde decarboxylase	1370147_at	1.7	ns	2.0	2.0	1.9	1.7	ns
Aco1	aconitase 1, soluble	1386916_at	1.9	1.8	2.1	2.0	1.8	1.9	ns
Acot1	acyl-CoA thioesterase 1	1398250_at	10.6	7.7	7.3	6.2	10.4	10.5	ns
Acot12	acyl-CoA thioesterase 12	1369485_at	3.3	3.0	2.9	2.6	3.4	3.3	ns
Acot2	acyl-CoA thioesterase 2	1391433_at	ns	1.6	ns	ns	ns	ns	ns
Acot2	acyl-CoA thioesterase 2	1388210_at	ns	2.1	ns	ns	ns	ns	ns
Acox1	acyl-Coenzyme A oxidase 1, palmitoyl	1367680_at	1.9	2.0	1.7	1.8	1.8	1.8	ns
Acs1	acyl-CoA synthetase long-chain family member 1	1370939_at	1.7	ns	1.7	1.6	1.7	ns	ns
Acs1	acyl-CoA synthetase long-chain family member 1	1388153_at	1.9	ns	2.3	1.9	ns	ns	ns
Acs13	acyl-CoA synthetase long-chain family member 3	1368177_at	ns	ns	ns	ns	1.6	ns	ns
Actn4	actinin alpha 4	1369942_at	ns	ns	ns	ns	ns	-1.6	ns
Adam15	a disintegrin and metallopeptidase domain 15 (metargidin)	1387135_at	ns	-1.6	ns	ns	ns	ns	ns
Adam2	ADAM metallopeptidase domain 2	1369833_at	-7.7	ns	ns	ns	ns	ns	ns
Adam8	ADAM metallopeptidase domain 8	1392754_at	ns	-4.5	ns	ns	ns	ns	ns
Adamts13	ADAM metallopeptidase with thrombospondin type 1 motif, 13	1375325_at	ns	ns	ns	ns	7.2	ns	ns

Symbol	Entrez gene name	Probeset ID	Fold change						
			UT		SC		siGCGR		
			LD	HD	LD	HD	LD	HD	C
Adarb1	adenosine deaminase, RNA-specific, B1	1391888_at	ns	5.3	4.9	5.6	ns	ns	ns
Adarb1	adenosine deaminase, RNA-specific, B1	1368933_at	ns	ns	ns	ns	2.3	2.3	ns
Adarb1	adenosine deaminase, RNA-specific, B1	1398370_at	2.1	2.0	2.6	2.6	2.2	2.4	ns
Adarb2	adenosine deaminase, RNA-specific, B2	1387475_at	ns	ns	ns	ns	-3.3	ns	ns
Adcy10	adenylate cyclase 10 (soluble)	1369337_at	ns	ns	ns	2.1	ns	ns	ns
Adcy6	adenylate cyclase 6	1386876_at	ns	ns	ns	ns	ns	ns	-1.7
Adh1	alcohol dehydrogenase 1 (class I)	1378260_at	ns	-2.2	ns	ns	ns	ns	ns
Adh7	alcohol dehydrogenase 7 (class IV), mu or sigma polypeptide	1369072_at	ns	ns	ns	ns	ns	-8.6	ns
Adipor2	adiponectin receptor 2	1397519_at	ns	ns	ns	ns	1.6	1.6	ns
Adm	adrenomedullin	1387219_at	-2.8	ns	ns	ns	ns	ns	ns
Adprh	ADP-ribosylarginine hydrolase	1370505_at	ns	1.6	ns	ns	ns	ns	ns
Adprh1	ADP-ribosylhydrolase like 1	1379392_at	ns	ns	ns	ns	-10.9	ns	ns
Afap1	actin filament associated protein 1	1381177_at	ns	-4.8	ns	ns	6.1	5.0	-8.7
Afmid	arylformamidase	1396300_at	1.7	ns	1.9	1.8	1.7	ns	ns
Afmid	arylformamidase	1396301_x_at	ns	ns	2.0	ns	ns	ns	ns
Afmid	arylformamidase	1394479_at	ns	ns	2.0	ns	1.8	ns	ns
Aftph	Aftphilin	1390295_at	ns	8.3	ns	ns	ns	ns	ns
Agap1	ArfGAP with GTPase domain, ankyrin repeat and PH domain 1	1377926_at	ns	ns	ns	1.9	ns	ns	ns
Agap2	ArfGAP with GTPase domain, ankyrin repeat and PH domain 2	1397549_at	ns	ns	ns	ns	ns	ns	-5.6
Agap3	ArfGAP with GTPase domain, ankyrin repeat and PH domain 3	1386458_x_at	ns	6.7	ns	ns	ns	ns	ns
Agps	alkylglycerone phosphate synthase	1370137_at	ns	ns	ns	ns	ns	2.7	ns
Agtbbp1	ATP/GTP binding protein 1	1383759_at	ns	ns	ns	ns	ns	-8.7	ns
Agtr1b	angiotensin II receptor, type 1b	1369439_at	ns	ns	ns	ns	-7.0	ns	ns
Ajap1	adherens junction associated protein 1	1395144_at	ns	ns	ns	-7.9	ns	ns	ns
Ak3l1	adenylate kinase 3-like 1	1398285_at	ns	ns	ns	ns	4.5	3.9	ns
Ak3l1	adenylate kinase 3-like 1	1371824_at	ns	ns	2.1	ns	2.1	ns	ns
Akap13	A kinase (PRKA) anchor protein 13	1382268_at	ns	ns	ns	-1.7	ns	ns	ns
Akr1d1	aldo-keto reductase family 1, member D1 (delta 4-3-ketosteroid-5-beta-reductase)	1398310_at	3.0	ns	2.8	ns	ns	ns	ns
Akr1d1	aldo-keto reductase family 1, member D1 (delta 4-3-ketosteroid-5-beta-reductase)	1392384_s_at	2.3	1.9	ns	ns	ns	ns	ns
Alas1	aminolevulinate, delta-, synthase 1	1367982_at	2.0	1.7	1.8	1.6	1.8	ns	ns
Alg10	asparagine-linked glycosylation 10, alpha-1,2-glucosyltransferase homolog (S. pombe)	1370317_at	ns	ns	ns	ns	ns	ns	-1.7
Alkbh	alkB, alkylation repair homolog (E. coli)	1380448_at	ns	ns	ns	ns	ns	ns	1.7
Alpl	alkaline phosphatase, liver/bone/kidney	1368139_s_at	1.6	1.6	1.5	1.7	ns	1.5	ns
Amelx	amelogenin X chromosome	1387634_a_at	7.2	6.6	ns	ns	ns	ns	ns
Ammecr1	AMME chromosomal region gene 1-like	1378338_at	ns	ns	ns	ns	ns	1.5	ns
Amy1a	amylase, alpha 1A (salivary)	1370359_at	ns	ns	ns	ns	ns	ns	-1.6
Amy1a	amylase, alpha 1A (salivary) / amylase 2, pancreatic	1369502_a_at	ns	ns	ns	ns	ns	ns	-1.6
Angptl2	angiopoietin-like 2	1369443_at	12.3	8.9	ns	4.8	10.6	19.2	ns
Angptl3	angiopoietin-like 3	1393403_at	2.6	2.6	2.3	2.3	2.3	2.3	ns
Ank1	ankyrin 1, erythrocytic	1381477_at	-9.2	ns	ns	ns	ns	ns	ns
Ankhd1	Ankhd1-Eif4ebp3 fusion transcript	1385965_at	ns	ns	ns	ns	ns	ns	-1.5
Ankrd42	ankyrin repeat domain 42	1389026_at	ns	ns	ns	ns	-1.7	-1.5	ns
Ankrd43	ankyrin repeat domain 43	1390073_at	ns	ns	ns	ns	3.3	ns	-3.1
Ankrd5	ankyrin repeat domain 5	1382488_at	ns	ns	ns	ns	ns	ns	-6.7
Ankrd54	ankyrin repeat domain 54	1389264_at	ns	ns	ns	ns	ns	-1.7	ns
Anks4b	ankyrin repeat and sterile alpha motif domain containing 4B	1374657_at	ns	ns	ns	-1.5	ns	ns	ns
Ap2a2	Adaptor-related protein complex 2, alpha 2 subunit	1371493_at	ns	ns	ns	ns	ns	-1.6	ns
Apbb1	amyloid beta (A4) precursor protein-binding, family B, member 1 (Fe65)	1367842_at	ns	ns	ns	-1.8	ns	ns	-1.6
Apbb2	amyloid beta (A4) precursor protein-binding, family B, member 2	1376678_at	ns	ns	ns	-1.6	ns	ns	ns
Apbb2	amyloid beta (A4) precursor protein-binding, family B, member 2	1378248_at	ns	ns	ns	ns	ns	ns	1.6

## 10 APPENDIX

Symbol	Entrez gene name	Probeset ID	Fold change						
			UT		SC		siGCGR		
			LD	HD	LD	HD	LD	HD	C
Apc2	adenomatosis polyposis coli 2	1395461_at	ns	-2.6	ns	ns	ns	ns	ns
Aplnr	apelin receptor	1379772_at	6.0	5.0	ns	ns	ns	ns	ns
Apoa4	apolipoprotein A-IV	1368520_at	ns	ns	ns	1.8	ns	ns	ns
Apoa5	apolipoprotein A-V	1369011_at	ns	-1.9	ns	ns	ns	ns	ns
Apol9a	apolipoprotein L 9a	1376496_at	ns	ns	ns	ns	ns	ns	5.1
Aqp7	aquaporin 7	1368317_at	ns	ns	-1.5	ns	ns	ns	ns
Aqp9	aquaporin 9	1368621_at	-1.7	-1.7	-1.9	-2.1	-1.8	-2.0	ns
Arfgef1	ADP-ribosylation factor guanine nucleotide-exchange factor 1 (brefeldin A-inhibited)	1395937_at	ns	7.3	ns	ns	ns	ns	ns
Arhgap20	Rho GTPase activating protein 20	1391673_at	ns	5.8	ns	ns	ns	ns	ns
Arhgap21	Rho GTPase activating protein 21	1374086_at	ns	ns	ns	-1.5	ns	-1.5	ns
Arhgap4	Rho GTPase activating protein 4	1374735_at	ns	ns	ns	ns	-4.5	ns	ns
Arhgef15	Rho guanine nucleotide exchange factor (GEF) 15	1383844_at	ns	ns	ns	ns	-10.5	ns	ns
Arhgef18	rho/rac guanine nucleotide exchange factor (GEF) 18	1383523_at	ns	ns	ns	ns	ns	-1.5	ns
Arid1b	AT rich interactive domain 1B (Swi1 like)	1383026_at	ns	ns	-2.0	-2.1	ns	ns	ns
Arid5a	AT rich interactive domain 5A (Mrf1 like)	1379311_at	ns	-2.2	ns	ns	ns	ns	-1.8
Arl5a	ADP-ribosylation factor-like 5A	1369729_at	1.8	ns	2.1	2.0	1.8	1.7	ns
Arl6ip6	ADP-ribosylation-like factor 6 interacting protein 6	1379005_at	ns	ns	ns	-2.1	ns	ns	ns
Arntl	aryl hydrocarbon receptor nuclear translocator-like	1370510_a_at	ns	-1.9	ns	-1.5	ns	ns	ns
Arpc5l	actin related protein 2/3 complex, subunit 5-like	1382016_at	ns	ns	ns	ns	2.7	ns	-2.8
Arpp19	cAMP-regulated phosphoprotein 19	1394318_at	ns	ns	ns	ns	ns	1.6	ns
Arpp-21	cyclic AMP-regulated phosphoprotein	1373257_at	ns	ns	ns	ns	ns	ns	-7.5
Asap1	ArfGAP with SH3 domain, ankyrin repeat and PH domain 1	1390441_at	ns	-2.2	ns	ns	ns	ns	ns
Asap1	ArfGAP with SH3 domain, ankyrin repeat and PH domain 1	1381019_x_at	-1.6	ns	-1.7	ns	ns	ns	ns
Asb18	ankyrin repeat and SOCS box-containing 18	1380076_at	-5.6	ns	ns	ns	ns	ns	ns
Asb5	ankyrin repeat and SOCS box-containing 5	1378848_at	ns	ns	-1.8	-2.0	ns	ns	ns
Ascl1	Achaete-scute complex homolog 1 (Drosophila)	1375258_at	6.2	ns	ns	ns	ns	ns	ns
Asns	asparagine synthetase	1387925_at	ns	ns	ns	1.5	ns	ns	ns
Aspa	aspartoacylase	1368563_at	ns	ns	ns	-2.0	-2.5	-2.5	ns
Aspg	asparaginase homolog (S. cerevisiae)	1387959_at	5.9	6.8	13.3	14.3	4.5	5.9	ns
Aspm	asp (abnormal spindle) homolog, microcephaly associated (Drosophila)	1393581_at	ns	-1.8	ns	-1.5	-1.7	-1.7	ns
Atf6	activating transcription factor 6	1392475_at	ns	1.5	ns	ns	ns	ns	ns
Atg4d	ATG4 autophagy related 4 homolog D (S. cerevisiae)	1385512_at	ns	ns	2.0	1.9	ns	ns	1.8
Atoh8	atonal homolog 8 (Drosophila)	1373287_at	ns	ns	-2.2	-2.8	ns	ns	ns
Atp13a2	ATPase type 13A2	1373949_at	ns	-1.8	ns	-1.6	ns	-1.7	ns
Atp13a5	ATPase type 13A5	1391104_at	ns	ns	ns	-5.9	ns	ns	ns
Atp1b1	ATPase, Na+/K+ transporting, beta 1 polypeptide	1367814_at	ns	1.6	ns	ns	ns	ns	ns
Atp2a2	ATPase, Ca++ transporting, cardiac muscle, slow twitch 2	1398862_at	ns	ns	1.7	ns	ns	ns	ns
Atp2b3	ATPase, Ca++ transporting, plasma membrane 3	1388237_s_at	ns	ns	-2.3	ns	ns	ns	ns
Atp6v0a1	ATPase, H+ transporting, lysosomal V0 subunit A1	1387045_at	ns	-1.6	ns	ns	ns	-2.2	ns
Atp7b	ATPase, Cu++ transporting, beta polypeptide	1370324_at	ns	ns	ns	-2.2	ns	ns	-1.9
Azgp1	alpha-2-glycoprotein 1, zinc-binding	1387234_at	ns	1.6	ns	ns	ns	ns	ns
B3galnt1	beta-1,3-N-acetylgalactosaminyltransferase 1	1398373_at	-2.1	-2.1	-2.3	-2.3	-2.9	-2.8	ns
Bach1	BTB and CNC homology 1, basic leucine zipper transcription factor 1	1377699_at	ns	2.8	ns	ns	ns	ns	ns
Bai2	brain-specific angiogenesis inhibitor 2	1378871_at	ns	ns	ns	ns	ns	-5.2	ns
Baiap2	BAI1-associated protein 2	1370074_at	ns	ns	ns	-1.6	-1.6	ns	ns
Baiap2	BAI1-associated protein 2	1374117_at	ns	-1.8	ns	-1.5	ns	-1.6	ns
Bard1	BRCA1 associated RING domain 1	1368777_at	ns	5.5	ns	ns	ns	ns	ns
Bcat1	branched chain aminotransferase 1, cytosolic	1370869_at	ns	ns	ns	6.0	ns	ns	ns

Symbol	Entrez gene name	Probeset ID	Fold change						
			UT		SC		siGCGR		
			LD	HD	LD	HD	LD	HD	C
Bche	butyrylcholinesterase	1387832_at	ns	ns	ns	-2.6	ns	ns	ns
Bcl2l1	Bcl2-like 1	1370485_a_at	ns	ns	ns	2.1	ns	1.8	ns
Bcl2l1	Bcl2-like 1	1370812_at	ns	1.6	ns	1.5	ns	ns	ns
Bcl9l	B-cell CLL/lymphoma 9-like	1384335_at	ns	-1.6	-1.6	-1.6	-1.5	-1.6	ns
Bcor1f	BCL6 co-repressor-like 1	1378730_at	ns	ns	ns	ns	-1.8	ns	ns
Bdh2	3-hydroxybutyrate dehydrogenase, type 2	1372613_at	ns	-2.1	ns	ns	ns	ns	ns
Bdkrb2	bradykinin receptor B2	1370649_at	ns	ns	ns	-9.8	ns	ns	-10.1
Bet1	blocked early in transport 1 homolog (S. cerevisiae)	1368881_at	ns	1.8	ns	ns	ns	ns	ns
Bex1 /// Bex2	brain expressed gene 1 /// brain expressed X-linked 2	1394299_at	ns	ns	ns	-6.0	ns	ns	ns
Bglap	bone gamma-carboxyglutamate (gla) protein	1369142_at	ns	2.3	ns	ns	ns	ns	ns
Bhlha15	basic helix-loop-helix family, member a15	1387212_at	ns	ns	ns	1.8	ns	ns	ns
Bhlhe40	basic helix-loop-helix family, member e40	1369415_at	ns	ns	ns	ns	1.7	1.6	ns
Bhlhe40	Basic helix-loop-helix family, member e40	1379483_at	ns	ns	ns	ns	1.6	1.6	ns
Bhlhe41	basic helix-loop-helix family, member e41	1368511_at	ns	ns	-6.1	ns	ns	ns	ns
Birc7	baculoviral IAP repeat-containing 7	1374889_at	ns	ns	ns	ns	-4.0	ns	ns
Blvra	biliverdin reductase A	1368164_at	ns	-1.5	ns	ns	ns	ns	ns
Bmp2	bone morphogenetic protein 2	1368945_at	-11.2	ns	ns	ns	ns	ns	ns
Bmp5	bone morphogenetic protein 5	1385127_at	ns	ns	ns	-8.6	ns	ns	ns
Bmp7	bone morphogenetic protein 7	1389403_at	2.0	2.4	ns	ns	ns	ns	ns
Bmper	BMP-binding endothelial regulator	1391345_at	ns	ns	ns	ns	13.4	ns	ns
Bnip3l	BCL2/adenovirus E1B interacting protein 3-like	1367898_at	1.6	1.6	1.7	1.6	1.6	ns	ns
Bnip3l	BCL2/adenovirus E1B interacting protein 3-like	1386978_at	1.6	ns	1.7	1.7	1.8	1.7	ns
Brd4	bromodomain containing 4	1393567_at	ns	2.2	ns	ns	ns	ns	ns
Bri3bp	Bri3 binding protein	1392839_at	ns	2.2	ns	ns	ns	ns	ns
Bst2	bone marrow stromal cell antigen 2	1390738_at	ns	ns	ns	ns	ns	ns	1.9
Btc	betacellulin	1387644_at	ns	ns	ns	-3.9	ns	ns	ns
Btg2	BTG family, member 2	1386995_at	-1.5	ns	ns	ns	ns	ns	ns
Btg2	BTG family, member 2	1386994_at	-1.7	-2.0	-1.7	-1.7	-1.7	ns	ns
Btnl5	butyrophilin-like 5	1398529_at	ns	ns	ns	ns	ns	-6.3	6.6
Bzw1	basic leucine zipper and W2 domains 1	1388554_at	ns	-1.5	ns	ns	ns	ns	ns
C1qtnf2	C1q and tumor necrosis factor related protein 2	1382185_at	ns	ns	ns	ns	-7.2	ns	ns
C1qtnf3	C1q and tumor necrosis factor related protein 3	1377086_at	ns	ns	-4.2	ns	ns	-6.4	ns
C1qtnf4	C1q and tumor necrosis factor related protein 4	1376707_at	ns	7.0	ns	ns	ns	ns	ns
C1s	complement component 1, s subcomponent	1387893_at	ns	-1.7	ns	ns	ns	ns	ns
C4-2 / C4b	complement component 4, gene 2 / complement component 4B (Chido blood group)	1370892_at	ns	ns	ns	ns	ns	ns	3.7
C4bpb	complement component 4 binding protein, beta	1368695_at	ns	-2.2	ns	ns	ns	ns	ns
Cabc1	chaperone, ABC1 activity of bc1 complex homolog (S. pombe)	1372536_at	ns	ns	ns	-1.7	ns	-1.5	ns
Cabp4	calcium binding protein 4	1385588_at	-10.0	ns	ns	ns	ns	ns	ns
Cacna1b	calcium channel, voltage-dependent, N type, alpha 1B subunit	1370444_at	ns	ns	ns	ns	-6.6	ns	ns
Cacna1d	calcium channel, voltage-dependent, L type, alpha 1D subunit	1370640_a_at	ns	ns	7.2	ns	ns	ns	ns
Cacna1i	calcium channel, voltage-dependent, T type, alpha 1I subunit	1370641_s_at	ns	4.8	ns	ns	ns	ns	ns
Cadm1	cell adhesion molecule 1	1376657_at	ns	-2.1	ns	ns	ns	-1.7	ns
Cadps2	Ca <sup>++</sup> -dependent secretion activator 2	1390865_at	ns	ns	ns	-1.5	ns	ns	ns
Calm3	calmodulin 3	1370873_at	ns	-1.7	-1.6	-2.2	-1.6	-1.9	ns
Camk1	calcium/calmodulin-dependent protein kinase I	1367889_at	ns	-1.6	ns	ns	ns	ns	ns
Capn10	calpain 10	1368904_at	ns	ns	-1.6	-1.7	ns	ns	ns
Car12	Carbonic anhydrase 12	1371922_at	1.6	2.0	2.2	2.8	ns	1.7	ns
Car2	carbonic anhydrase II	1386922_at	-1.5	ns	ns	ns	ns	ns	ns

## 10 APPENDIX

Symbol	Entrez gene name	Probeset ID	Fold change						
			UT		SC		siGCGR		
			LD	HD	LD	HD	LD	HD	C
Car2	carbonic anhydrase II	1367733_at	ns	ns	-1.6	-1.6	ns	ns	ns
Car4	carbonic anhydrase 4	1391132_at	-4.1	ns	ns	ns	ns	ns	ns
Car5b	carbonic anhydrase 5b, mitochondrial	1390807_at	ns	-1.6	ns	ns	-1.7	ns	ns
Car5b	carbonic anhydrase 5b, mitochondrial	1377573_at	ns	-1.8	ns	ns	ns	ns	ns
Caskin1	CASK interacting protein 1	1368425_at	ns	ns	ns	ns	-4.7	ns	ns
Casq2	calsequestrin 2 (cardiac muscle)	1387401_at	ns	ns	ns	ns	4.4	ns	-4.3
Catsper2	cation channel, sperm associated 2	1391231_at	ns	1.8	ns	ns	ns	ns	ns
Cav1	caveolin 1, caveolae protein	1372111_at	ns	-2.7	-3.0	-3.3	-3.4	-3.3	ns
Cav1	caveolin 1, caveolae protein	1393281_at	ns	ns	ns	-2.9	-3.2	ns	ns
Cav2	caveolin 2	1377642_at	ns	ns	ns	-2.5	ns	ns	ns
Ccdc101	Coiled-coil domain containing 101	1395038_at	ns	ns	-2.5	-2.9	-2.1	-2.7	ns
Ccdc117	coiled-coil domain containing 117	1379500_at	ns	ns	ns	ns	ns	1.5	ns
Ccdc158	coiled-coil domain containing 158	1396703_at	ns	ns	2.9	2.9	ns	ns	ns
Ccdc68	coiled-coil domain containing 68	1393952_at	ns	-1.7	ns	-1.5	ns	-1.6	ns
Ccdc69	coiled-coil domain containing 69	1391015_at	ns	2.5	ns	ns	ns	ns	ns
Ccl21b	chemokine (C-C motif) ligand 21b	1378015_at	ns	2.5	ns	ns	ns	ns	ns
Ccl5	chemokine (C-C motif) ligand 5	1369983_at	ns	ns	ns	ns	ns	ns	102.0
Ccnd1	cyclin D1	1371150_at	2.5	2.7	3.2	2.9	4.2	5.0	ns
Ccnd1	cyclin D1	1371643_at	4.1	3.4	4.0	4.2	5.4	6.4	ns
Ccnd1	cyclin D1	1383075_at	4.3	3.7	6.5	7.5	10.9	11.4	ns
Ccnj	cyclin J	1380997_at	ns	ns	ns	ns	ns	ns	1.7
Ccnjl	cyclin J-like	1374277_at	ns	4.5	ns	ns	ns	ns	ns
Cd209g	CD209g molecule	1384905_at	ns	-5.8	ns	-16.7	ns	ns	ns
Cd28	Cd28 molecule	1369865_at	ns	5.6	-6.7	ns	ns	ns	ns
Cd36	CD36 molecule (thrombospondin receptor)	1386901_at	-1.9	-2.1	-2.0	-2.1	-1.7	-1.7	ns
Cd36	CD36 molecule (thrombospondin receptor)	1367689_a_at	ns	-1.8	-1.8	-1.8	ns	ns	ns
Cd3e	CD3 molecule, epsilon polypeptide	1389997_at	4.3	4.2	ns	ns	ns	ns	ns
Cd79b	Cd79b molecule, immunoglobulin-associated beta	1387749_at	ns	-6.2	ns	ns	ns	ns	ns
Cdadcl1	cytidine and dCMP deaminase domain containing 1	1385329_at	ns	-1.5	ns	ns	ns	ns	ns
Cdc14a	CDC14 cell division cycle 14 homolog A (S. cerevisiae)	1376782_at	ns	ns	ns	ns	ns	-2.3	ns
Cdc16	cell division cycle 16 homolog (S. cerevisiae)	1396172_at	ns	ns	ns	ns	ns	ns	-1.9
Cdc20	cell division cycle 20 homolog (S. cerevisiae)	1387895_s_at	2.3	ns	ns	ns	3.2	3.3	-2.8
Cdc26	cell division cycle 26	1388727_at	ns	ns	ns	-1.7	-1.7	ns	ns
Cdc42ep2	CDC42 effector protein (Rho GTPase binding) 2	1389145_at	-1.6	-2.0	-2.0	-1.9	-2.1	-2.4	ns
Cdc42ep5	CDC42 effector protein (Rho GTPase binding) 5	1389378_at	ns	ns	-1.6	-1.5	ns	ns	ns
Cdca2	cell division cycle associated 2	1381833_at	ns	ns	ns	-4.2	ns	ns	ns
Cdca7	cell division cycle associated 7	1374540_at	ns	ns	-2.8	ns	ns	ns	ns
Cdgap	Cdc42 GTPase-activating protein	1395715_at	ns	ns	ns	-6.8	ns	ns	ns
Cdh16	cadherin 16	1390822_at	ns	ns	ns	ns	-4.5	ns	ns
Cdh22	cadherin 22	1388045_a_at	-1.7	ns	ns	ns	ns	ns	ns
Cdk10	cyclin-dependent kinase 10	1377402_at	-1.6	-2.1	ns	ns	ns	ns	ns
Cdkn1a	cyclin-dependent kinase inhibitor 1A	1388674_at	-1.8	-1.6	-1.9	-1.7	-1.6	-1.7	ns
Cds2	CDP-diacylglycerol synthase (phosphatidate cytidyltransferase) 2	1369505_at	ns	2.1	ns	ns	ns	ns	ns
Cenpb	centromere protein B	1372883_at	ns	-1.8	ns	ns	ns	ns	ns
Cep164	centrosomal protein 164kDa	1375950_a_at	ns	-1.8	ns	ns	ns	ns	ns
Cep164	centrosomal protein 164kDa	1375091_at	ns	ns	ns	ns	ns	-1.7	ns
Cerk	ceramide kinase	1375987_at	ns	-1.8	ns	ns	ns	ns	ns
Ces7	carboxylesterase 7	1396034_at	ns	3.1	ns	ns	ns	ns	ns
Cesl1	carboxylesterase-like 1/ carboxylesterase ES-4	1370352_at	2.2	ns	2.0	2.0	2.0	ns	ns
Cetn1	centrin 1	1393680_at	ns	ns	ns	ns	-5.2	ns	ns
Chaf1b	chromatin assembly factor 1, subunit B (p60)	1390982_at	ns	ns	ns	-3.5	ns	ns	ns
Chchd6	coiled-coil-helix-coiled-coil-helix domain containing 6	1372134_at	ns	1.5	ns	ns	ns	ns	ns

Symbol	Entrez gene name	Probeset ID	Fold change						
			UT		SC		siGCGR		
			LD	HD	LD	HD	LD	HD	C
Chia	chitinase, acidic	1381318_at	ns	ns	ns	ns	ns	-9.1	ns
Chic2	cysteine-rich hydrophobic domain 2	1383764_at	ns	ns	ns	ns	ns	ns	-1.6
Chic2	cysteine-rich hydrophobic domain 2	1378376_at	ns	ns	ns	ns	1.7	1.8	ns
Chpf	chondroitin polymerizing factor	1373561_at	ns	ns	ns	ns	ns	ns	1.5
Chrdl2	chordin-like 2	1393954_at	ns	ns	ns	ns	ns	-2.6	ns
Cidec	cell death-inducing DFFA-like effector c	1378739_at	ns	ns	ns	-1.8	ns	ns	ns
Cited2	Cbp/p300-interacting transactivator, with Glu/Asp-rich carboxy-terminal domain, 2	1367601_at	ns	ns	ns	ns	-2.5	-2.3	ns
Cited2	Cbp/p300-interacting transactivator, with Glu/Asp-rich carboxy-terminal domain, 2	1367602_at	ns	ns	ns	ns	-2.3	ns	ns
Cited4	Cbp/p300-interacting transactivator, with Glu/Asp-rich carboxy-terminal domain, 4	1370225_at	ns	ns	ns	-2.6	ns	ns	ns
Cited4	Cbp/p300-interacting transactivator, with Glu/Asp-rich carboxy-terminal domain, 4	1390008_at	ns	ns	ns	ns	ns	ns	6.7
Cklf	chemokine-like factor	1387984_at	ns	-1.7	ns	ns	ns	ns	ns
Cks2	CDC28 protein kinase regulatory subunit 2	1373823_at	-1.9	-1.6	-1.7	ns	-1.6	ns	ns
Clca3	chloride channel calcium activated 3	1390238_at	ns	-6.5	ns	-7.8	ns	ns	ns
Cldn1	claudin 1	1383946_at	-2.5	-2.5	-2.8	-3.1	-3.1	-3.1	ns
Cldn1	claudin 1	1387470_at	-2.1	-2.0	-2.2	-2.2	-2.0	-2.0	ns
Cldn1	claudin 1	1396150_at	-1.7	-1.7	-1.7	-1.8	-1.7	-1.9	ns
Cldn14	claudin 14	1393588_at	ns	-1.8	ns	ns	ns	ns	ns
Cldn3	claudin 3	1368115_at	ns	-1.6	-1.5	-1.6	ns	-1.6	ns
Clec4f	C-type lectin domain family 4, member f	1368755_at	ns	-8.4	ns	ns	ns	ns	ns
Clic1	chloride intracellular channel 1	1375633_at	-1.5	-1.6	ns	ns	ns	ns	ns
Cml3	camello-like 3	1370991_at	ns	ns	ns	ns	4.9	5.7	-5.3
Cmpk2	cytidine monophosphate (UMP-CMP) kinase 2, mitochondrial	1383424_at	ns	ns	ns	ns	ns	ns	2.9
Cmtm8	CKLF-like MARVEL transmembrane domain containing 8	1374491_at	1.8	1.8	2.0	1.9	2.0	1.9	ns
Cndp2	CNDP dipeptidase 2 (metallopeptidase M20 family)	1372132_at	2.6	2.2	2.7	2.9	2.7	2.8	ns
Cngb1	cyclic nucleotide gated channel beta 1	1370721_a_at	ns	ns	-1.9	ns	ns	ns	ns
Cnp	2',3'-cyclic nucleotide 3' phosphodiesterase	1387897_at	ns	-1.6	-1.7	-1.8	ns	ns	ns
Cnp	2',3'-cyclic nucleotide 3' phosphodiesterase	1370693_a_at	ns	ns	ns	-2.3	ns	ns	ns
Cnst	consortin, connexin sorting protein	1393264_at	ns	ns	ns	ns	ns	-2.5	ns
Cntn4	contactin 4	1369155_at	ns	5.9	ns	ns	ns	ns	ns
Col22a1	collagen, type XXII, alpha 1	1377813_at	ns	ns	ns	-2.1	ns	ns	ns
Col5a2	collagen, type V, alpha 2	1370895_at	ns	3.8	ns	ns	ns	ns	ns
Col5a3	collagen, type V, alpha 3	1368347_at	ns	3.3	ns	ns	ns	ns	ns
Colq	collagen-like tail subunit (single strand of homotrimer) of asymmetric acetylcholinesterase	1368475_at	ns	ns	ns	-1.9	ns	ns	ns
Commd6	COMM domain containing 6	1389144_at	ns	1.5	ns	1.6	ns	1.5	ns
Comp	cartilage oligomeric matrix protein	1387137_at	ns	ns	3.5	3.2	ns	ns	ns
Coq10b	coenzyme Q10 homolog B (S. cerevisiae)	1373866_at	ns	ns	1.6	ns	ns	ns	ns
Coro2a	coronin, actin binding protein 2A	1380960_at	ns	-11.0	ns	-4.9	ns	ns	ns
Cox5a	Cytochrome c oxidase, subunit Va	1375127_at	ns	ns	ns	ns	ns	ns	-1.6
Cpg1	candidate plasticity gene 1	1371129_at	ns	ns	-5.5	-8.2	-4.2	ns	ns
Cpne7	copine VII	1384863_at	ns	ns	ns	ns	ns	6.1	ns
Cpt1a	carnitine palmitoyltransferase 1a, liver	1386946_at	ns	-1.5	ns	-1.6	ns	ns	ns
Creb3l3	cAMP responsive element binding protein 3-like 3	1391483_at	ns	-2.1	ns	ns	ns	ns	ns
Crebbp	CREB binding protein	1387619_at	ns	ns	ns	ns	-13.2	ns	ns
Crhbp	corticotropin releasing hormone binding protein	1369908_at	ns	ns	7.0	ns	ns	ns	ns
Crhr2	corticotropin releasing hormone receptor 2	1369495_at	ns	ns	ns	ns	-2.3	ns	ns
Crispld2	cysteine-rich secretory protein LCCL domain containing 2	1376457_at	ns	ns	-3.1	-4.0	ns	ns	ns
Crot	carnitine O-octanoyltransferase	1368426_at	ns	-1.6	ns	-1.7	ns	-1.5	ns
Crot	carnitine O-octanoyltransferase	1387183_at	ns	-1.6	ns	-1.5	ns	ns	ns
Crp	C-reactive protein, pentraxin-related	1387830_at	3.3	ns	2.8	2.4	3.2	2.3	ns
Crtc3	CREB regulated transcription coactivator 3	1396538_at	-3.2	-5.4	ns	ns	ns	ns	ns

## 10 APPENDIX

Symbol	Entrez gene name	Probeset ID	Fold change						
			UT		SC		siGCCR		
			LD	HD	LD	HD	LD	HD	C
Cryl1	crystallin, lambda 1	1376051_at	ns	1.5	ns	1.5	ns	ns	ns
Csrp2	cysteine and glycine-rich protein 2	1370282_at	-1.6	-1.5	ns	ns	ns	ns	ns
Ctdspl	CTD (carboxy-terminal domain, RNA polymerase II, polypeptide A) small phosphatase-like	1374349_at	ns	-1.8	-1.6	-1.8	-1.6	-1.7	ns
Ctdspl	CTD (carboxy-terminal domain, RNA polymerase II, polypeptide A) small phosphatase-like	1375251_at	ns	ns	ns	-8.0	ns	ns	ns
Ctdspl	CTD (carboxy-terminal domain, RNA polymerase II, polypeptide A) small phosphatase-like	1379238_at	-2.4	-2.8	ns	ns	-2.4	-3.8	ns
Ctgf	connective tissue growth factor	1367631_at	ns	ns	ns	ns	ns	-1.9	ns
Ctps2	CTP synthase II	1374482_at	ns	ns	ns	-1.5	ns	ns	ns
Ctsq	cathepsin Q	1387980_at	ns	ns	ns	ns	ns	ns	-15.8
Cttnbp2	cortactin binding protein 2	1382913_at	ns	-3.0	ns	-3.4	ns	ns	ns
Cx3cr1	chemokine (C-X3-C motif) receptor 1	1369527_at	ns	ns	ns	-3.0	ns	ns	ns
Cxcl10	chemokine (C-X-C motif) ligand 10	1387969_at	ns	ns	ns	ns	ns	ns	4.7
Cxcl3	chemokine (C-X-C motif) ligand 3	1388032_a_at	ns	ns	ns	ns	ns	-4.3	ns
Cxcl3	chemokine (C-X-C motif) ligand 3	1370633_at	ns	ns	ns	-5.2	ns	ns	ns
Cxcl9	chemokine (C-X-C motif) ligand 9	1373544_at	2.4	ns	ns	ns	ns	ns	2.7
Cxcl9	chemokine (C-X-C motif) ligand 9	1382454_at	2.6	ns	2.2	ns	2.1	ns	2.5
Cxcr3	chemokine (C-X-C motif) receptor 3	1368192_at	ns	ns	ns	ns	ns	2.4	ns
Cxcr5	chemokine (C-X-C motif) receptor 5	1369911_at	ns	ns	ns	ns	-7.4	ns	ns
Cyb5r2	cytochrome b5 reductase 2	1391430_at	-2.7	ns	ns	ns	ns	ns	ns
Cym	chymosin	1369866_at	ns	ns	ns	-2.6	ns	ns	ns
Cyp17a1	cytochrome P450, family 17, subfamily a, polypeptide 1	1387123_at	ns	-4.8	ns	-2.8	ns	-3.7	ns
Cyp2b1 /Cyp2b2	cytochrome P450, family 2, subfamily b, polypeptide 1 / cytochrome P450, family 2, su	1371076_at	4.2	3.3	3.8	4.6	4.5	5.2	ns
Cyp2c11	cytochrome P450, subfamily 2, polypeptide 11	1387328_at	3.2	3.0	3.1	3.2	2.5	ns	ns
Cyp2c22	cytochrome P450, family 2, subfamily c, polypeptide 22	1387949_at	1.6	1.9	ns	1.5	1.5	1.6	ns
Cyp2c6	cytochrome P450, family 2, subfamily c, polypeptide 6 / cytochrome P450-like	1370580_a_at	5.8	5.5	6.7	6.8	7.3	7.1	ns
Cyp2j4	cytochrome P450, family 2, subfamily j, polypeptide 4	1387296_at	ns	ns	ns	-1.6	ns	ns	ns
Cyp2t1	cytochrome P450, family 2, subfamily t, polypeptide 1	1368265_at	ns	-1.6	ns	ns	ns	ns	ns
Cyp39a1	cytochrome P450, family 39, subfamily a, polypeptide 1	1385165_at	2.0	ns	1.8	ns	ns	ns	ns
Cyp3a18	cytochrome P450, family 3, subfamily a, polypeptide 18	1398307_at	6.5	5.4	5.2	5.3	5.2	4.7	ns
Cyp3a2	cytochrome P450, family 3, subfamily a, polypeptide 2	1370593_at	7.6	6.4	5.3	4.5	5.5	5.0	ns
Cyp3a23/3a1	cytochrome P450, family 3, subfamily a, polypeptide 23/polypeptide 1	1387118_at	8.5	9.2	6.2	6.6	9.9	9.9	-1.7
Cyp4f17	cytochrome P450, family 4, subfamily f, polypeptide 17	1392720_at	ns	ns	ns	ns	-1.7	-1.6	ns
Cyp4f5	cytochrome P450, family 4, subfamily f, polypeptide 5	1388055_at	ns	ns	ns	-3.3	ns	ns	ns
Cyp51	cytochrome P450, family 51	1367979_s_at	ns	-2.2	ns	ns	ns	-1.8	ns
Cyp51	cytochrome P450, family 51	1387020_at	ns	-1.8	ns	ns	ns	-1.8	ns
Cyp8b1	cytochrome P450, family 8, subfamily b, polypeptide 1	1368435_at	-3.6	-7.9	-4.8	-7.5	-6.6	-8.2	ns
Cyth1	cytohesin 1	1369517_at	ns	ns	ns	4.5	ns	ns	5.2
D2hgdh	D-2-hydroxyglutarate dehydrogenase	1382047_at	ns	ns	-1.8	ns	ns	ns	ns
Daam1	dishevelled associated activator of morphogenesis 1	1389318_at	ns	-1.7	ns	-1.5	ns	ns	ns
Daam1	dishevelled associated activator of morphogenesis 1	1374480_at	ns	-1.5	-1.5	-1.6	ns	ns	ns
Dab2ip	DAB2 interacting protein	1370335_at	ns	ns	1.5	ns	ns	ns	ns
Dact2	dapper, antagonist of beta-catenin, homolog 2 (Xenopus laevis)	1383205_at	1.7	1.9	1.9	1.9	1.7	1.9	ns
Dap	Death-associated protein	1395881_at	-1.6	ns	-1.6	ns	ns	ns	ns
Dapk1	death associated protein kinase 1	1376788_at	ns	ns	ns	ns	1.6	ns	ns
Dazap1	DAZ associated protein 1	1373046_at	ns	1.6	ns	ns	ns	ns	ns
Dbil5	diazepam binding inhibitor-like 5	1368631_at	ns	ns	ns	-6.0	ns	ns	ns
Dbt	dihydroliipoamide branched chain transacylase E2	1373201_at	ns	ns	ns	1.6	ns	1.7	ns



Symbol	Entrez gene name	Probeset ID	Fold change						
			UT		SC		siGCGR		
			LD	HD	LD	HD	LD	HD	C
Dcaf11	DDB1 and CUL4 associated factor 11	1371549_at	2.0	ns	1.9	ns	1.9	ns	ns
Dcaf6	DDB1 and CUL4 associated factor 6	1384402_a_at	ns	ns	ns	ns	1.9	ns	-2.3
Dcre1b	DNA cross-link repair 1B, PSO2 homolog (S. cerevisiae)	1388591_at	ns	-1.6	ns	ns	ns	ns	ns
Dda1	DET1 and DDB1 associated 1	1399031_at	ns	ns	ns	ns	ns	-1.6	ns
Ddah1	dimethylarginine dimethylaminohydrolase 1	1387111_at	ns	ns	ns	-1.5	ns	-1.6	ns
Ddah2	dimethylarginine dimethylaminohydrolase 2	1371436_at	ns	ns	-2.1	ns	ns	ns	-1.9
Ddit3	DNA-damage inducible transcript 3	1369590_a_at	ns	2.5	ns	ns	ns	ns	3.6
Ddx25	DEAD (Asp-Glu-Ala-Asp) box polypeptide 25	1368619_at	ns	ns	ns	ns	ns	-2.6	ns
Ddx58	DEAD (Asp-Glu-Ala-Asp) box polypeptide 58	1391463_at	ns	ns	ns	ns	ns	ns	2.2
Ddx60	DEAD (Asp-Glu-Ala-Asp) box polypeptide 60	1381556_at	ns	ns	-13.3	ns	ns	ns	27.3
Defa-rs1	defensin alpha-related sequence 1	1394174_at	4.4	4.1	6.8	7.9	4.7	6.7	ns
Defb1	defensin beta 1	1369660_at	6.6	10.7	5.3	8.3	4.6	6.7	ns
Dennd2a	DENN/MADD domain containing 2A	1378126_at	2.3	2.3	2.7	2.5	1.9	2.0	ns
Dennd2a	DENN/MADD domain containing 2A	1392267_at	2.5	2.6	2.7	2.5	2.2	2.3	ns
Depdc5	DEP domain containing 5	1373752_at	ns	ns	ns	-1.6	ns	ns	ns
Depdc7	DEP domain containing 7	1393612_a_at	1.5	ns	ns	ns	ns	ns	ns
Dffa	DNA fragmentation factor, alpha subunit	1389195_at	ns	ns	ns	-1.5	ns	ns	ns
Dhcr24	24-dehydrocholesterol reductase	1372012_at	1.9	ns	ns	ns	ns	ns	ns
Dhcr7	7-dehydrocholesterol reductase	1368189_at	ns	-2.3	ns	ns	ns	ns	ns
Dhrs1	dehydrogenase/reductase (SDR family) member 1	1389407_at	ns	ns	ns	-1.6	ns	ns	ns
Dhrs11	dehydrogenase/reductase (SDR family) member 11	1388952_at	-1.5	-1.5	ns	ns	ns	ns	ns
Dhx58	DEXH (Asp-Glu-X-His) box polypeptide 58	1385276_a_at	ns	ns	ns	ns	ns	ns	2.7
Dhx58	DEXH (Asp-Glu-X-His) box polypeptide 58	1385439_x_at	ns	ns	ns	ns	ns	ns	2.1
Disp1	dispatched homolog 1 (Drosophila)	1374219_at	-1.7	-2.0	-1.8	ns	-1.7	ns	ns
Dlc1	deleted in liver cancer 1	1389894_at	ns	ns	ns	ns	ns	-13.3	ns
Dlk2	delta-like 2 homolog (Drosophila)	1384906_at	ns	ns	3.5	ns	ns	-3.9	3.3
Dmbr1	deleted in malignant brain tumors 1	1368007_at	ns	ns	ns	ns	-3.2	ns	ns
Dmd	dystrophin	1369810_at	ns	ns	3.8	ns	ns	ns	ns
Dmgdh	dimethylglycine dehydrogenase	1370936_at	ns	-1.5	ns	ns	ns	ns	ns
Dnajb1	DnaJ (Hsp40) homolog, subfamily B, member 1	1383302_at	ns	ns	ns	1.5	ns	1.5	ns
Dnajb3	DnaJ (Hsp40) homolog, subfamily B, member 3	1390520_at	5.0	6.5	ns	5.4	15.8	17.0	ns
Dnajc12	DnaJ (Hsp40) homolog, subfamily C, member 12	1387905_at	ns	-1.6	-1.6	-1.6	ns	-1.5	ns
Dnajc17	DnaJ (Hsp40) homolog, subfamily C, member 17	1384670_at	ns	-6.0	ns	ns	ns	ns	ns
Dnajc22	DnaJ (Hsp40) homolog, subfamily C, member 22	1373198_at	ns	ns	1.6	ns	1.6	1.5	ns
Dnajc7	DnaJ (Hsp40) homolog, subfamily C, member 7	1378187_at	ns	4.1	ns	ns	ns	ns	ns
Doc2g	double C2, gamma	1382327_at	ns	ns	ns	-3.5	ns	ns	ns
Dolpp1	dolichyl pyrophosphate phosphatase 1	1389724_at	ns	ns	ns	-1.5	ns	ns	ns
Dph3	DPH3, KTI11 homolog (S. cerevisiae)	1383760_at	ns	ns	ns	-1.5	ns	ns	ns
Dpp7	dipeptidylpeptidase 7	1367722_at	-1.5	ns	-1.6	-1.6	ns	ns	ns
Dpy1911	dpy-19-like 1 (C. elegans)	1389483_at	ns	-1.5	ns	ns	ns	ns	ns
Dpys	dihydropyrimidinase	1387284_at	ns	-1.8	ns	-1.7	ns	ns	ns
Dpysl2	dihydropyrimidinase-like 2	1371694_at	ns	-2.2	ns	-1.7	ns	-2.0	ns
Drp2	dystrophin related protein 2	1380160_at	ns	6.4	ns	ns	ns	ns	ns
Dtnbp1	distrobrevin binding protein 1	1397473_at	ns	ns	ns	ns	ns	-5.7	ns
Dtx2	deltex homolog 2 (Drosophila)	1374564_at	-1.8	-1.8	-1.9	-1.6	-1.7	ns	ns
Dtx3l	deltex 3-like (Drosophila)	1374718_at	ns	ns	ns	ns	ns	ns	2.3
Duox2	dual oxidase 2	1387414_at	ns	ns	2.8	ns	ns	ns	ns
Duoxa1	dual oxidase maturation factor 1	1385189_at	ns	ns	ns	ns	2.0	ns	ns
Dusp13	dual specificity phosphatase 13	1377977_at	3.6	4.0	ns	ns	ns	ns	-3.4
Dusp14	dual specificity phosphatase 14	1373324_at	ns	ns	ns	ns	ns	-1.6	ns
Dusp15	dual specificity phosphatase 15	1385912_at	ns	ns	ns	-3.1	ns	ns	ns

## 10 APPENDIX

Symbol	Entrez gene name	Probeset ID	Fold change						
			UT		SC		siGCCR		
			LD	HD	LD	HD	LD	HD	C
Dvl1	dishevelled, dsh homolog 1 (Drosophila)	1397351_s_at	1.6	ns	1.5	ns	1.5	ns	ns
Dvl3	dishevelled, dsh homolog 3 (Drosophila)	1385420_at	-4.4	-5.3	ns	ns	ns	-4.1	ns
Dyrk2	dual-specificity tyrosine-(Y)-phosphorylation regulated kinase 2	1386063_at	ns	-1.8	ns	ns	ns	ns	ns
Ebpl	emopamil binding protein-like	1391462_at	ns	ns	ns	ns	1.5	ns	ns
Ece2	endothelin-converting enzyme 2 /// endothelin converting enzyme 2-like	1377387_a_at	ns	1.6	ns	ns	ns	ns	ns
Eef2k	eukaryotic elongation factor-2 kinase	1369638_at	ns	ns	ns	ns	ns	-4.7	ns
Efcab4a	EF-hand calcium binding domain 4A	1390285_at	ns	-2.0	-2.1	-2.0	ns	ns	ns
Efna4	ephrin A4	1384175_at	ns	ns	-1.5	ns	ns	ns	ns
Egfl6	EGF-like-domain, multiple 6	1393335_at	ns	ns	-6.0	ns	ns	ns	ns
Egfr	epidermal growth factor receptor	1370830_at	ns	ns	1.6	ns	ns	ns	ns
Egr4	Early growth response 4	1375784_at	ns	ns	ns	-5.9	ns	ns	ns
Ehhadh	enoyl-Coenzyme A, hydratase/3-hydroxyacyl Coenzyme A dehydrogenase	1368283_at	2.8	ns	2.5	2.1	2.3	ns	ns
Eid2b	EP300 interacting inhibitor of differentiation 2B	1382563_at	ns	ns	ns	ns	-4.2	ns	ns
Eif2ak2	eukaryotic translation initiation factor 2-alpha kinase 2	1387242_at	ns	ns	ns	ns	ns	ns	1.8
Elac1	elaC homolog 1 (E. coli)	1380412_at	ns	ns	ns	-1.8	ns	ns	ns
Elmod1	ELMO/CED-12 domain containing 1	1389781_at	-13.7	-7.9	ns	ns	ns	ns	ns
Elovl6	ELOVL family member 6, elongation of long chain fatty acids (yeast)	1394401_at	3.1	ns	4.6	3.2	3.4	ns	ns
Elovl6	ELOVL family member 6, elongation of long chain fatty acids (yeast)	1388108_at	2.4	ns	2.8	2.3	2.4	2.0	ns
Emilin2	elastin microfibril interfacer 2	1383936_at	ns	-5.1	ns	ns	ns	ns	ns
Eml4	echinoderm microtubule associated protein like 4	1376827_at	-1.7	-1.8	-1.7	-1.6	-1.7	-1.9	ns
Eml4	echinoderm microtubule associated protein like 4	1397552_at	-2.0	-2.0	ns	-1.7	-1.8	-2.0	ns
Eml4	echinoderm microtubule associated protein like 4	1378016_at	-1.9	-2.0	-1.6	-1.7	-1.8	-1.9	ns
Eng	endoglin	1372579_at	ns	ns	4.1	3.5	4.1	ns	ns
Enpep	glutamyl aminopeptidase	1368513_at	ns	ns	ns	-3.3	ns	ns	ns
Epb4.9	erythrocyte protein band 4.9	1397826_at	ns	ns	ns	ns	-3.7	ns	ns
Ephb6	Eph receptor B6	1378997_at	ns	ns	ns	-4.5	ns	ns	ns
Ephx2	epoxide hydrolase 2, cytoplasmic	1369663_at	ns	-1.5	ns	ns	ns	ns	ns
Eprs	glutamyl-prolyl-tRNA synthetase	1373418_at	ns	ns	ns	1.6	ns	ns	ns
Eprs	glutamyl-prolyl-tRNA synthetase	1382040_at	ns	ns	2.0	ns	ns	ns	ns
Ercc5	excision repair cross-complementing rodent repair deficiency, complementation group 5	1383953_at	ns	ns	ns	ns	ns	-1.8	ns
Erf	Ets2 repressor factor	1374055_at	ns	ns	ns	-1.6	-1.6	ns	ns
Ethe1	ethylmalonic encephalopathy 1	1372306_at	ns	1.6	ns	1.7	1.7	1.7	ns
Extl1	exostoses (multiple)-like 1	1377472_at	1.7	2.0	1.8	2.3	ns	2.0	ns
Ezh2	enhancer of zeste homolog 2 (Drosophila)	1373290_at	ns	-1.5	ns	ns	ns	ns	ns
Fabp2	fatty acid binding protein 2, intestinal	1369195_at	ns	-1.7	ns	ns	ns	ns	ns
Fabp5	fatty acid binding protein 5, epidermal	1370281_at	ns	ns	ns	1.7	ns	ns	ns
Fads2	fatty acid desaturase 2	1368453_at	ns	ns	3.2	ns	2.9	ns	ns
bi	Fas apoptotic inhibitory molecule 3	1382184_at	ns	ns	ns	ns	ns	ns	-2.9
Fam103a1	family with sequence similarity 103, member A1	1376780_at	ns	ns	-1.6	ns	ns	ns	ns
Fam110c	family with sequence similarity 110, member C	1385251_at	ns	-1.6	ns	ns	ns	ns	ns
Fam115a	family with sequence similarity 115, member A	1377580_at	ns	ns	-6.0	ns	ns	ns	ns
Fam116b	family with sequence similarity 116, member B	1375069_at	-1.7	ns	ns	ns	ns	-1.9	ns
Fam132a	family with sequence similarity 132, member A	1393975_a_at	ns	ns	ns	ns	4.2	ns	ns
Fam132a	family with sequence similarity 132, member A	1385792_at	ns	ns	-5.5	ns	ns	ns	ns
Fam155a	Family with sequence similarity 155, member A	1383800_at	ns	ns	ns	7.1	ns	ns	ns
Fam164a	family with sequence similarity 164, member A	1379625_at	ns	-1.8	ns	-1.6	ns	-1.5	ns
Fam169a	family with sequence similarity 169, member A	1395689_at	ns	ns	ns	7.6	ns	ns	ns

Symbol	Entrez gene name	Probeset ID	Fold change						
			UT		SC		siGCGR		
			LD	HD	LD	HD	LD	HD	C
Fam189b	family with sequence similarity 189, member B	1398446_at	ns	-1.7	ns	ns	-1.7	-2.2	ns
Fam198b	family with sequence similarity 198, member B	1384617_at	ns	ns	ns	ns	ns	ns	-7.3
Fam20b	family with sequence similarity 20, member B	1380993_at	ns	-4.3	ns	ns	ns	ns	ns
Fam26f	family with sequence similarity 26, member F	1391214_at	ns	ns	-2.2	ns	ns	ns	ns
Fam63b	family with sequence similarity 63, member B	1393505_x_at	ns	ns	1.7	ns	ns	ns	ns
Fam82a2	family with sequence similarity 82, member A2	1372302_at	ns	1.7	ns	ns	ns	ns	ns
Fam83f	family with sequence similarity 83, member F	1391012_at	ns	-6.9	ns	ns	ns	ns	ns
Fam89a	family with sequence similarity 89, member A	1377307_at	ns	-2.7	ns	ns	ns	ns	ns
Fam92a1	family with sequence similarity 92, member A1	1386378_at	ns	ns	ns	ns	ns	ns	7.8
Fam96a	family with sequence similarity 96, member A	1374487_at	ns	ns	ns	ns	ns	ns	1.6
Fasn	fatty acid synthase	1367707_at	3.6	ns	3.6	3.2	ns	ns	ns
Fasn	fatty acid synthase	1367708_a_at	2.9	ns	2.9	2.7	3.0	2.4	ns
Fbrsl1	fibrosin-like 1	1376809_at	ns	-1.8	ns	-1.6	ns	ns	ns
Fbrsl1	fibrosin-like 1	1379816_at	ns	-1.6	ns	ns	ns	ns	ns
Fbxl4	F-box and leucine-rich repeat protein 4	1392875_at	ns	ns	ns	-1.7	ns	ns	ns
Fbxl7	F-box and leucine-rich repeat protein 7	1381675_at	-4.6	ns	ns	ns	ns	ns	ns
Fbxl8	F-box and leucine-rich repeat protein 8	1386543_at	ns	ns	ns	ns	-3.4	ns	ns
Fbxo23	F-box only protein 23	1386614_at	ns	ns	ns	-1.6	ns	ns	ns
Fbxo31	F-box protein 31	1372600_at	1.7	1.6	1.6	ns	1.6	1.6	ns
Fbxo46	F-box protein 46	1378266_at	ns	ns	ns	ns	ns	-9.8	ns
Fer1l5	fer-1-like 5 (C. elegans)	1396729_at	ns	ns	5.0	8.9	ns	ns	ns
Fermt2	fermitin family homolog 2 (Drosophila)	1384182_at	ns	ns	1.6	ns	ns	ns	ns
Fgd6	FYVE, RhoGEF and PH domain containing 6	1381882_at	ns	ns	ns	ns	ns	-2.8	ns
Fgf1	fibroblast growth factor 1	1387301_at	ns	ns	ns	ns	ns	ns	1.7
Fgf18	fibroblast growth factor 18	1370106_at	ns	10.6	ns	ns	ns	ns	ns
Fgf20	fibroblast growth factor 20	1369606_at	-4.7	-4.2	ns	ns	ns	ns	ns
Fgfr2	fibroblast growth factor receptor 2	1373829_at	ns	ns	ns	ns	1.6	1.6	ns
Fgfr4	fibroblast growth factor receptor 4	1389801_at	ns	-1.7	ns	ns	ns	ns	ns
Fgr	Gardner-Rasheed feline sarcoma viral (v-fgr) oncogene homolog	1368693_at	-2.0	-2.0	-2.0	ns	ns	ns	ns
Fhl3	four and a half LIM domains 3	1372569_at	ns	-2.0	ns	ns	-2.1	-1.9	ns
Fhod1	formin homology 2 domain containing 1	1378477_a_at	ns	-3.0	ns	ns	ns	ns	ns
Fibin	fin bud initiation factor homolog (zebrafish)	1393696_at	ns	2.3	ns	2.1	ns	ns	ns
Fibin	fin bud initiation factor homolog (zebrafish)	1373727_at	ns	ns	ns	3.8	ns	ns	ns
Fitm2	fat storage-inducing transmembrane protein 2	1374278_at	ns	ns	ns	ns	1.5	ns	ns
Fkbp5	FK506 binding protein 5	1388901_at	-1.8	-1.8	-1.9	-1.8	-1.8	-1.9	ns
Fit3	fms-related tyrosine kinase 3	1377882_at	ns	ns	ns	-3.5	ns	ns	ns
Flvcr2	feline leukemia virus subgroup C cellular receptor family, member 2	1376036_at	ns	1.9	ns	2.0	ns	ns	ns
Fmo1	flavin containing monooxygenase 1	1387053_at	ns	ns	-2.0	-2.3	ns	ns	ns
Fnbp4	formin binding protein 4	1376470_at	ns	ns	ns	-1.7	ns	ns	ns
Foxa3	forkhead box A3	1387506_at	ns	ns	ns	ns	ns	-1.8	ns
Fxyd6	FXYD domain-containing ion transport regulator 6	1370248_at	ns	ns	ns	ns	-7.4	ns	ns
Fzd1	frizzled homolog 1 (Drosophila)	1370256_at	ns	ns	ns	-2.3	ns	ns	ns
Fzd8	frizzled homolog 8 (Drosophila)	1383721_at	ns	-1.6	ns	ns	ns	ns	ns
G3bp1	GTPase activating protein (SH3 domain) binding protein 1	1372635_at	ns	ns	ns	ns	ns	-1.8	ns
G6pc	glucose-6-phosphatase, catalytic subunit	1386944_a_at	ns	ns	ns	ns	2.7	ns	ns
G6pc	glucose-6-phosphatase, catalytic subunit	1370725_a_at	3.2	ns	ns	ns	3.6	ns	ns
Gabarap	GABA(A) receptor-associated protein	1378279_at	-1.7	ns	ns	ns	ns	-1.9	ns
Gabarapl2	GABA(A) receptor-associated protein like 2	1380170_at	ns	ns	ns	ns	ns	ns	-1.5
Gabre	gamma-aminobutyric acid (GABA) A receptor, epsilon	1388049_a_at	7.6	ns	ns	ns	ns	ns	ns

Symbol	Entrez gene name	Probeset ID	Fold change						
			UT		SC		siGCCR		
			LD	HD	LD	HD	LD	HD	C
Gadd45a	growth arrest and DNA-damage-inducible, alpha	1368947_at	ns	ns	ns	1.5	ns	1.5	ns
Gadd45b	growth arrest and DNA-damage-inducible, beta	1372016_at	2.2	2.3	2.2	2.2	2.0	2.0	ns
Galnt13	UDP-N-acetyl-alpha-D-galactosamine:polypeptide N-acetylgalactosaminyltransferase 13 (Ga	1383021_at	ns	ns	ns	ns	7.1	ns	ns
Galnt2	UDP-N-acetyl-alpha-D-galactosamine:polypeptide N-acetylgalactosaminyltransferase 2 (Gal	1390775_at	ns	ns	ns	ns	ns	8.7	ns
Gata6	GATA binding protein 6	1368827_at	ns	ns	ns	-1.6	ns	ns	ns
Gba2	glucosidase beta 2	1399040_at	ns	ns	-3.3	ns	ns	ns	ns
Gba3	glucosidase, beta, acid 3 (cytosolic)	1398628_at	ns	ns	ns	-8.3	ns	ns	ns
Gbp2	guanylate binding protein 2	1368332_at	ns	ns	ns	ns	ns	ns	4.4
Gbp4	guanylate binding protein 4	1385051_at	ns	ns	ns	ns	ns	ns	12.3
Gca	grancalcin	1379031_at	-1.6	-1.6	ns	ns	-1.7	-1.9	ns
Gcgr	glucagon receptor	1370522_at	ns	ns	ns	ns	ns	ns	-4.9
Gch1	GTP cyclohydrolase 1	1387221_at	1.6	1.8	1.7	1.9	1.6	1.7	ns
Gch1	GTP cyclohydrolase 1	1368503_at	ns	ns	ns	1.9	2.2	2.2	ns
Gckr	glucokinase (hexokinase 4) regulator	1387203_at	1.6	ns	1.7	ns	1.7	ns	ns
Gcnt3	glucosaminyl (N-acetyl) transferase 3, mucin type	1392209_at	ns	ns	ns	ns	ns	-7.4	ns
Gdap111	Ganglioside-induced differentiation-associated protein 1-like 1	1382498_x_at	ns	ns	ns	-4.3	ns	ns	ns
Gdf15	growth differentiation factor 15	1370153_at	2.0	2.4	2.2	2.7	2.1	2.8	ns
Gdpd3	glycerophosphodiester phosphodiesterase domain containing 3	1379992_at	ns	-6.4	ns	ns	ns	ns	ns
Gfap	glial fibrillary acidic protein	1368353_at	ns	ns	ns	ns	-8.0	ns	ns
Ggct	gamma-glutamyl cyclotransferase	1392541_at	1.6	ns	1.8	1.9	1.8	1.7	ns
Ggt1	gamma-glutamyltransferase 1	1368374_a_at	2.3	2.7	2.7	2.9	2.5	2.3	ns
Ggta1	Glycoprotein, alpha-galactosyltransferase 1	1391112_at	ns	ns	ns	ns	ns	ns	-5.7
Ghdc	GH3 domain containing	1390462_at	ns	ns	ns	ns	-1.5	-1.5	ns
Giyd2	GIY-YIG domain containing 2	1378215_at	ns	ns	ns	ns	ns	-1.5	ns
Gkn2	gastrokine 2	1393737_at	ns	ns	-10.8	ns	ns	ns	ns
Glb1l	galactosidase, beta 1-like	1393637_at	ns	-1.7	ns	ns	ns	ns	ns
Glcc1	glucocorticoid induced transcript 1	1389679_at	ns	ns	ns	ns	1.7	ns	ns
Glcc1	glucocorticoid induced transcript 1 /// hypothetical LOC296884	1375724_at	ns	ns	ns	ns	1.7	ns	ns
Gldc	glycine dehydrogenase (decarboxylating)	1376427_a_at	ns	-1.6	-1.6	ns	ns	ns	ns
Glrx1	glutaredoxin 1	1367705_at	ns	-2.0	-1.7	-2.3	ns	-1.6	ns
Glrx1	glutaredoxin 1	1386908_at	ns	-2.0	-1.7	-2.3	ns	-1.9	ns
Gls2	glutaminase 2 (liver, mitochondrial)	1370375_at	1.7	1.7	2.0	2.2	2.1	2.3	ns
Glt8d3	glycosyltransferase 8 domain containing 3	1373600_at	ns	ns	ns	ns	ns	ns	-1.6
Glud1	glutamate dehydrogenase 1	1370200_at	ns	-1.5	ns	ns	ns	ns	ns
Glyat	glycine-N-acyltransferase	1391652_at	ns	-1.9	ns	-2.0	ns	-1.9	ns
Glycam1	glycosylation dependent cell adhesion molecule 1	1368337_at	ns	9.9	ns	ns	ns	ns	ns
Gmfb	glia maturation factor, beta	1387663_at	ns	1.8	ns	ns	ns	ns	ns
Gmip	Gem-interacting protein	1384070_at	ns	ns	ns	ns	-2.0	ns	ns
Gmnn	geminin	1378056_at	ns	-1.7	ns	ns	ns	ns	ns
Gmnn	Geminin	1392700_at	ns	ns	ns	-4.1	ns	ns	ns
Gnai2	guanine nucleotide binding protein (G protein), alpha inhibiting 2	1367844_at	ns	ns	ns	ns	ns	-1.5	ns
Gnat3	guanine nucleotide binding protein, alpha transducing 3	1388223_at	ns	-3.2	ns	ns	ns	ns	ns
Gnb4	guanine nucleotide binding protein (G protein), beta polypeptide 4	1371071_at	ns	ns	ns	-2.9	ns	ns	ns
Gng11	guanine nucleotide binding protein (G protein), gamma 11	1367902_at	ns	ns	ns	2.4	ns	ns	ns
Gnrh1	gonadotropin-releasing hormone 1 (luteinizing-releasing hormone)	1370417_at	-9.7	ns	ns	ns	ns	ns	ns
Gpc3	glypican 3	1368395_at	-17.1	-11.3	ns	ns	ns	ns	ns
Gpd1	glycerol-3-phosphate dehydrogenase 1 (soluble)	1369560_at	2.3	2.2	2.7	2.3	2.9	2.5	ns
Gpd1	glycerol-3-phosphate dehydrogenase 1 (soluble)	1371363_at	2.0	2.0	1.7	1.8	1.9	1.8	ns

Symbol	Entrez gene name	Probeset ID	Fold change						
			UT		SC		siGCGR		
			LD	HD	LD	HD	LD	HD	C
Gpd2	glycerol-3-phosphate dehydrogenase 2, mitochondrial	1387670_at	1.8	1.9	2.0	2.1	2.1	2.3	ns
Gpd2	Glycerol-3-phosphate dehydrogenase 2, mitochondrial	1369666_at	1.7	1.9	ns	ns	ns	1.9	ns
Gpr116	G protein-coupled receptor 116	1376767_at	-6.4	ns	ns	ns	ns	ns	ns
Gpr135	G protein-coupled receptor 135	1381738_at	ns	ns	ns	-5.2	ns	ns	ns
Gpr137	G protein-coupled receptor 137	1376064_at	ns	ns	ns	ns	ns	ns	-3.3
Gpr146	G protein-coupled receptor 146	1382266_at	ns	-1.9	ns	ns	ns	ns	ns
Gpr146	G protein-coupled receptor 146	1373158_at	ns	ns	-1.7	-1.6	-1.5	-1.7	ns
Gpr177	G protein-coupled receptor 177	1383129_at	ns	ns	-2.5	ns	ns	ns	ns
Gpr44	G protein-coupled receptor 44	1396674_at	ns	3.8	ns	ns	ns	ns	ns
Gpsm1	G-protein signaling modulator 1 (AGS3-like, <i>C. elegans</i> )	1372383_at	ns	-1.7	ns	ns	-1.7	-1.5	ns
Gramd3	GRAM domain containing 3	1398664_at	1.6	ns	ns	ns	ns	ns	ns
Gria2	glutamate receptor, ionotropic, AMPA 2	1387171_at	ns	9.6	ns	ns	ns	ns	ns
Grk5	G protein-coupled receptor kinase 5	1368408_at	2.9	2.2	3.2	2.8	2.9	2.7	ns
Gsr	glutathione reductase	1369061_at	2.8	2.6	2.5	2.4	2.9	2.9	ns
Gss	glutathione synthetase	1370365_at	ns	1.5	ns	1.5	ns	ns	ns
Gsta2	glutathione S-transferase A2 /// LOC494499 protein	1368180_s_at	6.2	6.8	4.7	4.7	5.8	5.3	ns
Gsta4	glutathione S-transferase alpha 4	1372297_at	1.9	1.6	1.9	1.7	2.1	2.0	ns
Gstm2	glutathione S-transferase mu 2	1370952_at	1.9	ns	1.7	1.7	1.7	1.7	ns
Gstm3	glutathione S-transferase mu 3	1369921_at	3.4	ns	3.5	3.1	3.6	2.7	ns
Gtf2h5	general transcription factor IIH, polypeptide 5	1384085_at	ns	ns	ns	ns	ns	2.9	ns
Gtbp2	GTP binding protein 2	1374489_at	ns	1.9	ns	1.8	ns	ns	ns
Gtse1	G-2 and S-phase expressed 1	1379386_at	ns	ns	-2.0	ns	ns	ns	ns
Guca2b	guanylate cyclase activator 2B	1387253_at	ns	ns	-4.8	-3.2	3.4	4.2	-3.5
Gucy2e	guanylate cyclase 2E	1369360_at	ns	ns	ns	ns	6.6	4.2	-9.4
Gulp1	GULP, engulfment adaptor PTB domain containing 1	1376285_at	ns	-6.7	ns	ns	ns	ns	ns
Gylt1b	glycosyltransferase-like 1B	1395652_at	ns	ns	ns	ns	ns	-1.5	ns
H2afx	H2A histone family, member X	1378847_x_at	ns	ns	ns	ns	-2.2	ns	ns
Hace1	HECT domain and ankyrin repeat containing, E3 ubiquitin protein ligase 1	1382779_at	ns	-1.5	ns	ns	ns	ns	ns
Hacl1	2-hydroxyacyl-CoA lyase 1	1371012_at	2.6	ns	2.2	ns	2.6	ns	ns
Hadhb	hydroxyacyl-Coenzyme A dehydrogenase/3-ketoacyl-Coenzyme A thiolase/enoyl-Coenzyme A hydratase	1367694_at	ns	1.6	ns	ns	ns	ns	ns
Hand1	heart and neural crest derivatives expressed 1	1370128_at	ns	ns	-3.6	ns	ns	ns	ns
Hao1	hydroxyacid oxidase (glycolate oxidase) 1	1394112_at	ns	-1.7	ns	-1.7	ns	ns	ns
Hao2	hydroxyacid oxidase 2 (long chain)	1387139_at	ns	-1.7	ns	ns	ns	ns	ns
Hapln3	hyaluronan and proteoglycan link protein 3	1394561_at	ns	ns	ns	-4.2	ns	ns	ns
Haus4	HAUS augmin-like complex, subunit 4	1374802_at	ns	ns	ns	-1.5	ns	ns	ns
Haus8	HAUS augmin-like complex, subunit 8	1388923_at	ns	1.7	ns	ns	ns	ns	ns
Haus8	HAUS augmin-like complex, subunit 8	1381289_at	ns	ns	ns	1.8	ns	1.6	ns
Hbs1l	Hbs1-like ( <i>S. cerevisiae</i> )	1398535_at	ns	ns	ns	1.5	ns	1.6	ns
Hdac11	histone deacetylase 11	1374954_at	-2.1	-2.4	ns	ns	-2.2	-2.0	ns
Hdac5	Histone deacetylase 5	1397587_at	ns	3.3	ns	ns	ns	ns	ns
Heatr5b	HEAT repeat containing 5B	1383710_at	ns	ns	-1.5	ns	ns	ns	ns
Herc6	hect domain and RLD 6	1382902_at	ns	ns	ns	ns	ns	ns	4.4
Hgd	homogentisate 1, 2-dioxygenase	1398514_at	2.3	ns	ns	ns	2.4	ns	ns
Hint1	histidine triad nucleotide binding protein 1	1369620_at	ns	ns	ns	ns	ns	ns	-6.9
Hirip3	HIRA interacting protein 3	1371813_at	ns	ns	ns	1.5	ns	ns	ns
Hisppd2a	histidine acid phosphatase domain containing 2A	1390876_at	ns	-1.8	ns	-1.6	ns	-1.7	ns
Hist1h2bc	histone cluster 1, H2bc / histone cluster 1, H2bc-like 1 / histone cluster 1, H2bm	1391301_at	ns	ns	ns	ns	-17.2	ns	ns
Hist1h2bh	histone cluster 1, H2bh	1390021_at	ns	ns	ns	ns	ns	ns	1.6
Hist1h3f	histone cluster 1, H3f	1388276_at	-8.7	ns	ns	ns	ns	ns	ns
Hivep3	human immunodeficiency virus type I enhancer binding protein 3	1393703_at	ns	ns	ns	ns	ns	-2.7	ns

## 10 APPENDIX

Symbol	Entrez gene name	Probeset ID	Fold change						
			UT		SC		siGCGR		
			LD	HD	LD	HD	LD	HD	C
Hmgb3	high mobility group box 3	1371887_at	-1.5	-1.6	-1.6	-1.6	ns	ns	ns
Hmgcs1	3-hydroxy-3-methylglutaryl-Coenzyme A synthase 1 (soluble)	1367932_at	ns	-2.6	ns	ns	ns	-2.1	ns
Hmgcs2	3-hydroxy-3-methylglutaryl-Coenzyme A synthase 2 (mitochondrial)	1370310_at	ns	-2.7	-2.0	-2.8	ns	-2.3	ns
Homer1	homer homolog 1 (Drosophila)	1370997_at	ns	-6.0	ns	ns	ns	ns	ns
Hoxa10	homeo box A10	1389670_at	ns	ns	ns	ns	ns	ns	4.2
Hoxb4	homeo box B4	1386125_at	ns	ns	ns	ns	ns	ns	-4.1
Hoxb7	homeo box B7	1388287_at	-6.6	ns	ns	ns	ns	ns	ns
Hr	hairless	1369336_at	ns	ns	ns	ns	ns	ns	-2.3
Hrasls5	HRAS-like suppressor family, member 5	1375834_at	1.8	1.7	ns	ns	ns	ns	ns
Hrk	harakiri, BCL2 interacting protein (contains only BH3 domain)	1368535_at	ns	1.6	ns	1.8	ns	ns	ns
Hsd17b13	hydroxysteroid (17-beta) dehydrogenase 13	1377758_at	ns	-2.2	ns	-1.9	ns	-2.3	ns
Hsd12	hydroxysteroid dehydrogenase like 2	1384244_at	ns	1.5	ns	ns	ns	ns	ns
Hsd12	hydroxysteroid dehydrogenase like 2	1397468_at	ns	ns	ns	ns	2.2	2.0	ns
Hspa1a	heat shock 70kD protein 1A	1370912_at	ns	ns	ns	2.7	ns	2.5	ns
Hspa1a / Hspa1b	heat shock 70kD protein 1A /// heat shock 70kD protein 1B (mapped)	1368247_at	ns	ns	ns	2.2	ns	2.6	ns
Hspa4l	heat shock protein 4 like	1378002_at	ns	ns	ns	1.9	ns	ns	ns
Hspa9	heat shock protein 9	1370690_at	ns	1.6	ns	1.6	ns	1.5	ns
Hspb11	Heat shock protein family B (small), member 11	1397940_at	ns	ns	ns	ns	ns	6.3	ns
Hspb8	heat shock protein B8	1387282_at	ns	ns	ns	ns	ns	1.7	ns
Htatsf1	HIV-1 Tat specific factor 1	1384652_at	ns	ns	ns	ns	ns	1.9	-2.1
Htr1f	5-hydroxytryptamine (serotonin) receptor 1F	1370093_at	ns	5.0	-5.4	ns	ns	ns	ns
Htr3b	5-hydroxytryptamine (serotonin) receptor 3b	1371077_at	-4.0	ns	ns	-3.8	ns	ns	ns
Htr7	5-hydroxytryptamine (serotonin) receptor 7	1371290_a_at	ns	9.9	ns	ns	ns	ns	ns
Iars	isoleucyl-tRNA synthetase	1386583_at	ns	ns	ns	ns	1.5	ns	-1.5
Id4	Inhibitor of DNA binding 4	1385923_at	ns	-2.0	-1.6	-1.8	ns	ns	ns
Id4	inhibitor of DNA binding 4	1394022_at	-1.6	-2.1	ns	-1.9	-2.0	-2.2	ns
Id4	Inhibitor of DNA binding 4	1375183_at	ns	-1.7	ns	ns	ns	ns	ns
Id4	inhibitor of DNA binding 4	1375120_at	ns	-1.9	ns	ns	ns	-1.8	ns
Idh2	isocitrate dehydrogenase 2 (NADP+), mitochondrial	1388403_at	ns	ns	ns	-1.7	ns	-1.6	ns
Idi1	isopentenyl-diphosphate delta isomerase 1	1368878_at	ns	-2.4	ns	-2.0	ns	-2.4	ns
Iifo1	intermediate filament family orphan 1	1393215_at	ns	ns	-2.2	ns	ns	ns	ns
Iifi27	interferon, alpha-inducible protein 27	1387770_at	ns	ns	ns	ns	ns	ns	1.6
Iifi35	interferon-induced protein 35	1374551_at	ns	ns	ns	ns	ns	ns	1.6
Iifi44	interferon-induced protein 44	1381014_at	ns	ns	ns	ns	ns	ns	2.5
Iifi44l	Interferon-induced protein 44-like	1379748_at	ns	ns	ns	ns	ns	ns	2.3
Iifit2	interferon-induced protein with tetratricopeptide repeats 2	1384180_at	ns	ns	ns	ns	ns	ns	1.9
Iifit3	interferon-induced protein with tetratricopeptide repeats 3	1376908_at	ns	ns	ns	ns	ns	ns	24.5
Iifitm3	interferon induced transmembrane protein 3	1387995_a_at	ns	ns	ns	ns	ns	ns	4.4
Iifng	interferon gamma	1370790_at	-9.5	ns	ns	ns	ns	ns	ns
Iift57	intraflagellar transport 57 homolog (Chlamydomonas)	1380548_at	ns	ns	ns	ns	-1.6	-1.5	ns
Igf2bp2	Insulin-like growth factor 2 mRNA binding protein 2	1382609_at	ns	ns	ns	-1.9	ns	ns	-1.9
Igh-6 /// LOC314509	immunoglobulin heavy chain 6 /// similar to single chain Fv antibody fragment scFv 7-10	1388166_at	6.7	ns	7.8	5.5	9.5	6.8	ns
Igh-6 /// LOC314509	immunoglobulin heavy chain 6 /// similar to single chain Fv antibody fragment scFv 7-10	1380366_at	10.0	ns	ns	ns	7.8	ns	ns
Igtp	interferon gamma induced GTPase	1397304_at	ns	ns	ns	ns	ns	ns	3.2
Ikbkb	Inhibitor of kappa light polypeptide gene enhancer in B-cells, kinase beta	1397547_at	ns	ns	ns	-2.5	ns	ns	ns
Il10ra	interleukin 10 receptor, alpha	1387728_at	-7.1	ns	ns	ns	ns	ns	ns
Il18	interleukin 18	1369665_a_at	ns	-1.8	ns	-1.9	ns	ns	ns
Il18bp	interleukin 18 binding protein	1369031_at	ns	ns	ns	ns	ns	ns	3.3

Symbol	Entrez gene name	Probeset ID	Fold change						
			UT		SC		siGCGR		
			LD	HD	LD	HD	LD	HD	C
Il1a	interleukin 1 alpha	1371170_a_at	ns	ns	ns	-7.6	ns	ns	ns
Il1f8	interleukin 1 family, member 8	1385842_at	ns	-2.1	ns	-2.1	-1.7	-2.5	ns
Il6ra	interleukin 6 receptor, alpha	1386987_at	-1.7	-1.9	ns	-1.9	-1.7	-1.9	ns
Il6st	interleukin 6 signal transducer	1383489_at	ns	-1.6	ns	ns	-1.5	-1.6	ns
Il6st	interleukin 6 signal transducer	1373140_at	ns	ns	ns	ns	-1.5	-1.6	ns
Immt	inner membrane protein, mitochondrial	1380154_at	-2.1	ns	ns	ns	ns	ns	ns
Impact	imprinted and ancient	1375754_at	ns	3.3	ns	ns	ns	ns	ns
Inpp1	inositol polyphosphate-1-phosphatase	1399125_at	-1.5	-1.5	ns	ns	ns	ns	ns
Inpp1	inositol polyphosphate-1-phosphatase	1394340_at	-1.5	ns	-1.5	-1.5	ns	ns	ns
Ins1	insulin 1	1387815_at	ns	ns	-4.3	ns	ns	ns	ns
Insig1	insulin induced gene 1	1367894_at	1.8	1.6	1.8	1.8	1.9	1.6	ns
Insig2	insulin induced gene 2	1393690_at	2.3	ns	2.4	1.9	2.8	2.4	ns
Insig2	insulin induced gene 2	1389377_at	2.5	1.6	2.9	2.3	2.8	2.4	ns
Insrr	insulin receptor-related receptor	1369514_at	ns	3.2	ns	ns	2.9	ns	ns
Irak1	interleukin-1 receptor-associated kinase 1	1394991_at	ns	ns	ns	ns	ns	ns	-1.6
Irf6	interferon regulatory factor 6	1377379_at	ns	ns	ns	ns	ns	-1.5	ns
Irf6	interferon regulatory factor 6	1386568_at	-1.6	-1.7	-1.6	-1.6	-1.8	-1.7	ns
Irf7	interferon regulatory factor 7	1383564_at	ns	ns	ns	ns	ns	ns	15.6
Irf9	interferon regulatory factor 9	1383448_at	ns	ns	ns	ns	ns	ns	3.1
Irgm	immunity-related GTPase family, M	1391489_at	ns	ns	ns	ns	ns	ns	2.4
Irx3	Iroquois homeobox 3	1386520_at	ns	ns	ns	-12.4	ns	ns	-14.5
Irx4	iroquois homeobox 4	1390081_at	8.5	ns	ns	ns	ns	ns	ns
Isg15	ISG15 ubiquitin-like modifier	1382314_at	ns	ns	ns	ns	ns	ns	23.2
Isg20	interferon stimulated exonuclease gene 20	1390507_at	ns	ns	ns	ns	ns	ns	2.6
Itfg2	integrin alpha FG-GAP repeat containing 2	1397078_at	-1.5	ns	ns	ns	ns	ns	ns
Itgad	integrin, alpha D	1369038_at	-5.7	ns	ns	ns	ns	ns	ns
Itgb5	integrin, beta 5	1398358_a_at	ns	ns	1.5	ns	ns	ns	ns
Ith4	inter alpha-trypsin inhibitor, heavy chain 4	1368707_at	ns	ns	1.5	1.9	ns	ns	ns
Itpka	inositol 1,4,5-trisphosphate 3-kinase A	1368462_at	ns	ns	-2.2	-1.8	ns	ns	ns
Jsrp1	junctional sarcoplasmic reticulum protein 1	1375055_at	ns	ns	-8.6	ns	ns	ns	ns
Katnb1	katanin p80 (WD repeat containing) subunit B 1	1375188_at	ns	ns	ns	-1.6	ns	ns	ns
Kcna2	potassium voltage-gated channel, shaker-related subfamily, member 2	1370612_at	ns	2.9	ns	ns	ns	ns	ns
Kcnab1	potassium voltage-gated channel, shaker-related subfamily, beta member 1	1378738_at	ns	ns	ns	ns	ns	-13.4	ns
Kcng3	potassium voltage-gated channel, subfamily G, member 3	1387845_at	-5.9	-6.1	ns	ns	ns	ns	ns
Kcnk1	potassium channel, subfamily K, member 1	1369500_at	ns	ns	ns	-5.1	ns	ns	ns
Kcnk5	potassium channel, subfamily K, member 5	1371898_at	2.0	2.0	1.8	2.1	1.7	1.7	ns
Kcnma1	potassium large conductance calcium-activated channel, subfamily M, alpha member 1	1369334_at	-8.3	ns	ns	ns	ns	ns	ns
Kctd14	potassium channel tetramerisation domain containing 14	1395966_at	ns	ns	ns	ns	2.1	1.9	ns
Kdelr3	KDEL (Lys-Asp-Glu-Leu) endoplasmic reticulum protein retention receptor 3	1372870_at	ns	ns	ns	ns	ns	ns	-1.6
Kif11	kinesin family member 11	1390891_at	ns	1.5	ns	ns	1.7	1.8	ns
Kif11	kinesin family member 11	1385619_at	2.0	1.6	1.8	ns	1.9	2.1	ns
Kif12	kinesin family member 12	1391611_at	ns	-2.6	ns	-2.7	ns	ns	ns
Kif16b	kinesin family member 16B	1391526_at	ns	-1.6	ns	ns	ns	ns	ns
Kif1a	kinesin family member 1A	1384133_at	ns	ns	ns	ns	ns	3.3	-3.4
Klf1	Kruppel-like factor 1 (erythroid)	1382033_at	ns	ns	ns	-5.8	ns	ns	ns
Klf11	Kruppel-like factor 11	1379914_at	ns	ns	ns	-1.8	ns	ns	ns
Klf13	Kruppel-like factor 13	1383013_at	-1.5	-1.6	ns	ns	ns	ns	ns
Klf15	Kruppel-like factor 15	1368249_at	ns	ns	ns	ns	ns	ns	1.5
Klf2	Kruppel-like factor 2 (lung)	1376569_at	ns	ns	9.9	ns	ns	ns	ns
Klf3	Kruppel-like factor 3 (basic)	1393150_at	-1.6	ns	ns	ns	ns	ns	ns
Klf3	Kruppel-like factor 3 (basic)	1378332_at	ns	-1.6	ns	ns	ns	ns	ns

Symbol	Entrez gene name	Probeset ID	Fold change						
			UT		SC		siGCGR		
			LD	HD	LD	HD	LD	HD	C
Klhdc3	kelch domain containing 3	1392378_at	ns	ns	ns	-3.6	ns	ns	ns
Klkb1	kallikrein B, plasma 1	1387323_at	3.2	2.4	3.9	4.0	3.1	2.8	ns
Klra5	killer cell lectin-like receptor, subfamily A, member 5	1370740_at	ns	8.1	ns	ns	ns	ns	ns
Klrg1	killer cell lectin-like receptor subfamily G, member 1	1387297_at	ns	ns	ns	-6.3	ns	ns	ns
Kmo	kynurenine 3-monooxygenase (kynurenine 3-hydroxylase)	1368915_at	ns	ns	ns	-1.7	ns	ns	ns
Kng1, Kng11, Kng2	kininogen 1 /// kininogen 1-like 1 /// kininogen 2	1387050_s_at	ns	ns	ns	1.5	ns	ns	ns
Krba1	KRAB-A domain containing 1	1375914_at	ns	ns	ns	ns	ns	-1.5	ns
Krt17	keratin 17	1397645_at	ns	ns	-1.6	ns	ns	ns	ns
Kynu	kynureninase (L-kynurenine hydrolase)	1398282_at	ns	-1.7	ns	-1.8	ns	-1.5	ns
Lactb2	Lactamase, beta 2	1390851_at	2.1	1.6	2.2	1.7	1.9	1.6	ns
Lactb2	lactamase, beta 2	1389551_at	1.7	1.5	1.7	1.7	1.6	1.6	ns
Lalba	lactalbumin, alpha	1387838_at	ns	ns	ns	ns	9.4	ns	ns
Lamb2	laminin, beta 2	1367880_at	ns	ns	-5.8	ns	ns	-17.4	ns
Lao1	L-amino acid oxidase 1	1385064_at	ns	ns	ns	ns	-7.3	ns	ns
Lcat	lecithin cholesterol acyltransferase	1367887_at	ns	ns	ns	-1.6	ns	ns	ns
Ldb2	LIM domain binding 2	1383824_at	ns	ns	ns	8.3	ns	ns	ns
Ldhb	lactate dehydrogenase B	1370218_at	ns	-2.2	-2.6	-3.2	-2.3	-2.3	ns
Leng8	leukocyte receptor cluster (LRC) member 8	1375327_at	ns	-2.4	ns	ns	ns	ns	ns
Leng8	leukocyte receptor cluster (LRC) member 8	1392932_at	ns	ns	ns	ns	ns	-1.6	ns
Lep	leptin	1387748_at	4.5	ns	ns	ns	ns	ns	ns
Lepr	leptin receptor	1371223_a_at	ns	ns	ns	1.7	ns	ns	ns
Lepr	leptin receptor	1388260_a_at	ns	ns	ns	ns	ns	ns	-4.6
Letm1	leucine zipper-EF-hand containing transmembrane protein 1	1396013_at	ns	ns	1.7	1.7	1.6	1.7	ns
Lgals12	lectin, galactoside-binding, soluble, 12	1394058_at	ns	ns	ns	ns	-7.2	ns	ns
Lgals3bp	lectin, galactoside-binding, soluble, 3 binding protein	1387946_at	ns	ns	ns	ns	ns	ns	4.6
Lgals5 / Lgals9	lectin, galactose binding, soluble 5 /// lectin, galactoside-binding, soluble, 9	1369716_s_at	ns	ns	ns	ns	ns	ns	2.3
Lgals9	lectin, galactoside-binding, soluble, 9	1387027_a_at	ns	ns	ns	ns	ns	ns	2.3
Lgmn	legumain	1380609_at	ns	ns	ns	ns	ns	6.1	-7.6
Lgr4	leucine-rich repeat-containing G protein-coupled receptor 4	1388104_at	ns	-1.8	ns	ns	ns	ns	ns
Lhfp14	lipoma HMGIC fusion partner-like 4	1395649_at	6.3	ns	-4.4	ns	ns	ns	ns
Lim2	lens intrinsic membrane protein 2	1368493_at	ns	9.6	ns	ns	ns	ns	ns
Lime1	Lck interacting transmembrane adaptor 1	1391044_s_at	ns	ns	ns	-2.2	ns	ns	ns
Lime1, Zgpat	Lck interacting transmembrane adaptor 1 /// zinc finger, CCCH-type with G patch domain	1378319_at	ns	ns	ns	-1.5	ns	ns	ns
Limk2	LIM domain kinase 2	1387090_a_at	1.6	ns	1.6	1.7	1.8	1.8	ns
Lims2	LIM and senescent cell antigen like domains 2	1388422_at	ns	ns	ns	ns	1.6	ns	ns
Lin7a	lin-7 homolog a (C. elegans)	1370108_a_at	ns	ns	ns	ns	ns	-5.0	ns
Lix1	Lix1 homolog (chicken)	1379505_at	ns	ns	ns	-5.5	ns	ns	ns
Lmna	lamin A	1368054_at	ns	ns	ns	ns	-1.6	ns	ns
LOC100302372	hypothetical protein LOC100302372	1377675_at	ns	ns	ns	ns	-1.5	ns	ns
LOC100359435	cleavage stimulation factor, 3 pre-RNA, subunit 3 (predicted)-like	1393166_at	-2.9	ns	ns	ns	ns	ns	ns
LOC100359529	rCG61688-like	1385480_at	ns	ns	1.5	1.8	ns	ns	ns
LOC100360294	spermatogenesis associated, serine-rich 2-like	1395336_at	ns	ns	ns	ns	-9.6	ns	ns
LOC100360384	hypothetical protein LOC100360384	1384123_at	ns	ns	ns	ns	7.6	ns	-7.3
LOC100360582 / LOC688261	5',3'-nucleotidase, cytosolic /// similar to 5(3)-deoxyribonucleotidase, cytosolic type	1389425_at	ns	-1.7	ns	ns	ns	ns	ns
LOC100360867	yippee-like 1	1393924_s_at	-5.1	ns	-6.8	-7.1	ns	ns	ns
LOC100360908 / Pde4c	Pde4c protein-like /// phosphodiesterase 4C, cAMP-specific (phosphodiesterase E1 dunce	1384400_at	ns	-2.0	ns	ns	ns	ns	ns



Symbol	Entrez gene name	Probeset ID	Fold change						
			UT		SC		siGCGR		
			LD	HD	LD	HD	LD	HD	C
LOC100361007	rCG32064-like	1376296_at	ns	ns	ns	ns	-1.6	ns	ns
LOC100361136	hypothetical LOC100361136	1395162_at	ns	-7.4	ns	ns	ns	ns	ns
LOC100361349 /// LOC100361455	hypothetical protein LOC100361349 /// hypothetical protein LOC100361455	1384721_at	ns	ns	ns	ns	ns	ns	-4.7
LOC100361585	rCG31991-like	1385211_at	ns	ns	ns	ns	-1.6	ns	ns
LOC100361733	rCG57079-like	1375056_at	ns	-1.5	ns	ns	ns	ns	ns
LOC100361913	rCG54286-like	1375706_at	ns	ns	ns	ns	ns	-1.5	ns
LOC100362394 / LOC100365991	rCG54026-like /// rCG54026-like	1391756_at	ns	ns	ns	-2.5	ns	ns	ns
LOC100362471	hypothetical protein LOC100362471	1380990_at	ns	-3.9	ns	ns	ns	ns	ns
LOC100362940 / LOC100364126	sorting nexin 21-like /// sorting nexin 21-like	1374791_at	ns	ns	ns	ns	ns	1.5	ns
LOC100363841	mCG54481-like	1381082_at	ns	12.1	ns	ns	ns	ns	ns
LOC100364854 / LOC290071	similar to RIKEN cDNA A430107P09 gene-like /// similar to RIKEN cDNA A430107P09 gene	1371016_at	ns	ns	ns	ns	ns	2.3	ns
LOC100365106	rCG32755-like	1376151_a_at	ns	ns	ns	ns	ns	ns	2.3
LOC100365542	rCG41957-like	1396788_at	ns	3.1	ns	ns	ns	ns	ns
LOC100365770	histone variant H2al2-like	1390988_at	ns	1.6	ns	1.6	ns	1.5	ns
LOC100365872	eukaryotic translation initiation factor 4E binding protein 3-like	1373692_at	ns	ns	ns	-3.3	ns	-3.0	ns
LOC100365876	hypothetical protein LOC100365876	1381927_at	ns	ns	ns	-2.9	ns	ns	ns
LOC100365904	hypothetical protein LOC100365904	1390076_at	-9.5	ns	ns	-10.2	ns	ns	ns
LOC100365921	rCG31672-like	1384455_at	ns	ns	ns	2.1	ns	ns	ns
LOC100366121	rCG29408-like	1371496_at	ns	ns	ns	-1.8	ns	ns	ns
LOC100366273	rCG30986-like	1380631_at	ns	ns	ns	ns	ns	-2.0	ns
LOC287167	globin, alpha	1375519_at	ns	ns	ns	-5.1	ns	ns	ns
LOC292199	hypothetical LOC292199	1394946_at	ns	ns	ns	ns	ns	ns	-6.7
LOC302999	similar to tripartite motif protein 32	1374356_at	ns	ns	ns	-7.5	ns	ns	ns
LOC305633	similar to Antr2 protein	1379988_a_at	ns	ns	ns	ns	5.4	ns	ns
LOC311026	similar to mKIAA1461 protein	1382897_at	ns	-4.2	ns	ns	-3.3	ns	ns
LOC312502	similar to RAB11 family interacting protein 5 (class I) isoform 1	1371468_at	-1.8	ns	-1.9	-1.6	-2.1	-2.0	ns
LOC361100	similar to topoisomerase (DNA) II beta	1395871_at	ns	ns	ns	ns	ns	1.7	ns
LOC361346	Similar to chromosome 18 open reading frame 54	1379740_at	ns	1.6	ns	ns	ns	ns	ns
LOC363188	similar to ubiquitin protein ligase E3 component n-recogin 2	1382970_at	ns	ns	ns	ns	ns	2.2	ns
LOC363188	similar to ubiquitin protein ligase E3 component n-recogin 2	1381349_a_at	ns	1.5	ns	ns	ns	ns	ns
LOC363331	similar to plasma membrane associated protein, S3-12	1372856_at	ns	-2.2	ns	-2.2	-2.5	-2.7	ns
LOC498145	similar to RIKEN cDNA 2810453I06	1373688_at	ns	ns	1.5	ns	ns	ns	ns
LOC498145	similar to RIKEN cDNA 2810453I06	1378399_at	1.7	ns	1.6	ns	1.5	ns	ns
LOC498154	hypothetical protein LOC498154	1383301_at	ns	ns	ns	ns	ns	ns	-1.9
LOC498222	similar to specifically androgen-regulated protein	1374434_at	ns	ns	ns	-5.3	ns	ns	ns
LOC498236	LRRGT00186	1391265_at	ns	ns	-5.8	ns	6.1	8.2	-17.0
LOC498453	Similar to transcription elongation factor A 1 isoform 2	1392658_at	ns	1.5	ns	ns	ns	ns	ns

10 APPENDIX

Symbol	Entrez gene name	Probeset ID	Fold change							
			UT		SC		siGCGR			
			LD	HD	LD	HD	LD	HD	C	
LOC498525	Bm403207	1375718_at	ns	ns	ns	ns	ns	ns	ns	-1.5
LOC498675	hypothetical LOC498675	1381729_at	ns	-6.2	ns	ns	ns	ns	ns	ns
LOC499749	similar to RIKEN cDNA C430004E15	1390602_a_at	ns	ns	ns	ns	ns	ns	-1.5	ns
LOC500013	similar to sterile alpha motif domain containing 9-like	1376920_at	ns	ns	ns	ns	ns	ns	ns	6.4
LOC500013, Samd9l	similar to sterile alpha motif domain containing 9-like /// similar to sterile alpha mo	1390312_at	ns	ns	ns	ns	ns	ns	ns	4.2
LOC502201	similar to CG8272-PA	1381362_at	ns	ns	ns	-2.1	ns	ns	ns	ns
LOC503165	similar to ADP-ribosylation factor GTPase-activating protein 3 (ARF GAP 3)	1388981_at	ns	ns	ns	1.5	ns	ns	ns	ns
LOC678910	similar to CG9967-PA, isoform A	1383713_at	ns	-2.4	ns	-2.5	ns	ns	ns	ns
LOC679692	Similar to lysophosphatidylglycerol acyltransferase 1	1389219_at	ns	ns	1.5	1.5	ns	1.5	ns	ns
LOC679692	Similar to lysophosphatidylglycerol acyltransferase 1	1389358_at	ns	ns	1.5	ns	ns	ns	ns	ns
LOC679811	similar to RIKEN cDNA D930015E06	1391414_at	ns	ns	-1.5	-1.5	ns	-1.5	ns	ns
LOC679885 / Ndr3	similar to N-myc downstream regulated gene 3 /// N-myc downstream regulated gene 3	1370903_a_at	ns	ns	ns	-2.1	ns	ns	ns	ns
LOC679958	similar to CG10806-PB, isoform B	1384679_at	ns	ns	ns	8.2	ns	ns	ns	ns
LOC680199	Hypothetical protein LOC680199	1373604_at	-4.2	ns	ns	ns	ns	ns	ns	ns
LOC680656	hypothetical protein LOC680656	1378755_at	ns	ns	-1.7	-1.9	ns	ns	ns	ns
LOC681383	similar to Protein C10orf11 homolog	1396323_at	2.4	2.3	3.5	3.0	3.4	3.2	ns	ns
LOC683722	Similar to Fgfr1 oncogene partner	1398006_at	5.2	ns	ns	ns	ns	ns	ns	ns
LOC684112	similar to KIAA0999 protein	1383379_at	1.5	1.7	1.7	1.7	1.6	1.8	ns	ns
LOC684122	similar to development and differentiation enhancing factor-like 1	1383149_at	ns	ns	2.1	2.2	2.4	2.3	ns	ns
LOC684352	similar to twinfilin-like protein	1372135_at	ns	ns	ns	ns	ns	-2.0	ns	ns
LOC684425	similar to Adenylosuccinate synthetase isozyme 1 (Adenylosuccinate synthetase, muscle i	1374677_at	ns	ns	ns	2.1	2.2	2.4	ns	ns
LOC684568	similar to solute carrier family 17 (sodium phosphate), member 4	1397268_at	1.7	2.1	1.6	1.9	1.8	2.1	ns	ns
LOC684811	similar to Rho guanine nucleotide exchange factor (GEF) 10-like	1392537_at	ns	-1.5	ns	ns	ns	ns	ns	ns
LOC684871	similar to Protein C8orf4 (Thyroid cancer protein 1) (TC-1)	1373403_at	ns	ns	-1.5	-1.6	-1.5	ns	ns	ns
LOC685045	similar to Protein C6orf115	1383912_at	ns	-2.2	ns	-2.2	ns	ns	ns	ns
LOC685079	similar to Protein SYS1 homolog	1381926_at	ns	ns	ns	ns	ns	ns	ns	-1.7
LOC686393	similar to Protease-associated domain-containing protein of 21 kDa precursor	1392975_at	ns	ns	ns	ns	ns	ns	ns	-1.6
LOC686779	similar to C1q domain containing 1 isoform 1	1373260_at	ns	-1.6	-1.5	ns	ns	ns	ns	ns
LOC687047	similar to coiled-coil domain containing 13	1384930_at	ns	ns	-3.5	-5.3	ns	ns	ns	-3.8
LOC687536	similar to Forkhead box protein F1 (Forkhead-related protein FKHL5) (Forkhead-related t	1383488_at	ns	ns	ns	ns	-6.4	ns	ns	ns
LOC687565	similar to density-regulated protein	1391644_at	ns	ns	ns	-4.4	ns	ns	ns	ns
LOC687711	similar to small nuclear ribonucleoprotein D3	1371848_at	ns	1.6	ns	ns	ns	ns	ns	ns
LOC687713	similar to Protein C22orf13 homolog	1372997_at	2.0	2.4	1.9	2.1	1.8	1.9	ns	ns
LOC687758	similar to phosphatidylinositol-4-phosphate 5-kinase-like 1	1396389_at	ns	ns	ns	ns	6.5	8.9	-9.0	ns
LOC688495	hypothetical protein LOC688495	1394524_at	ns	ns	ns	ns	ns	ns	ns	-1.7
LOC688832	Hypothetical protein LOC688832	1395044_at	ns	-2.4	ns	ns	ns	ns	ns	ns
LOC688966	Similar to K11B4.2	1380921_at	ns	ns	ns	ns	ns	7.2	-14.3	ns
LOC689574	hypothetical protein LOC689574	1388441_at	ns	ns	ns	ns	ns	ns	ns	-1.6

Symbol	Entrez gene name	Probeset ID	Fold change						
			UT		SC		siGCGR		
			LD	HD	LD	HD	LD	HD	C
LOC689755	hypothetical protein LOC689755	1390805_at	ns	ns	ns	ns	ns	ns	-2.0
LOC689791	Hypothetical protein LOC689791	1377279_at	ns	ns	ns	-8.6	ns	ns	ns
LOC690344	similar to Protein UNQ655/PRO1286 homolog precursor	1374390_at	ns	ns	ns	ns	ns	ns	-1.6
LOC690728	similar to Protein C12orf11 (Sarcoma antigen NY-SAR-95)	1385265_a_at	ns	ns	ns	-2.1	ns	ns	ns
LOC691083	hypothetical protein LOC691083	1391679_at	ns	ns	ns	-1.5	ns	ns	ns
LOC691396	Similar to Zinc finger protein 551 (Zinc finger protein KOX23)	1381224_at	ns	ns	ns	ns	ns	ns	-1.6
Lonp1	lon peptidase 1, mitochondrial	1398247_at	ns	2.1	ns	1.7	ns	ns	ns
Lor	loricrin	1372975_at	ns	-4.4	ns	ns	ns	ns	ns
Loxl3	lysyl oxidase-like 3	1385695_at	ns	ns	-4.8	ns	ns	ns	-5.9
Lpar2	lysophosphatidic acid receptor 2	1382962_at	ns	-2.1	ns	-2.3	ns	ns	ns
Lpar6	lysophosphatidic acid receptor 6	1377702_at	ns	-1.6	ns	ns	ns	-1.6	ns
Lpcat3	lysophosphatidylcholine acyltransferase 3	1393915_at	1.6	1.5	1.6	1.6	1.7	1.6	ns
Lpcat3	lysophosphatidylcholine acyltransferase 3	1376813_at	1.7	1.6	1.8	1.8	1.7	1.5	ns
Lphn2	latrophilin 2	1369643_a_at	ns	ns	ns	-1.8	ns	ns	ns
Lrba	LPS-responsive vesicle trafficking, beach and anchor containing	1384601_at	ns	ns	ns	ns	-16.3	ns	ns
Lrfn4	leucine rich repeat and fibronectin type III domain containing 4	1392313_at	ns	ns	ns	-5.5	ns	ns	ns
Lrg1	leucine-rich alpha-2-glycoprotein 1	1374626_at	ns	ns	-4.9	ns	ns	ns	ns
Lrig3	leucine-rich repeats and immunoglobulin-like domains 3	1375531_at	ns	-1.7	ns	ns	ns	ns	ns
Lrp3	low density lipoprotein receptor-related protein 3	1368239_at	ns	ns	ns	-1.5	ns	-1.5	ns
Lrp3	low density lipoprotein receptor-related protein 3	1378136_at	ns	-2.1	ns	ns	ns	-2.1	ns
Lrpprc	leucine-rich PPR-motif containing	1395338_at	ns	ns	ns	2.1	ns	ns	ns
Lrrc16a	leucine rich repeat containing 16A	1383743_at	ns	ns	ns	ns	ns	-2.1	ns
Lrrc28	leucine rich repeat containing 28	1378555_at	1.5	ns	1.6	ns	1.6	ns	ns
Lrrc39	leucine rich repeat containing 39	1373755_at	ns	ns	ns	ns	ns	3.2	ns
Lrrc61	leucine rich repeat containing 61	1398501_at	ns	ns	ns	ns	ns	2.1	-2.2
Lrtomt	leucine rich transmembrane and O-methyltransferase domain containing	1385810_at	1.7	1.8	ns	ns	ns	ns	ns
Lsm8	LSM8 homolog, U6 small nuclear RNA associated (S. cerevisiae)	1388772_at	ns	ns	ns	ns	ns	ns	-1.9
Lsr	lipolysis stimulated lipoprotein receptor	1368368_a_at	ns	ns	-1.6	ns	ns	ns	ns
Lss	Lanosterol synthase (2,3-oxidosqualene-lanosterol cyclase)	1372973_at	ns	ns	1.6	ns	ns	ns	ns
Luzp5	Leucine zipper protein 5	1378199_at	ns	6.0	ns	ns	ns	ns	ns
Ly86	lymphocyte antigen 86	1393280_at	ns	ns	ns	4.7	ns	ns	ns
Lyzl6	lysozyme-like 6	1381789_at	ns	ns	ns	ns	ns	ns	-5.7
Lztr1	leucine-zipper-like transcription regulator 1	1383959_at	ns	ns	ns	-2.3	ns	ns	ns
Lzts2	leucine zipper, putative tumor suppressor 2	1389190_at	ns	-1.9	-1.5	-1.7	ns	ns	ns
Magee1	melanoma antigen, family E, 1	1377267_at	-2.5	-3.8	-2.7	-3.4	-2.8	-3.4	ns
Mal2	mal, T-cell differentiation protein 2	1384361_at	2.4	ns	2.8	2.4	2.5	2.6	ns
Mal2	mal, T-cell differentiation protein 2	1372755_at	2.0	1.9	2.0	1.8	2.0	1.9	ns
Maml3	Mastermind like 3 (Drosophila)	1398708_at	ns	ns	ns	ns	-2.6	ns	ns
Man2a2	mannosidase 2, alpha 2	1379355_at	ns	-6.5	ns	ns	ns	ns	ns
Man2b1	Mannosidase, alpha, class 2B, member 1	1390012_at	ns	ns	ns	-2.9	ns	ns	ns
Manba	mannosidase, beta A, lysosomal	1371875_at	ns	ns	ns	1.6	ns	1.6	ns
Mansc1	MANSC domain containing 1	1393806_at	ns	ns	ns	ns	-2.1	ns	ns
Map1b	microtubule-associated protein 1B	1371003_at	ns	ns	ns	ns	-1.9	ns	ns
Map2k3	mitogen activated protein kinase kinase 3	1388858_at	ns	-1.5	ns	ns	ns	ns	ns
Map2k6	mitogen-activated protein kinase kinase 6	1387809_at	-1.8	-2.4	-1.9	-2.7	-2.0	-1.8	ns
Map3k12	mitogen activated protein kinase kinase 12	1368886_at	ns	-1.5	ns	ns	ns	ns	ns
Mapk8ip1	mitogen-activated protein kinase 8 interacting protein 1	1387971_a_at	ns	ns	ns	-2.7	ns	ns	ns
Mapre3	microtubule-associated protein, RP/EB	1374062_x_at	1.6	ns	ns	ns	ns	ns	ns

Symbol	Entrez gene name	Probeset ID	Fold change							
			UT		SC		siGCGR			
			LD	HD	LD	HD	LD	HD	C	
	family, member 3									
March6	membrane-associated ring finger (C3HC4) 6	1393593_at	ns	ns	2.7	2.3	ns	ns	ns	ns
March6	Membrane-associated ring finger (C3HC4) 6	1372395_at	1.8	1.7	1.8	1.7	1.7	1.7	1.7	ns
Mast4	Microtubule associated serine/threonine kinase family member 4	1390905_at	ns	ns	-1.6	ns	-1.6	ns	ns	ns
Mast4	microtubule associated serine/threonine kinase family member 4	1390658_at	ns	ns	ns	4.8	ns	ns	ns	ns
Mat1a	methionine adenosyltransferase I, alpha	1371031_at	1.6	1.9	1.5	1.6	1.5	1.6	1.6	ns
Matn1	matrilin 1, cartilage matrix protein	1380579_at	ns	ns	-2.7	ns	ns	ns	ns	ns
Mbnl2	Muscleblind-like 2	1375675_at	ns	1.5	ns	ns	ns	ns	ns	ns
Mboat1	membrane bound O-acyltransferase domain containing 1	1382776_at	ns	-2.4	ns	-2.4	ns	-2.2	ns	ns
Mc4r	melanocortin 4 receptor	1370622_at	ns	ns	ns	ns	ns	-10.4	ns	ns
Mcam	melanoma cell adhesion molecule	1374933_at	ns	ns	ns	-9.0	ns	ns	ns	ns
Mcart1	mitochondrial carrier triple repeat 1	1386478_at	ns	ns	1.7	1.6	ns	1.7	1.7	ns
Mcart2	mitochondrial carrier triple repeat 2	1395621_at	ns	ns	ns	ns	1.6	2.0	ns	ns
Mcoln1	mucoilin 1	1389032_at	1.6	1.6	1.6	1.5	1.5	ns	ns	ns
Mcpt4	mast cell protease 4	1369573_at	ns	ns	ns	ns	ns	ns	ns	-7.1
Me1	malic enzyme 1, NADP(+)-dependent, cytosolic	1370870_at	2.2	1.9	2.7	2.7	2.2	1.9	1.9	ns
Me1	malic enzyme 1, NADP(+)-dependent, cytosolic	1370067_at	2.1	2.1	2.7	2.6	1.9	1.7	1.7	ns
Med16	mediator complex subunit 16	1376528_at	ns	ns	ns	ns	-3.1	ns	ns	ns
Med19	mediator complex subunit 19	1376644_at	ns	ns	ns	ns	ns	ns	ns	1.6
Med31	Mediator complex subunit 31	1392659_at	ns	ns	ns	ns	ns	ns	ns	-1.5
Mfap5	microfibrillar associated protein 5	1373674_at	ns	ns	-4.9	-5.7	ns	ns	ns	ns
Mfng	MFNG O-fucosylpeptide 3-beta-N-acetylglucosaminyltransferase	1377041_at	ns	ns	7.6	ns	ns	ns	ns	ns
Mfsd9	major facilitator superfamily domain containing 9	1374604_at	ns	-1.5	ns	ns	ns	ns	ns	ns
MGC114529	similar to melanoma antigen family A, 10	1382906_at	ns	14.0	ns	ns	ns	ns	ns	ns
Mgp	matrix Gla protein	1367568_a_at	ns	ns	ns	ns	-7.3	-8.3	ns	ns
Mgst3	microsomal glutathione S-transferase 3	1388300_at	ns	-1.8	-1.6	-1.6	ns	-1.6	ns	ns
Micall2	MICAL-like 2	1379059_at	-2.0	ns	ns	ns	ns	ns	ns	ns
Mid1ip1	MID1 interacting protein 1 (gastrulation specific G12 homolog (zebrafish))	1372091_at	1.7	1.6	1.7	1.7	1.6	1.6	1.6	ns
Mier2	mesoderm induction early response 1, family member 2	1376342_at	-1.6	ns	ns	ns	ns	ns	ns	ns
Mier2	mesoderm induction early response 1, family member 2	1395908_at	ns	ns	ns	ns	ns	ns	ns	-4.4
Mif	macrophage migration inhibitory factor	1367609_at	ns	1.5	ns	ns	ns	ns	ns	ns
Mir351	microRNA mir-351	1381473_at	ns	ns	ns	ns	-4.5	ns	ns	ns
Mitd1	MIT, microtubule interacting and transport, domain containing 1	1393085_at	ns	ns	ns	ns	ns	ns	ns	2.2
Mll4	myeloid/lymphoid or mixed-lineage leukemia 4	1395786_at	ns	ns	ns	ns	ns	ns	ns	6.6
Mll4	myeloid/lymphoid or mixed-lineage leukemia 4	1388951_at	-1.6	ns	ns	ns	ns	ns	ns	ns
Mllt3	myeloid/lymphoid or mixed-lineage leukemia (trithorax homolog, Drosophila); translocate	1384478_at	ns	-2.1	ns	ns	ns	ns	ns	ns
Mmd	monocyte to macrophage differentiation-associated	1371883_at	ns	ns	ns	ns	ns	6.1	ns	ns
Mme	membrane metallo endopeptidase	1370072_at	15.8	12.0	ns	ns	11.8	11.3	ns	ns
Mmp11	matrix metalloproteinase 11	1367858_at	ns	ns	ns	ns	ns	-5.5	ns	ns
Mmp12	matrix metalloproteinase 12	1368530_at	-4.3	ns	ns	ns	ns	ns	ns	ns
Mmp14	matrix metalloproteinase 14 (membrane-inserted)	1367860_a_at	-2.0	-2.1	ns	ns	-1.9	-2.5	ns	ns
Mmp14	Matrix metalloproteinase 14 (membrane-inserted)	1378225_at	-1.8	-2.1	-1.7	-1.9	-1.5	-1.7	ns	ns
Mmp16	matrix metalloproteinase 16	1368590_at	-6.8	ns	ns	ns	ns	ns	ns	ns
Mocs2	molybdenum cofactor synthesis 2	1372177_at	ns	ns	ns	1.5	ns	ns	ns	ns
Mocs3	Molybdenum cofactor synthesis 3	1386800_at	-3.7	ns	ns	ns	ns	ns	ns	ns
Mogat1	monoacylglycerol O-acyltransferase 1	1385308_at	ns	ns	-4.5	ns	ns	ns	ns	ns
Morc2	MORC family CW-type zinc finger 2	1392303_at	ns	-1.5	ns	ns	ns	ns	ns	ns
Mov10	Moloney leukemia virus 10	1374725_at	ns	ns	-1.6	ns	ns	ns	ns	ns

Symbol	Entrez gene name	Probeset ID	Fold change						
			UT		SC		siGCGR		
			LD	HD	LD	HD	LD	HD	C
Mpdz	multiple PDZ domain protein	1368133_at	ns	ns	ns	-1.7	ns	ns	ns
Mphosph8 /// Parp4	M-phase phosphoprotein 8 /// poly (ADP-ribose) polymerase family, member 4	1376810_at	ns	-1.5	ns	-1.6	ns	ns	ns
Mpnd	MPN domain containing	1371990_at	ns	ns	ns	-1.5	ns	ns	ns
Mrpl34	mitochondrial ribosomal protein L34	1371604_at	ns	ns	ns	ns	ns	ns	-1.6
Ms4a6b	membrane-spanning 4-domains, subfamily A, member 6B	1390510_at	ns	ns	ns	ns	-7.2	ns	ns
Msh3	mutS homolog 3 (E. coli)	1395488_at	ns	ns	ns	-1.5	ns	ns	ns
Mstn	myostatin	1369550_at	ns	ns	5.0	ns	ns	ns	ns
Mtf2	metal response element binding transcription factor 2	1391042_at	ns	ns	ns	ns	ns	ns	1.7
Mthfd2	methylenetetrahydrofolate dehydrogenase (NADP+ dependent) 2, methenyltetrahydrofolate c	1372808_at	ns	ns	ns	1.8	ns	ns	ns
Mtss1	metastasis suppressor 1	1385433_at	1.6	ns	ns	ns	ns	ns	ns
Mug1	murinoglobulin 1	1388229_a_at	ns	-2.0	ns	ns	ns	ns	ns
Mvd	mevalonate (diphospho) decarboxylase	1368020_at	ns	-1.7	ns	ns	ns	ns	ns
Mvk	mevalonate kinase	1368232_at	ns	-1.5	ns	ns	ns	ns	ns
Mx2	myxovirus (influenza virus) resistance 2	1369202_at	ns	ns	ns	ns	ns	ns	20.8
Mxd4	Max dimerization protein 4	1374085_at	ns	-1.7	ns	ns	ns	ns	ns
Mxd4	Max dimerization protein 4	1373779_at	ns	ns	ns	-1.6	ns	ns	ns
Myh6	myosin, heavy chain 6, cardiac muscle, alpha	1387049_at	ns	ns	ns	ns	ns	5.3	ns
Myo10	myosin X	1385409_at	ns	ns	ns	ns	ns	10.1	ns
Myo6	myosin VI	1376804_at	ns	-1.6	ns	-1.5	ns	-1.5	ns
Myof	myoferlin	1375857_at	ns	ns	ns	ns	ns	-3.0	ns
Myt1	myelin transcription factor 1	1395161_at	ns	ns	ns	ns	ns	ns	-3.2
N4bp1	Nedd4 binding protein 1	1390859_at	1.5	ns	1.6	ns	ns	ns	ns
Nadk	NAD kinase	1371559_at	1.6	1.6	1.7	1.7	1.6	1.7	ns
Nadk	NAD kinase	1384467_at	1.5	ns	ns	1.6	ns	1.6	ns
Nadsyn1	NAD synthetase 1	1379472_at	ns	ns	ns	ns	ns	-1.6	ns
Nav2	neuron navigator 2	1381892_at	ns	ns	ns	-4.9	ns	ns	ns
Ncam1	neural cell adhesion molecule 1	1368320_at	ns	ns	3.7	ns	ns	ns	ns
Ncln	nicalin homolog (zebrafish)	1374497_at	ns	1.6	ns	ns	ns	ns	ns
Ncor2	Nuclear receptor co-repressor 2	1398140_at	ns	ns	-3.3	ns	ns	ns	ns
Ndufa9	NADH dehydrogenase (ubiquinone) 1 alpha subcomplex, 9	1396282_at	ns	ns	ns	ns	ns	-2.3	ns
Nedd4l	neural precursor cell expressed, developmentally down-regulated 4-like	1389507_at	ns	ns	ns	-1.5	ns	ns	ns
Nedd9	neural precursor cell expressed, developmentally down-regulated 9	1396053_at	ns	1.5	1.7	ns	ns	ns	ns
Nedd9	neural precursor cell expressed, developmentally down-regulated 9	1374650_at	1.7	1.5	1.5	ns	ns	ns	ns
Nefl	neurofilament, light polypeptide	1370058_at	ns	-16.6	-16.8	ns	ns	ns	ns
Neo1	neogenin homolog 1 (chicken)	1381467_at	-2.1	ns	ns	ns	ns	ns	ns
Neo1	neogenin homolog 1 (chicken)	1390468_at	ns	ns	ns	-1.6	ns	ns	ns
Nes	nestin	1386948_at	ns	ns	ns	ns	ns	ns	-4.4
Neu2	sialidase 2 (cytosolic sialidase)	1368127_at	1.8	1.6	ns	ns	1.8	1.5	ns
Neu3	sialidase 3 (membrane sialidase)	1369420_at	ns	ns	ns	-2.0	ns	ns	ns
Nf1	neurofibromin 1	1369014_at	ns	ns	4.0	3.8	ns	ns	ns
Nfe2l1	nuclear factor, erythroid derived 2,-like 1	1390068_at	1.6	ns	1.8	1.6	1.7	ns	ns
Nfkbia	nuclear factor of kappa light polypeptide gene enhancer in B-cells inhibitor, alpha	1389538_at	1.7	1.6	ns	ns	ns	ns	ns
Nfu1	NFU1 iron-sulfur cluster scaffold homolog (S. cerevisiae)	1389162_at	ns	1.5	ns	1.5	ns	ns	ns
Nfyb	nuclear transcription factor-Y beta	1387452_a_at	ns	ns	ns	ns	ns	1.6	ns
Ngdn	Neuroguidin, EIF4E binding protein	1392401_s_at	ns	ns	ns	-2.9	ns	ns	ns
Ngfrap1	nerve growth factor receptor (TNFRSF16) associated protein 1	1385534_at	ns	-1.8	ns	ns	ns	ns	ns
Ngfrap1	nerve growth factor receptor (TNFRSF16) associated protein 1	1369948_at	ns	-1.6	-1.5	-1.8	ns	ns	ns
Nhej1	nonhomologous end-joining factor 1	1374245_at	ns	2.2	ns	ns	ns	ns	ns
Ninj1	ninjurin 1	1370348_at	ns	ns	ns	ns	ns	ns	-1.5
Ninj2	ninjurin 2	1368135_at	ns	1.7	ns	ns	ns	ns	ns
Nlgn2	neuroligin 2	1397705_at	ns	ns	ns	-5.3	ns	ns	ns

Symbol	Entrez gene name	Probeset ID	Fold change						
			UT		SC		siGCCR		
			LD	HD	LD	HD	LD	HD	C
Nme3	non-metastatic cells 3, protein expressed in	1368863_at	ns	-1.5	ns	ns	ns	ns	ns
Nolc1	nucleolar and coiled-body phosphoprotein 1	1382893_at	ns	ns	ns	ns	ns	9.8	-10.6
Notch1	Notch homolog 1, translocation-associated ( <i>Drosophila</i> )	1371491_at	ns	ns	-2.0	-2.2	ns	ns	ns
Npas2	neuronal PAS domain protein 2	1383439_at	ns	-2.0	-1.7	-2.2	-1.7	-2.0	ns
Npffr2	neuropeptide FF receptor 2	1387607_at	ns	ns	ns	-8.0	ns	ns	ns
Nr0b1	nuclear receptor subfamily 0, group B, member 1	1369478_at	6.5	ns	ns	ns	ns	6.5	ns
Nr0b2	nuclear receptor subfamily 0, group B, member 2	1368376_at	42.2	94.9	ns	7.2	16.4	51.6	ns
Nr2f6	nuclear receptor subfamily 2, group F, member 6	1398826_s_at	ns	-1.6	ns	-1.5	ns	ns	ns
Nr4a2	nuclear receptor subfamily 4, group A, member 2	1387410_at	-6.5	ns	ns	ns	ns	ns	ns
Nradd	neurotrophin receptor associated death domain	1369917_at	ns	ns	ns	-2.1	ns	ns	ns
Nrarp	Notch-regulated ankyrin repeat protein	1375277_at	ns	ns	ns	ns	-3.9	ns	ns
Nrbp	nuclear receptor binding protein	1372057_at	ns	ns	ns	1.6	ns	ns	ns
Nrf1	nuclear respiratory factor 1	1381895_at	ns	ns	ns	2.4	ns	ns	ns
Nrg1	neuregulin 1	1369783_a_at	-1.7	ns	-1.6	ns	-1.6	ns	ns
Nrg2	neuregulin 2	1391033_s_at	ns	-4.4	ns	ns	ns	ns	ns
Nrip3	nuclear receptor interacting protein 3	1396173_at	ns	3.0	ns	ns	ns	ns	ns
Nrm	nrin (nuclear envelope membrane protein)	1390469_at	ns	ns	ns	ns	ns	ns	-2.5
Nrtn	neurturin	1374048_at	ns	ns	ns	ns	ns	-1.6	ns
Nudc	nuclear distribution gene C homolog (A. nidulans)	1368436_at	ns	ns	ns	1.5	ns	ns	ns
Nxn1	nucleoredoxin-like 1	1395235_at	ns	ns	-3.9	ns	ns	ns	ns
Oas1a	2'-5' oligoadenylate synthetase 1A	1371152_a_at	ns	ns	ns	ns	ns	ns	29.4
Oasl	2'-5'-oligoadenylate synthetase-like	1377497_at	ns	ns	ns	ns	ns	ns	10.1
Obp3	alpha-2u globulin PGCL4	1370479_x_at	ns	ns	ns	ns	ns	ns	-1.9
Olfml2a	olfactomedin-like 2A	1382072_at	ns	-7.9	ns	ns	ns	ns	ns
Olfml2b	olfactomedin-like 2B	1389295_at	ns	ns	ns	ns	-2.0	ns	ns
Omd	osteomodulin	1387197_at	ns	-1.8	-1.6	-2.1	ns	-1.9	ns
Onecut1	one cut homeobox 1	1371034_at	-2.3	-2.3	ns	-2.0	-2.4	-2.9	ns
Onecut1	one cut homeobox 1	1387760_a_at	ns	ns	ns	ns	ns	-2.0	ns
Opn3	opsin 3	1393373_at	ns	-2.2	ns	ns	ns	ns	ns
Orai2	ORAI calcium release-activated calcium modulator 2	1379159_at	ns	ns	ns	ns	-5.6	ns	ns
Orai2	ORAI calcium release-activated calcium modulator 2	1377955_at	ns	ns	5.4	ns	ns	ns	ns
Oraov1	oral cancer overexpressed 1	1379074_at	ns	ns	1.6	ns	1.6	1.6	ns
Osbp16	oxysterol binding protein-like 6	1384871_at	ns	ns	ns	ns	ns	ns	10.5
Otub2	OTU domain, ubiquitin aldehyde binding 2	1385154_at	2.1	2.7	ns	2.4	2.5	2.3	ns
P2ry10	purinergic receptor P2Y, G-protein coupled, 10	1394051_at	ns	ns	ns	5.2	ns	ns	ns
P2ry2	purinergic receptor P2Y, G-protein coupled, 2	1368940_at	1.7	1.7	1.9	1.8	1.9	1.7	ns
Pah	phenylalanine hydroxylase	1387034_at	-1.8	-2.4	-1.9	-2.1	-1.7	-2.1	ns
Pak3	p21 protein (Cdc42/Rac)-activated kinase 3	1368902_at	ns	4.9	ns	ns	ns	ns	ns
Palb2	partner and localizer of BRCA2	1376695_at	ns	ns	-1.7	ns	ns	ns	ns
Pank1	pantothenate kinase 1	1382924_at	1.8	ns	1.7	ns	1.8	1.7	ns
Parp14	poly (ADP-ribose) polymerase family, member 14	1372034_at	ns	ns	ns	ns	ns	ns	1.9
Parp14	poly (ADP-ribose) polymerase family, member 14	1379613_at	ns	ns	ns	ns	ns	ns	1.7
Parp9	poly (ADP-ribose) polymerase family, member 9	1376144_at	ns	ns	ns	ns	ns	ns	2.2
Pax8	paired box 8	1378692_at	ns	ns	ns	ns	ns	1.9	-1.8
Pbld	phenazine biosynthesis-like protein domain containing	1370320_at	ns	-2.0	-1.8	-2.3	ns	-1.8	ns
Pbld	phenazine biosynthesis-like protein domain containing	1390993_at	-1.9	-2.8	-2.1	-2.6	-2.3	-2.7	ns
Pcdh19	protocadherin 19	1382130_at	ns	ns	ns	ns	ns	12.1	ns
Pcdh20	protocadherin 20	1385229_at	ns	ns	ns	ns	ns	-8.3	ns
Pcdh24	protocadherin 24	1390366_at	ns	ns	ns	-2.1	ns	ns	ns

Symbol	Entrez gene name	Probeset ID	Fold change						
			UT		SC		siGCGR		
			LD	HD	LD	HD	LD	HD	C
Pcdh8	protocadherin 8	1368956_at	ns	-4.8	ns	ns	ns	ns	ns
Pcdh9	protocadherin 9	1397688_at	-5.0	ns	ns	ns	ns	ns	ns
Pcdhb22	protocadherin beta 22	1392002_at	-10.6	ns	ns	ns	ns	ns	ns
Pcdhb9	protocadherin beta 9	1389653_at	ns	ns	ns	-5.7	ns	ns	ns
Pcdhga1 / Pcdhga10	protocadherin gamma subfamily A, 1 / protocadherin gamma subfamily A, 10 / protocad	1388551_at	ns	ns	ns	-1.5	ns	ns	ns
Pcp2	Purkinje cell protein 2	1372936_at	ns	ns	ns	-2.3	ns	ns	ns
Pcsk9	proprotein convertase subtilisin/kexin type 9	1385640_at	ns	-1.6	ns	ns	ns	ns	ns
Pctk1	PCTAIRE protein kinase 1	1370326_at	ns	ns	ns	ns	ns	ns	1.5
Pctp	phosphatidylcholine transfer protein	1387058_at	ns	ns	ns	1.5	ns	ns	ns
Pde11a	phosphodiesterase 11A	1369349_a_at	4.6	ns	ns	ns	ns	ns	ns
Pde3b	phosphodiesterase 3B, cGMP-inhibited	1369157_at	ns	ns	1.7	ns	1.9	1.8	ns
Pde4b	phosphodiesterase 4B, cAMP specific	1369044_a_at	ns	-7.5	ns	ns	ns	ns	ns
Pde8a	Phosphodiesterase 8A	1376057_at	1.6	ns	ns	ns	ns	ns	ns
Pdhb	pyruvate dehydrogenase (lipoamide) beta	1371388_at	1.7	1.7	1.8	1.8	1.7	1.7	ns
Pdk2	pyruvate dehydrogenase kinase, isozyme 2	1386975_at	ns	ns	ns	3.0	ns	ns	ns
Pdk3	pyruvate dehydrogenase kinase, isozyme 3	1384315_at	ns	ns	ns	ns	-5.7	ns	ns
Pdk4	pyruvate dehydrogenase kinase, isozyme 4	1369150_at	ns	ns	ns	ns	2.5	3.6	ns
Pdlim2	PDZ and LIM domain 2	1375367_at	-2.2	-2.4	-2.3	-2.4	-2.3	-2.0	ns
Pdlim3	PDZ and LIM domain 3	1370291_at	ns	ns	ns	-1.9	ns	ns	ns
Pdlim7	PDZ and LIM domain 7	1370347_at	ns	ns	ns	-2.6	ns	ns	ns
Pdp2	pyruvate dehydrogenase phosphatase catalytic subunit 2	1380045_at	ns	ns	ns	ns	2.3	ns	ns
Pdp2	Pyruvate dehydrogenase phosphatase isoenzyme 2	1396062_at	2.0	ns	2.2	ns	3.1	2.8	ns
Pdzk1	PDZ domain containing 1	1368178_at	1.9	ns	2.2	1.8	2.1	1.9	ns
Per1	period homolog 1 (Drosophila)	1374855_at	-2.0	-1.6	-2.1	-2.4	-1.9	-2.0	ns
Pex11a	peroxisomal biogenesis factor 11 alpha	1387740_at	ns	-2.9	ns	ns	ns	ns	ns
Pex19	peroxisomal biogenesis factor 19	1382028_at	ns	-1.6	ns	ns	ns	ns	ns
Pfkfb3	6-phosphofructo-2-kinase/fructose-2,6-biphosphatase 3	1369794_a_at	ns	ns	ns	ns	ns	ns	-8.4
Pfkfbm	phosphofructokinase, muscle	1367864_at	ns	ns	ns	-1.7	ns	ns	ns
Pgs1	phosphatidylglycerophosphate synthase 1	1371863_at	ns	ns	1.8	1.9	1.6	1.6	ns
Phactr1	phosphatase and actin regulator 1	1382303_at	ns	ns	ns	ns	-7.9	ns	8.6
Phf11	PHD finger protein 11	1382546_at	ns	ns	ns	ns	ns	ns	2.9
Pi4kb	phosphatidylinositol 4-kinase, catalytic, beta	1369039_at	ns	ns	ns	ns	ns	-1.5	ns
Pias3	protein inhibitor of activated STAT, 3	1370196_at	-1.5	-1.7	ns	-1.8	ns	-1.5	ns
Picalm	phosphatidylinositol binding clathrin assembly protein	1369452_a_at	ns	ns	ns	ns	1.6	1.6	ns
Pik3c2g	phosphoinositide-3-kinase, class 2, gamma polypeptide	1369050_at	ns	-2.1	-2.4	-2.3	ns	-1.7	ns
Pik3r2	phosphoinositide-3-kinase, regulatory subunit 2 (beta)	1370100_at	ns	ns	ns	ns	ns	-1.6	ns
Pik3r3	phosphoinositide-3-kinase, regulatory subunit 3 (gamma)	1369518_at	ns	-7.7	ns	ns	ns	ns	ns
Pik3r6	Phosphoinositide-3-kinase, regulatory subunit 6	1374317_at	-3.0	ns	ns	ns	ns	ns	ns
Pikfyve	phosphoinositide kinase, FYVE finger containing	1380216_at	ns	1.8	ns	ns	ns	ns	ns
Pim3	pim-3 oncogene	1367725_at	ns	ns	ns	ns	-1.6	-1.5	ns
Pion	pigeon homolog (Drosophila)	1382181_at	ns	-1.5	ns	ns	ns	ns	ns
Pitpnm1	phosphatidylinositol transfer protein, membrane-associated 1	1389347_at	ns	ns	ns	ns	-1.7	ns	ns
Pla1a	phospholipase A1 member A	1370445_at	ns	-1.8	ns	ns	-1.9	ns	ns
Pla2g12a	phospholipase A2, group XIIA	1373810_at	1.5	1.5	ns	ns	ns	ns	ns
Pla2g6	phospholipase A2, group VI (cytosolic, calcium-independent)	1370385_at	ns	2.3	ns	2.0	ns	1.5	ns
Pla2g6	phospholipase A2, group VI (cytosolic, calcium-independent)	1377408_at	ns	1.7	ns	ns	ns	ns	ns
Pla2g6	phospholipase A2, group VI (cytosolic, calcium-independent)	1387941_s_at	ns	1.5	1.6	1.9	ns	1.5	ns
Plcd4	phospholipase C, delta 4	1387065_at	ns	ns	ns	ns	7.5	ns	ns

Symbol	Entrez gene name	Probeset ID	Fold change						
			UT		SC		siGCCR		
			LD	HD	LD	HD	LD	HD	C
Pld2	phospholipase D2	1368954_at	ns	ns	ns	-3.0	ns	ns	ns
Plekha1	Pleckstrin homology domain containing, family A (phosphoinositide binding specific) mem	1392230_at	ns	3.7	ns	ns	ns	ns	ns
Plekha4	pleckstrin homology domain containing, family A (phosphoinositide binding specific) mem	1384570_at	2.7	ns	ns	2.9	3.7	4.7	ns
Plekha5	pleckstrin homology domain containing, family A member 5	1373272_at	ns	ns	ns	ns	1.7	ns	ns
Plekha6	Pleckstrin homology domain containing, family A member 6	1379536_at	ns	ns	ns	ns	ns	ns	1.6
Plekhf1	pleckstrin homology domain containing, family F (with FYVE domain) member 1	1373532_at	ns	ns	ns	-1.6	ns	-1.5	ns
Plekhh1	pleckstrin homology domain containing, family H (with MyTH4 domain) member 1	1384277_at	ns	ns	ns	-1.6	ns	-1.7	ns
Plekhh2	pleckstrin homology domain containing, family H (with MyTH4 domain) member 2	1391845_at	ns	ns	ns	ns	ns	4.2	ns
Plekhh3	pleckstrin homology domain containing, family H (with MyTH4 domain) member 3	1377384_at	ns	-1.8	ns	ns	ns	ns	ns
Plin5	perilipin 5	1381722_at	ns	ns	ns	ns	ns	-1.8	ns
Plp2	proteolipid protein 2 (colonic epithelium-enriched)	1388393_at	ns	-1.5	ns	ns	ns	ns	ns
Plxna2	plexin A2	1384355_at	ns	ns	ns	-3.0	ns	ns	ns
Plxnd1	plexin D1	1389341_at	ns	ns	ns	-6.1	ns	ns	ns
Pmvk	phosphomevalonate kinase	1373243_at	ns	-1.6	ns	ns	ns	ns	ns
Pnkd	paroxysmal nonkinesigenic dyskinesia	1373312_at	ns	-1.9	-1.7	-1.9	ns	-1.9	ns
Pnpla3	patatin-like phospholipase domain containing 3	1380013_at	5.8	ns	7.6	6.2	7.4	ns	ns
Pnpla8	Patatin-like phospholipase domain containing 8	1375528_at	ns	-5.3	ns	ns	ns	ns	ns
Pnrc1	proline-rich nuclear receptor coactivator 1	1370381_at	ns	ns	ns	-1.8	ns	ns	ns
Podn	podocan	1381088_at	ns	ns	ns	3.7	ns	ns	ns
Podxl	podocalyxin-like	1385823_s_at	4.8	4.2	ns	-3.6	ns	ns	ns
Poll	polymerase (DNA directed), lambda	1389268_at	ns	ns	ns	ns	-1.6	ns	ns
Pols	polymerase (DNA directed) sigma	1371987_at	1.9	1.6	2.0	1.8	1.9	1.7	ns
Pom121	nuclear pore membrane protein 121	1386957_at	ns	ns	ns	1.6	ns	ns	ns
Popdc2	popeye domain containing 2	1376646_at	ns	-2.0	ns	-2.4	ns	ns	ns
Por	P450 (cytochrome) oxidoreductase	1387109_at	3.5	3.3	2.9	2.8	2.5	2.3	ns
Por	P450 (cytochrome) oxidoreductase	1368213_at	3.8	2.9	3.3	3.2	3.7	3.4	ns
Porcn	porcupine homolog (Drosophila)	1397965_at	3.9	4.4	ns	ns	ns	ns	ns
Pot1a	protection of telomeres 1A	1386777_at	ns	ns	ns	ns	-1.6	ns	ns
Ppap2a	phosphatidic acid phosphatase type 2A	1369961_at	ns	-1.7	ns	ns	ns	-1.5	ns
Ppard	peroxisome proliferator-activated receptor delta	1374914_at	ns	ns	ns	ns	1.8	ns	ns
Ppcdc	phosphopantothienoylcysteine decarboxylase	1373236_at	ns	ns	ns	ns	1.8	1.6	ns
Ppp1r10	protein phosphatase 1, regulatory subunit 10	1396682_at	ns	ns	ns	ns	ns	ns	5.5
Ppp1r12a	protein phosphatase 1, regulatory (inhibitor) subunit 12A	1382307_at	ns	ns	1.7	ns	ns	ns	ns
Ppp1r12a	protein phosphatase 1, regulatory (inhibitor) subunit 12A	1381850_at	ns	ns	1.8	ns	ns	ns	ns
Ppp1r15a	protein phosphatase 1, regulatory (inhibitor) subunit 15A	1370174_at	ns	1.5	ns	1.6	ns	1.7	ns
Ppp2r5a	Protein phosphatase 2, regulatory subunit B', alpha isoform	1392241_at	ns	ns	ns	ns	ns	ns	-6.7
Prdm1	PR domain containing 1, with ZNF domain	1390221_at	ns	ns	ns	-6.2	ns	ns	ns
Prex2	phosphatidylinositol-3,4,5-trisphosphate-dependent Rac exchange factor 2	1380817_at	-11.8	ns	ns	ns	ns	ns	ns
Prf1	perforin 1 (pore forming protein)	1370096_at	ns	ns	ns	ns	6.2	ns	ns
Prg2	proteoglycan 2, bone marrow	1387633_at	ns	ns	ns	ns	ns	ns	-10.8
Pric285	peroxisomal proliferator-activated receptor A interacting complex 285	1390531_at	ns	ns	ns	ns	ns	ns	1.8
Prkab2	Protein kinase, AMP-activated, beta 2 non-catalytic subunit	1378845_at	ns	7.5	ns	ns	ns	ns	ns
Prkag3	protein kinase, AMP-activated, gamma 3 non-catalytic subunit	1394711_at	-2.0	ns	ns	ns	ns	ns	ns
Prkar1b	protein kinase, cAMP dependent regulatory, type I, beta	1389463_at	ns	ns	-1.9	ns	ns	ns	ns
Prkar2a	Protein kinase, cAMP dependent regulatory, type II alpha	1375620_at	ns	ns	-2.9	ns	ns	ns	ns



Symbol	Entrez gene name	Probeset ID	Fold change						
			UT		SC		siGCGR		
			LD	HD	LD	HD	LD	HD	C
Prkcq	protein kinase C, theta	1376259_at	ns	ns	ns	-11.6	ns	ns	ns
Prlr	prolactin receptor	1370384_a_at	ns	ns	ns	-2.0	ns	ns	ns
Prmt6	protein arginine methyltransferase 6	1373910_at	ns	ns	ns	ns	-1.6	ns	1.6
Prokr2	prokineticin receptor 2	1369532_at	ns	ns	ns	ns	ns	ns	-5.1
Prp2l1	proline rich protein 2-like 1	1388207_at	ns	ns	-5.2	ns	ns	ns	ns
Prr13	proline rich 13	1388408_at	ns	-1.6	ns	ns	ns	ns	ns
Psca	prostate stem cell antigen	1374345_at	3.0	3.0	1.8	ns	ns	1.9	ns
Psd3	pleckstrin and Sec7 domain containing 3	1379108_at	-1.7	-1.8	ns	-1.5	-1.7	-1.8	ns
Psen2	presenilin 2	1370064_at	ns	-1.9	ns	ns	-1.7	-1.6	ns
Psmb8	proteasome (prosome, macropain) subunit, beta type 8 (large multifunctional peptidase 7)	1367786_at	ns	ns	ns	ns	ns	ns	2.0
Psmc3ip	PSMC3 interacting protein	1370008_at	-1.6	ns	ns	ns	ns	ns	ns
Psmc1	Proteasome (prosome, macropain) activator subunit 1	1394006_at	ns	-3.6	ns	ns	ns	ns	ns
Psmc4	proteasome (prosome, macropain) activator subunit 4	1387345_at	ns	ns	ns	ns	1.6	1.5	ns
Pspc1	Paraspeckle component 1	1392162_at	ns	ns	ns	ns	ns	-1.7	ns
Ptdss2	phosphatidylserine synthase 2	1372663_at	1.6	ns	1.6	1.6	1.5	ns	ns
Ptger2	prostaglandin E receptor 2 (subtype EP2)	1369766_at	ns	ns	ns	ns	ns	ns	-4.3
Ptger3	prostaglandin E receptor 3 (subtype EP3)	1369187_a_at	-1.8	ns	-1.7	ns	-1.6	-1.6	ns
Ptgs1	prostaglandin-endoperoxide synthase 1	1368259_at	ns	ns	ns	ns	4.8	5.0	ns
Ptprd	protein tyrosine phosphatase, receptor type, D	1374591_at	-1.6	-1.9	ns	-2.1	-1.7	-2.0	ns
Ptprd	protein tyrosine phosphatase, receptor type, D	1376619_at	ns	-2.2	ns	-2.0	ns	ns	ns
Ptprs	protein tyrosine phosphatase, receptor type, S	1369094_a_at	ns	ns	ns	ns	ns	ns	-1.9
Ptprv	protein tyrosine phosphatase, receptor type, V	1387136_at	ns	ns	-1.7	ns	ns	ns	-1.7
Punc	Putative neuronal cell adhesion molecule	1382825_at	ns	ns	3.9	4.3	8.5	11.7	ns
Purb	purine rich element binding protein B	1391303_at	-5.9	ns	ns	ns	ns	ns	ns
Pvrl2	poliovirus receptor-related 2	1375216_at	-1.7	-1.6	-1.5	ns	ns	-1.6	ns
Pycard	PYD and CARD domain containing	1389873_at	-2.8	ns	ns	ns	ns	ns	ns
Pycr1	pyrroline-5-carboxylate reductase 1	1383434_at	ns	1.9	ns	ns	ns	2.0	ns
Pygm	phosphorylase, glycogen, muscle	1375476_at	ns	ns	ns	-5.3	ns	ns	ns
Pzp	pregnancy-zone protein	1370547_at	ns	ns	ns	ns	ns	-1.5	ns
Qprt	Quinolate phosphoribosyltransferase	1382244_at	ns	ns	ns	-1.9	ns	ns	ns
Qprt	quinolate phosphoribosyltransferase	1372672_at	ns	-1.7	-1.6	-1.9	ns	-1.7	ns
Qrs1	glutamyl-tRNA synthase (glutamine-hydrolyzing)-like 1	1380842_at	ns	ns	ns	2.4	ns	ns	ns
Rab11fip1	RAB11 family interacting protein 1 (class I)	1377790_at	-1.6	-1.7	ns	ns	ns	-1.6	ns
Rab13	RAB13, member RAS oncogene family	1388140_at	ns	-1.5	ns	-1.6	ns	ns	ns
Rab17	RAB17, member RAS oncogene family	1383437_at	ns	-1.5	ns	ns	ns	ns	ns
Rab27a	RAB27A, member RAS oncogene family	1384852_at	ns	ns	ns	ns	ns	ns	-1.8
Rab33b	RAB33B, member of RAS oncogene family	1383232_at	ns	ns	ns	1.5	ns	ns	ns
Rab39	RAB39, member RAS oncogene family	1385653_at	ns	ns	ns	ns	-18.4	ns	16.4
Rab3il1	RAB3A interacting protein (rabin3)-like 1	1369305_at	-17.0	ns	ns	ns	ns	ns	ns
Rabgap1l	RAB GTPase activating protein 1-like	1391897_at	ns	ns	ns	-1.5	ns	ns	ns
Rabggta	Rab geranylgeranyltransferase, alpha subunit	1369899_s_at	ns	ns	ns	ns	-1.6	-1.6	ns
Rad50	RAD50 homolog (S. cerevisiae)	1397642_at	ns	ns	ns	-1.6	ns	ns	ns
Rad50	RAD50 homolog (S. cerevisiae)	1385565_at	ns	12.2	ns	ns	ns	ns	ns
Rad50	RAD50 homolog (S. cerevisiae)	1387427_at	ns	ns	ns	2.8	ns	ns	2.4
Rad51ap1	RAD51 associated protein 1	1380277_at	ns	ns	ns	ns	-2.8	ns	ns
Rai1	retinoic acid induced 1	1373966_at	ns	ns	ns	-1.9	ns	ns	ns
Rap2ip	Rap2 interacting protein	1391532_at	ns	ns	ns	-1.6	ns	ns	ns
Rap2ip	Rap2 interacting protein	1379552_s_at	ns	-9.1	ns	-21.1	-9.0	-23.6	ns
Rap2ip	Rap2 interacting protein	1387928_at	ns	ns	ns	-2.6	-2.6	-2.7	ns
Rapgef1	Rap guanine nucleotide exchange factor (GEF) 1	1371199_at	ns	ns	ns	-7.6	ns	ns	ns
Rapgef1l	Rap guanine nucleotide exchange factor	1383335_at	ns	4.4	ns	ns	ns	ns	ns

## 10 APPENDIX

Symbol	Entrez gene name	Probeset ID	Fold change							
			UT		SC		siGCGR			
			LD	HD	LD	HD	LD	HD	C	
	(GEF)-like 1									
Raph1	Ras association (RalGDS/AF-6) and pleckstrin homology domains 1	1374369_at	ns	ns	ns	-1.7	ns	ns	ns	ns
Rapsn	receptor-associated protein of the synapse	1395946_at	ns	5.9	ns	ns	ns	ns	ns	ns
Rarres1	retinoic acid receptor responder (tazartone induced) 1	1382274_at	2.1	ns	2.3	2.0	2.2	2.2	2.2	ns
Rasa2	RAS p21 protein activator 2	1384386_at	ns	ns	ns	ns	ns	ns	ns	2.3
Rasgrp3	RAS guanyl releasing protein 3 (calcium and DAG-regulated)	1390159_at	ns	ns	ns	-2.9	ns	ns	ns	ns
Rassf1	Ras association (RalGDS/AF-6) domain family member 1	1392688_at	ns	-2.4	ns	ns	ns	ns	ns	ns
Rassf1	Ras association (RalGDS/AF-6) domain family member 1	1382449_at	ns	-8.1	ns	ns	ns	ns	ns	ns
Rassf5	Ras association (RalGDS/AF-6) domain family member 5	1370415_at	ns	ns	ns	ns	-1.9	ns	ns	ns
RatNP-3b	defensin RatNP-3 precursor	1370791_at	ns	7.7	ns	ns	ns	ns	ns	ns
Raver2	ribonucleoprotein, PTB-binding 2	1378471_at	ns	ns	ns	-13.1	ns	ns	ns	ns
Rbm38	RNA binding motif protein 38	1372271_at	ns	ns	-1.6	ns	ns	ns	ns	ns
Rbp7	retinol binding protein 7, cellular	1374863_at	ns	-2.7	ns	ns	ns	ns	-2.0	ns
Rcc2	regulator of chromosome condensation 2	1395396_at	ns	ns	ns	2.0	ns	ns	ns	ns
Rcl1	RNA terminal phosphate cyclase-like 1	1373452_at	ns	ns	-1.6	-1.6	ns	-1.7	ns	ns
Rdh10	Retinol dehydrogenase 10 (all-trans)	1373923_at	ns	ns	ns	-1.9	ns	ns	ns	ns
Rdh10	Retinol dehydrogenase 10 (all-trans)	1393351_at	ns	-1.5	ns	-1.5	ns	-1.6	ns	ns
Rdm1	RAD52 motif 1	1389453_at	ns	ns	ns	ns	ns	ns	ns	-1.5
Rem2	RAS (RAD and GEM) like GTP binding 2	1374035_at	ns	ns	ns	ns	ns	ns	-2.8	ns
Renbp	renin binding protein	1398254_at	-1.8	-1.6	ns	ns	ns	ns	ns	ns
Rfwd2	Ring finger and WD repeat domain 2	1375172_at	ns	5.0	ns	ns	ns	ns	ns	ns
RGD1304693	similar to CG14803-PA	1390321_at	ns	ns	-2.0	ns	ns	-1.8	ns	ns
RGD1304810	similar to 6430573F11Rik protein	1393353_at	ns	ns	ns	-2.2	ns	ns	ns	ns
RGD1304827	hypothetical LOC316091	1376156_at	ns	ns	-1.5	ns	ns	ns	ns	ns
RGD1305090	similar to CD2-associated protein	1385351_at	ns	ns	ns	ns	7.8	ns	-12.4	ns
RGD1305158	Similar to RIKEN cDNA 1810030N24	1394240_at	ns	ns	ns	ns	ns	ns	ns	-1.9
RGD1306063	similar to HT021	1374882_at	ns	-1.6	ns	ns	ns	ns	ns	ns
RGD1306072	hypothetical LOC304654	1385062_at	ns	1.9	ns	ns	ns	ns	ns	ns
RGD1306622	similar to KIAA0954 protein	1373321_at	ns	ns	-1.5	-1.7	ns	-1.7	ns	ns
RGD1306625	LOC360508	1393892_at	ns	-10.3	ns	ns	ns	ns	ns	ns
RGD1307235	similar to RIKEN cDNA 2310035C23	1397730_at	ns	ns	ns	ns	-5.6	ns	ns	ns
RGD1308114	similar to cDNA sequence AF397014	1385574_at	ns	-2.0	ns	ns	ns	ns	ns	ns
RGD1308116	similar to hypothetical protein MGC42105	1377014_at	ns	-10.0	ns	ns	ns	ns	ns	ns
RGD1308117	similar to 9930012K11Rik protein	1383414_at	ns	ns	-2.0	-2.1	-1.6	-1.5	-1.7	ns
RGD1308165	Similar to hypothetical protein MGC17337	1390346_at	ns	ns	ns	-5.0	ns	ns	ns	ns
RGD1308350	similar to hypothetical protein MGC13251	1388848_at	ns	ns	1.8	1.7	ns	ns	ns	ns
RGD1308470	similar to RIKEN cDNA 493343P14 gene	1389269_at	ns	ns	ns	ns	ns	ns	ns	1.8
RGD1308616	similar to KIAA0467 protein	1385556_at	ns	ns	ns	ns	ns	-1.5	ns	ns
RGD1308759	similar to KIAA0892 protein	1377205_at	ns	ns	ns	ns	ns	ns	ns	-1.6
RGD1308958	similar to chromosome 9 open reading frame 5	1396228_at	ns	1.5	ns	ns	ns	ns	ns	ns
RGD1309079	similar to Ab2-095	1389199_at	ns	ns	ns	ns	ns	1.8	ns	ns
RGD1309095	similar to hypothetical protein BC015148	1384252_at	ns	ns	ns	1.6	ns	ns	ns	ns
RGD1309414	similar to KIAA0913 protein	1390315_a_at	ns	ns	ns	ns	ns	-1.6	ns	ns
RGD1309453	Similar to hypothetical protein FLJ32884	1374486_at	ns	ns	ns	-1.8	ns	ns	ns	ns
RGD13095	similar to RIKEN cDNA 4931406C07	1371763_at	3.3	2.4	3.1	2.7	3.2	2.7	ns	ns

Symbol	Entrez gene name	Probeset ID	Fold change							
			UT		SC		siGCGR			
			LD	HD	LD	HD	LD	HD	C	
34										
RGD1309621	similar to hypothetical protein FLJ10652	1395297_at	ns	-3.3	ns	ns	ns	ns	ns	ns
RGD1309823	similar to hypothetical protein FLJ21156	1374808_at	ns	ns	ns	ns	ns	ns	-1.5	ns
RGD1310348	similar to Ser/Thr-rich protein T10 in DGCR region	1386503_at	ns	ns	ns	-1.8	ns	ns	ns	ns
RGD1310686	similar to chromosome 16 open reading frame 5	1374217_at	ns	-1.9	ns	-1.9	ns	ns	-1.6	ns
RGD1310686	similar to chromosome 16 open reading frame 5	1374169_at	ns	ns	-1.5	-1.5	ns	ns	ns	ns
RGD1310877	similar to RIKEN cDNA 1810063B07 gene	1374807_at	ns	ns	ns	1.5	ns	1.5	ns	ns
RGD1311084	similar to 1700113K14Rik protein	1393913_at	ns	ns	ns	ns	-2.9	ns	ns	ns
RGD1311595	similar to KIAA2026 protein	1390699_at	ns	-1.5	ns	ns	ns	ns	ns	ns
RGD1311612	similar to hypothetical protein FLJ12118	1383134_at	ns	ns	-1.5	ns	ns	ns	ns	ns
RGD1311739	similar to RIKEN cDNA 1700037H04	1372430_at	-1.6	-1.8	ns	-1.7	-1.7	-1.7	-1.7	ns
RGD1311823	Similar to RIKEN cDNA 1700016G05	1386822_s_at	5.5	ns	ns	ns	ns	ns	ns	ns
RGD1359616	similar to 2010321M09Rik protein	1380707_at	ns	-4.5	ns	ns	ns	ns	ns	ns
RGD1559600	RGD1559600	1392825_at	ns	ns	ns	ns	-2.0	-2.1	ns	ns
RGD1559896	similar to RIKEN cDNA 2310022B05	1376878_at	ns	-1.5	ns	ns	ns	ns	ns	ns
RGD1560108	similar to RIKEN cDNA 2700081O15	1374321_at	-1.8	-1.9	ns	-1.8	ns	ns	ns	ns
RGD1560171	similar to PRO0149 protein	1384130_at	ns	ns	ns	ns	ns	-5.8	ns	ns
RGD1560433	similar to 1500019C06Rik protein	1382797_at	ns	ns	1.5	1.5	ns	ns	ns	ns
RGD1560925	similar to 2610034M16Rik protein	1374375_at	ns	ns	ns	-1.6	ns	ns	ns	ns
RGD1561042	similar to RIKEN cDNA 5730509K17 gene	1374874_at	ns	ns	ns	-2.0	ns	ns	ns	ns
RGD1561067	Similar to RNA binding protein gene with multiple splicing	1375898_at	ns	-1.5	ns	ns	ns	ns	ns	ns
RGD1561238	similar to ring finger protein 122 homolog	1373485_at	-3.3	ns	ns	ns	ns	ns	ns	ns
RGD1561551	similar to Hypothetical protein MGC75664	1390691_at	ns	1.9	1.7	2.2	ns	2.0	ns	ns
RGD1561852	similar to Protein C20orf29	1374041_at	ns	ns	1.6	1.8	ns	ns	ns	1.6
RGD1562284	similar to Glutaminyl-peptide cyclotransferase precursor (QC)	1377867_at	ns	-4.4	ns	ns	ns	ns	ns	ns
RGD1562310	similar to hypothetical protein FLJ21415	1381366_at	ns	2.3	ns	ns	ns	ns	ns	ns
RGD1562342	similar to RIKEN cDNA 1110012D08	1385060_at	ns	ns	ns	ns	ns	-3.4	ns	ns
RGD1562552	similar to hypothetical protein LOC340061	1390226_at	ns	ns	ns	ns	ns	ns	ns	9.0
RGD1562704	RGD1562704	1392028_at	ns	14.0	ns	ns	ns	ns	ns	ns
RGD1563060	similar to AVLV472	1378398_at	ns	ns	ns	-7.7	ns	ns	ns	ns
RGD1563072	similar to hypothetical protein FLJ38984	1393074_at	ns	-1.6	ns	-1.5	-1.6	ns	ns	ns
RGD1563091	similar to OEF2	1376693_at	ns	ns	ns	ns	ns	ns	ns	5.5
RGD1563440	similar to hypothetical protein	1377397_at	ns	ns	ns	ns	ns	5.7	-9.2	ns
RGD1564053	similar to hypothetical protein	1397890_at	-12.2	ns	ns	ns	ns	ns	ns	ns
RGD1564163	Similar to RIKEN cDNA 1700025K23	1386053_at	ns	2.3	ns	ns	ns	ns	ns	ns
RGD1564722	similar to C19orf36 protein	1391920_at	ns	ns	ns	-11.1	ns	ns	ns	ns
RGD1564865	similar to 20-alpha-hydroxysteroid dehydrogenase	1393221_at	ns	-4.6	ns	-4.3	ns	ns	ns	ns
RGD1564952	similar to zinc finger, RAN-binding domain containing 3	1383217_at	-2.0	ns	ns	ns	ns	ns	ns	ns
RGD1565096	similar to TSG118.1	1396572_at	ns	5.9	ns	ns	ns	ns	ns	ns
RGD1565210	RGD1565210	1386337_at	ns	ns	-1.5	ns	ns	ns	ns	-1.6
RGD1565350	Similar to Shb protein	1389639_at	1.7	1.8	1.8	1.9	1.8	1.9	ns	ns

## 10 APPENDIX

Symbol	Entrez gene name	Probeset ID	Fold change						
			UT		SC		siGCCR		
			LD	HD	LD	HD	LD	HD	C
RGD1565591	similar to Ski protein	1375463_at	ns	ns	ns	ns	-1.7	ns	ns
RGD1565787	similar to RIKEN cDNA 1810065E05	1381572_at	ns	ns	ns	ns	ns	ns	-3.6
RGD1565926	RGD1565926	1380065_at	ns	ns	ns	ns	ns	7.6	ns
RGD1566029	Similar to mKIAA1644 protein	1395068_at	ns	ns	ns	ns	5.7	ns	ns
RGD1566085	similar to pyridoxal (pyridoxine, vitamin B6) kinase	1387826_at	ns	ns	ns	ns	1.7	1.7	ns
RGD1566266	similar to hypothetical protein FLJ21127	1386121_at	ns	-6.2	ns	ns	ns	ns	ns
Rgn	regucalcin (senescence marker protein-30)	1368627_at	ns	ns	-1.5	ns	-1.6	ns	ns
Rgs8	regulator of G-protein signaling 8	1387403_at	ns	ns	-6.6	ns	ns	ns	ns
Rgs9	regulator of G-protein signaling 9	1368500_a_at	ns	ns	-5.4	ns	ns	ns	ns
Rhebl1	Ras homolog enriched in brain like 1	1382623_at	ns	1.8	ns	ns	ns	ns	ns
Rhobtb2	Rho-related BTB domain containing 2	1382279_at	ns	-3.4	ns	ns	ns	ns	ns
Rhobtb3	Rho-related BTB domain containing 3	1395358_at	ns	-8.0	ns	ns	ns	ns	ns
Rhoc	ras homolog gene family, member C	1371659_at	-1.5	-1.7	-1.5	ns	ns	ns	ns
Rhox4g	reproductive homeobox 4G	1385785_at	ns	ns	ns	ns	6.3	ns	ns
Rhpn2	rhopilin, Rho GTPase binding protein 2	1383012_at	1.6	ns	2.0	1.9	ns	ns	ns
Rims2	regulating synaptic membrane exocytosis 2	1369333_a_at	ns	ns	ns	ns	ns	-8.0	ns
Rin2	Ras and Rab interactor 2	1372365_at	-2.5	-2.9	-2.2	-2.1	-1.9	-1.9	ns
Rin2	Ras and Rab interactor 2	1375602_at	-22.0	ns	ns	ns	ns	ns	ns
Riok3	RIO kinase 3 (yeast)	1395699_at	1.7	3.2	1.9	2.8	1.7	2.5	ns
Riok3	RIO kinase 3 (yeast)	1394363_at	ns	3.1	1.7	2.7	ns	2.1	ns
Riok3	RIO kinase 3 (yeast)	1393236_at	ns	1.9	ns	1.9	ns	1.7	ns
Rnase4	ribonuclease, RNase A family 4	1368943_at	2.3	ns	2.2	ns	2.9	2.4	ns
Rnase4	ribonuclease, RNase A family 4	1371475_at	2.0	ns	1.9	1.6	1.9	1.8	ns
Rnf114	ring finger protein 114	1375955_at	ns	ns	ns	ns	ns	ns	1.5
Rnf125	ring finger protein 125	1384098_at	ns	ns	1.9	ns	ns	ns	ns
Rnf213	ring finger protein 213	1374337_at	ns	ns	ns	ns	ns	ns	2.0
Rnf213	ring finger protein 213	1373514_at	ns	ns	ns	ns	ns	ns	2.5
Rnf25	ring finger protein 25	1398336_at	ns	ns	ns	ns	ns	ns	1.6
Rnf41	ring finger protein 41	1391252_at	ns	-1.9	ns	ns	ns	ns	ns
Rnls	renalase, FAD-dependent amine oxidase	1381816_at	ns	-1.5	ns	ns	ns	ns	ns
Robo2	roundabout, axon guidance receptor, homolog 2 (Drosophila)	1379750_at	ns	ns	ns	ns	ns	ns	-2.3
Ropn1l	ropporin 1-like	1381960_at	ns	-7.5	ns	ns	ns	ns	ns
Rp2	retinitis pigmentosa 2 homolog (human)	1386027_at	ns	-1.9	ns	ns	-1.8	-1.8	ns
Rpesp	RPE-spondin	1396035_at	3.2	ns	3.1	3.3	2.9	3.3	ns
Rpia	Ribose 5-phosphate isomerase A	1376559_at	ns	ns	ns	ns	ns	ns	-1.7
Rpl7	Ribosomal protein L7	1375788_at	ns	ns	ns	ns	ns	ns	-1.8
Rprm	reprimin, TP53 dependent G2 arrest mediator candidate	1390672_at	ns	-3.9	ns	-3.3	ns	ns	ns
Rsad2	radical S-adenosyl methionine domain containing 2	1370913_at	ns	5.8	ns	5.7	ns	ns	19.4
RT1-A2	RT1 class Ia, locus A2	1380436_at	ns	8.7	ns	ns	ns	ns	ns
RT1-Db1	RT1 class II, locus Db1	1370382_at	7.9	11.6	ns	ns	ns	ns	ns
RT1-M3-1	RT1 class Ib, locus M3, gene 1	1387205_at	-1.5	-1.6	ns	ns	ns	ns	ns
RT1-S3	RT1 class Ib, locus S3	1388213_a_at	ns	ns	ns	ns	ns	ns	3.8
RT1-S3	RT1 class Ib, locus S3	1388164_at	ns	ns	ns	ns	ns	ns	3.0
RT1-S3	RT1 class Ib, locus S3	1388212_a_at	ns	ns	ns	ns	ns	ns	3.8
RT1-S3	RT1 class Ib, locus S3	1371123_x_at	ns	ns	ns	ns	ns	ns	3.1
Rtn4	reticulin 4	1368888_a_at	ns	ns	ns	-1.5	ns	ns	ns
Rtn4	reticulin 4	1388027_a_at	ns	-1.7	-1.5	-1.6	ns	ns	ns
Rtn4r1	reticulin 4 receptor-like 1	1372690_at	ns	-1.8	-2.0	-2.1	-1.8	-1.9	ns
Rtn4r1	reticulin 4 receptor-like 1	1393404_at	ns	-2.6	-2.1	-2.3	-1.9	-2.2	ns
Rtp4	receptor (chemosensory) transporter protein 4	1379285_at	ns	ns	ns	ns	ns	ns	10.7
Rwdd2a	RWD domain containing 2A	1380403_at	-1.8	ns	ns	-2.6	-1.7	-1.7	ns
Ryr2	ryanodine receptor 2, cardiac	1382775_at	ns	ns	ns	ns	ns	ns	-5.6

Symbol	Entrez gene name	Probeset ID	Fold change						
			UT		SC		siGCGR		
			LD	HD	LD	HD	LD	HD	C
S100a13	S100 calcium binding protein A13	1375954_at	ns	ns	ns	ns	ns	-1.5	ns
S100g	S100 calcium binding protein G	1368339_at	4.6	4.4	3.9	3.5	3.4	3.3	ns
S1pr1	sphingosine-1-phosphate receptor 1	1371840_at	ns	ns	ns	-2.4	ns	ns	ns
Safb	scaffold attachment factor B	1368058_at	ns	ns	ns	ns	ns	ns	1.7
Sall1	Sal-like 1 (Drosophila)	1391194_at	ns	ns	-1.7	-1.6	-1.7	-1.7	ns
Sash3	SAM and SH3 domain containing 3	1385831_at	ns	ns	ns	ns	9.9	8.8	ns
Sbk1	SH3-binding domain kinase 1	1388072_at	ns	3.9	ns	ns	ns	ns	ns
Sc4mol	sterol-C4-methyl oxidase-like	1368275_at	ns	-2.4	ns	ns	ns	-1.9	ns
Scai	suppressor of cancer cell invasion	1397394_at	ns	ns	ns	ns	-3.1	ns	ns
Scarb1	scavenger receptor class B, member 1	1367855_at	ns	ns	-1.7	ns	ns	ns	ns
Scd	stearoyl-CoA desaturase (delta-9-desaturase)	1367668_a_at	7.1	ns	26.0	11.7	22.0	10.1	ns
Scd1	stearoyl-Coenzyme A desaturase 1	1370355_at	1.6	2.0	1.6	1.7	2.1	2.2	ns
Scg5	secretogranin V	1367992_at	ns	ns	ns	-4.4	ns	ns	ns
Scnn1b	sodium channel, nonvoltage-gated 1, beta	1370482_at	ns	ns	ns	-3.6	ns	ns	ns
Sdcbp2	syndecan binding protein (syntenin) 2	1376973_at	ns	ns	ns	2.5	ns	ns	ns
Sdpr	serum deprivation response	1375638_at	1.9	ns	ns	ns	ns	ns	ns
Sdr39u1	short chain dehydrogenase/reductase family 39U, member 1	1393673_at	ns	ns	ns	1.8	1.7	2.0	ns
Sdr39u1	short chain dehydrogenase/reductase family 39U, member 1	1376222_at	ns	ns	ns	1.5	ns	ns	ns
Sec14l2	SEC14-like 2 (S. cerevisiae)	1374308_at	ns	-1.8	ns	ns	ns	ns	ns
Selp	selectin P	1369374_at	ns	ns	ns	ns	4.7	5.9	-6.6
Sema4b	sema domain, immunoglobulin domain (Ig), transmembrane domain (TM) and short cytoplasmic	1374678_at	ns	-1.6	ns	ns	-1.6	-1.6	ns
Sema6d	sema domain, transmembrane domain (TM), and cytoplasmic domain, (semaphorin) 6D	1389353_at	ns	ns	ns	ns	-6.6	ns	ns
Senp8	Sumo1/sentrin/SMT3 specific peptidase 8	1397187_at	ns	ns	ns	-6.7	ns	ns	ns
Sepp1	selenoprotein P, plasma, 1	1387339_at	ns	-3.5	ns	-2.5	ns	ns	ns
Serf1	small EDRK-rich factor 1	1392856_at	ns	ns	ns	ns	ns	ns	-1.5
Serf2	small EDRK-rich factor 2	1374547_at	ns	ns	ns	ns	ns	ns	-1.5
Serinc5	serine incorporator 5	1386979_at	ns	-1.7	ns	ns	ns	-1.5	ns
Serp1	stress-associated endoplasmic reticulum protein 1	1386900_at	ns	1.6	ns	ns	ns	ns	ns
Serpina11	serine (or cysteine) peptidase inhibitor, clade A (alpha-1 antitrypsin)	1376174_at	-1.6	ns	ns	ns	ns	ns	ns
Serpina3n	serine (or cysteine) peptidase inhibitor, clade A, member 3N	1368224_at	-1.7	ns	ns	ns	-1.7	-1.5	ns
Serpina7	serine (or cysteine) peptidase inhibitor, clade A (alpha-1 antitrypsin)	1371143_at	ns	-2.8	ns	ns	ns	ns	ns
Serpib12	serine (or cysteine) peptidase inhibitor, clade B (ovalbumin), member 12	1376243_at	ns	5.4	ns	ns	ns	ns	ns
Serpib1a	serine (or cysteine) proteinase inhibitor, clade B, member 1a	1380346_at	ns	ns	-6.9	ns	ns	ns	ns
Serpib1a	serine (or cysteine) proteinase inhibitor, clade B, member 1a	1377034_at	ns	ns	ns	ns	ns	-4.2	ns
Serpib3	serine protease inhibitor B3	1384973_at	ns	ns	ns	ns	-10.2	ns	ns
Serpind1	serine (or cysteine) peptidase inhibitor, clade D, member 1	1398260_a_at	ns	-2.0	ns	-1.9	ns	ns	ns
Sesn1	sestrin 1	1372248_at	ns	-1.6	ns	-1.8	-1.5	-1.8	ns
Sez6	seizure related 6 homolog (mouse)	1391032_at	ns	-6.5	ns	-5.2	ns	ns	ns
Sfn	stratifin	1374806_at	ns	4.1	ns	ns	ns	ns	ns
Sfrp2	secreted frizzled-related protein 2	1396614_at	ns	3.4	ns	ns	ns	ns	ns
Sfrp4	secreted frizzled-related protein 4	1388021_at	ns	ns	ns	ns	ns	6.8	ns
Sfrs16	splicing factor, arginine/serine-rich 16	1376054_at	ns	1.6	ns	ns	ns	ns	ns
Sfrs3	splicing factor, arginine/serine-rich 3	1376252_at	ns	-1.5	ns	ns	ns	ns	ns
Sfxn3	sideroflexin 3	1387008_at	ns	ns	ns	ns	ns	-1.9	ns
Sgk1	serum/glucocorticoid regulated kinase 1	1367802_at	ns	ns	-1.8	-1.6	-2.2	-1.8	ns
Sgk493	protein kinase-like protein Sgk493	1372316_at	-3.3	-4.6	-4.1	-5.6	-3.6	-4.7	ns
Sgsm2	small G protein signaling modulator 2	1388768_at	ns	ns	ns	ns	ns	-1.7	ns
Sh2d4a	SH2 domain containing 4A	1389779_at	-1.5	ns	ns	ns	ns	ns	ns

## 10 APPENDIX

Symbol	Entrez gene name	Probeset ID	Fold change						
			UT		SC		siGCGR		
			LD	HD	LD	HD	LD	HD	C
Sh3glb2	SH3-domain GRB2-like endophilin B2	1376486_at	ns	-1.8	-1.5	ns	-1.5	-1.6	ns
Shank2	SH3 and multiple ankyrin repeat domains 2	1369776_a_at	ns	ns	ns	ns	-8.1	ns	ns
Shc1	SHC (Src homology 2 domain containing) transforming protein 1	1377594_at	ns	ns	ns	ns	1.5	ns	ns
Shc2	SHC (Src homology 2 domain containing) transforming protein 2	1384347_at	ns	ns	ns	ns	-1.9	ns	ns
Shh	sonic hedgehog	1387584_at	ns	ns	-4.7	ns	ns	ns	ns
Shisa5	shisa homolog 5 ( <i>Xenopus laevis</i> )	1388776_at	ns	ns	ns	ns	ns	ns	1.7
Shmt2	serine hydroxymethyltransferase 2 (mitochondrial)	1388695_at	ns	ns	ns	1.7	ns	ns	ns
Shoc2	soc-2 (suppressor of clear) homolog (C. elegans)	1380435_at	ns	ns	ns	ns	-1.6	ns	ns
Si	sucrase-isomaltase (alpha-glucosidase)	1387539_at	ns	ns	ns	ns	ns	4.6	ns
Siglec10	sialic acid binding Ig-like lectin 10	1394501_at	ns	ns	ns	-2.7	ns	ns	ns
Sin3b	SIN3 homolog B, transcription regulator (yeast)	1388653_at	ns	ns	-1.7	ns	ns	ns	ns
Sirt4	sirtuin (silent mating type information regulation 2 homolog) 4 ( <i>S. cerevisiae</i> )	1397836_at	1.7	ns	ns	ns	ns	ns	ns
Ska2	spindle and kinetochore associated complex subunit 2	1379261_at	ns	ns	ns	-1.6	ns	ns	ns
Slc10a2	solute carrier family 10 (sodium/bile acid cotransporter family), member 2	1368745_at	-2.4	-3.9	-3.2	-3.2	-2.3	-3.1	ns
Slc14a2	solute carrier family 14 (urea transporter), member 2	1398312_s_at	ns	-12.8	ns	ns	ns	ns	ns
Slc15a1	solute carrier family 15 (oligopeptide transporter), member 1	1369381_a_at	ns	ns	4.6	ns	ns	ns	ns
Slc16a10	solute carrier family 16 (monocarboxylic acid transporters), member 10	1370548_at	ns	ns	-2.0	-2.0	-1.8	ns	ns
Slc16a13	Solute carrier family 16, member 13 (monocarboxylic acid transporter 13)	1385352_at	ns	ns	ns	ns	ns	-1.9	ns
Slc18a2	solute carrier family 18 (vesicular monoamine), member 2	1369132_at	ns	ns	ns	ns	ns	-5.5	ns
Slc18a2	solute carrier family 18 (vesicular monoamine), member 2	1369131_at	ns	ns	ns	ns	2.1	ns	ns
Slc1a3	solute carrier family 1 (glial high affinity glutamate transporter), member 3	1368565_at	ns	ns	ns	-2.2	ns	ns	ns
Slc22a17	solute carrier family 22, member 17	1371889_at	ns	ns	ns	-1.5	ns	ns	ns
Slc22a8	solute carrier family 22 (organic anion transporter), member 8	1368461_at	ns	ns	ns	ns	-1.7	ns	ns
Slc23a1	solute carrier family 23 (nucleobase transporters), member 1	1369169_at	2.1	1.7	2.1	ns	1.8	ns	ns
Slc24a2	solute carrier family 24 (sodium/potassium/calcium exchanger), member 2	1383444_at	ns	ns	ns	ns	ns	-2.9	ns
Slc25a15	Solute carrier family 25 (mitochondrial carrier; ornithine transporter) member 15	1393947_at	ns	ns	ns	ns	ns	-1.5	ns
Slc25a23	solute carrier family 25 (mitochondrial carrier; phosphate carrier), member 23	1379169_at	ns	ns	ns	ns	ns	2.8	ns
Slc25a28	solute carrier family 25, member 28	1392978_at	1.6	ns	1.8	ns	1.8	1.7	ns
Slc25a37	solute carrier family 25, member 37	1382688_at	ns	1.8	1.6	1.6	ns	ns	ns
Slc25a4	solute carrier family 25 (mitochondrial carrier; adenine nucleotide translocator), memb	1388112_at	ns	-2.1	-2.0	-2.6	-1.8	-2.1	ns
Slc25a44	solute carrier family 25, member 44	1373306_at	ns	ns	1.5	ns	ns	ns	ns
Slc25a45	solute carrier family 25, member 45	1375080_at	3.4	3.3	3.2	2.6	7.7	6.6	ns
Slc25a5	solute carrier family 25 (mitochondrial carrier; adenine nucleotide translocator), memb	1388163_at	ns	ns	ns	ns	ns	ns	-1.6
Slc2a4	solute carrier family 2 (facilitated glucose transporter), member 4	1367989_at	ns	ns	ns	ns	ns	2.8	ns
Slc31a2	solute carrier family 31 (copper transporters), member 2	1373657_at	ns	-2.1	ns	ns	ns	ns	ns
Slc34a1	solute carrier family 34 (sodium phosphate), member 1	1370745_at	ns	ns	ns	ns	ns	ns	-1.7
Slc34a1	solute carrier family 34 (sodium phosphate), member 1	1370610_at	ns	ns	ns	ns	ns	7.4	-7.8
Slc35a2	solute carrier family 35, member A2	1373227_at	ns	ns	ns	ns	ns	ns	1.5
Slc35a5	Solute carrier family 35, member A5	1384413_at	ns	ns	ns	ns	ns	-1.6	ns
Slc35b2	solute carrier family 35, member B2	1373460_at	ns	ns	ns	ns	ns	-1.5	ns
Slc38a6	solute carrier family 38, member 6	1399089_at	ns	ns	-1.5	ns	ns	ns	ns
Slc3a2	solute carrier family 3 (activators of dibasic and neutral amino acid transport), membe	1398771_at	ns	1.7	ns	1.7	ns	1.6	ns
Slc43a1	solute carrier family 43, member 1	1378196_at	1.6	1.6	2.1	1.8	1.9	1.8	ns

Symbol	Entrez gene name	Probeset ID	Fold change						
			UT		SC		siGCGR		
			LD	HD	LD	HD	LD	HD	C
Slc44a1	solute carrier family 44, member 1	1370935_at	-1.7	ns	ns	-1.7	-1.6	ns	ns
Slc44a1	solute carrier family 44, member 1	1373054_at	-1.5	-1.7	-1.6	-1.7	ns	-1.6	ns
Slc5a12	solute carrier family 5 (sodium/glucose cotransporter), member 12	1383832_at	ns	ns	ns	ns	ns	9.7	ns
Slc6a11	solute carrier family 6 (neurotransmitter transporter, GABA), member 11	1369715_at	ns	ns	ns	ns	7.3	13.3	-12.0
Slc6a13	solute carrier family 6 (neurotransmitter transporter, GABA), member 13	1387372_at	ns	ns	ns	ns	2.1	ns	ns
Slc6a8	solute carrier family 6 (neurotransmitter transporter, creatine), member 8	1367810_at	ns	ns	-1.5	-1.6	ns	ns	ns
Slc6a8	solute carrier family 6 (neurotransmitter transporter, creatine), member 8	1386934_at	-1.8	-1.8	-1.8	-1.8	-1.7	-1.6	ns
Slc6a9	solute carrier family 6 (neurotransmitter transporter, glycine), member 9	1373787_at	ns	1.8	ns	1.8	ns	ns	ns
Slc6a9	solute carrier family 6 (neurotransmitter transporter, glycine), member 9	1369772_at	ns	ns	1.5	1.9	ns	ns	ns
Slc6a9	solute carrier family 6 (neurotransmitter transporter, glycine), member 9	1387693_a_at	2.1	1.9	2.4	2.6	ns	2.4	ns
Slc7a1	solute carrier family 7 (cationic amino acid transporter, y+ system), member 1	1387167_at	ns	-4.4	ns	ns	ns	ns	ns
Slc7a10	solute carrier family 7, (neutral amino acid transporter, y+ system) member 10	1370115_at	2.9	5.3	ns	ns	ns	ns	ns
Slc9a3r1	solute carrier family 9 (sodium/hydrogen exchanger), member 3 regulator 1	1387793_at	1.7	ns	1.9	1.7	1.6	ns	ns
Slc9a3r2	solute carrier family 9 (sodium/hydrogen exchanger), member 3 regulator 2	1387976_at	ns	ns	ns	-1.6	ns	ns	ns
Slco1a4	solute carrier organic anion transporter family, member 1a4	1387094_at	9.1	4.3	11.3	6.9	9.3	6.4	ns
Slco1a4	solute carrier organic anion transporter family, member 1a4	1387093_at	6.7	3.5	6.5	4.0	8.8	6.3	ns
Slco1b3	solute carrier organic anion transporter family, member 1b3	1387679_at	ns	-1.7	ns	-1.8	ns	ns	ns
Slco3a1	Solute carrier organic anion transporter family, member 3a1	1373734_at	ns	ns	ns	-5.9	ns	ns	ns
Smarca2	SWI/SNF related, matrix associated, actin dependent regulator of chromatin, subfamily a	1376337_at	1.6	ns	1.5	ns	ns	ns	ns
Smek1	SMEK homolog 1, suppressor of mek1 (Dictyostelium)	1389933_at	ns	-4.1	ns	ns	ns	ns	ns
Smox	spermine oxidase	1394621_at	ns	2.0	1.7	1.7	ns	1.7	ns
Smox	spermine oxidase	1374556_at	1.9	1.9	1.8	1.9	1.7	1.7	ns
Snap29	synaptosomal-associated protein 29	1373213_at	ns	ns	ns	ns	ns	ns	-1.6
Snrnp25	small nuclear ribonucleoprotein 25 (U11/U12)	1393361_at	2.0	1.8	2.1	2.0	2.3	2.2	ns
Snrnp25	small nuclear ribonucleoprotein 25 (U11/U12)	1393242_at	2.1	2.0	2.4	2.2	2.5	2.3	ns
Snrpa	small nuclear ribonucleoprotein polypeptide A	1388436_at	ns	ns	ns	ns	ns	1.6	ns
Snrpd1	Small nuclear ribonucleoprotein D1	1379320_at	ns	ns	ns	ns	ns	1.5	ns
Snx10	sorting nexin 10	1379275_at	ns	2.2	2.0	2.3	ns	2.0	ns
Snx27	sorting nexin family member 27	1381394_at	ns	-1.5	ns	ns	ns	ns	ns
Snx8	sorting nexin 8	1380802_at	1.7	1.9	ns	ns	1.8	1.9	ns
Sor11	sortilin-related receptor, LDLR class A repeats-containing	1390710_x_at	ns	ns	-1.5	ns	ns	ns	ns
Sor11	sortilin-related receptor, LDLR class A repeats-containing	1386268_at	ns	ns	ns	-7.6	ns	ns	ns
Sor11	sortilin-related receptor, LDLR class A repeats-containing	1377458_at	ns	ns	ns	-1.6	ns	ns	ns
Sost	sclerosteosis	1368969_at	ns	ns	ns	ns	ns	-6.0	ns
Sox13	SRY (sex determining region Y)-box 13	1374682_at	ns	-1.6	ns	ns	ns	ns	ns
Sox17	SRY (sex determining region Y)-box 17	1392990_at	ns	ns	ns	-8.0	ns	ns	ns
Sp110	SP110 nuclear body protein	1372930_at	ns	ns	ns	ns	ns	ns	1.5
Spats2l	spermatogenesis associated, serine-rich 2-like	1388791_at	ns	ns	ns	ns	ns	ns	7.9
Spink5	serine peptidase inhibitor, Kazal type 5	1398688_at	ns	ns	ns	-4.1	ns	ns	ns
Spinlw1	serine peptidase inhibitor-like, with Kunitz and WAP domains 1 (eppin)	1392781_at	ns	ns	-7.2	ns	ns	ns	ns
Sppl2a	signal peptide peptidase-like 2A	1375362_at	ns	ns	ns	ns	ns	ns	-1.8
Sprn	Shadow of prion protein homolog (zebrafish)	1397231_at	ns	ns	ns	-14.5	ns	ns	ns
Spry4	sprouty homolog 4 (Drosophila)	1392529_at	ns	ns	ns	ns	ns	2.1	-2.4
Sptbn1	spectrin, beta, non-erythrocytic 1	1371046_at	ns	ns	-1.7	-2.2	ns	ns	-1.6
Sqle	squalene epoxidase	1387017_at	ns	-1.7	ns	ns	ns	-1.8	ns

Symbol	Entrez gene name	Probeset ID	Fold change						
			UT		SC		siGCCR		
			LD	HD	LD	HD	LD	HD	C
Sreb1	sterol regulatory element binding transcription factor 1	1388426_at	2.4	4.3	2.1	3.3	2.5	3.9	ns
Sreb1	sterol regulatory element binding transcription factor 1	1371104_at	2.0	3.9	1.6	2.2	2.0	3.0	ns
Sreb2	sterol regulatory element binding transcription factor 2	1371979_at	ns	ns	ns	ns	ns	-1.8	1.6
Srm	spermidine synthase	1367834_at	ns	1.8	ns	1.6	ns	ns	ns
Srp14	signal recognition particle 14	1367476_at	ns	ns	ns	ns	ns	ns	-1.6
Ssbp3	single stranded DNA binding protein 3	1368517_at	ns	ns	ns	ns	ns	-1.7	ns
Ssr3	signal sequence receptor, gamma	1369718_at	1.6	ns	ns	ns	ns	ns	ns
St5	suppression of tumorigenicity 5	1373288_at	ns	-1.6	ns	-1.5	ns	ns	ns
St8sia3	ST8 alpha-N-acetyl-neuraminide alpha-2,8-sialyltransferase 3	1387435_at	ns	-1.8	-2.0	-2.2	ns	ns	ns
Stap2	signal transducing adaptor family member 2	1389420_at	ns	ns	ns	-2.1	ns	-1.9	ns
Star	steroidogenic acute regulatory protein	1368406_at	-10.2	ns	ns	ns	ns	ns	ns
Stard5	StAR-related lipid transfer (START) domain containing 5	1393183_at	ns	-1.7	ns	ns	ns	ns	ns
Stat1 /// Stat4	signal transducer and activator of transcription 1 /// signal transducer and activator	1387354_at	ns	ns	ns	ns	ns	ns	2.1
Stat1 /// Stat4	signal transducer and activator of transcription 1 /// signal transducer and activator	1368835_at	ns	ns	ns	ns	ns	ns	1.7
Stat2	signal transducer and activator of transcription 2	1389571_at	ns	ns	ns	ns	ns	ns	1.8
Stat2	Signal transducer and activator of transcription 2	1373670_at	ns	ns	ns	ns	ns	ns	1.5
Stbd1	starch binding domain 1	1372602_at	ns	1.8	ns	1.7	ns	ns	ns
Stc1	stanniocalcin 1	1377404_at	ns	ns	ns	ns	-10.0	ns	ns
Stfa2l3	stefin A2-like 3	1393978_at	ns	ns	-8.4	-8.4	ns	ns	ns
Stk32c	serine/threonine kinase 32C	1377534_at	6.9	ns	ns	ns	5.9	ns	-9.5
Ston2	Stonin 2	1380981_at	ns	ns	ns	ns	-2.2	-2.1	ns
Stra6	stimulated by retinoic acid gene 6	1385475_a_at	ns	ns	-6.1	ns	ns	ns	ns
Stx18	syntaxin 18	1372512_at	1.5	ns	1.7	1.7	1.6	ns	ns
Stx3	syntaxin 3	1369308_at	ns	ns	4.3	4.3	ns	ns	ns
Sulf1	sulfatase 1	1375492_at	ns	ns	ns	-9.6	ns	ns	ns
Sulf2	sulfatase 2	1388753_at	-1.7	-1.9	-1.8	-1.9	-1.6	-1.8	ns
Sult1c2 /// Sult1c2a	sulfotransferase family, cytosolic, 1C, member 2 /// sulfotransferase family, cytosolic	1370943_at	-2.4	-2.2	-2.4	-1.9	-1.9	-2.0	ns
Sult2a1	sulfotransferase family 2A, dehydroepiandrosterone (DHEA)-preferring-like 1	1387006_at	5.2	2.6	3.5	2.5	3.4	2.4	ns
Supt3h	suppressor of Ty 3 homolog (S. cerevisiae)	1385624_at	ns	ns	ns	ns	ns	1.8	ns
Susd2	sushi domain containing 2	1398511_at	ns	ns	ns	-2.2	ns	ns	ns
Susd2	sushi domain containing 2	1392594_at	ns	ns	ns	-8.1	ns	ns	ns
Syn3	synapsin III	1369423_at	ns	14.6	ns	ns	ns	ns	ns
Syngap1	synaptic Ras GTPase activating protein 1 homolog (rat)	1368110_a_at	ns	ns	ns	ns	ns	ns	-3.9
Synj2bp	synaptotagmin 2 binding protein	1368038_at	ns	-1.6	ns	ns	ns	ns	ns
Sypl2	synaptophysin-like 2	1374012_at	ns	ns	-5.7	-6.5	ns	ns	ns
Tapbp	TAP binding protein	1369726_at	ns	ns	ns	ns	ns	ns	1.7
Tasp1	taspase, threonine aspartase 1	1382428_at	ns	ns	-1.8	ns	-1.7	ns	ns
Tbc1d19	TBC1 domain family, member 19	1396309_at	ns	-1.5	ns	ns	-1.6	ns	ns
Tbc1d22b	TBC1 domain family, member 22B	1373622_at	ns	ns	-1.8	ns	ns	ns	ns
Tbc1d2b	TBC1 domain family, member 2B	1372748_at	-2.1	-2.2	-1.8	-2.9	-1.7	-1.8	ns
Tbl1xr1	Transducin (beta)-like 1 X-linked receptor 1	1379309_at	ns	ns	ns	ns	ns	ns	-3.4
Tbx2	T-box 2	1375556_at	2.1	3.2	ns	ns	ns	ns	ns
Tcea3	transcription elongation factor A (SII), 3	1388611_at	ns	-2.2	ns	-2.2	ns	-2.1	ns
Tchp	trichoplein, keratin filament binding	1377798_at	ns	ns	ns	ns	ns	-5.7	ns
Tcp11l2	t-complex 11 (mouse) like 2	1388471_at	1.8	2.6	ns	2.4	ns	2.2	ns
Tex19	testis expressed 19	1390666_at	ns	ns	ns	-10.6	ns	ns	ns
Tex2	testis expressed 2	1376038_at	2.0	ns	2.1	1.7	2.1	1.8	ns
Tfpt	TCF3 (E2A) fusion partner	1388099_a_at	ns	ns	ns	ns	ns	ns	1.6
Tg	thyroglobulin	1370764_a_at	ns	ns	ns	-2.6	ns	ns	ns



Symbol	Entrez gene name	Probeset ID	Fold change						
			UT		SC		siGCGR		
			LD	HD	LD	HD	LD	HD	C
Tgif1	TGFB-induced factor homeobox 1	1373421_at	ns	ns	-1.9	-1.8	ns	ns	ns
Tgm3	transglutaminase 3, E polypeptide	1378675_at	ns	ns	ns	-4.3	ns	ns	ns
Thra	thyroid hormone receptor alpha	1367726_at	ns	ns	ns	ns	ns	-2.3	ns
Thrsp	thyroid hormone responsive	1371400_at	2.2	ns	ns	ns	ns	ns	ns
Thrsp	thyroid hormone responsive	1387852_at	2.5	ns	2.3	ns	2.5	ns	ns
Thy1	Thy-1 cell surface antigen	1369652_at	ns	ns	ns	ns	ns	-9.6	ns
Tia1	TIA1 cytotoxic granule-associated RNA binding protein	1382991_at	ns	-8.4	ns	ns	ns	ns	ns
Timp4	tissue inhibitor of metalloproteinase 4	1377632_at	ns	-4.6	ns	ns	ns	ns	ns
Tjap1	tight junction associated protein 1	1375865_at	ns	ns	-1.5	ns	ns	ns	ns
Tk1	thymidine kinase 1, soluble	1389858_at	ns	ns	ns	ns	2.0	ns	ns
Tk1	thymidine kinase 1, soluble	1372631_at	ns	ns	2.2	ns	ns	ns	ns
Tkt	transketolase	1386859_at	1.7	1.8	1.6	1.7	1.8	1.7	ns
Tle1	transducin-like enhancer of split 1 (E(sp1) homolog, Drosophila)	1374425_at	1.7	ns	1.5	ns	1.6	ns	ns
Tm4sf4	transmembrane 4 L six family member 4	1368706_at	-1.5	-2.0	-1.9	-2.3	ns	-1.8	ns
Tm9sf3	transmembrane 9 superfamily member 3	1380053_at	ns	ns	ns	ns	ns	ns	-2.8
Tm9sf3	transmembrane 9 superfamily member 3	1398973_at	ns	ns	ns	ns	ns	ns	-1.8
Tmbim1	transmembrane BAX inhibitor motif containing 1	1376102_at	2.1	2.6	2.3	2.7	2.3	2.8	ns
Tmem109	transmembrane protein 109	1372369_at	ns	-1.6	ns	ns	-1.5	ns	ns
Tmem119	transmembrane protein 119	1372935_at	ns	ns	ns	-4.4	ns	ns	ns
Tmem135	transmembrane protein 135	1392466_at	ns	ns	ns	ns	1.6	ns	ns
Tmem140	transmembrane protein 140	1390042_at	-1.7	-2.0	ns	-1.8	ns	ns	ns
Tmem14a	transmembrane protein 14A	1391684_at	ns	-2.7	ns	ns	ns	ns	ns
Tmem158	transmembrane protein 158	1370210_at	ns	ns	ns	ns	ns	ns	2.0
Tmem171	transmembrane protein 171	1373006_at	2.2	2.2	2.0	2.1	2.0	1.9	ns
Tmem176a	transmembrane protein 176A	1373204_at	ns	-1.5	ns	ns	ns	ns	ns
Tmem182	transmembrane protein 182	1385201_at	ns	4.8	ns	ns	ns	ns	-4.5
Tmem19	transmembrane protein 19	1386346_at	-1.8	-1.9	-1.7	-1.7	-1.7	-1.8	ns
Tmem19	transmembrane protein 19	1394842_at	-1.8	-2.0	-1.7	-1.7	-1.7	-1.7	ns
Tmem206	transmembrane protein 206	1393165_at	ns	ns	ns	ns	ns	ns	-1.6
Tmem212	transmembrane protein 212	1378042_at	ns	ns	ns	-13.3	ns	ns	ns
Tmem38a	transmembrane protein 38a	1379206_at	ns	-1.5	ns	ns	ns	ns	ns
Tmem51	Transmembrane protein 51	1380378_at	3.3	3.2	ns	ns	ns	ns	ns
Tmem56	Transmembrane protein 56	1383593_at	ns	ns	1.6	1.6	1.6	1.5	ns
Tmem63a	transmembrane protein 63a	1377102_at	ns	ns	ns	-1.7	ns	ns	ns
Tmod2	tropomodulin 2	1393418_at	ns	ns	-9.6	-9.9	ns	ns	ns
Tmod4	tropomodulin 4	1372407_at	ns	ns	ns	-2.6	ns	ns	ns
Tmprss2	transmembrane protease, serine 2	1373329_at	ns	ns	2.3	1.9	2.2	2.2	ns
Tnfrsf11a	Tumor necrosis factor receptor superfamily, member 11a	1394313_at	ns	ns	ns	ns	-2.0	ns	ns
Tnfrsf14	tumor necrosis factor receptor superfamily, member 14 (herpesvirus entry mediator)	1376327_at	ns	ns	ns	-5.1	ns	-5.1	ns
Tnfrsf1b	tumor necrosis factor receptor superfamily, member 1b	1392731_at	ns	ns	ns	ns	ns	ns	2.0
Tnk2	tyrosine kinase, non-receptor, 2	1372692_at	-1.6	-1.5	-1.6	ns	ns	ns	ns
Tnni1	troponin I type 1 (skeletal, slow)	1386873_at	ns	ns	ns	-5.2	ns	ns	ns
Tnni2	troponin I type 2 (skeletal, fast)	1367964_at	-4.5	ns	ns	ns	ns	ns	ns
Tom1l2	target of myb1-like 2 (chicken)	1392724_at	ns	ns	ns	ns	ns	1.9	ns
Tor1aip2	torsin A interacting protein 2	1375969_at	ns	-1.8	ns	ns	ns	ns	ns
Tox	thymocyte selection-associated high mobility group box	1379824_at	ns	ns	-5.5	ns	ns	ns	ns
Tpm1	Tropomyosin 1, alpha	1371241_x_at	ns	ns	ns	1.6	ns	ns	ns
Tpm3	Tropomyosin 3, gamma	1389846_at	ns	-1.5	ns	ns	ns	ns	ns
Tpm3	tropomyosin 3, gamma	1387617_at	ns	ns	ns	ns	ns	ns	-1.8
Trafd1	TRAF type zinc finger domain containing 1	1373757_at	ns	ns	-1.5	ns	-1.6	ns	ns
Tram1	Translocation associated membrane protein 1	1390077_at	ns	ns	ns	ns	ns	ns	-2.0
Trib3	tribbles homolog 3 (Drosophila)	1370695_s_at	ns	1.7	ns	1.8	ns	1.8	ns
Trib3	tribbles homolog 3 (Drosophila)	1386321_s_at	ns	ns	ns	1.9	ns	ns	ns

Symbol	Entrez gene name	Probeset ID	Fold change						
			UT		SC		siGCCR		
			LD	HD	LD	HD	LD	HD	C
Trib3	tribbles homolog 3 (Drosophila)	1370694_at	ns	ns	ns	1.9	ns	1.8	ns
Trim2	tripartite motif-containing 2	1375278_at	ns	-2.0	ns	ns	ns	-2.0	ns
Trim2	tripartite motif-containing 2	1373578_at	ns	-1.6	ns	ns	ns	ns	ns
Trim32	tripartite motif-containing 32	1389163_at	ns	-1.7	ns	ns	ns	ns	ns
Trim54	tripartite motif-containing 54	1372639_at	ns	ns	ns	ns	ns	3.1	ns
Trim6	tripartite motif-containing 6	1377886_at	ns	ns	ns	-4.0	ns	ns	ns
Trpv2	transient receptor potential cation channel, subfamily V, member 2	1368735_a_at	-7.2	ns	ns	ns	ns	ns	ns
Tsc22d1	TSC22 domain family, member 1	1398759_at	ns	ns	-1.6	-1.6	-1.6	ns	ns
Tsc22d3	TSC22 domain family, member 3	1367771_at	ns	ns	-1.6	-1.8	-1.9	-1.9	ns
Tshb	thyroid stimulating hormone, beta	1369750_at	ns	ns	ns	ns	ns	-6.0	ns
Tshz3	teashirt zinc finger homeobox 3	1377853_at	ns	ns	-15.6	ns	ns	ns	ns
Tsku	tsukushin	1383315_at	3.4	4.1	2.6	3.0	2.6	2.6	ns
Tspan5	tetraspanin 5	1377089_a_at	ns	ns	ns	ns	-1.7	ns	ns
Tspan5	tetraspanin 5	1380725_at	ns	ns	ns	ns	ns	2.8	-2.6
Tspan8	tetraspanin 8	1368052_at	ns	3.9	ns	ns	ns	ns	ns
Ttc14	tetratricopeptide repeat domain 14	1393758_at	ns	2.3	ns	ns	ns	ns	ns
Ttc25	tetratricopeptide repeat domain 25	1398551_at	ns	ns	1.8	ns	ns	ns	ns
Ttc3	tetratricopeptide repeat domain 3	1389957_at	ns	-1.5	ns	ns	ns	-1.6	ns
Ttc36	tetratricopeptide repeat domain 36	1393061_at	4.2	3.1	3.6	ns	3.8	3.1	ns
Ttc39b	tetratricopeptide repeat domain 39B	1377860_at	1.5	1.5	ns	1.6	ns	ns	ns
Ttc8	tetratricopeptide repeat domain 8	1378416_at	ns	-1.8	ns	ns	ns	ns	ns
Ttl12	Tubulin tyrosine ligase-like family, member 12	1388959_at	ns	ns	ns	1.6	ns	ns	ns
Ttl7	tubulin tyrosine ligase-like family, member 7	1394422_at	ns	-1.8	ns	ns	ns	ns	ns
Tuba8	tubulin, alpha 8	1390766_at	ns	ns	ns	ns	ns	ns	-5.4
Tubb3	tubulin, beta 3	1369901_at	ns	ns	ns	ns	ns	ns	-8.6
Tubb6	tubulin, beta 6	1376100_at	ns	ns	ns	1.5	ns	ns	ns
Tufm	Tu translation elongation factor, mitochondrial	1395647_at	ns	ns	-2.1	ns	ns	ns	ns
Tusc4	tumor suppressor candidate 4	1394580_at	ns	ns	ns	ns	ns	ns	-1.8
Txnip	thioredoxin interacting protein	1371131_a_at	ns	-2.0	-1.8	-2.2	-1.8	-1.9	ns
Tyms	thymidylate synthetase	1369499_at	ns	ns	-1.8	-2.3	ns	ns	ns
Uap111	UDP-N-acetylglucosamine pyrophosphorylase 1-like 1	1379673_at	ns	ns	-1.9	ns	ns	ns	ns
Uba7	ubiquitin-like modifier activating enzyme 7	1386277_at	ns	ns	ns	ns	ns	ns	4.5
Uba7	ubiquitin-like modifier activating enzyme 7	1379633_a_at	-8.4	ns	ns	ns	ns	ns	26.7
Ube2h	ubiquitin-conjugating enzyme E2H	1383023_at	ns	ns	ns	ns	ns	1.7	ns
Ube2h	ubiquitin-conjugating enzyme E2H	1390157_at	ns	1.7	ns	1.6	ns	ns	ns
Ube2l6	ubiquitin-conjugating enzyme E2L 6	1373037_at	ns	ns	ns	ns	ns	ns	2.4
Ubr4	ubiquitin protein ligase E3 component n-recognin 4	1399063_at	ns	1.6	ns	ns	ns	ns	1.7
Ubsd1	ubiquitin domain containing 1	1393126_at	ns	-1.9	ns	ns	ns	ns	ns
Ugt2a1	UDP glucuronosyltransferase 2 family, polypeptide A1	1369850_at	ns	ns	1.9	ns	ns	ns	ns
Ugt2b1	UDP glucuronosyltransferase 2 family, polypeptide B1	1370698_at	7.0	7.9	4.9	5.1	6.7	6.7	ns
Ulk1	Unc-51 like kinase 1 (C. elegans)	1375869_at	ns	ns	1.8	ns	ns	ns	ns
Unc5cl	unc-5 homolog C (C. elegans)-like	1376953_at	ns	ns	-2.0	ns	-1.8	ns	ns
Uox	urate oxidase	1387963_a_at	ns	ns	ns	-1.9	ns	ns	ns
Usf2	upstream transcription factor 2, c-fos interacting	1368591_at	ns	ns	ns	ns	-1.5	ns	ns
Usp18	ubiquitin specific peptidase 18	1389034_at	ns	ns	ns	ns	ns	ns	17.9
Usp2	ubiquitin specific peptidase 2	1387703_a_at	ns	2.4	ns	2.0	ns	ns	ns
Usp25	ubiquitin specific peptidase 25	1378679_at	ns	ns	ns	ns	ns	ns	1.7
Usp42	ubiquitin specific peptidase 42	1384767_at	ns	ns	ns	ns	ns	7.4	ns
Usp49	ubiquitin specific peptidase 49	1378999_a_at	10.1	ns	ns	ns	ns	ns	ns
Usp54	ubiquitin specific peptidase 54	1372356_at	ns	ns	-1.5	-1.6	ns	-1.6	ns
Ust5r	integral membrane transport protein UST5r	1369450_at	ns	-2.5	ns	ns	ns	ns	ns
Vav1	vav 1 guanine nucleotide exchange factor	1369387_at	ns	ns	ns	-8.6	ns	ns	ns

Symbol	Entrez gene name	Probeset ID	Fold change						
			UT		SC		siGCGR		
			LD	HD	LD	HD	LD	HD	C
Vav2	vav 2 guanine nucleotide exchange factor	1384171_x_at	ns	-1.9	ns	ns	ns	ns	ns
Vax2	ventral anterior homeobox 2	1369582_at	ns	ns	ns	ns	ns	ns	-2.5
Vcpip1	valosin containing protein (p97)/p47 complex interacting protein 1	1377849_at	ns	ns	ns	ns	1.5	ns	ns
Vegp1 / Vegp2	von Ebners gland protein 1 /// von Ebners gland protein 2	1368557_s_at	ns	ns	ns	ns	ns	-3.6	ns
VeZF1	Vascular endothelial zinc finger 1	1377806_at	ns	-1.6	ns	ns	ns	ns	ns
Vil1	villin 1	1379393_at	ns	-8.2	ns	-18.5	ns	-6.6	ns
Vipr1	vasoactive intestinal peptide receptor 1	1383695_at	ns	6.1	ns	ns	ns	ns	ns
Vipr2	vasoactive intestinal peptide receptor 2	1387177_at	ns	ns	ns	-3.9	ns	ns	ns
Vldlr	very low density lipoprotein receptor	1387455_a_at	ns	ns	2.5	3.9	ns	2.8	ns
Vldlr	very low density lipoprotein receptor	1389611_at	ns	2.8	2.2	3.6	1.9	2.6	ns
Vldlr	very low density lipoprotein receptor	1369098_at	ns	2.2	2.0	2.5	ns	2.0	ns
Vom1r100	vomer nasal 1 receptor, 100	1370732_at	ns	ns	ns	ns	-7.4	-6.3	11.2
Vom1r102	vomer nasal 1 receptor, 102	1370712_at	ns	ns	ns	ns	ns	-9.7	ns
Vom2r-ps45	vomer nasal 2 receptor, pseudogene 45	1388047_at	ns	14.1	ns	ns	ns	ns	ns
Vps13a	vacuolar protein sorting 13 homolog A (S. cerevisiae)	1392571_at	ns	ns	ns	ns	ns	ns	-3.1
Vps36	Vacuolar protein sorting 36 homolog (S. cerevisiae)	1379843_at	ns	ns	2.5	ns	ns	ns	ns
Vps45	vacuolar protein sorting 45 homolog (S. cerevisiae)	1370549_at	ns	ns	ns	-1.7	ns	ns	ns
Vps4a	vacuolar protein sorting 4 homolog A (S. cerevisiae)	1396462_at	ns	-1.6	ns	ns	ns	ns	ns
Vps52	vacuolar protein sorting 52 homolog (S. cerevisiae)	1369668_x_at	ns	ns	ns	ns	ns	ns	-9.0
Vps52	vacuolar protein sorting 52 homolog (S. cerevisiae)	1369667_at	1.7	1.8	1.6	1.8	ns	ns	1.6
Vsn1	visinin-like 1	1368853_at	ns	6.8	ns	ns	ns	ns	ns
Vwc2	von Willebrand factor C domain containing 2	1398659_at	ns	ns	-10.0	-10.0	ns	-7.9	ns
Wasf1	WAS protein family, member 1	1392974_at	ns	-1.5	ns	ns	ns	ns	ns
Wbp2	WW domain binding protein 2	1369592_at	ns	ns	ns	ns	ns	6.5	ns
Wdr6	WD repeat domain 6	1373399_at	ns	ns	ns	-1.5	ns	-1.5	ns
Wif1	Wnt inhibitory factor 1	1369203_at	1.9	1.9	ns	1.9	ns	ns	ns
Wnk1	WNK lysine deficient protein kinase 1	1396919_at	-7.0	ns	ns	ns	ns	ns	ns
Wnt7a	wingless-type MMTV integration site family, member 7A	1398645_at	ns	ns	ns	ns	ns	-6.1	ns
Wnt8b	wingless-type MMTV integration site family, member 8B	1386122_at	ns	7.4	ns	ns	ns	ns	ns
Wrmip1	Werner helicase interacting protein 1	1389090_at	ns	-1.7	ns	ns	ns	ns	ns
Xpo4	exportin 4	1385428_at	ns	ns	ns	1.5	ns	ns	ns
Xpo4	exportin 4	1385864_at	ns	1.6	ns	ns	ns	ns	ns
Ybx2	Y box binding protein 2	1388914_at	ns	ns	-6.9	ns	ns	ns	ns
Yeats4	YEATS domain containing 4	1378100_at	ns	ns	1.6	ns	ns	ns	ns
Ythdf1	YTH domain family, member 1	1379215_at	ns	ns	-4.4	ns	9.0	ns	ns
Zadh2	zinc binding alcohol dehydrogenase, domain containing 2	1385015_at	ns	ns	ns	ns	2.0	ns	ns
Zadh2	zinc binding alcohol dehydrogenase, domain containing 2	1388731_at	ns	ns	ns	ns	1.8	1.5	ns
Zbtb39	zinc finger and BTB domain containing 39	1391642_at	ns	-12.8	ns	ns	ns	ns	ns
Zbtb39	zinc finger and BTB domain containing 39	1390476_at	ns	ns	ns	ns	ns	ns	1.6
Zbtb45	zinc finger and BTB domain containing 45	1378116_at	ns	-2.0	ns	ns	ns	ns	ns
Zbtb7b	zinc finger and BTB domain containing 7B	1385398_at	ns	3.4	ns	ns	ns	ns	ns
Zbtb8a	zinc finger and BTB domain containing 8a	1397882_at	ns	ns	-2.8	ns	ns	ns	ns
Zc3h7b	zinc finger CCCH-type containing 7B	1395943_at	ns	2.8	ns	ns	ns	ns	ns
Zdhhc1	zinc finger, DHHC-type containing 1	1396149_at	ns	ns	ns	-3.0	ns	-1.9	ns
Zdhhc7	zinc finger, DHHC-type containing 7	1368152_at	ns	1.5	ns	1.6	ns	ns	ns
Zfand2a	zinc finger, AN1-type domain 2A	1373767_at	ns	ns	ns	1.8	ns	ns	ns
Zfand2b	zinc finger, AN1 type domain 2B	1373606_at	ns	ns	ns	1.5	ns	ns	ns
Zfx4	zinc finger homeobox 4	1375582_at	ns	ns	ns	ns	-1.9	ns	ns
Zfp189	zinc finger protein 189	1376628_at	-1.7	ns	-1.8	ns	-1.7	-1.8	ns

## 10 APPENDIX

Symbol	Entrez gene name	Probeset ID	Fold change						
			UT		SC		siGCGR		
			LD	HD	LD	HD	LD	HD	C
Zfp278	zinc finger protein 278	1372205_at	ns	ns	ns	-1.7	-2.0	ns	ns
Zfp324	zinc finger protein 324	1375395_at	ns	ns	ns	ns	ns	-7.1	6.1
Zfp346	zinc finger protein 346	1392699_at	ns	ns	ns	ns	ns	ns	2.3
Zfp395	zinc finger protein 395	1390148_a_at	ns	-1.8	-1.6	-1.8	ns	-1.6	ns
Zfp426l2	zinc finger protein 426-like 2	1391564_at	ns	ns	ns	ns	-1.7	ns	ns
Zfp469	zinc finger protein 469	1372483_at	ns	-1.6	-1.9	ns	ns	ns	ns
Zfp84	zinc finger protein 84	1382411_at	ns	ns	-1.6	ns	ns	ns	ns
Zfpm2	zinc finger protein, multitype 2	1377568_at	ns	ns	ns	ns	ns	5.0	ns
Zic4	Zic family member 4	1380514_at	ns	ns	ns	ns	ns	ns	-5.4
Zmat4	zinc finger, matrin type 4	1380847_at	ns	5.1	ns	ns	ns	ns	ns
Zmiz2	zinc finger, MIZ-type containing 2	1372288_at	ns	ns	ns	ns	-1.5	ns	ns
Zmynd8	zinc finger, MYND-type containing 8	1390305_at	ns	ns	ns	ns	ns	ns	1.7
Znf467	zinc finger protein 467	1391507_at	ns	ns	ns	-1.5	ns	-1.5	ns
Znf503	Zinc finger protein 503	1375366_at	ns	ns	ns	-6.6	ns	ns	ns
Znf509	zinc finger protein 509	1391216_at	ns	-1.8	ns	ns	ns	ns	ns
Znf580	zinc finger protein 580	1377433_at	ns	ns	ns	ns	ns	ns	-1.9
Znf597	zinc finger protein 597	1370705_at	ns	-1.8	ns	ns	ns	ns	ns
Znf763	zinc finger protein 763	1385597_at	ns	ns	ns	-2.4	ns	ns	ns